Physico-chemical characterization of beta-amyloid oligomers and study of their function in biological processes at molecular level

Dóra Simon

Ph.D. Thesis

Szeged
2011.

Physico-chemical characterization of beta-amyloid oligomers and study of their function in biological processes at molecular level

Dóra Simon

Ph.D. Thesis

Supervisors:

Lívia Fülöp Ph.D.
Botond Penke D.Sc.

Department of Medical Chemistry
University of Szeged

Szeged
2011.

Publications providing the basis of the thesis

I.

Two pyridine derivatives as potential Cu(II) and Zn(II) chelators in therapy for Alzheimer's disease.

Lakatos A, Zsigó E, Hollender D, Nagy NV, Fülöp L, Simon D, Bozsó Z, Kiss T.
Dalton Trans. 2010. Feb. 7; 39 (5):1302-15.

II.

Controlled in situ preparation of A beta(1-42) oligomers from the isopeptide "iso-A beta(1-42)", physicochemical and biological characterization.

Bozso Z, Penke B, Simon D, Laczkó I, Juhász G, Szegedi V, Kasza A, Soós K, Hetényi A, Wéber E, Tóháti H, Csete M, Zarándi M, Fülöp L.
Peptides. 2010. Feb; 31 (2):248-56.

III.

Protein array based interactome analysis of amyloid-β indicates an inhibition of protein translation.

Virok DP[#], Simon D[#], Bozsó Z, Rajkó R, Datki Z, Bálint É, Szegedi V, Janáky T, Penke B, Fülöp L.
J. Proteome Res. 2011. Apr. 1;10 (4):1538-47.

IV.

Interactions of pathological hallmark proteins: Tubulin polymerization promoting protein/p25, {beta}-amyloid and {alpha}-synuclein.

Olah J, Vincze O, Virok D, Simon D, Bozso Z, Tokesi N, Horvath I, Hlavanda E, Kovacs J, Magyar A, Szucs M, Orosz F, Penke B, Ovadi J.
J. Biol. Chem. 2011. Aug. 8.

Table of Contents

1 Introduction

1.1 Major pathological hallmarks of Alzheimer's disease

Alzheimer's disease (AD), described by Alois Alzheimer in 1907, is one of the most common neurodegenerative disorders in the aged population. More than 25 million people in the world today are affected by dementia, most of them are suffering from Alzheimer's disease. It is the seventh leading cause of death in the United States (Alzheimer 2008). In both developed and developing nations, Alzheimer's disease has had tremendous impact on the affected individuals, caregivers, and society. The etiological factors, other than older age and genetic susceptibility, remain to be determined (Qiu, Kivipelto et al. 2009).

The main pathological hallmarks are senile plaques, composed of extracellularly accumulated amyloid-beta (Aβ) fibrils and intracellularly hyperphosphorylated-tau protein filaments, called neurofibrillar tangles (NFT).

A major advance in the study of AD came with the sequencing of the main peptide constituent of the senile plaque, the Aβ peptide(Glenner, Wong et al. 1984). This led to four key discoveries. *First*, the Aβ peptide is a part of a large type I membrane protein, the amyloid precursor protein (APP), which is encoded by the *APP* gene on chromosome 21. *Second*, the *APP* gene is mutated in a significant fraction of the cases of familial Alzheimer's disease. *Third*, individuals with Down's syndrome, who have three copies of chromosome 21 and hence three copies of the *APP* gene, develop clinical and pathological signs of early-onset Alzheimer's. And *fourth*, mutations in the presenilin-1 (*PSEN1*) and presenilin-2 (*PSEN2*) genes can behave as dominant familial AD genes. Presenilin is the catalytic subunit of the γ-secretase activity that liberates the Aβ peptide from the C-terminus of AP (Herrup 2010). These observations led to the so-called 'amyloid cascade hypothesis', which states that the deposition of amyloid, made up principally of Aβ 1-42, would be the central event in the initial pathogenesis of AD (Hutton and Hardy 1997)(Fig. 1.)(Hardy and Higgins 1992; Herrup 2010). In familial AD (Fig. 1. top left), missense mutations in either *APP* or one of the *PSEN* genes lead to the accumulation of the amyloid peptide in the brain that has a high tendency to aggregate by forming beta-sheet structures. The amyloid cascade hypothesis proposes that these Aβ aggregates lead to a series of downstream events including synapse loss, plaque

deposition, inflammation, triggering of tau hyperphosphorylation and consequently to the death of susceptible neurons. The hypothesis also proposes that sporadic AD develops when an individual has an accelerated age-dependent process of Aβ accumulation, including the failure of the clearance mechanisms (Fig. 1, top right). At some point, sufficient Aβ becomes deposited thus the amyloid cascade evolves. Subsequently, the sporadic disease follows the same pathway to dementia as the familial form (Fig. 1, top left) (Herrup 2010).

Biochemical studies show that NFTs contain hyperphosphorylated tau proteins. Tau protein is a microtubular associated protein (MAP), that ensures the construction of the microtubular network. During neurodegeneration, tau is abnormally phosphorylated at proline-directed serine/ threonine phosphorylation sites (Castellani, Rolston et al. 2010). NFTs are located primarily in large pyramidal neurons of cornu ammonis (CA) and the cerebral neocortex, although neurofibrillary pathology is also encountered in deep structures, including midbrain and pontine tegmentum, basal nucleus of Meynert, and hypothalamus (Braak and Braak 1991). NFTs are cross-beta, congophilic structures, like Aβ and morphologically classically described as consisting of numerous paired helical filaments (Kidd 1963), that are composed of 2 axially opposed helical filaments with a diameter of 10 nm and a half-period of 80 nm (Kidd 1964) (Terry, Gonatas et al. 1964; Wisniewski, Narang et al. 1976). The distribution and amount of neurofibrillary tangles are correlated with the severity of cognitive impairment in patients with AD (Arriagada, Growdon et al. 1992) (Garcia-Sierra, Mondragon-Rodriguez et al. 2008). No direct evidence has firmly established a causal role of tau hyperphosphorylation and the presence of neurofibrillary tangles in Alzheimer disease, however several mutations in the tau gene are known to lead to another type of dementia—the familial frontotemporal dementia with Parkinsonism linked to chromosome 17 (FTDP-17) (Hutton, Lendon et al. 1998; Poorkaj, Bird et al. 1998; Spillantini, Murrell et al. 1998). In addition, overexpression of tau causes exaggregated and facilitated pathogenesis in transgenic mice carrying mutant APP (Gotz, Chen et al. 2001; Lewis, Dickson et al. 2001). Genetic removal of tau from these transgenic mice led to reduced Alzheimer disease–type pathologic features (Roberson, Scearce-Levie et al. 2007), suggesting that tau is essential for Aβ–induced neuronal toxicity (at least in transgenic mice).

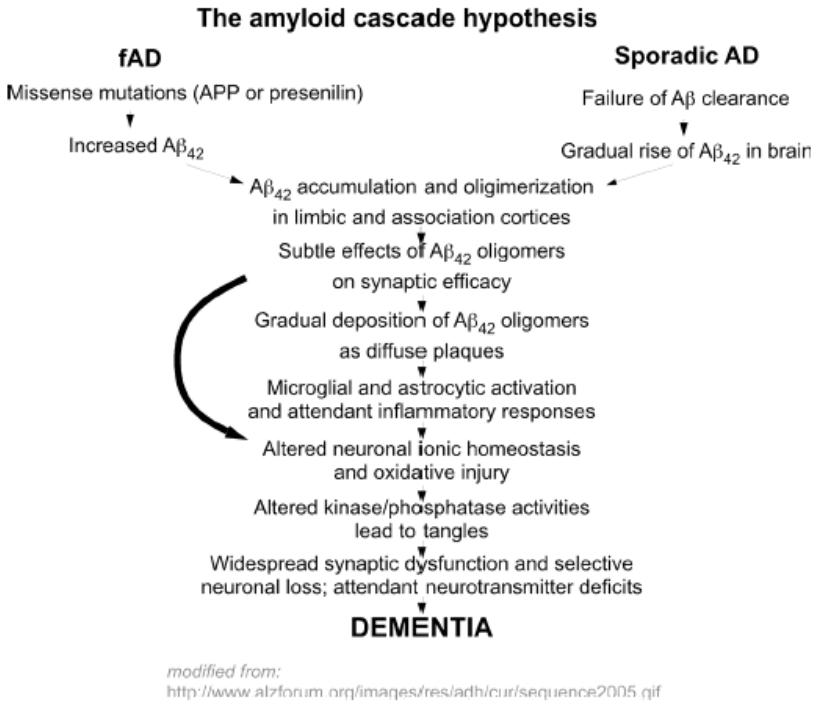

Figure 1. The amyloid cascade hypothesis of Alzheimer's disease (Herrup K., 2010.). This hypothesis represents the classic theory of the origins of Alzheimer's disease. The diagram is modified from that found on the AlzForum web site (http://www.alzforum.org/images/res/adh/cur/sequence2005.gif)

1.1.1 Diagnosis and treatment

AD must be differentiated from other causes of dementia: vascular dementia, dementia with Lewy bodies, Parkinson's disease with dementia, frontotemporal dementia, and reversible dementias (Castellani, Rolston et al. 2010). Memory impairment alone is not sufficient for a diagnosis of AD. According to the Diagnostic and Statistical Manual of Mental Disorders, 4th edition (DSM-IV), dementia is defined as memory impairment plus one or more of the following symptoms: *aphasia*-impairment of any language modality; *apraxia*-loss of the ability to execute or carry out learned purposeful movements; *agnosia*-loss of ability to recognize objects, persons, sounds, shapes, or smells, and impaired executive functioning (http://www.alzforum.org). Recent studies indicate that individuals diagnosed with mild cognitive impairment (MCI) may in fact be showing very early symptoms of Alzheimer's (Shah, Tangalos et al. 2000). It is important to point out that MCI is not a distinct entity.

Rather, MCI lacks a pathologic substrate, genetic predispositions, and discernible treatment benefits, remain clinically stable for many years, and even improve over time. The MCI is therefore a case of early AD or not, comprises a mixture of subjects with genuine AD, subjects with neurodegenerative conditions, and subjects who would not develop neurodegeneration for many years. (Castellani, Rolston et al. 2010).

The diagnosis is based on clinical observations, i.e. on the presence of characteristic neurological and neuropsychological features. (Klafki, Staufenbiel et al. 2006; Mendez 2006). Medical imaging with computed tomography (CT) or magnetic resonance imaging (MRI), and with single photon emission computed tomography (SPECT) are used more and more frequently. Recently positron emission tomography (PET) contributes to the recognition of the disease. A new PET-ligand, the Pittsburgh Compound B (PiB), a Thioflavin-T homologue, can cross the blood-brain-barrier (BBB) and binds to β-sheet structures, like Aβ (Bacskai, Frosch et al. 2007). PiB opened the door to visualizing *in vivo* brain function in a manner relevant to amyloid plaque buildup in AD. It allows also a direct measurement of the efficacy of anti-amyloid therapy (Castellani, Rolston et al. 2010) and it can be used to help excluding other cerebral pathology or subtypes of dementia. The techniques mentioned have provided mapping of morphological and functional brain alterations during the progress of Alzheimer's disease. On the other hand, Alzheimer’s disease is diagnosed through several clinical interviews and tests. Even though there is no cure today, an early diagnosis can help patients and families in taking advantage of available treatments and make informed decisions about long-term care, participation in research and clinical trials, and legal and financial arrangements (http://www.alzforum.org).

Brain autopsy helps to confirm the diagnosis of Alzheimer after death. Brain banks are also critically important for research, as they provide tissue essential for understanding the disease and for identifying diagnostic and therapeutic targets.

Currently AD can't be cured. Still, drug and non-drug treatments may help with both cognitive and behavioral symptoms. Treatment teams of several clinics work with patients to develop a treatment program tailored to their individual needs. The U.S. Food and Drug Administration (FDA) has approved two types of medications: cholinesterase inhibitors, like Aricept (Exelon, Razadyne, Cognex), and memantine (Namenda) for treating the cognitive symptoms (memory loss, confusion, and problems with thinking and reasoning) of AD.

Cholinesterase inhibitors play a major role in treatment of the disease, because there is selective loss of choline acetyltransferase (ChAT) activity in different parts of the AD brain samples including cortex, hippocampus and amygdala (Bowen, Smith et al. 1976). The most consistent losses throughout the progression of AD are seen in long projection neurons, including cholinergic neurons of the basal forebrain (Auld, Kornecook et al. 2002). These neurons provide the major source of cholinergic innervation to the cerebral cortex and hippocampus and play therefore a key role in memory and attentional function (Auld, Kornecook et al. 2002).

Memantine is the first in a novel class of Alzheimer's disease medications acting on the glutamatergic system by blocking NMDA glutamate receptors. Dysfunction of glutamatergic neurotransmission, manifested as neuronal excitotoxicity, is hypothesized to be involved in the etiology of Alzheimer's disease. Memantine is a low-affinity voltage-dependent uncompetitive antagonist at glutamatergic NMDA receptors (Rogawski and Wenk 2003) (Robinson and Keating 2006). By binding to the NMDA receptor with a higher affinity than Mg^{2+} ions, memantine is able to inhibit the prolonged influx of Ca^{2+} ions, which forms the basis of neuronal excitotoxicity.

Several studies show that diet rich in docosahexaenoic acid (DHA) may delay or even prevent the developement of the disease. Mice fed with meal rich in omega-3 fatty acid had lower levels of Aβ and tau proteins than those in the control groups.

While current medications cannot stop the damage caused by AD to brain cells, they may help lessen or stabilize symptoms for a limited time. Neurologists sometimes prescribe both types of medications together (http//www.alz.org).

1.1.2 Aggregation of Aβ 1-42

Aβ peptides consist of 39-42 amino acids and generated after enzymatic cleavage by β-and γ-secretases from a membrane protein, called amyloid precursor protein (APP), encoded on chromosome 21. Initially these peptides possess α-helical/ random coil conformation, which turns readily into β-sheet in aqueous environment. This conformational transition induces aggregation producing Aβ-oligomers, protofibrils and fibrils. Simultaneously the water solubility of these Aβ-species substantially decrease (Bozso, Penke et al. 2010). Aβ 1-42 has a higher tendency of β-amyloid fibril formation than Aβ 1-40 (Kim, Onstead et al. 2007; Yan

and Wang 2007; Jan, Gokce et al. 2008). Fibrillar Aβ was suspected of being the primary agent that causes the AD-related histopathology and eventually clinical symptoms. However, the accumulation of the predominantly fibrillar Aβ containing plaques does not correlate well with the clinical symptoms (Terry, Gonatas et al. 1964; Lue, Kuo et al. 1999; McLean, Cherny et al. 1999), and plaque accumulation appears later than the observed histopathology in animal models (Westerman, Cooper-Blacketer et al. 2002) (Billings, Oddo et al. 2005). Nowadays it is evident, that extracellular plaques, including fibrillar form of Aβ, are the consequence of several processes and alterations that contribute to the development of the disease and Aβ 1-42 in soluble oligomeric form is considered to be the main toxic species and most likely responsible for neuronal disfunction in AD (Armstrong 2011) (Hardy and Selkoe 2002). The term 'soluble' refers to any form of Aβ that is soluble in aqueos solution after high-speed centrifugation, indicating that it is not the insoluble fibrillar Aβ. Assemblies ranging from dimers to 24-mers, or even those of higher molecular weight (MW), have been reported as Aβ oligomers (Haass and Selkoe 2007; Glabe 2008; Roychaudhuri, Yang et al. 2009; Sakono and Zako 2010). The amount of Aβ oligomers is increased in AD in both brain tissue and plasma (Xia, Yang et al. 2009). The original amyloid cascade hypothesis proposed that Aβ aggregation is the central event associated with neurotoxicity (Hardy, 1992, 2002). This hypothesis had been reformulated to focus on soluble aggregates as the pathogenic molecular form of Aβ (Hardy and Selkoe 2002). The analysis of the aggregation pathway *in vitro* and biochemical characterization of Aβ deposits isolated from AD brains indicate that Aβ oligomerization occurs via distinct intermediates, including oligomers of 3 to 50 Aβ monomers, annular oligomers, protofibrils, fibrils and plaques (Jellinger 2009). Among these, the most toxic species appear to be low-n Aβ oligomers (Finder and Glockshuber 2007). Nevertheless, knowledge about the detailed mechanism underlying Aβ aggregation and β-amyloid fibril formation is still limited (Finder, Vodopivec et al. 2010) since the structure of soluble oligomers and different aggregated forms is very challenging to study, because they are generally difficult to obtain in large quantities for high resolution structural techniques, and they are temporally unstable, rapidly aggregating into more mature fibrillar forms, caused by the presence of high number of hydrophobic amino acids in the sequence (Meredith 2005) (Bozso, Penke et al. 2010). Studies using conformation-dependent antibodies suggest that structural variants could exist among even morphologically similar Aβ oligomers. A

difference in antibody-binding properties indicates a difference in epitope exposure. For example there are two antibodies: OC and A11 which are specific for fibrils and oligomers, respectively (Glabe 2008). According to these studies, there are two distinct type of oligomers: prefibrillar ones that are A11-positive and fibrillar ones that are OC-positive. The prefibrillar oligomers may align into fibrillar ones, which posses the structural characteristics of fibrillar aggregates (protofibrils, fibrils) and might represent fibril nuclei to which the monomers can attach before elongation. These results strongly suggest the existence of a structural polymorphism of Aβ oligomers (Sakono and Zako 2010).

Until recently the synthetic peptide samples were not homogenous concerning their solubility and aggregation grade. Using synthetic Aβ from different sources led to poorly reproducible experimental results. To obtain well caracterized, water soluble and reproducible peptide solutions of Aβ, several preparation protocols were formulated and published in the literature (Catalano, Dodson et al. 2006; Hepler, Grimm et al. 2006) (Lambert, Barlow et al. 1998; Dahlgren, Manelli et al. 2002) To overcome the problem of solubility and high aggregation propensity of Aβ, we used a precursor of human Aβ synthetized in our laboratory instead of the convenient synthetic form. This synthetic peptide is a so-called ’depsi-peptide’ containing an ester bond in the peptide chain. It was described recently independently by (Carpino, Krause et al. 2004; Sohma, Sasaki et al. 2004) and (Dos Santos, Chandravarkar et al. 2005). The precursor peptide (`iso Aβ´) has a low tendency for aggregation. The ester bond in the backbone is between Gly^{25}-Ser^{26}, thus Ser^{26} has a free α-amino group. The ester bond decreases the propensity of the peptide to aggregate, thus it has an enhanced water solubility. The depsipeptide form is stable at acidic pH. When the pH is raised to the physiological value, a fast O→N acyl-transfer reaction occurs resulting in the natural, unmodified Aβ 1–42 sequence. The O→N acyl-shift can occur in a short time both in vitro and in vivo, thus iso Aβ 1–42 can be used as a good precursor for Aβ 1–42 (Fig. 2.).

The most important factors in the toxicity of Aβ oligomers are the aggregation grade and the peptide conformation. Thus one of our aim was to characterize the assemblies of Aβ with a series of biochemical methods. These methods are: 1, fast protein liquid chromatography-size exclusion chromatography (FPLC-SEC), which separates mixtures of samples according to their size (hydrodynamic diameter); 2, sodium dodecyl sulfate-polyacrylamide gelelectrophoresis (SDS-PAGE); 3, Western blot (WB); 4, dinamic light scattering (DLS), by

which the size distribution of the protein aggregates can be determined in solution; 5, and transmission electron microscopy (TEM), which is a high resolution visualizing technique, where an image is formed from the interaction of the species and the electrons transmitted through the sample.

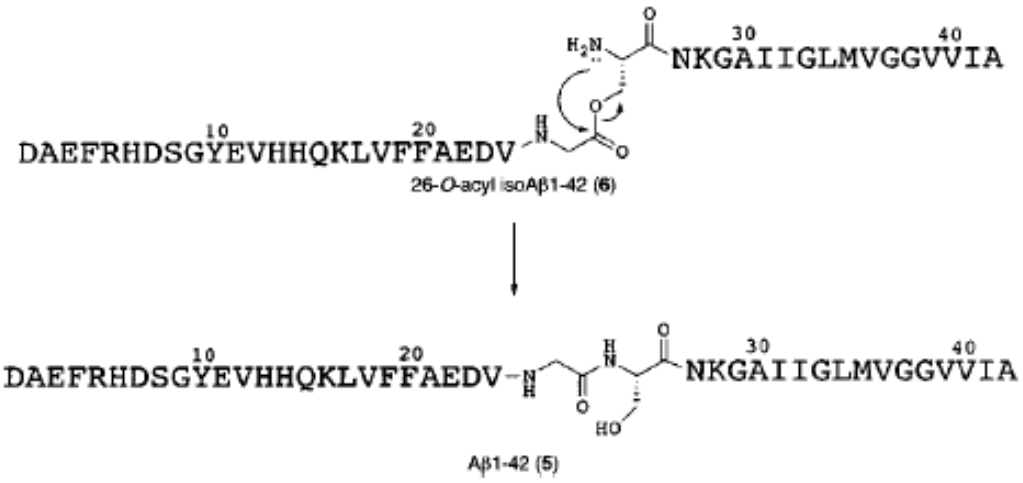

Fig. 2.: O→ N acyl-shift occurs at pH 7.4 at Ser^{26} in the sequence of isopeptide resulting Aβ 1-42 (Sohma, Sasaki et al. 2004).

1.1.3 Factors, that influence the aggregation of Aβ 1-42: metals in Alzheimer's disease

There are several scientists who think, that self-aggregating properties of Aβ are insufficient to explain the accumulation of the peptide in diffrent brain regions and assume the presence of other neurochemical factors that have to play an important role in the aggregation process (Bush and Tanzi 2008; Lakatos, Zsigo et al. 2010). One of these outstanding factors might be the pathological interaction between Aβ and metal ions Zn^{2+} and Cu^{2+} that are presented in the brain (Huang, Cuajungco et al. 2000). These ions are found in living organisms and have defined physiological functions that serve to maintain normal cellular processes. There is an extensive literature demonstrating their potential involvement and interaction with biochemical substrates in cognitive impairment and other processes that may contribute to neurodegeneration, including AD (Adlard and Bush 2006).

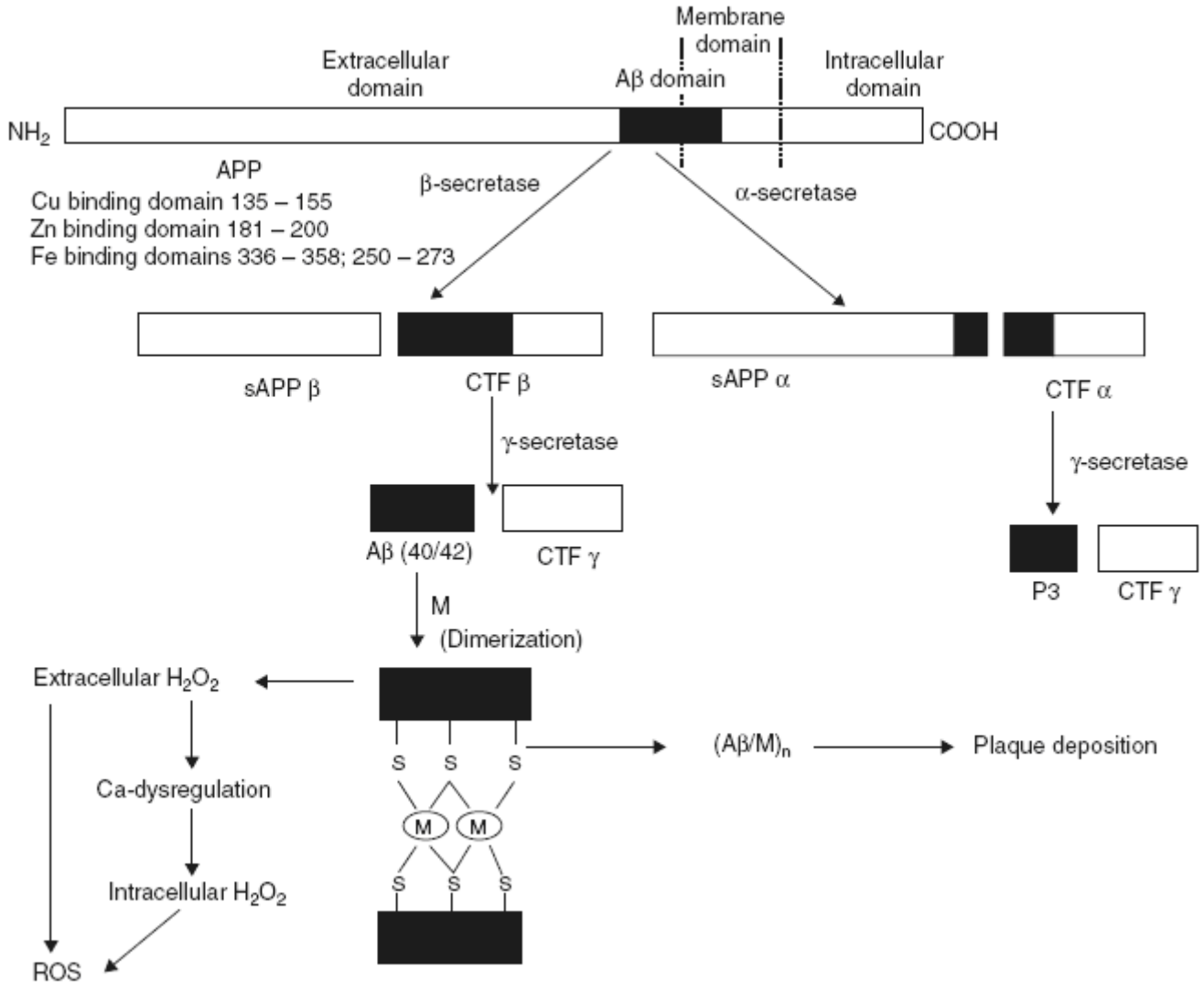

Fig. 3, The proteolytic processing of amyloid precursor protein (APP) to produce Aβ that coordinates the metal ions (M: Zn^{2+}, Cu^{2+} and Fe^{2+}) to induce aggregation, and generation of ROS. The hyper-metallated (by Zn^{2+}, Cu^{2+} and Fe^{2+}) state of Aβ as a consequence of age-dependent elevations in tissue metal concentrations can induce Aβ aggregation. H_2O_2 can initiate a number of oxidative events, including Fenton reactions to form toxic hydroxyl radicals and calcium dysregulation, and subsequent reactive oxygen species (ROS) generation (Bandyopadhyay, Huang et al. 2010).

The high affinity binding of transition metals to Aβ (Bush, Pettingell et al. 1994)has been extensively studied and shown to result in a pH dependent induction of protease resistant aggregation and precipitation of Aβ (Miura, Suzuki et al. 2000). In this way, a „metal hypothesis" has established, wich points out the metal induced aggregation of Aβ as a key step in place of the self aggregation (Fig. 3,). On the average there are up to 3.5 metal binding sites on Aβ (probably as an oligomer) (Atwood, Scarpa et al. 2000). At least two of these sites are selective for zinc and copper, but some substitution can occur at each site. The proportion of binding of Zn^{2+} and Cu^{2+} to Aβ will depends on the respective stability constants (K = [ML]/[M][L], where M = metal ion and L = ligand) of each metal ion for different ligands, their total concentrations, and the pH of the microenvironment. (Atwood, Scarpa et al. 2000) (Yang, McLaurin et al. 2000).

1.1.3.1 Zinc in AD

Zn^{2+} has a well documented interaction with Aβ pepide and its modulation with age may initiate AD related pathology (Lin, Huang et al. 2010). In AD, due to the abundantly expressed Zn^{2+} transporter proteins (ZnTs) that induce an abnormal uptake and distribution of Zn^{2+} (Bush, Pettingell et al. 1994), high local Zn^{2+} release is observed from the presynaptic vesicles to the postsynaptic membrane in depolarization-dependent manner in several parts of the brain, including neocortex, hippocampus and amygdala (Bandyopadhyay, Huang et al. 2010). It is well known that high affinity binding is observed between Zn^{2+} and Aβ (Bush, Pettingell et al. 1994). In this way the sequestration of Zn^{2+} in Aβ-Zn^{2+} complexes further leads to reduced Zn^{2+} availability at synaptic terminals (Frederickson, Koh et al. 2005). The increase of synaptic Zn^{2+} correlates well with higher levels of insoluble Aβ in aging females, and these sex differences completely disappear in $ZnT3^{-/-}$mice, suggesting the role for synaptic Zn^{2+} in the sex differences in AD (Lee, Cole et al. 2002) Bandyopadhyay, 2010). The Zn^{2+}-Aβ binding prevents the formation of the regular amyloid fibrils, it induces the accumulation of large unorganized aggregates of smaller non-fibrillar forms of Aβ (Tougu, Karafin et al. 2009) (Noy, Solomonov et al. 2008). Zinc-induced aggregation of Aβ occurs over a broad pH range (pH 5.5–7.5) (Atwood, Moir et al. 1998) (Yoshiike, Tanemura et al. 2001) (Cherny, Legg et al. 1999).

Since the Aβ-Zn^{2+} complex is proven to be toxic as confirmed by Zsolt Datki (in personal communication) and his collagues, metal chelators may act as potential blockers of Aβ fibrillization and Aβ-dependent oxidative stress induced neurotoxicity, in this way may serve as drugs in AD (Bandyopadhyay, Huang et al. 2010). There is a potent Zn^{2+} chelator molecule, a novel derivative of the N,N,N',N'-tetrakis (2-pyridylmethyl)ethylenediamine (TPEN)-a widely used high affinity membrane permeable Zn^{2+} chelator.) derivative: *N*1,*N*2-bis(pyridine-2-yl-methyl)ethane-1,2-diamine (ENDIP, Fig. 4.). The effect of ENDIP was extensively studied in *in vitro* experiments in our laboratory.

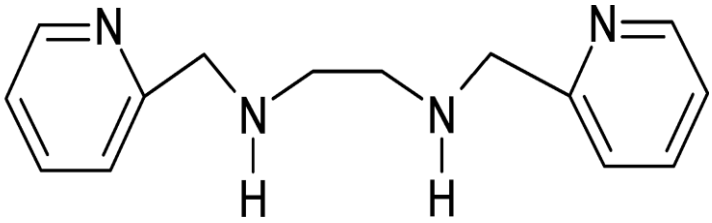

Fig. 4.: Structure of *N*1,*N*2-bis(pyridine-2-yl-methyl)ethane-1,2-diamine (ENDIP).

1.1.4 Interactions of Aβ 1-42 oligomers

The other aim of this work was to present the experiments designed for seeking interaction partners of Aβ 1–42 oligomers in a high-throughput manner, using protein array technology. Protein–protein interactions provide the molecular basis for the structural and functional organization within cells. Alterations in binding affinities can have serious consequences on some essential cellular processes (Van Gassen, Annaert et al. 2000). As it was discussed previously, in the beginning, fibrillar Aβ was thougt to play the central role in the disease, but currently oligomeric Aβ is of interest in Aβ-mediated toxicity and the pathogenesis of Alzheimer's disease. It is possible that the fibril itself is not toxic and fibrillization would be an efficient way for the cell to sequester potentially toxic protofibrils (Lansbury 1999). APP localizes to the plasma membrane, trans-Golgi network, endoplasmic reticulum (ER) and endosomal, lysosomal and mitochondrial membranes, hence Aβ is released and thus can be accumulated extra-and intracellularly. Multiple Aβ oligomer conformations are produced via different pathways, indicating that the mechanisms of formation may also differ for extracellular and intracellular oligomers (Glabe 2008). The liberation of Aβ could potentially occur wherever APP and β-and γ-secretases are localized for example in several cellular

compartments. If this cleavage takes place within the confines of the cell, Aβ will be intracellular. If liberation occurs at the plasma membrane or in the secretory pathway, it will be released extracellularly (LaFerla, Green et al. 2007). Intracellular Aβ can be produced in two ways: first, by sequential cleavage of secretases in endosomes and membranes inside of the cell (mentioned above), and second by taking up the previously secreted Aβ by cells and internalizing into intracellular pools through various receptors, transporters or via endocytotic pathways. Intracellular accumulation of Aβ in the multivesicular body (MVB, which is considered as late endosome and is formed from the early endosome system) is linked to cytosolic proteasome inhibition (Almeida, Takahashi et al. 2006). This inhibition suggests that Aβ is also located within the cytosolic compartment (Oh, Hong et al. 2005). Although most of Aβ is formed in endosomes and normally degraded within lysosomes, Aβ can accumulate in lysosomes hence destabilizes its membrane (Yang, Chandswangbhuvana et al. 1998), which could also lead to the presence of Aβ in the cytosolic compartment (Sakono and Zako 2010).

How intra-and/or extracellular Aβ oligomers could be formed and affect brain cells is yet unclear. Accumulation of Aβ may initiate a complex cascade that induces gliosis, inflammatory and synaptic changes, the formation of neurofibrillary tangles and transmitter loss (Verdier, Zarandi et al. 2004). Perhaps there is no single molecular pathological mechanism behind AD and Aβ modulates cellular functions by binding to a large group of functionally important proteins in the cellular protein network and also to a variety of biomolecules, including lipids (apolipoproteins and High Density Lipoprotein, HDL), and proteoglycans. Aβ is known to interact with the cell membrane, membrane proteins and also with the membranes of subcellular organelles such as lysosome, mitochondria, Golgi complex and endoplasmic reticulum in concequence of its lipophilicity.

There are several ways how Aβ oligomers may cause neuronal damage:

1, Extracellular Aβ: The binding of Aβ to the plasma membranes is a potential point of intervention in the events leading to the development of AD, although it is also known that toxic intracellular Aβ accumulation can be detected in neurons before extracellular Aβ deposits (Talaga and Quere 2002) and extracellular Aβ may originate from intraneuronal pools (LaFerla, 2007.). There is a growing body of evidence showing an association between cholesterol and AD (Hartmann 2001). This biochemical relation is bidirectional. Several

studies have demonstrated that extracellular Aβ affects the cellular cholesterol dynamics, such as cellular transport, which in turn has a variety of effects on AD related pathologies, including the modulation of tau phosphorylation and synapse formation. On the other hand, cholesterol-and glycosphingolipid-rich microdomains known as lipid rafts are implicated in APP processing, Aβ generation and oligomerization and can modulate protein folding dynamics and rates of aggregation (Waschuk, Elton et al. 2001), leading to the development of the disease (Chochina, Avdulov et al. 2001) (Michikawa 2003). A subset of membrane proteins also bind, hereby may internalize extracellular Aβ, such as the insulin receptor, serpin complex receptor (SEC-R), acetylcholine receptors (AChRs), integrins, receptor for advanced glycosylation end products (RAGE), formyl peptide receptor-like 1 (FPRL1), NMDAR, etc., inducing various effects on neurons. Binding of Aβ to some membrane proteins may be protective for the cell, e. g. by mediation of Aβ adhesion, internalization into early endosomes and degradation. Perturbation of these functions (membrane fluidity, membrane structure) may facilitate the development of AD (Verdier, 2004.). Among others, binding of Aβ oligomer to the NGF receptor (p75NTR) mediates apoptotic cell death and the activation of downstream signaling molecules, such as c-Jun N-terminal kinase (Coulson 2006). Several reports show that Aβ oligomers interact with NMDAR, causing abnormal calcium homeostasis, leading to increased oxidative stress and synapse loss (De Felice, Velasco et al. 2007; Shankar, Bloodgood et al. 2007) and can also induce the loss of insulin receptors from the neuronal surface. Such insulin receptor impairment is inhibited by extracellular insulin, suggesting that insulin plays an important role in oligomer-induced cell death (De Felice, Vieira et al. 2009) (Zhao, De Felice et al. 2008) (Magdesian, Carvalho et al. 2008). Aβ oligomers bind to the Frizzled (Fz) receptor, an acceptor of Wnt protein, inhibiting Wnt signaling pathway, which promotes progenitor cell proliferation during brain development, inactivating glycogen synthase kinase-3β (GSK-3β) and increased β-catenin. This inhibition causes tau phosphorylation and neurofibrillary tangles, which suggest a Wnt/β-catenin toxicity pathway (Magdesian, Carvalho et al. 2008). These observations show that cell death, caused by Aβ oligomers might occur via multiple pathways.

2, Intracellular Aβ: As mentioned above, there are two main known possibilities for intracellular Aβ formation and accumulation. Prefoldin, a cytosolic molecular chaperon may have a potential role in formation of high-MW toxic oligomers *in vitro* (Sakono, Zako et al.

2008). Aβ oligomer-prefoldin complex can bind to the proteasome, causing proteasome dysfunction and cell death (Tseng, Green et al. 2008). Moreover, molecular chaperons stabilize and mediate the folding of unfolded proteins and several results show that the interaction between prefoldin and Aβ oligomers prevents further aggregation and stabilizes the oligomer structure (Sakono and Zako 2010). In neurodegenerative disorders, (e.g. Parkinson disease (PD), Huntington's disease (HD)), various molecular chaperons, such as cytosolic chaperonin (CCT), are upregulated in patients and co-localize with aggregated proteins in plaques/ inclusion bodies, preventing further aggregation. It is possible, that the supression of the protein aggregation may cause the formation of toxic oligomers. These assumptions suggest that intracellular Aβ may exert its toxic effect through the interactions with various cellular proteins and the toxicity mechanisms of extra-and intracellular Aβ oligomers may be different (Sakono and Zako 2010).

Because of the interactions mentioned above, Aβ causes a mistuning of the cellular protein network at several spots at a time rather than attacking a single protein molecule (Juhasz, Foldi et al. 2011). A little molecular change in the composition of organized protein complexes could alter its functioning rapidly, specifically and even reversibly (Bashor, Horwitz et al. 2010) Aβ probably works in a similar way because it is an unspecific „glue" that sticks to functionally important elements of the molecular machines of nerve cells and imposes its rigidity (Juhasz, Foldi et al. 2011). Changing the functioning protein network of nerve cells, Aβ triggers signalling system responses regulating gene transcription. Aβ also interacts with the mitochondrial metabolic network and almost all functional protein networks of nerve cells and extracellular matrices. The intracellular and extracellular forms of Aβ oligomers influence cell functions at many different spots. It has to be noted as well that diffusible small oligomers can enter the synaptic gap, but large fibrils cannot. This suggests that synaptic action and, in turn, memory impairment (induced by Aβ oligomers), are dependent on the size of the oligomers (Juhasz, Foldi et al. 2011). Therefore, several researchers believe that the multimolecular targets of Aβ and its consequences in the cellular machinery of nerve cells, particularly on the synapse, are the main issues for making progress in the development of the early diagnosis, prevention and better treatment of AD (Shankar and Walsh 2009).

Despite its important role in the disease, the binding partners (on which the oligomeric Aβ exerts its toxicity) have not been investigated at a proteome or subproteome level. Mapping the Aβ interaction partners could help to discover novel pathways in disease pathogenesis. The identification of new binding partners is important, because these interactors might function as physiological ligands and hence could be the molecular targets of novel therapeutic strategies.

Our aim was to identify binding proteins of Aβ, thus we applied a microarray-based analysis for understanding the basic cellular events which mediate complex cellular processes, like interactions between proteins/protein networks and Aβ oligomers.

This method is an effective tool, as it is a rapid and economic way to interpret molecular processes, which may occur in AD (Haab 2001) (Cahill 2001) (Templin, Stoll et al. 2002) (Zhu and Snyder 2001) (Yanagida 2002). These protein microarrays, also known as protein chips, are miniaturized, parallel assay systems that contain small amounts of purified proteins in a high-density format (Chen and Zhu 2006) (Yang, Guo et al. 2011). The first breakthrough came from a report by (Zhu, Bilgin et al. 2001), in which protein microarrays consisting of 5800 unique yeast proteins on a modified microscopic slide were fabricated. The arrays are prepared by immobilizing purified proteins onto a microscope slide in an active state at high densities in such a fashion that the proteins remain in a moisturized environment (Zhu and Snyder 2003). A variety of slide surfaces can be used: aldehyde-and epoxy-derivatized glass surfaces (MacBeath and Schreiber 2000) , nitrocellulose (Kramer, Feilner et al. 2004) (Stillman and Tonkinson 2000), or gel coated slides (Angenendt, Glokler et al. 2002) (Charles, Goldman et al. 2004) for attachment of proteins. After proteins are immobilized on the slides, they can be probed for a variety of functions. The reaction signals are usually measured and recorded by fluorescent or radoisotope labeling.

2 Aims of the study

It is very important to know what kind of Aβ aggregates we use during our biological experiments, therefore we characterized our Aβ solutions versatilely. There are several unanswered questions on the pathological role of Aβ oligomers in the central nervous system, e.g. which aggregation form of the peptide has deleterious effect on neurons, which factors influence the aggregation, wich receptors, membrane proteins or intracellular systems are involved in these processes, etc. There are certain unclearified issues regarding in this subject, since AD is a very complex disease. The main concept of my work is to address the following questions:

1) The physico-chemical characterization of Aβ 1-42 oligomers before use in biological experiments:

The high number of hydrophobic amino acids in the sequence cause low water solubility and rapid aggregation of Aβ-peptides. It is very important to obtain well characterized, relatively stable oligomer solutions for reproducible results during biological experiments. In order to achieve this, synthetic Aβ 1-42 was prepared in our lab from its precursor peptide, called „isopeptide". By using the precursor and elaborating a standardized sample preparation protocol, we are able to prepare well characterized peptide solutions in a reproducible manner, which could be therefore succesfully used in several chemical and biological experiments. For the characterization, we used numerous physico-chemical methods, such as FPLC-SEC, SDS-PAGE, WB, DLS and TEM, to follow the aggregational processes during different incubation times.

2) Studies on the influence of Zn^{2+} and a metal ion chelator molecule, ENDIP on the aggregation and the hydrodynamic diameter of the Aβ aggregates, pretreated with Zn^{2+}.

3) Investigation of Aβ 1-42 oligomer-protein interactions *in vitro* by protein array technology (as a novel postgenomic method), in a high throughput manner:

In this method, different human proteins were affixed in ordered manner at separate locations of a plate thus forming a microscopic array. These arrays contain 8163 human proteins covering a significant portion of the human proteome. Thus the results may show the most important interactions between human proteins with Aβ oligomers.

3 Materials and Methods

3.1 Synthesis of the Aß peptides

Peptide synthesis was carried out in our Alzheimers's research group: Iso Aβ 1-42 precursor peptide was synthesized as it was described previously (Bozso, Penke et al. 2010), on a Boc-Ala-PAM resin. It is a stable form of Aβ 1-42 and can be stored at -20 °C for months. In our experiments we used Aβ 1-42 oligomers freshly prepared from iso Aβ 1-42 with O→N acyl transfer at pH 7.4.

The sequence of the control scrambled Aβ 1-42 peptide was

^{1}LKAFD^{6}IGVEY^{11}NKVGE^{16}GFAIS^{21}HGVAH^{26}LDVSM^{31}FGEIG^{36}RVDVH^{41}QA.

The peptide was synthesized on a Fmoc-Ala-Wang resin using N^{α}-Fmoc protected amino acids with a CEM Liberty microwave peptide synthesizer (Matthews, NC).

3.2 Preparation of iso Aβ peptide-derived amyloid oligomers

For studying the aggregation of Aβ oligomers, iso Aβ 1-42 was dissolved in 1,1,1,3,3,3-hexafluoro-2-propanol (HFIP, Sigma, Saint Louis, MO), and incubated for 24 h at room temperature. HFIP was removed in vacuo, followed by dissolution of the oligomeric peptide in Milli-Q ultrapure water (pH 5.0) to 500 μM and sonicated for 5 min.

For preparation of Aβ 1-42 oligomers, the peptide stock solution was diluted to 50 μM in 20 mM $NaHCO_3$, 150 mM NaCl pH 8.1 (Hydrocarbonate-buffered saline, HCBS) for FPLC-SEC measurements), in 20 mM $NaHCO_3$ pH 8.3 for (SDS-PAGE, WB) and in 25 mM HEPES, 125 mM NaCl, 2 mM KCl, 12 mM D-glucose, 2 mM $MgCl_2$, 2 mM $CaCl_2$, pH 7.4 (for DLS studies of the effect of ENDIP on the Aβ aggregation.)

For binding studies the peptide stock solution was diluted to 50 μM in a BSA-free protein array washing buffer (10 mM NaHCO3 buffer, containing 0.45% NaCl, 1% BSA, 5 mM MgCl2, 0.5 mM DTT, 0.05% Triton X-100, 5% glycerol). The Aβ 1-42 oligomer solution was incubated for 15 min at ambient temperature, and diluted to 10 μM with washing buffer prior to its application on the array. For the consequent DLS experiments, TEM studies, ELISA and *in vitro* translation assay Aβ oligomers were prepared identically, with

only one difference: instead of the washing buffer, the aqueous peptide stock solution was diluted in a solution of 10 mM NaHCO3 and 0.45% NaCl (pH 7.2) to the required peptide concentration.

3.3 Transmission Electron Microscopy

For TEM experiments ten microliter droplets of Aβ 1-42 oligomer or purified ribosome solutions were placed on 400 mesh Formvar-carboncoated copper grids (Electron Microscopy Sciences, Washington, PA), incubated for 2 min, fixed with a 0.5% (v/v) glutaraldehyde solution, washed three times with Milli-Q water, and finally stained with 2% (w/v) uranyl acetate. Specimens were studied with a Philips CM 10 transmission electron microscope (FEI Company, Hillsboro, OR) operating at 100 kV. Images were taken by a Megaview II Soft Imaging System and analyzed by an AnalySis 3.2 software package (Soft Imaging System, Munster, Germany). Ribosomal images were taken at magnifications of x 64 000 and x 92 000, and x 130 000. The statistical analysis of Aβ 1-42 oligomers was performed by analyzing the size distribution of the aggregates on 10 images taken from different areas of the grid.

3.4 Dynamic Light Scattering

This technique uses light to hit small particles thus light scatters in all directions. These molecules undergo Brownian motion, while scattered light undergoes either constructive or destructive interference by the surrounding particles and within this intensity fluctuation, information is contained about the time scale of movement of the scatterers (www.wikipedia.org). Assuming the scattering particles to be hard spheres, their apparent hydrodynamic radius can be calculated from the diffusion parameters by using the Stokes-Einstein equation $Rh = kBT/(6\pi\eta DT)$, where kB is the Boltzmann constant, T is the absolute temperature, η is the viscosity of the medium, and DT is the translational diffusion coefficient. The correlation function and distribution of the apparent hydrodynamic radii (Rh) over the scattered intensity of the samples can be monitored for the expected time interval.

For the chelator-measurements: The Aβ 1-42 peptide solution was filtered through a syringe filter equipped with a 0.1 μm pore size PVDF membrane (Millex, Millipore Ireland,

Carrigtwohill, Ireland) in order to remove the interfering dust particles. Prior to the measurements, 0.1 M metal stock solution of known concentration was diluted with MilliQ water to get a working solution with a concentration of 500 μM. Working solution of the examined chelator was similarly prepared: material was dissolved in MilliQ water to a concentration 2.5 mM (in the case of 1 : 5 molar ratio, Aβ: chelator). All experiments were performed at 25 ^{0}C with a Malvern Zetasizer Nano ZS instrument (Malvern Instruments Ltd., Worcestershire, U.K.). The instrument was equipped with a He-Ne laser (633 nm) applying the Non-Invasive Back Scatter (NIBS) technology, detecting the scattered light at an angle of 173^0. The translational diffusion coefficients were obtained from the measured autocorrelation functions using the regularization algorithm CONTIN built in the software package Dispersion Technology Software 4.0 (Malvern Instruments Ltd., Worcestershire, U.K.). The scattering intensity of the background could be neglected compared to the signal intensity of the peptide sample. The DLS instrument was programmed to execute 12 measurements consecutively with 5min delays in each case. Measurements were conducted either without disturbing the aggregating system (upon the examination of the aggregation of pure Aβ), or aliquots of the working solutions were added between two measurements, routinely after the first and the fourth measurements by pipetting a calculated amount of the stock solution carefully into the cell without removing it from the instrument. Control measurements were conducted without the administration of iso Aβ in each experimental set-up, in order to determine the effect of the working solutions on the scattering intensity. It was found, that the working solutions were able to raise the scattering intensity of the vehicle only to a negligible amount (generally about 1% of the experienced total scattering intensity derived from the measurements with iso Aβ), therefore their effect on the measurement could be neglected.

To model the aggregation under the conditions of the on-array binding studies, change of the hydrodynamic radius was monitored for 3 h at 4 ^{0}C in a 10 μM iso Aβ oligomer solution with the same DLS instrument. The results were obtained from three parallel experiments.

3.5 FPLC-SEC experiments

For the experiment, iso Aβ was dissolved and transformed to Aβ 1-42 as discussed above and aggregated for different time intervals: 0 min, 3 hours, overnight and 3 days at 37 ^{0}C. These samples were loaded onto a Superose 6 10 300 FPLC column and the aggregates were separated at 0.5 ml/min flow in HCBS as elution buffer at 25 °C. Compared with protein calibration standards (Vitamine B_{12} 1,350 kDa, Equine myoglobin 17,000 kDa, Chicken ovalbumin 44,000 kDa, Bovine gamma-globulin 158,000 kDa, Thyroglobulin 670,000 kDa; Bio-Rad)., exact size of the aggregates could be calculated.

3.6 SDS-PAGE, Western blot

For the Aβ Western blot, 50 uM samples were loaded onto 15% SDS-polyacrylamide gel (2,5 ug/ lane). The gel was then transferred to a nitrocellulose membrane using an electroblotting apparatus. After blotting, the nitrocellulose membrane was blocked in TBS, 0.5% Tween-20 (TBST) and 5% non-fat dry milk., and probed with anti-Aβ antibody (Bam-10, 1:2500) (Sigma, St. Louis, MO) or rabbit polyclonal anti-amyloid fibril specific OC antibody (1: 1000) (Millipore, Billerica, USA), diluted in blocking solution overnight at 4 ^{0}C. The following day, the membranes were incubated with an anti-mouse-HRP secondary antibody (1:10000; DakoCytomation, Glostrup, Denmark) and Pierce ECL Western blotting Substrate (PIERCE, Rockford, IL). Blots were exposed to Kodak film (Sigma).

For preparation and Western-blot analysis of purified ribosomes: The ribosome purification from human hippocampus is described in section *3.12*. Protein concentrations of purified ribosomes were determined by the BCA protein assay kit (Novagen, EMD Chemicals, Gibbstown, NJ). To assess the purity of the purified ribosomes, a Western-blot was performed with the ribosomal protein specific anti-RPL36A antibody (Sigma). Equal amounts (10 μg/ lane) of the original homogenized samples and the purified ribosomes were loaded onto a 15% SDS-polyacrylamide gel. The gel was then transferred to a nitrocellulose membrane using an electroblotting apparatus. After blotting, the nitrocellulose membrane was blocked in TBS, 0.5% Tween-20 (TBST) and 5% non-fat dry milk. The membranes were probed with the ribosome specific anti-RPL36A antibody (1:1000) and anti-β-actin antibody (1: 2500) (Sigma, St. Louis, MO), diluted in blocking solution overnight at 4 ^{0}C. The following day, the

membranes were incubated with an anti-mouse-HRP secondary antibody (1:10000; DakoCytomation, Glostrup, Denmark) and Pierce ECL Western blotting Substrate (PIERCE, Rockford, IL). Blots were exposed to Kodak film (Sigma).

3.7 Labeling of the monoclonal antibody with Alexa fluor-647 succinimidyl ester

Alexa Fluor 647 succinimidyl ester (Invitrogen, Carlsbad, CA) was used for labeling monoclonal anti-Aβ antibody, BAM10 (Sigma, Saint Louis, MO). The antibody was placed in a 3000 MWCO Microcon tube (Millipore, Billerica, MA), repeatedly washed, and finally resuspended in a 50 mM $NaHCO_3$ buffer. A 5-fold excess of the fluorescein dye, dissolved in dimethylformamide, was added to the gently stirred solution of the protein in an ice-bath, and then allowed to warm to ambient temperature in 2 h protected from light in the meantime. To neutralize the excess of the succinimidyl ester, 0.1 M of aqueous hydroxylamine solution (pH 8.0) was applied. The labeled antibody was separated from the free dye in the Microcon tube, reconstituted, and stored in the original buffer under the same conditions as that used for the unlabeled antibody.

3.8 Probing the ProtoArray human protein microarray

All reagents were purchased from Sigma (Saint Louis, MO). All the steps were performed at 4 ^{0}C. The ProtoArray Human Protein microarray 4.0 (Invitrogen, Carlsbad, CA) was blocked in a 10 mM $NaHCO_3$ buffer containing 0.45% NaCl, 1% BSA, and 0.1% Tween-20, pH 7.2, for 1 h with gentle shaking. After the blocking step, excess buffer was drained and Aβ 1-42 oligomer, prepared as described before, was diluted in washing buffer (10 mM $NaHCO_3$ buffer, containing 0.45% NaCl, 1% BSA, 5 mM $MgCl_2$, 0.5 mM DTT, 0.05% Triton X-100, 5% glycerol) to a final concentration of 10 μM and was added on the top of the array in a total volume of 120 μL. The protein array was covered with a HybriSlip Coverslip (Grace Bio-Laboratories, Brend, OR) and incubated for 1.5 h without shaking at 4 ^{0}C. After incubation, the array was washed three times with washing buffer, incubated with Alexa-647 labeled anti-Aβ mAb (BAM10, 1:1000) for 30 min at room temperature protected from light, and finally washed again three times with washing buffer. Excess solution was decanted, the

protein array was centrifuged for 4 min at 800g and dried at ambient temperature protected from light. Scanning was carried out using a GenePix Personal 4100A microarray scanner (Molecular Devices, Sunnyvale, CA).

3.9 ProtoArray data processing

The procedure of data processing was carried out by Róbert Rajkó: The signal intensity of each protein spot was calculated by subtracting the median background value from the median spot value. Protein spots were normalized to median so that the median signal intensity of each array became 1. Since every protein had duplicate spots, the average of each duplicate was used as the final signal intensity for a given protein. The corresponding spotted protein concentrations were also averaged. Furthermore, protein signal intensities were normalized to concentration so that the signal intensities normalized to median were divided by the protein concentration values of the spots. In a two-step procedure, we eliminated the low-concentrations spots and identified the proteins with high signal intensity normalized to concentration, which could be the putative Aβ interactors. For the functional analysis of the protein array data, a Gene Ontology-based functional grouping was performed using the DAVID Web-based knowledge database.

3.10 Aurora A kinase activity assay

To study the effect of Aβ oligomers on the activity of Aurora A kinase we used an HTScan® Aurora A Kinase Assay Kit (Cell Signaling, Cat. No.: 7510). The oligomers were prepared as for the protein array experiments.

0 min and 24 h Aβ aggregates or staurosporine (inhibitor of protein kinases through the prevention of ATP binding to the kinase) in different concentrations: (0 min: 0.001, 0.01, 0.1, 1, 10, 100 μM; 24h: 1, 10, 100 μM; staurosporine 1, 10 μM) were incubated with Aurora A kinase and ATP for 5 min, and biotinylated substrate was added for 30 min. After stopping the reaction with 50 mM EDTA, pH 8.0 aliquots were transfered to a 96-well streptavidine-coated plate, and incubated at RT for 60 min. The plate was washed three times with PBS-Tween-20. After incubation with the primary antibody phospho-PLK (Ser137) in

PBS-Tween-20 and 1% BSA 1:1000) for 2h at RT, wells were washed three times with PBS-Tween-20. HRP-labelled secondary antibody in PBS-Tween-20 and 1% BSA was incubated for 30 min with the samples in 1:1000 dilution. After washing, tetra-methylbenzidine (TMB) solution and stop solution (Cell Signaling Technology, Inc., Danvers, MA) was added. Absorbance was read at 450 nm with FLUOstar OPTIMA Multidetection Microplate Reader (BMG LABTECH, Offenburg, Germany).

3.11 Ribosome purification

Purification of the ribosomes was carried out according to Langstrom N. S. (Langstrom, Anderson et al. 1989). All the steps were performed at 4 ^{0}C. The frozen tissue was homogenized in a 5-volume excess of buffer containing 50 mM Tris-HCl pH 7.4, 0.25 mM sucrose, 0.3 M KCl, 5 mM $MgCl_2$, 10 U/ml RNasin. After centrifugation at 8000g for 10 min the supernatant was layered over a sucrose step gradient of 2M to 1M sucrose. The sample was centrifuged at 95000 g for 19h and the pellet was resuspended in storage buffer (0.1 M NaCl, 5 mM $MgCl_2$, 50 mM Tris-HCl pH 7.4, 10 U/ml RNasin. Samples were stored at -80 ^{0}C or used for further experiments (TEM, WB, ELISA, *in vitro* translation).

3.12 Enzyme-Linked Immunosorbent Assay (ELISA): measurement of oligomeric Aβ ribosome binding

0.1 μg of purified ribosome was coated in each well of a 96 well plate for 18-20 h at 4 ^{0}C, using a coating solution (15 mM Na_2CO_3, 35 mM $NaHCO_3$,, 3 mM NaN_3). After the incubation, the wells were blocked using a blocking solution (10 mM $NaHCO_3$, 0.45% NaCl, 0.1% Tween-20, 1% BSA) at room temperature. Aβ 1-42 (prepared as mentioned before) was diluted in a modified washing buffer (10 mM $NaHCO_3$, 0.45% NaCl, 0.05% Tween-20, 1% BSA, 5 mM $MgCl_2$) and was added to the wells in a final concentration of 1, 0.2, 0.1, 0.02, 0.01, 0.002, 0.001, 0.0005, and 0.0001 μM. After 1 h of incubation with gentle shaking at room temperature, the plate was washed three times with a washing buffer (10 mM $NaHCO_3$, 0.45% NaCl, 0.1% Tween-20). A monoclonal Aβ antibody (BAM10, SIGMA) was added to the wells in blocking solution for 1 h at room temperature. After washing twice, the wells

were incubated with HRP-conjugated anti-mouse secondary antibody (DakoCytomation, Denmark, Glostrup) in blocking solution. The plate was washed two times, an TMB reagent (Cell Signaling Technology) was added to the wells. Without using a stopping reagent, the absorbance at 370 nm was constantly monitored using a FLUOstar OPTIMA Multidetection Microplate Reader (BMG LABTECH, Offenburg, Germany). Data values were read at the saturation point of the signal curves.

3.13 *In vitro* translation assay

To permit ribosomal binding, Aβ 1-42 oligomer was preincubated with the Rabbit Reticulocyte Lysate System, Nuclease Treated *in vitro* translation mix (Promega, WI) in a series of concentration (25, 10, 5, 2.5, 1, 0.5 μM) at 37 ^{0}C for 60 min. As a control, scrambled Aβ was used in two concentrations (10 and 25 μM). After the preincubation step, 1 μg of the kit's Luciferase control RNA template was added to the reactions, and incubated for 90 min at 30 ^{0}C. The luminescence produced by the translated luciferase was measured in 1:10 dilution of the reaction mixtures according to the Promega Luciferase Assay protocol on a LumiStar Optima luminometer (BMG Labtech, Offenburg, Germany). Expressed luciferase control protein was also investigated by Western-blot. Promega Transcend Biotin-Lysyl-tRNA was added to the *in vitro* translation reaction, in order to detect the de novo synthesized biotinylated luciferase, using streptavidin-HRP and chemiluminescent detection. From the translation reaction mixtures, 2 μL aliquots were removed and loaded onto a 10% SDS-polyacrylamide gel. The gel was transferred to a nitrocellulose membrane using an electroblotting apparatus (Bio-Rad Laboratories, CA). The membrane was blocked in TBS 0.5% Tween-20. For the chemiluminescent detection of the biotinylated proteins, the membrane was incubated in a Streptavidin-HRP solution diluted in TBST for one hour at room temperature and Pierce ECL Western blotting Substrate (PIERCE, Rockford, IL). Blots were exposed to Kodak film (Sigma, Saint Louis, MO).

4 Results

4.1 Physico-chemical characterization of Aβ 1-42 oligomers, study of the aggregation processes

In order to generate Aβ oligomers for the experiments, a new protocol was developed. Synthetic peptide was treated with HFIP overnight to dissolve the evolving aggregates during the synthesis and after evaporation of the HFIP, the peptide was dissolved in MilliQ water followed by the adjustment of the pH to 7.4, because O→N acyl-transfer reaction occurs when the pH is raised to the physiological value. Finally it was incubated for different time intervals according to the demands of the experiments.

4.1.1 FPLC-SEC measurements

We characterized the size distribution of our Aβ 1-42 aggregates under non-denaturing conditions by size exclusion chromatography. Aβ aggregates, incubated for different time intervals, fractionated on a Superose 6 10 300 column. The elution profile detected by UV absorbance at 280 nm is shown in Fig. 5. The estimated molecular masses of the aggregates were calculated by using a calibration curve, based on the retention times (RT) of molecular weight (MW) standards fractionated with the same conditions (Vitamine B_{12} 1,350 kDa, Equine myoglobin 17,000 kDa, Chicken ovalbumin 44,000 kDa, Bovine gamma-globulin 158,000 kDa, Thyroglobulin 670,000 kDa). It can be seen, that in the freshly dissolved sample (0 min) there is an intensive peak (II. peak) at the smaller molecular masses between~2300 and ~12000 Da. This means, that the great majority of the aggregates consist of approximately monomers, dimers and trimers. In case of the sample incubated for 3 hours, there is a significant difference, namely this time seemed to be enough for the developement of larger aggregates. There is a broad distribution of aggregates between ~ 83000 and ~ 480000 Da (I. peak). Compared to the third sample, which was incubated overnight, the amount of low-n aggregates decreased for the benefit of the high n-aggregates. In case of the sample incubated for 3 days we used NaN_3 to prevent infections (a visible peak at ~45-50 min.). The tendency is the same as in case of the overnight sample, but the intensities are lower, because in this case we applied the half of the protein amount of the other three samples.

A

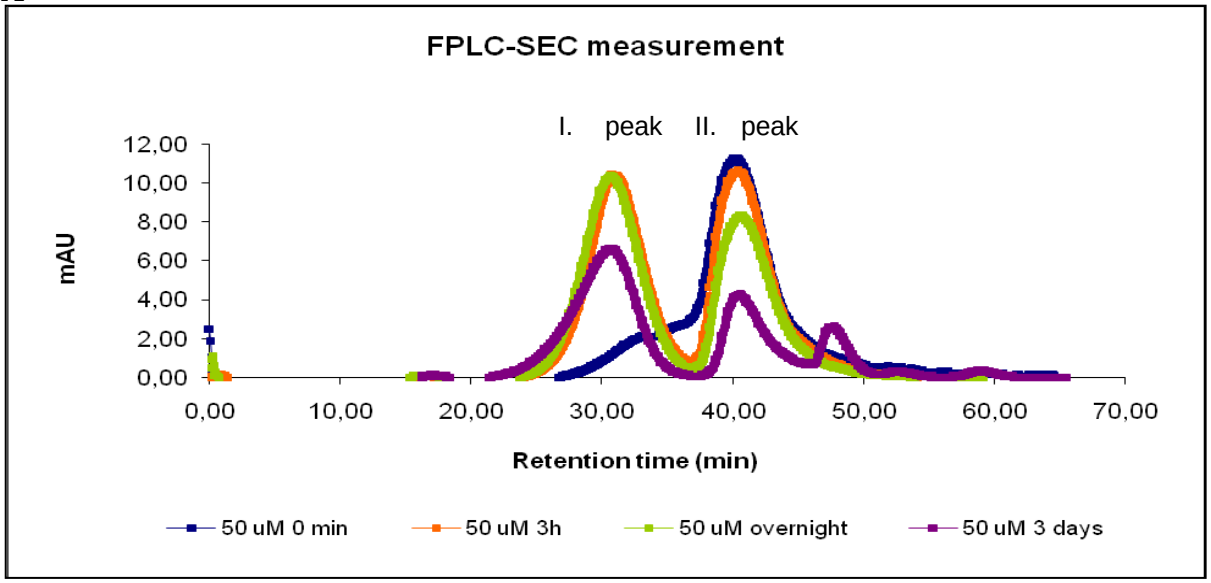

B

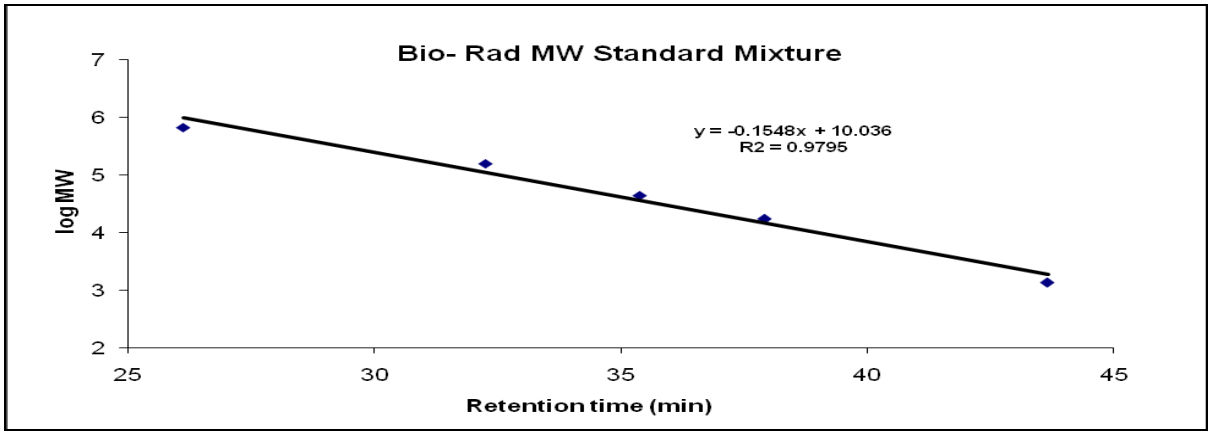

C

	I. peak			II. peak		
	FWHM	MAX	FWHM	FWHM	MAX	FWHM
RT (min)	28.26	30.63	33.2	38.6	40.6	43.2
MW (Da)	476387.1	205579.6	82641.8	12178.6	5992.4	2383.4

Fig 5.: A: Size distribution of Aβ samples, incubated for different time intervals by FPLC-SEC at 280 nm. In case of the sample incubated for 3 days we used NaN_3 to prevent infections (a visible peak at ~45-50 retention min.). **B**: Bio-Rad molecular weight standard mixture separated by FPLC-SEC: Vitamin B_{12} 1,350 kDa, Equine myoglobin 17,000 kDa, Chicken ovalbumin 44,000 kDa, Bovine gamma-globulin 158,000 kDa, Thyroglobulin 670,000 kDa. **C:** Compared with protein calibration standards size distribution of the aggregates could be calculated.

4.1.2 Western blot experiments

For Western blot (Fig. 6.), we loaded the same Aβ samples as for the FPLC-SEC measurements. We used two types of antibodies, a sequence specific monoclonal antibody: Bam-10, and a conformation (fibril) specific polyclonal antibody: OC. OC recognizes a generic epitope that is associated with the fibrillar amyloid conformation regardless of the sequence (Kayed, Head et al. 2007). On the membrane incubated with Bam-10, the freshly dissolved samples are mostly low-n oligomers. It can be seen that, with progress of time, high-n aggregates appear and possess a strong signal compared to that of the low-n oligomers. On the second membrane, incubated with OC antibody, a broad range of aggregates are present, but they are not distinct as much as on the first membrane. In case of the 0 min sample, low-n oligomers (dimers, trimers, tetramers) show enhanced reactivity compared to the high-n ones in contrast with the membrane incubated with Bam-10 antibody.

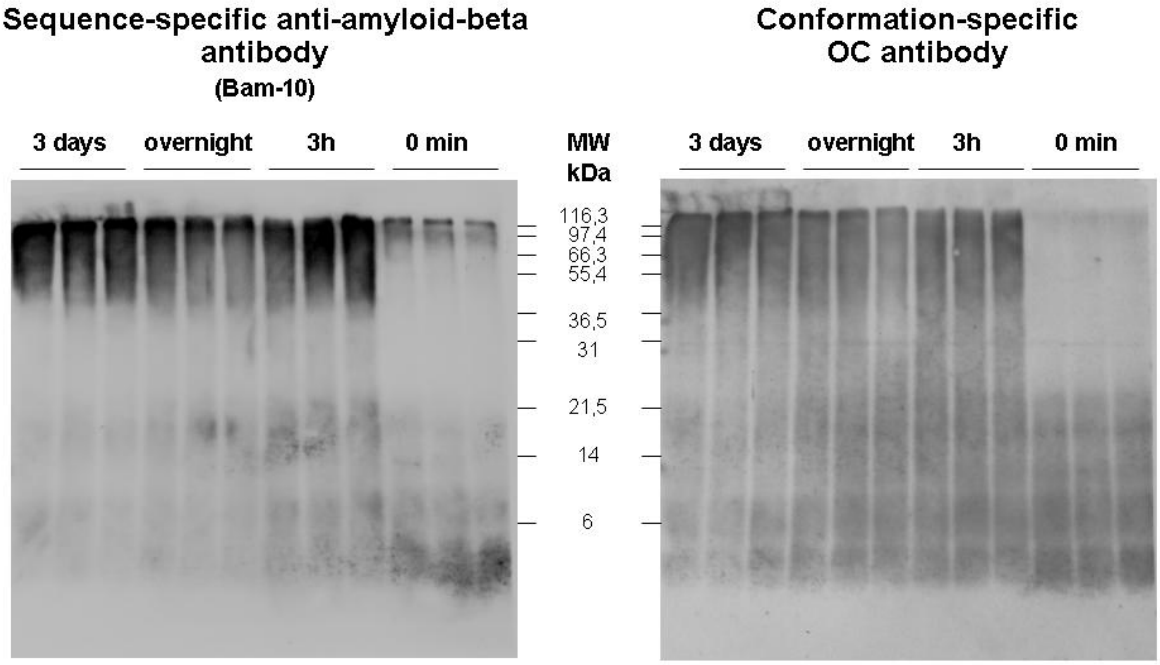

Fig 6.: Western blot analysis of Aβ aggregates. The same samples as in the FPLC-SEC measurements were loaded onto 15% SDS gels and blotted onto nitrocellulose membranes. Membranes were probed with a sequence-(Bam-10) and a conformation-specific antibody (OC).

4.2 Analysis of the effect of ENDIP on the aggregation and the size of the aggregates of Aβ after adding Zn^{2+}

In order to determine the changes in the size of the aggregates, we used DLS measurement, a well established technique for measuring the size of small particles in solution, typically in the submicron region. The population of the Aβ 1-42 -derived oligomers is proven to be outstandingly stable without the disturbance of extrinsic effects, such as administration of chelating ions, change of ionic strength of the medium, or application of preformed fibrils as seeds. The change in the Aβ size (*d*H) over time was monitored applying DLS measurements in 50 μM iso-Aβ 1–42 oligomer solutions with and without addition of metal ion, Zn^{2+} and chelator, ENDIP (Fig. 7.). In the sample containing only Aβ 1–42, d_H of the peptide did not change during the time of the experiment (~ 2 h), When metal ion was added to the peptide solution (after the first measurement) a significant increase in d_H could be observed, proving that Zn^{2+} could promote Aβ precipitation. ENDIP applied in five fold excess after the fourth measurement, lowered d_H back to its initial value, showing that ENDIP was able to displace Zn^{2+}.

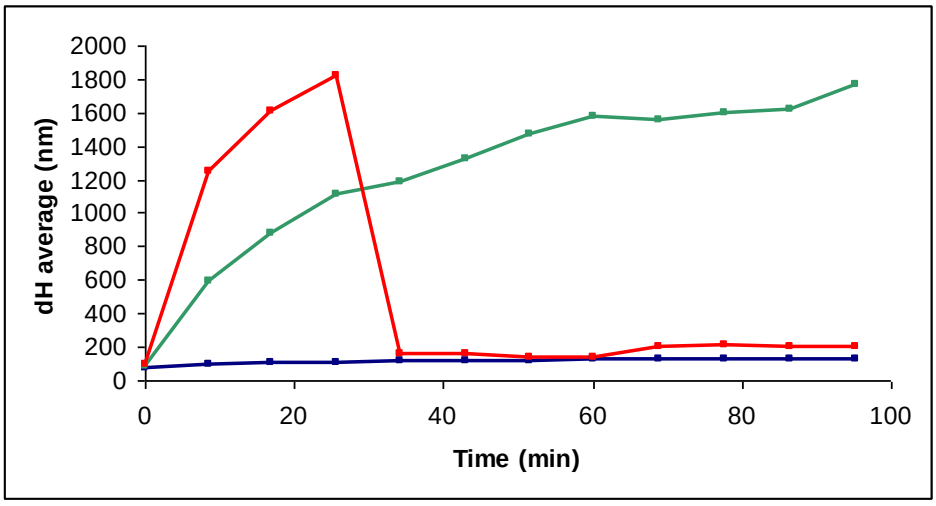

Fig. 7.: Time-dependent analysis of the hydrodynamic diameter of Aβ in different conditions: Blue points: 50 μM Aβ 1-42; Green points: 50 μM Aβ 1-42 +1 equivalent Zn^{2+} after the first measurement; Red points: 50 μM Aβ 1-42 +1 equivalent Zn^{2+} after the first measurement and addition of 5 equivalent of ENDIP after the fourth measurement.

4.3 Mapping of the binding partners of Aβ 1-42 oligomers

4.3.1 Protein array experiments

4.3.1.1 Oligomerization of Aβ 1-42

By using a standardized protocol, an exceptionally stable oligomeric population can be obtained. The stability of the Aβ 1-42 oligomers was examined by dynamic light scattering. DLS provides quantitative information about the size distribution of an oligomer population. In parallel, the actual shape of the oligomers has to be characterized by microscopic techniques working in the submicrometer range. Therefore, we conducted TEM investigations as well. The results of the DLS measurements are summarized in Fig. 8A. The stability of Aβ 1-42 oligomers was monitored at 4 ^{0}C for the time interval typically applied in the microarray experiments. Experimental results revealed that the oligomers possessed an average hydrodynamical diameter of 55.1 ± 3.9 nm and were proven to retain their size distribution during the time examined. At the end of the incubation period, oligomers were visualized by TEM (Fig. 8B). The shape of the oligomers could be considered to be spherical, as no sign of anisotropic forms could be observed on the TEM images. The statistical analysis of the TEM images revealed an average diameter of 7 ± 3 nm for the aggregates. The discrepancy between the average sizes measured with DLS and TEM can be explained by two phenomena: (i) DLS measures the hydrodynamical sizes; therefore, if the protein chains are fully hydrated, exert an expanded structure and are measured together with their hydrate shell; on the contrary on TEM grids, the particles are measured in their dehydrated state, and (ii) statistically underrepresented, atypical large aggregates, which are not observed by TEM, can distort the size distribution in DLS, as it is determined from the intensity of the scattered light, resulting in an apparently increased average diameter. Size data derived from DLS measurements were used, therefore, only to demonstrate the stability of the oligomers during the experiment.

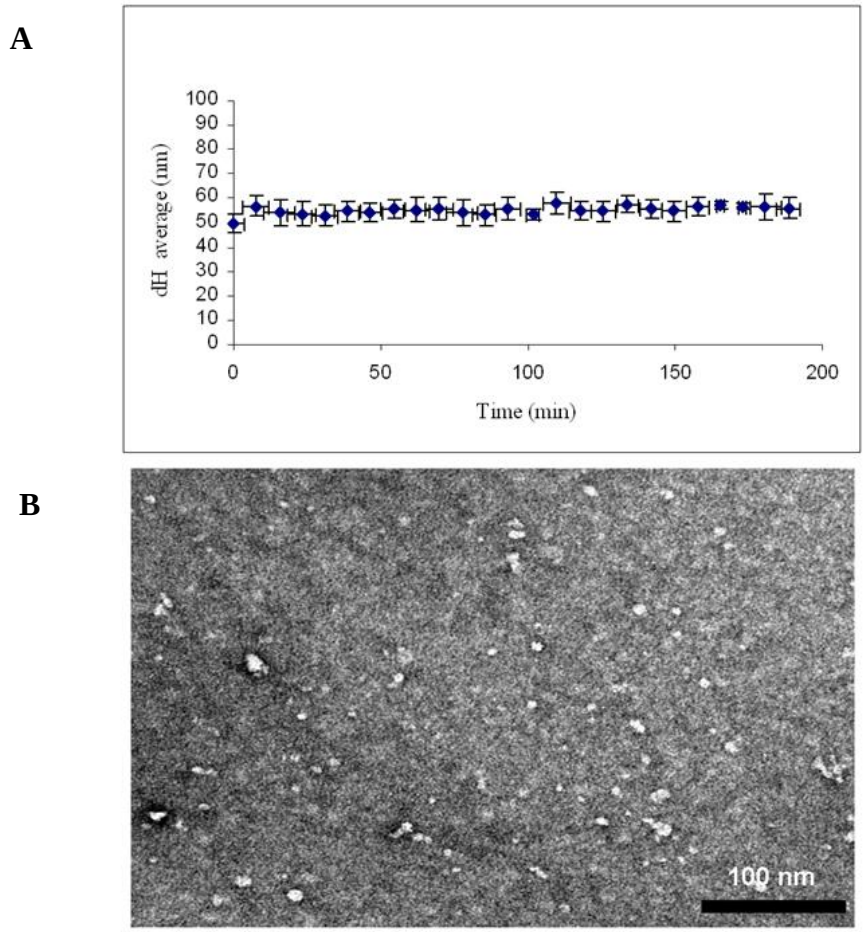

Fig. 8.: Aggregation of oligomeric Aβ 1-42. **A.** DLS measurements of Aβ 1-42 oligomers. Measurements were performed in a $NaHCO_3$-solution at pH = 7.2 at 4 ^{0}C. Aggregation was monitored for 3h. **B.** TEM image of the Aβ 1-42 oligomers prepared by following the protocol applied in the on-array binding studies. The TEM bar is 100 nm.

4.3.1.2 Protein array based oligomeric Aβ 1-42 interactome screen

We applied two parallel Protoarray 4.0 protein arrays for the Aβ 1-42 interactome analysis. These arrays contain duplicate spots for 8163 unique recombinantly expressed human proteins and also control spots. The recombinant expression is performed in an insect cell line; hence, the eukaryotic post-translational modifications are likely present. Since the Aβ binding was visualized with a monoclonal Aβ-antibody, first we measured the aspecific binding of the antibody onto the array proteins. Applying the antibody alone, the hybridization resulted only a dim background fluorescence (Fig. 9A).

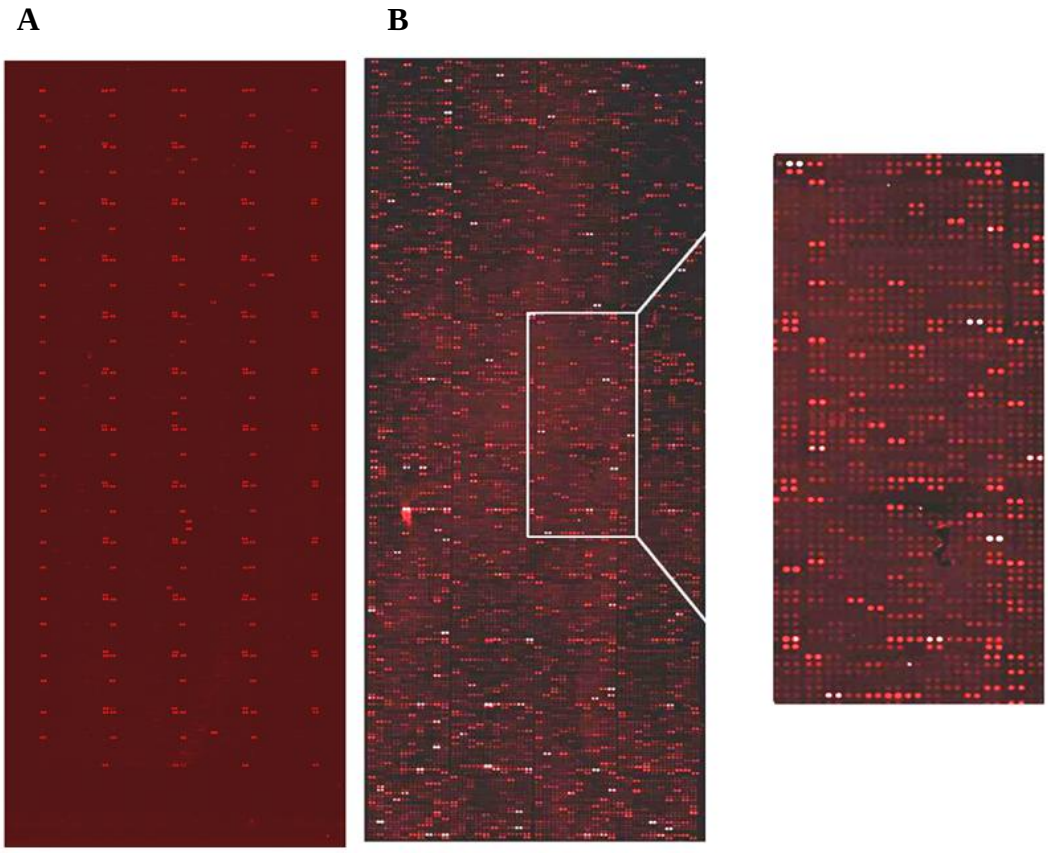

Fig. 9.: Protein array hybridization. Represenative image of the protein array **A:** after we applied the fluorescent antibody alone and **B:** after Aβ hybridization.

Analysis of the raw images and signal intensities revealed that Aβ 1-42 could bind to numerous proteins on the array (Fig. 9B), such as proteins that take part in regulation of transcription, translation, gene expression, metabolic processes, in nucleosome organisation, in processes of mitosis, etc. To identify the most likely Aβ interactors, a multistep analysis was performed. To identify spots with high normalized signal intensities, Róbert Rajkó applied a two-step LTS-based (least trimmed squares) robust fitting statistical filtering. First, LTS analysis calculated a cutoff value of 2021 arbitrary units for the averaged spot concentration for the two arrays. Only spots with a higher concentration were used further. Second, the signal values were normalized with the spot concentration. LTS analysis calculated 560.3 and 647.5 arbitrary units concentration normalized signal intensity cutoff values for the applied two protein arrays. Only proteins that had higher concentration normalized signal intensities than the cutoff values of both arrays were included in the final

analysis. Altogether, 324 proteins had higher normalized signal intensities than the cutoff values on both arrays. In a consequent study (described in the following section) one of these potential interactors of Aβ 1-42, was chosen for further analysis.

We used another analysis method after the concentration normalization of the signal intensities, by ordering the potential binding partners in functional groups. To gain functional information about the Aβ interactors, we performed a Gene Ontology (GO) analysis, using the DAVID Web-based knowledgebase (Fig. 10). (GO co-ordinates denominations of genes and their products, developing an agreed standard terminology, and provide a solution for scientists searching for all information in their research area.) DAVID analyzes the GO terms-words, identifiers and definitions of genes or gene products-relating to the significantly altered genes/proteins, identifies the terms that contain multiple proteins, and calculates a significance value for the observed enrichment compared to a background protein set—in our case all the proteins on the array.

The DAVID analysis revealed that the most highly impacted GO Biological Function category was the protein translation. The “translation” functional category contained 24 proteins, including several mitochondrial and nonmitochondrial ribosome components along with other proteins required for translation, such as translation initiation factors (Fig. 10).

GO term	protein count	P value	Benjamini
translational elongation	13	4,57E-07	2,76E-04
translation	24	7,12E-07	2,15E-04
RNA metabolic process	39	1,22E-05	2,45E-03
RNA processing	26	2,25E-04	3,35E-02
regulation of transcription	55	4,12E-04	4,85E-02
regulation of nucleobase, nucleoside, nucleotide and nucleic a	59	4,32E-04	4,25E-02
regulation of gene expression	61	4,96E-04	4,19E-02
regulation of macromolecule biosynthetic process	58	1,34E-03	9,66E-02
mitosis	12	2,68E-03	1,65E-01
M phase of mitotic cell cycle	12	3,20E-03	1,76E-01
nucleosome organization	7	3,21E-03	1,62E-01
regulation of cellular biosynthetic process	58	3,48E-03	1,61E-01
regulation of RNA metabolic process	37	4,50E-03	1,89E-01
M phase	14	4,93E-03	1,92E-01
somatic diversification of immune receptors	4	6,91E-03	2,44E-01
mRNA metabolic process	16	7,43E-03	2,45E-01
nucleosome assembly	6	8,77E-03	2,69E-01
chromatin assembly or disassembly	7	9,96E-03	2,85E-01
regulation of transcription, DNA-dependent	34	1,29E-02	3,38E-01
protein-DNA complex assembly	6	1,35E-02	3,37E-01
ncRNA processing	9	4,70E-02	7,50E-01
somatic diversification of immunoglobulins	3	5,08E-02	7,61E-01
mRNA processing	12	6,25E-02	8,16E-01
immunoglobulin production	3	6,34E-02	8,07E-01
axon cargo transport	3	6,34E-02	8,07E-01
spindle organization	4	6,43E-02	7,99E-01
DNA metabolic process	16	7,04E-02	8,17E-01
transcription initiation	5	7,90E-02	8,41E-01
ncRNA metabolic process	9	9,54E-02	8,85E-01
RNA catabolic process	4	9,98E-02	8,88E-01

ID	protein name	CHIP A	CHIP B
BC034488	ATP-binding cassette, sub-family F (GCN20), member 1	600,09	1029,27
BC036109	SECIS binding protein 2	2813,28	9535,04
BC007847	eukaryotic translation elongation factor 1 delta	633,78	1274,81
BC007888	eukaryotic translation initiation factor 2, subunit 2 beta, 38kDa	745,63	1777,20
NM_139242	mitochondrial methionyl-tRNA formyltransferase	819,35	1342,51
NM_024540	mitochondrial ribosomal protein L24	803,78	1274,03
NM_007208	mitochondrial ribosomal protein L3	1148,20	1455,62
NM_023937	mitochondrial ribosomal protein L34	1193,89	2393,34
BC020651	mitochondrial ribosomal protein L35	593,32	1644,57
NM_004927	mitochondrial ribosomal protein L49	903,54	2476,34
NM_018135	mitochondrial ribosomal protein S18A	1921,66	2847,10
BC019069	ribosomal L1 domain containing 1	964,00	1216,25
NM_000975	ribosomal protein L11	1175,84	2011,34
NM_005061	ribosomal protein L3-like	1362,03	1458,56
NM_000989	ribosomal protein L30	612,85	839,55
NM_000993	ribosomal protein L31	2099,69	2492,06
NM_015414	ribosomal protein L36	603,51	695,31
NM_021104	ribosomal protein L41	835,05	662,95
NM_001014	ribosomal protein S10	751,96	1037,52
NM_001015	ribosomal protein S11	720,69	1446,54
NM_001020	ribosomal protein S16	2054,42	3402,04
NM_022551	ribosomal protein S18	562,21	717,14
NM_001022	ribosomal protein S19	971,33	1304,54
NM_001029	ribosomal protein S26	692,52	865,72
	MEDIAN	108,81	98,45

Fig. 10.: GO functional analysis of human proteins interacting with Aβ. The Aβ 1-42 binder proteins were analysed for enriched GO functional groups by using the DAVID Web-based knowledge database. The significantly enriched ($P < 0.01$) functional groups are shown with the number of proteins in each group. The second table represents the members of the GO Biological Function category „translation”. The concentration normalized signal intesities from both protein array experiments are shown. On the last row the median concentration normalized signal intesities on the protein arrays are highlighted .

4.3.1.3 Results of the first analysis

By using the first analysis method, among others we identified several binding partners, such as Aurora A kinase (AURKA), fibroblast growth factor (FGF), γ-tubulin, beta-secretase 1 (BACE1), mitogen-activated protein kinase 7 (MAPK7) and TAO kinase 3 (TAOK3) with relatively high binding intensities (Fig 11.). All these proteins can be related to AD:

FGFs has neuroprotective role (Alzheimer and Werner 2002), the level of some of these factors are diminished in the brains of Alzheimer's patients (Brinton and Wang 2006).

Changes in the phosphorylation state of various MAPKs by Aβ lead to synaptic dysfunction and cognitive decline, as well as development of inflammatory responses in AD (Origlia, Arancio et al. 2009).

TAOK3 has inhibitory effect on JNK signaling patway. JNK pathway is considered to be a key regulator of various inflammatory pathways which are activated during normal aging and Alzheimer's disease (Mehan, Meena et al. 2011).

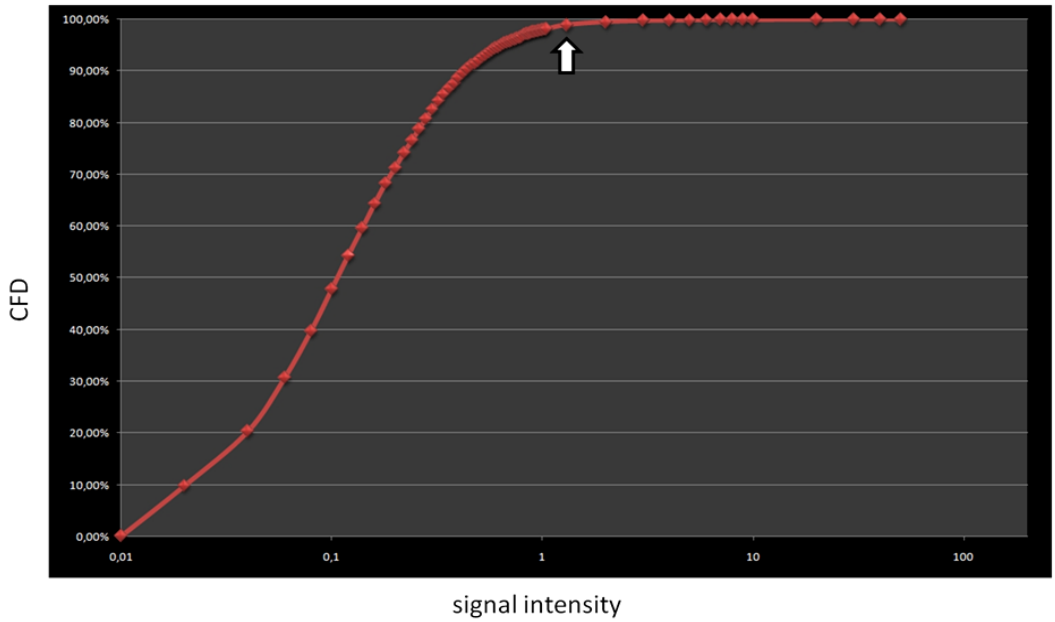

Fig. 11.: Cumulative Frequency Distribution (CFD) of the Aβ 1-42 binding signal intesities detected on the protein array. The arrow shows that the AURKA protein with 1.3 signal intensity had higher signal intensity than 98.92% of the proteins on the array. Some proteins with higher signal intensities than AURKA: TAOK3: 1.32; MAPK7:1.54; BACE1: 2.84; γ-tubulin:3.16; FGF12: 6.16.

γ-Tubulin is a member of the tubulin superfamily required for microtubule nucleation.It is well known, that microtubular network is impaired during the development of the disease. Our protein array data suggested as well, that Aβ 1-42 could bind to TPPP/p25 and other members of the microtubular network. Utilizing these results, the group of Judit Ovádi performed several experiments to confirm the conception, that Tubulin Polymerization

Promoting Protein (TPPP/p25) as a new factor could be involved in multiple pathological interactions leading to protein aggregations characteristic for a subtype of neurological disorders. TPPP/p25 was identified as a disordered protein, and it has a significant role in the rearrangement of the microtubular network during the differentiation of oligodendrocytes in human brain. In their work multiple interactions between Aβ 1-42 oligomers and TPPP/p25 were characterized at molecular and cellular levels. By these results the output of the initial high-throughput interactome screening could be validated.

We assumed that AURKA can be a target of our further experiments for several reasons: i) it is a serine/ threonine-protein kinase, its function is related to phosphorylation, ii) it has a central role in mitotic processes, it regulates mitotic spindles and involved in key cell cycle events such as centrosome duplication, and iii) it is also related to Alzheimer's disease, because it has regulatory role in tau phosphorylation through the activation of Gsk-3β protein. Therefore we decided that we try to confirm this binding by other *in vitro* techniques. To further support the result of the array, we utilized HTScan® Aurora A Kinase Assay Kit. In this assay we aimed to study if Aβ, in different incubation time (0 min, 24h) and in different concentrations, is able to inhibit the function of AURKA. The primary antibody, used in the assay, detects the phosphorylated (Ser137) form of the substrate of AURKA. This phosphorylation may be inhibited by our Aβ 1-42 preparations. As positive control, we used staurosporine, a phosphatase inhibitor in 1 and 10 μM concentration.

The results show that, our Aβ 1-42 preparations were unable to inhibit the phosphorylation of the substrate of the enzyme (Fig. 12.), compared to staurosporine, but there is some difference between their effect. The freshly dissolved Aβ 1-42 (1 nM-1 mM) did not influence the activity of Auora at all, whereas 24h Aβ (1-10-100 μM) had a slight inhibitory effect. The reason of the difference might be that in the fresh preparation there are more low-n oligomers, that may be not as much effective in this assay because of their size or improper conformation.

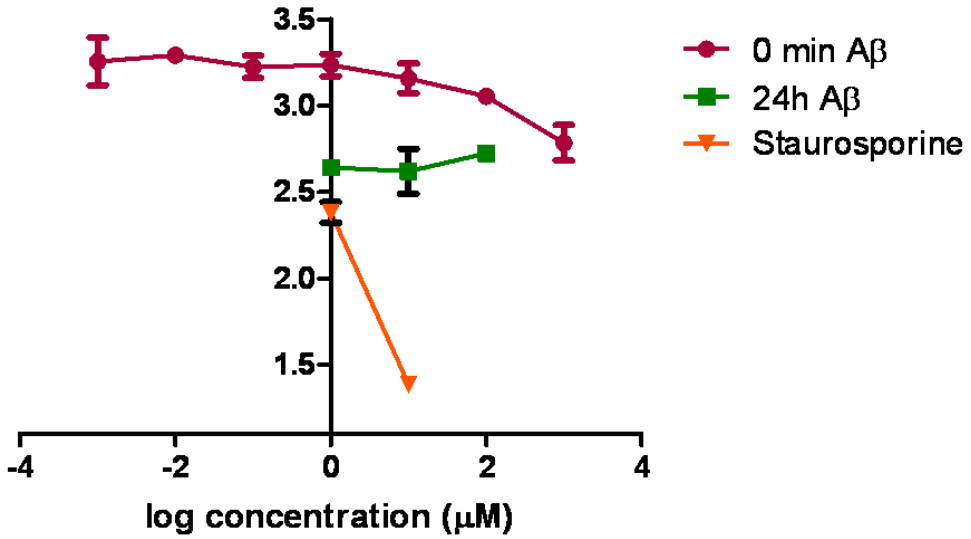

Fig. 12.: Aurora A kinase aktivity assay. Red data points show the effect of 0 min Aβ 1-42 in different concentrations. Green data points show the effect of 25h Aβ 1-42 in three different concentrations. Two orange data points indicate Staurosporin, a phosphatase inhibitor. It is shown that neither 0 min, nor 24h Aβ was able to inhibit the activity of the enzyme.

4.3.1.4 Oligomeric Aβ 1-42 binding to purified ribosomal complexes

To support the protein array binding data, we performed an ELISA binding assay on purified rat hippocampal ribosomes. The ribosome purification/enrichment was performed using a sucrose gradient centrifugation. The degree of enrichment was verified using a ribosomal protein (RPL36A) specific and actin specific Western blot (Fig. 13A). The Western blots clearly showed that RPL36A was highly enriched in the purified fraction compared to the initial homogenate. On the other hand, the actin signal was only detected in the initial homogenate, but not in the purified fraction, indicating that the purification was specific for ribosomes and ribosomal proteins. The presence of purified intact ribosomes in the purified fraction was also visualized by TEM (Fig. 13B). Purified ribosomes and unpurified hippocampus homogenates as controls were adsorbed onto an ELISA plate, and Aβ 1-42 oligomer (1 μM to 0.0001 μM) was added to the immobilized ribosomes and homogenates. As shown in Figure 13C, Aβ bound to immobilized ribosomes in a dose-dependent manner.

Moreover, there was a significantly higher binding to the purified ribosomes compared to the hippocampus homogenates when we applied Aβ between 0.01 and 1μM. Aβ binding to the hippocampus homogenates supported the protein array data showing that Aβ probably had multiple targets in the homogenate (Fig. 13C). On the other hand, binding of Aβ to purified ribosomes was stronger, indicating that the binding strength to ribosomal proteins was significantly higher than the binding to the "background" protein population in the hippocampus homogenate.

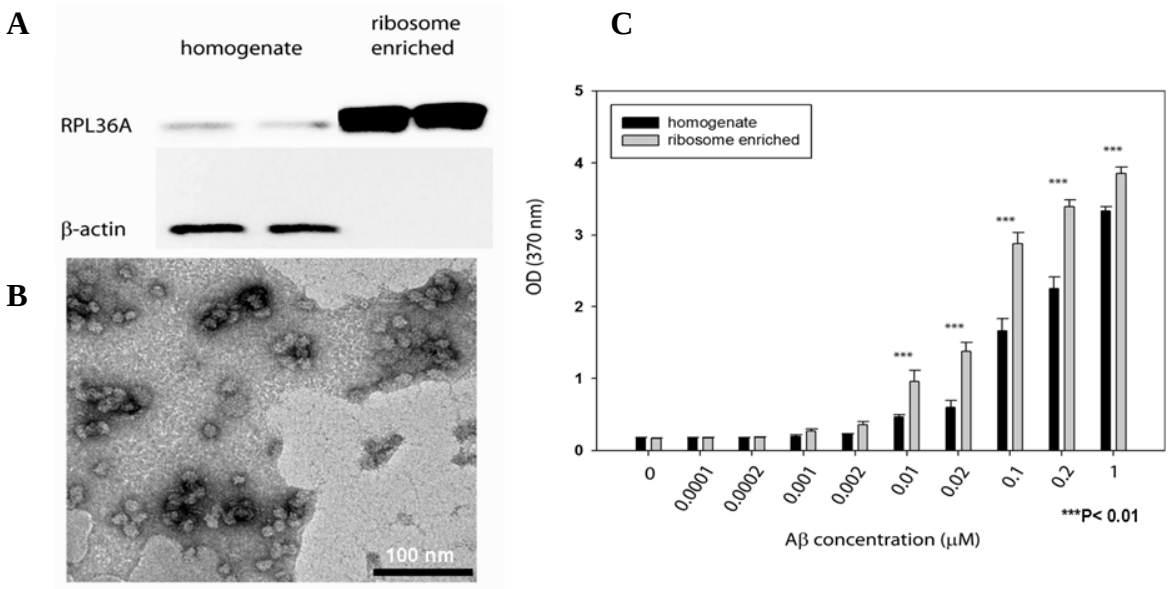

Fig. 13.: Binding of oligomeric Aβ 1-42 to purified hippocampal ribosomes. **A**: Western blot validation of ribosome purification. Ten micrograms of protein from two rat hippocampus homogenates and two purified ribosomal fractions were loaded. The ribosomal enrichment was verified using the ribosomal protein specific anti-RPL36A antibody. As control, the β-actin levels were also measured int he samples. **B**: TEM visualization of the purified ribosomes. The image shows round-shaped organelles with an average diameter of 15-20 nm, resembling intact riosomes. TEM bar is 100 nm. **C:** Concentration dependent Aβ 1-42 binding to purified ribosomal complexes and control homogenates. (n = 6; values are mean ± SEM, P-values were calculated using the Student's t-test).

4.3.1.5 Aβ 1-42-mediated inhibition of *in vitro* protein translation

To test the effect of Aβ 1-42 on the efficiency of translation, an *in vitro* translation involved a nuclease treatment in order to eliminate the endogenous RNA background. Hence we could detect the translation of luciferase control RNA template only. The same Aβ binding parameters that were used in the protein array study (90min, 4 ^{0}C) were applied, except the temperature was raised to the physiological 37 ^{0}C. As a negative control, scrambled Aβ 1-42 was used, because its sequence is not the same as the native Aβ 1-42, but contains the same amino acids. The 90 min Aβ preincubation step enabled the Aβ-ribosomal binding. After the preincubation step, a luciferase template was added to the reaction and a standard translation reaction was performed. The *in vitro* translation results clearly showed a concentration dependent inhibitory effect on the luminescent activity of the luciferase enzyme (Fig. 14A) which validates the former protein binding data.The inhibitory effect was significant, even at 1 μM Aβ 1-42 concentration. The inhibitory effect was correlated with the applied Aβ 1-42 concentration reaching a close to 50% reduction in luminescence at 25 μM. To exclude the possibility that the reduction of the luminescent signal intensity was due to the Aβ-mediated inhibition of luciferase enzyme function and not to the decreased luciferase translation, a Western-blot experiment was performed. The Western-blot data clearly showed that the observed reduction of luciferase function was the result of the reduction of luciferase protein expression (Fig. 14C). Notably, there was a significant difference between the inhibitory activity of the native and scrambled Aβ 1-42. The native form showed a ~25% inhibitory activity at a 10 μM concentration, while the scrambled form showed a ~10% inhibition. The difference between the native and scrambled forms was even higher at the 25 μM concentration. Twenty-five micromolar native β-amyloid 1-42 caused a ~50% translation inhibition, while the scrambled form showed a ~25% translation inhibition. The translation inhibitory activity was about equal of the 10 μM native Aβ 1-42 and the 25 μM scambled Aβ (Fig. 14B).

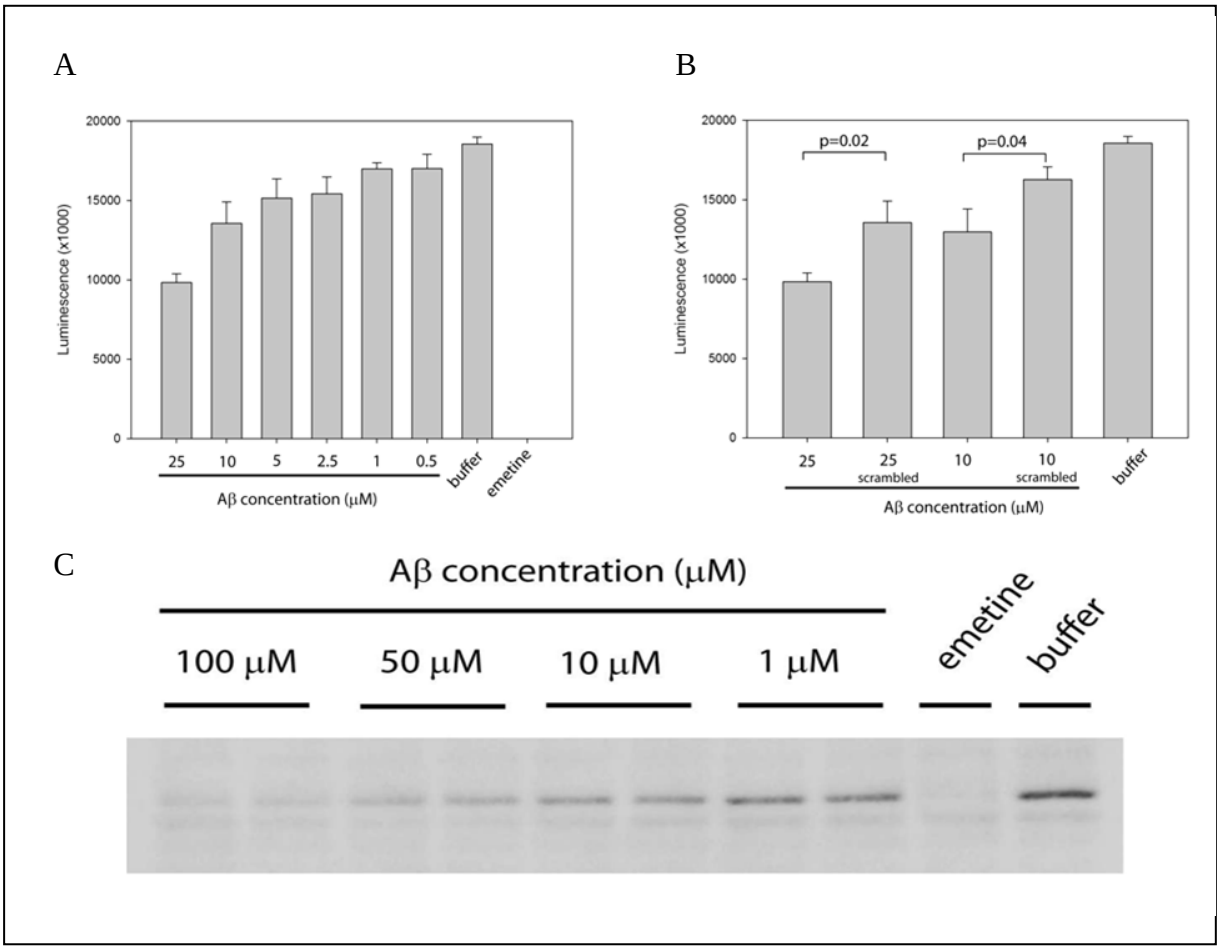

Fig. 14.: *In vitro* analysis of Aβ 1-42 mediated translation inhibition. **A:** The effect of Aβ 1-42 on *in vitro* luciferase expression. Aβ was applied in different concentrations in an *in vitro* translation system. The luminescent activity of the translated luciferase was measured with a standard luminometer. The luminescence values were significantly different ($P < 0.05$) from the conrtol „buffer only" values in all applied Aβ concentration except the 0.5 μM case ($n = 3$, values are mean ± SEM, P-values were calculated using the Student's t-test). **B:** Comparison of the translation inhibition effect of native and scrambled Aβ 1-42 ($n = 3$, values are mean ± SEM, P-values were calculated using the Student t-test). **C:** Western blot analysis of luciferase expression. The applied concentration ranged from 1 to 100 μM. The known translational inhibitor emetine was used as a positive control in both the luminescent measurements and the Western blot experiments. The inhibitory activity of Aβ 1-42 was compared to the buffer controls containing no β-amyloid peptide.

5 Discussion

5.1 Physico-chemical characterization of beta-amyloid 1-42 oligomers and aggregation studies

Aβ aggregation is a complicated process and appears to involve more than a simple conversion of soluble monomers to a fiber. More recent evidence has pointed to the role of soluble amyloid oligomers or prefibrillar aggregation intermediates as the primary toxic species in degenerative amyloid diseases (Hardy and Selkoe 2002) (Glabe 2005) (Necula, Kayed et al. 2007). TEM analysis identified 5-10 nm spherical particles, that appear at early times of incubation and disappear or their amount decreases as time goes by as shown in our WB and FPLC-SEC measurements. These oligomers appear to be precursors of high-n aggregates and fibrils, because they are transiently observed at the beginning of the incubation during fibril formation (Necula, Kayed et al. 2007).

For our experiments we used isopeptide (iso Aβ 1-42) as a precursor, in which the incorporated ester bond decreases the propensity of the peptide to aggregate, thus it has an enhanced water solubility. When the pH is raised to the physiological value, a fast O→N acyl-transfer reaction occurs resulting in Aβ 1–42 with more controllable aggregation. With the aid of this Aβ 1-42 peptide we can study the aggregation process from the early phase. It is very important to have well characterized Aβ 1-42 solutions in the course of the experiments. To achieve this, we used several methods, such as FPLC-SEC, WB and DLS measurements. DLS is a well established technique for measuring the size of small particles in solution, typically in the submicron region. Care must be taken with the interpretation of DLS results, since the increase of the diameters detected by DLS are always distorted by the large particles, as the observed scattering intensity is proportional to the sixth power of the hydrodynamical radius of the scattering particle (the bigger is the scattering particle, the larger is its contribution to the scattering intensity). Thus, the increase of the average size in a given time interval is possibly smaller, than that measured by DLS.

To monitor the changes in the aggregation process of Aβ 1-42, we standardized our experiments according to the incubation time and the buffers. FPLC-SEC and WB studies (using sequence specific monoclonal antibody) show that Aβ 1-42 solutions in our experiments contained a wide range of species, from low-molecular-weight to

high-molecular-weight assemblies, the size of which increases with time (0 min, 3h, overnight, 3 days). In case of FPLC-SEC measurements we added NaN3 to the 3 days incubated sample in order to avoid bacterial infections. WB analysis with OC antibody confirms that our preparations contained oligomers from low-n to high-n aggregates. The oligomers which were present shortly after sample preparation were mainly low-n ones. Already after overnight incubation high-n oligomers could also be observed, therefore a broad range oligomer population was detected. The results have great importance, because amyloidogenic proteins and peptides can adopt a number of distinct conformations and a key issue is, which of them are closely associated with the pathogenesis. Conformation dependent antibodies that recognize these different assembly states offer the potential of providing insight into which conformations accumulate in the disease and can be pathologically significant. It is known that fibril assembly is a nucleation dependent process and these soluble fibrillar oligomers may represent fibril nuclei or seeds. (Kayed, Head et al. 2007).

5.2 Study of the aggregation process in the presence of Zn2+ and ENDIP

There are numerous studies, that emphasize the role of metal ions in neurodegenerative diseases, especially in AD. These ions can interact with several proteins, such as Aβ, α-synuclein, prion protein (Gaeta and Hider 2005) (Pattison, Clarke et al. 1971) contributing to changes in their function, conformation or aggregation state. In this work I only detail the role of Zn2+. It is well known that this ion influences Aβ aggregation and thus it may have a crucial role in the pathology of AD. One therapeutic approach is to develop new chelating agents to inhibit or turn back the effect of the metal ions on the aggregation of Aβ, because Aβ-Zn2+-complexes are toxic, confirmed by several studies (Maynard, Bush et al. 2005). We studied the effect of TPEN derivative ENDIP on the aggregation and the size of the assemblies of Aβ after adding Zn2+ using DLS technology. In the sample containing only 50 uM Aβ 1-42, the size of the aggregates did not change during the time of the experiment (~2h), which means that no considerable aggregation occured. When we added equal amount of Zn2+ to the Aβ solution after the first measurement, we observed a rapid increase of the hydrodynamic diameter (d_H) of these particles, proving that Zn^{2+} could promote Aβ precipitation. The addition of ENDIP, in five fold excess, lowered d_H back to its initial value.

From these data we can conclude that ENDIP is able to prevent the metal-induced aggregation and to resolubilize Aβ. Based on these results ENDIP seems to be a good compound for designing drug candidates of AD as a so-called metal-protein attenuating compound (MPAC). MPACs are molecules that can reduce the aberrant metal-protein interactions by chelating metal ions.

5.3 Interactome sreening of Aβ 1-42 oligomers

To explore the Aβ cellular interactome, a protein array method was applied. The applied Protoarray 4.0 array contained 8163 recombinantly expressed human proteins spotted in a defined order onto the array. Our protein array analysis revealed that the Aβ-related protein interaction is not specific; the peptide could interact with at least 324 cellular proteins. The observed nonspecific binding is most likely related to the oligomeric Aβ structure. According to a recent theory, oligomers belong to the new class of proteins called "intrinsically disordered proteins" (IDPs; (Ball, Phillips et al. 2011) (Uversky 2003). The primary amino acid sequence may determine weather a protein will have an IDP structure or not. Since IDPs exist as an ensemble of rapidly interconverting structures (Metallo 2010), there can be more conformations and aggregation states that may have different binding partners. The flexibility of their structure provides versatile interactions and causes the lack of specificity of binding to partner molecules (Tompa 2010). The IDP theory can be fitted also to the phenomenon of conformation specific antibodies. By using these antibodies scientists aimed to identify the 'guilty' conformation/ conformations of Aβ 1-42, if they exist at all. Despite of the efforts made, it is still unclear, which one of these forms is the main toxic species having cardinal interactions. Conformation specific antibodies, like OC and A11 in case of Aβ 1-42, recognize a certain conformation from the ensemble of the interconverting metastable conformations and stabilize it by changing to a stable Aβ 1-42-antibody complex.

In the first analysis we categorized the binding partners according to the signal intensities. In this way we found that AURKA protein, (a serine/ threonine-protein kinase) which has a potential role in Alzheimer's disease possessed a high Aβ-binding intensity. This enzyme can be coupled to GSK-3β protein and in immunoprecipitation studies they coexist in the same protein complex. Therefore, it is possible that AURKA regulates GSK-3β phosphorylation through a direct interaction (Dar, Belkhiri et al. 2009). GSK-3β has been found to be bound to

non hyperphosphorylated tau associated with microtubular network, (Sun, Qureshi et al. 2002) as well as with the hyperphosphorylated tau deposits in the AD brain (Yamaguchi, Ishiguro et al. 1996; Ferrer, Barrachina et al. 2002). We assumed that our Aβ 1-42 oligomers would be able to affect the function of the AURKA protein, hereby influence tau phosphorylation indirectly. To determine the effect of our oligomers on the enzyme we used an Aurora kinase assay kit. In this test, Aβ 1-42 was applied in different concentrations and incubation times (0 min, 24h.). Based on our results, we can conclude that, no effect of our Aβ preparations on the enzyme activity could be observed compared to staurosporine, a protein kinase inhibitor. The explanation for the controversy between the observed binding and the lack of the enzyme modulating effect can be that Aβ 1-42 may interact with AURKA, but the binding side may not influence the activity of the enzyme.

We also tried another analysis method, in which we classified Aβ-bound proteins in functional groups. The GO-based functional analysis showed that the most highly impacted cellular process was the translation. We were able to identify 24 proteins involved in the mechanism of protein translation, which possessed a strong binding to oligomeric Aβ 1-42. Translation consists of three basic processes: initiation, elongation and termination. The protein array data indicates that Aβ might interfere with the initiation and elongation steps. We found that Aβ bound to the important initiation factor eukaryotic initiation factor 2 (EIF2) (Schmitt, Naveau et al. 2010). Aβ 1-42 also bound to the mitochondrial methionyl-tRNA formyltransferase, a protein involved in mitochondrial translation initiation (Takeuchi, Ueda et al. 1998). Besides translation initiation, Aβ bound to several ribosomal proteins involved in elongation. Despite their importance, the precise roles of ribosomal proteins are not known. These proteins are probably involved in the correct folding and processing of rRNA and in the assembly of the ribosome (Steitz and Moore 2003). (Robledo, Idol et al. 2008) showed that the individual depletion of 9 different small and 6 large ribosomal subunit genes led to a decrease in all ribosomal proteins of both the small and the large subunits sinking also the number of the assembled ribosomes and polysomes. The knockdown of ribosomal proteins also led to an increase of rRNA precursors, suggesting their roles in rRNA processing (Robledo, Idol et al. 2008). Among the ribosomal proteins tested by Robledo et al., we also proved that Aβ binds to ribosomal protein S16 (RPS16), RPS19 and RPL11. One of the cellular compartment involved in AD pathogenesis is the mitochondrium. The mechanism(s)

of the well described Aβ-mediated mitochondrial damage (Wang, Su et al. 2009) (Fukui and Moraes 2008) is not exactly known, but it probably involves direct binding of Aβ peptides to mitochondrial proteins (Oppermann, Salim et al. 1999) Our experiments showed that six mitochondrial ribosomal proteins and the mitochondrial methionyl-tRNA formyltransferase bound to Aβ. If the Aβ binding also has an inhibitory effect on mitochondrial translation, as we showed in the *in vitro* translation system, then the translational blockade might lead to mitochondrial dysfunction. Indeed, the intact protein synthesis is essential to the normal mitochondrial function, as described earlier in the case of genetic diseases such as the Pearson syndrome and the Kearns-Sayre syndrome (DiMauro 2004). It is important to note that, while we confirmed the Aβ 1-42 binding to several translation-related proteins, a simple interaction detection by protein array does not necessarily mean that these proteins bind also *in vivo* to Aβ or the binding has functional consequences. There could be several reasons for that. First, the Aβ 1-42 and its interactors might not be expressed at the same time or in the same cellular compartment. Second, the Aβ binding site of the interactors can face to another molecule in a protein or other complex. Therefore, additional binding and functional studies are needed to validate the protein array results. One of the technical limitations associated with the protein array technology is that the proteins are *individually* printed onto the array; hence, the binding of Aβ to protein complexes (such as ribosomes) is not possible. Therefore, we decided to investigate the binding of Aβ 1-42 to native ribosomes purified from rat hippocampus. Our experiments prove that Aβ is able to bind to correctly folded ribosomal complexes. Although we clearly showed that Aβ 1-42 can bind to ribosomal proteins and also to native ribosomal complexes, this binding can occur on ribosomal regions that are not important in translation. Therefore, we functionally tested the inhibitory effect of oligomeric Aβ 1-42 in an *in vitro* translation system. We found that Aβ binding had a concentration dependent inhibitory effect on translation starting at 1 μM and became prominent in 2.5-10 μM concentration. Importantly, the scrambled Aβ 1-42 also had some aspecific inhibitory effect, but this inhibitory effect was significantly lower than that of the native Aβ 1-42, indicating that effective inhibition requires the native amino acid sequence and peptide structure. The detection of Aβ 1-42 mediated translation inhibition is novel scientific result, however, the significant inhibitory effect could be observed only in a relatively high (2.5-25 μM) Aβ 1-42 concentrations. These results can be still relevant, as the intracellular Aβ 1-42 could get via

active or passive transports into cell compartments such as in the endoplasmic reticulum, and accumulate in there, reaching a relatively high local concentration. It was recently described that neuronal cells could take up Aβ oligomers (Sakono and Zako 2010), and this peptide later accumulated in cellular compartments such as late endosomes or lysosomes. The accumulation of Aβ oligomers reached a 2.5 μM local concentration, which was 2 orders of magnitude higher than the extracellular Aβ concentration (25 nM, (Hu, Crick et al. 2009)).

We also have to underline that although we confirmed the binding of Aβ 1-42 to several proteins involved in translation *in vitro*, and we proved that it was able to decrease the *de novo* protein expression in an *in vitro* translation system, these findings do not mechanistically mean that this inhibition occurs *in vivo* and contributes to the pathogenesis of AD. The difficulty of the *in vivo* validation of in vitro results, can be that, detection of the decreased protein content in an AD tissue could just also be a circumstantial evidence, since various AD-and Aβ-related pathways may also lead to the same effect. These altered pathways include the increased apoptosis (Ohyagi, Asahara et al. 2005) impaired neurotrophin function (Schindowski, Belarbi et al. 2008) mitochondrial respiration (Wang, Su et al. 2009) and microtubular transport (Islam and Levy 1997; King, Kan et al. 2006). A more definitive *in vivo* validation of our finding could be the isolated investigation of the translation machinery in the brains of AD patients and age matched controls. In fact, these measurements have already been performed by two independent groups (Langstrom, Anderson et al. 1989) (Ding, Markesbery et al. 2005). In a comparative study (Ding, Markesbery et al. 2005), polyribosomal complexes isolated from different brain areas of 8-8 patients with AD and mild cognitive impairment (MCI) and 10 controls were tested for protein synthesis capability. Ribosomes isolated from AD-related cortical areas (such as superior middle temporal gyri and inferior parietal lobule) showed a significantly (30-60%) inhibited protein synthesis compared to non-AD controls. Ribosomes from other regions that are less involved in AD pathogenesis (such as the cerebellum) were unaffected. This difference indicates that the decline of protein synthesis is not a general metabolic effect of the disease, but rather occurs only in the AD-involved brain areas. Moreover, the fact that patients with MCI, a (potentially pre-AD state), also have a significantly decreased protein synthesis indicates that the decreased translation might be one of the causes and not the result of AD. Since cellular translation requires a complex system, the observed inhibition could have various sources. Previous studies focused

on the AD-related increased oxidation of ribosomal RNA and mRNA pools (Ding, Markesbery et al. 2005). Our novel data indicate that Aβ could bind to various ribosomal and other translation related proteins and, this binding had a functional effect, a significantly decreased protein synthesis. It is possible that *in vivo* the increased oxidation of rRNA and mRNA and the direct binding of Aβ 1-42 to various translation-related proteins are parallel mechanisms that might result a decreased protein synthesis in the diseased tissues.

6 Summary

Even though researchers have little knowledge about the developement and the main cause of Alzheimer's disease, there are different theories. By using technologies given in our laboratory, we tried to answer some ambiguous questions.

The first point is the aggregation of Aβ peptide during different time intervals and the identification of the aggregated species that may affect the neurons.

With the application of an Aβ precursor peptide we succeeded in preparing relatively stable and well characterized oligomer population, which were analyzed by DLS, FPLC-SEC and WB. The shape of the aggregates was characterized by TEM analysis. The changes in the size of these aggregates during the incubation time intervals were studied using FPLC-SEC and WB method. The results demonstrate that the amount of high-n aggregates increased with time, while the percentage of the low-n aggregates decreased.

We confirmed that our oligomers have a fibrillar nature according to our WB studies using conformation-and sequence-specific antibodies.

The role of heavy metal ions, primarily of Zn^{2+} is not yet clear in the etiopathology of Alzheimer's disease. Therefore we studied the effect of Zn^{2+} on the aggregation and the effect of ENDIP on the size of the Aβ aggregates previously treated with Zn^{2+} by using DLS technique. The results demonstrate the promiscuous role of the metal chelator in the therapy of AD, because the Aβ-Zn^{2+} complex has deleterious effect on mice nervous system was demonstrated in our laboratory (publication is under submission).

Aβ oligomers have specific and non-specific interactions with large variety of proteins. We identified several binding partners of Aβ oligomers in a human protein array study, and our results confirmed that Aβ oligomers can bind to ribosomes *in vitro* and consequently decrease the effectiveness of the translational processes. In this way the role of ribosomes in the pathomechanism of AD can be a promising objective of further research.

7 Aknowledgements

I would like to express my gratitude to my supervisors, *Lívia Fülöp Ph.D.* and *Botond Penke D.Sc.* for allowing me to join their research group and for securing the background to my experiments and supported me in all aspects of the laboratory work, and guided me through the difficulties of designing and performing the experiments.

I would like to thank to all of the members of the laboratories taking part in this research group for the special atmosphere they have provided, for their help and expert support on this work and last but not least my consultant. *Dezső Virók M.D., Ph.D.*, for the scientific guidance, encouragement and support me during the laboratory work.

I am grateful for the technical assistance of *Szilvia Pataki*.

Special thanks go to my *parents* and my brother, *Krisztián* for constant encouragment and furtherance to complete my thesis, especially to my husband, *Zsolt* for their support and love, and to friends who were with me during this period.

8 References

Adlard, P. A. and A. I. Bush (2006). "Metals and Alzheimer's disease." J Alzheimers Dis **10**(2-3): 145-163.

Almeida, C. G., R. H. Takahashi, et al. (2006). "Beta-amyloid accumulation impairs multivesicular body sorting by inhibiting the ubiquitin-proteasome system." J Neurosci **26**(16): 4277-4288.

Alzheimer, A. (2008). "2008 Alzheimer's disease facts and figures." Alzheimers Dement **4**(2): 110-133.

Alzheimer, C. and S. Werner (2002). "Fibroblast growth factors and neuroprotection." Adv Exp Med Biol **513**: 335-351.

Angenendt, P., J. Glokler, et al. (2002). "Toward optimized antibody microarrays: a comparison of current microarray support materials." Anal Biochem **309**(2): 253-260.

Armstrong, R. A. (2011). "The pathogenesis of Alzheimer's disease: a reevaluation of the "amyloid cascade hypothesis"." Int J Alzheimers Dis **2011**: 630865.

Arriagada, P. V., J. H. Growdon, et al. (1992). "Neurofibrillary tangles but not senile plaques parallel duration and severity of Alzheimer's disease." Neurology **42**(3 Pt 1): 631-639.

Atwood, C. S., R. D. Moir, et al. (1998). "Dramatic aggregation of Alzheimer abeta by Cu(II) is induced by conditions representing physiological acidosis." J Biol Chem **273**(21): 12817-12826.

Atwood, C. S., R. C. Scarpa, et al. (2000). "Characterization of copper interactions with alzheimer amyloid beta peptides: identification of an attomolar-affinity copper binding site on amyloid beta1-42." J Neurochem **75**(3): 1219-1233.

Auld, D. S., T. J. Kornecook, et al. (2002). "Alzheimer's disease and the basal forebrain cholinergic system: relations to beta-amyloid peptides, cognition, and treatment strategies." Prog Neurobiol **68**(3): 209-245.

Bacskai, B. J., M. P. Frosch, et al. (2007). "Molecular imaging with Pittsburgh Compound B confirmed at autopsy: a case report." Arch Neurol **64**(3): 431-434.

Ball, K. A., A. H. Phillips, et al. (2011). "Homogeneous and heterogeneous tertiary structure ensembles of amyloid-beta peptides." Biochemistry **50**(35): 7612-7628.

Bandyopadhyay, S., X. Huang, et al. (2010). "Novel drug targets based on metallobiology of Alzheimer's disease." Expert Opin Ther Targets **14**(11): 1177-1197.

Bashor, C. J., A. A. Horwitz, et al. (2010). "Rewiring cells: synthetic biology as a tool to interrogate the organizational principles of living systems." Annu Rev Biophys **39**: 515-537.

Billings, L. M., S. Oddo, et al. (2005). "Intraneuronal Abeta causes the onset of early Alzheimer's disease-related cognitive deficits in transgenic mice." Neuron **45**(5): 675-688.

Bowen, D. M., C. B. Smith, et al. (1976). "Neurotransmitter-related enzymes and indices of hypoxia in senile dementia and other abiotrophies." Brain **99**(3): 459-496.

Bozso, Z., B. Penke, et al. (2010). "Controlled in situ preparation of A beta(1-42) oligomers from the isopeptide "iso-A beta(1-42)", physicochemical and biological characterization." Peptides **31**(2): 248-256.

Braak, H. and E. Braak (1991). "Neuropathological stageing of Alzheimer-related changes." Acta Neuropathol **82**(4): 239-259.

Brinton, R. D. and J. M. Wang (2006). "Therapeutic potential of neurogenesis for prevention and recovery from Alzheimer's disease: allopregnanolone as a proof of concept neurogenic agent." Curr Alzheimer Res **3**(3): 185-190.

Bush, A. I., W. H. Pettingell, Jr., et al. (1994). "Modulation of A beta adhesiveness and secretase site cleavage by zinc." J Biol Chem **269**(16): 12152-12158.

Bush, A. I., W. H. Pettingell, et al. (1994). "Rapid induction of Alzheimer A beta amyloid formation by zinc." Science **265**(5177): 1464-1467.

Bush, A. I. and R. E. Tanzi (2008). "Therapeutics for Alzheimer's disease based on the metal hypothesis." Neurotherapeutics **5**(3): 421-432.

Cahill, D. J. (2001). "Protein and antibody arrays and their medical applications." J Immunol Methods **250**(1-2): 81-91.

Carpino, L. A., E. Krause, et al. (2004). "Synthesis of 'difficult' peptide sequences: application of a depsipeptide technique to the Jung-Redemann 10- and 26-mers and the amyloid peptide A beta(1-42)." Tetrahedron Letters **45**(40): 7519-7523.

Castellani, R. J., R. K. Rolston, et al. (2010). "Alzheimer disease." Dis Mon **56**(9): 484-546.

Catalano, S. M., E. C. Dodson, et al. (2006). "The role of amyloid-beta derived diffusible ligands (ADDLs) in Alzheimer's disease." Curr Top Med Chem **6**(6): 597-608.

Charles, P. T., E. R. Goldman, et al. (2004). "Fabrication and characterization of 3D hydrogel microarrays to measure antigenicity and antibody functionality for biosensor applications." Biosens Bioelectron **20**(4): 753-764.

Chen, C. S. and H. Zhu (2006). "Protein microarrays." Biotechniques **40**(4): 423, 425, 427 passim.

Cherny, R. A., J. T. Legg, et al. (1999). "Aqueous dissolution of Alzheimer's disease Abeta amyloid deposits by biometal depletion." J Biol Chem **274**(33): 23223-23228.

Chochina, S. V., N. A. Avdulov, et al. (2001). "Amyloid beta-peptide1-40 increases neuronal membrane fluidity: role of cholesterol and brain region." J Lipid Res **42**(8): 1292-1297.

Coulson, E. J. (2006). "Does the p75 neurotrophin receptor mediate Abeta-induced toxicity in Alzheimer's disease?" J Neurochem **98**(3): 654-660.

Dahlgren, K. N., A. M. Manelli, et al. (2002). "Oligomeric and fibrillar species of amyloid-beta peptides differentially affect neuronal viability." J Biol Chem **277**(35): 32046-32053.

Dar, A. A., A. Belkhiri, et al. (2009). "The aurora kinase A regulates GSK-3beta in gastric cancer cells." Oncogene **28**(6): 866-875.

De Felice, F. G., P. T. Velasco, et al. (2007). "Abeta oligomers induce neuronal oxidative stress through an N-methyl-D-aspartate receptor-dependent mechanism that is blocked by the Alzheimer drug memantine." J Biol Chem **282**(15): 11590-11601.

De Felice, F. G., M. N. Vieira, et al. (2009). "Protection of synapses against Alzheimer's-linked toxins: insulin signaling prevents the pathogenic binding of Abeta oligomers." Proc Natl Acad Sci U S A **106**(6): 1971-1976.

DiMauro, S. (2004). "Mitochondrial diseases." Biochim Biophys Acta **1658**(1-2): 80-88.

Ding, Q., W. R. Markesbery, et al. (2005). "Ribosome dysfunction is an early event in Alzheimer's disease." J Neurosci **25**(40): 9171-9175.

Dos Santos, S., A. Chandravarkar, et al. (2005). "Switch-peptides: controlling self-assembly of amyloid beta-derived peptides in vitro by consecutive triggering of acyl migrations." J Am Chem Soc **127**(34): 11888-11889.

Ferrer, I., M. Barrachina, et al. (2002). "Glycogen synthase kinase-3 is associated with neuronal and glial hyperphosphorylated tau deposits in Alzheimer's disease, Pick's disease, progressive supranuclear palsy and corticobasal degeneration." Acta Neuropathol **104**(6): 583-591.

Finder, V. H. and R. Glockshuber (2007). "Amyloid-beta aggregation." Neurodegener Dis **4**(1): 13-27.

Finder, V. H., I. Vodopivec, et al. (2010). "The recombinant amyloid-beta peptide Abeta1-42 aggregates faster and is more neurotoxic than synthetic Abeta1-42." J Mol Biol **396**(1): 9-18.

Frederickson, C. J., J. Y. Koh, et al. (2005). "The neurobiology of zinc in health and disease." Nat Rev Neurosci **6**(6): 449-462.

Fukui, H. and C. T. Moraes (2008). "The mitochondrial impairment, oxidative stress and neurodegeneration connection: reality or just an attractive hypothesis?" Trends Neurosci **31**(5): 251-256.

Gaeta, A. and R. C. Hider (2005). "The crucial role of metal ions in neurodegeneration: the basis for a promising therapeutic strategy." Br J Pharmacol **146**(8): 1041-1059.

Garcia-Sierra, F., S. Mondragon-Rodriguez, et al. (2008). "Truncation of tau protein and its pathological significance in Alzheimer's disease." J Alzheimers Dis **14**(4): 401-409.

Glabe, C. C. (2005). "Amyloid accumulation and pathogensis of Alzheimer's disease: significance of monomeric, oligomeric and fibrillar Abeta." Subcell Biochem **38**: 167-177.

Glabe, C. G. (2008). "Structural classification of toxic amyloid oligomers." J Biol Chem **283**(44): 29639-29643.

Glenner, G. G., C. W. Wong, et al. (1984). "The amyloid deposits in Alzheimer's disease: their nature and pathogenesis." Appl Pathol **2**(6): 357-369.

Gotz, J., F. Chen, et al. (2001). "Formation of neurofibrillary tangles in P301l tau transgenic mice induced by Abeta 42 fibrils." Science **293**(5534): 1491-1495.

Haab, B. B. (2001). "Advances in protein microarray technology for protein expression and interaction profiling." Curr Opin Drug Discov Devel **4**(1): 116-123.

Haass, C. and D. J. Selkoe (2007). "Soluble protein oligomers in neurodegeneration: lessons from the Alzheimer's amyloid beta-peptide." Nat Rev Mol Cell Biol **8**(2): 101-112.

Hardy, J. and D. J. Selkoe (2002). "The amyloid hypothesis of Alzheimer's disease: progress and problems on the road to therapeutics." Science **297**(5580): 353-356.

Hardy, J. A. and G. A. Higgins (1992). "Alzheimer's disease: the amyloid cascade hypothesis." Science **256**(5054): 184-185.

Hartmann, T. (2001). "Cholesterol, A beta and Alzheimer's disease." Trends Neurosci **24**(11 Suppl): S45-48.

Hepler, R. W., K. M. Grimm, et al. (2006). "Solution state characterization of amyloid beta-derived diffusible ligands." Biochemistry **45**(51): 15157-15167.

Herrup, K. (2010). "Reimagining Alzheimer's disease--an age-based hypothesis." J Neurosci **30**(50): 16755-16762.

Hu, X., S. L. Crick, et al. (2009). "Amyloid seeds formed by cellular uptake, concentration, and aggregation of the amyloid-beta peptide." Proc Natl Acad Sci U S A **106**(48): 20324-20329.

Huang, X., M. P. Cuajungco, et al. (2000). "Alzheimer's disease, beta-amyloid protein and zinc." J Nutr **130**(5S Suppl): 1488S-1492S.

Hutton, M. and J. Hardy (1997). "The presenilins and Alzheimer's disease." Hum Mol Genet **6**(10): 1639-1646.

Hutton, M., C. L. Lendon, et al. (1998). "Association of missense and 5'-splice-site mutations in tau with the inherited dementia FTDP-17." Nature **393**(6686): 702-705.

Islam, K. and E. Levy (1997). "Carboxyl-terminal fragments of beta-amyloid precursor protein bind to microtubules and the associated protein tau." Am J Pathol **151**(1): 265-271.

Jan, A., O. Gokce, et al. (2008). "The ratio of monomeric to aggregated forms of Abeta40 and Abeta42 is an important determinant of amyloid-beta aggregation, fibrillogenesis, and toxicity." J Biol Chem **283**(42): 28176-28189.

Jellinger, K. A. (2009). "Recent advances in our understanding of neurodegeneration." J Neural Transm **116**(9): 1111-1162.

Juhasz, G., I. Foldi, et al. (2011). "Systems biology of Alzheimer's disease: How diverse molecular changes result in memory impairment in AD." Neurochem Int.

Kayed, R., E. Head, et al. (2007). "Fibril specific, conformation dependent antibodies recognize a generic epitope common to amyloid fibrils and fibrillar oligomers that is absent in prefibrillar oligomers." Mol Neurodegener **2**: 18.

Kidd, M. (1963). "Paired helical filaments in electron microscopy of Alzheimer's disease." Nature **197**: 192-193.

Kidd, M. (1964). "Alzheimer's Disease--an Electron Microscopical Study." Brain **87**: 307-320.

Kim, J., L. Onstead, et al. (2007). "Abeta40 inhibits amyloid deposition in vivo." J Neurosci **27**(3): 627-633.

King, M. E., H. M. Kan, et al. (2006). "Tau-dependent microtubule disassembly initiated by prefibrillar beta-amyloid." J Cell Biol **175**(4): 541-546.

Klafki, H. W., M. Staufenbiel, et al. (2006). "Therapeutic approaches to Alzheimer's disease." Brain **129**(Pt 11): 2840-2855.

Kramer, A., T. Feilner, et al. (2004). "Identification of barley CK2alpha targets by using the protein microarray technology." Phytochemistry **65**(12): 1777-1784.

LaFerla, F. M., K. N. Green, et al. (2007). "Intracellular amyloid-beta in Alzheimer's disease." Nat Rev Neurosci **8**(7): 499-509.

Lakatos, A., E. Zsigo, et al. (2010). "Two pyridine derivatives as potential Cu(II) and Zn(II) chelators in therapy for Alzheimer's disease." Dalton Trans **39**(5): 1302-1315.

Lambert, M. P., A. K. Barlow, et al. (1998). "Diffusible, nonfibrillar ligands derived from Abeta1-42 are potent central nervous system neurotoxins." Proc Natl Acad Sci U S A **95**(11): 6448-6453.

Langstrom, N. S., J. P. Anderson, et al. (1989). "Alzheimer's disease-associated reduction of polysomal mRNA translation." Brain Res Mol Brain Res **5**(4): 259-269.

Lansbury, P. T., Jr. (1999). "Evolution of amyloid: what normal protein folding may tell us about fibrillogenesis and disease." Proc Natl Acad Sci U S A **96**(7): 3342-3344.

Lee, J. Y., T. B. Cole, et al. (2002). "Contribution by synaptic zinc to the gender-disparate plaque formation in human Swedish mutant APP transgenic mice." Proc Natl Acad Sci U S A **99**(11): 7705-7710.

Lewis, J., D. W. Dickson, et al. (2001). "Enhanced neurofibrillary degeneration in transgenic mice expressing mutant tau and APP." Science **293**(5534): 1487-1491.

Lin, C. J., H. C. Huang, et al. (2010). "Cu(II) interaction with amyloid-beta peptide: a review of neuroactive mechanisms in AD brains." Brain Res Bull **82**(5-6): 235-242.

Lue, L. F., Y. M. Kuo, et al. (1999). "Soluble amyloid beta peptide concentration as a predictor of synaptic change in Alzheimer's disease." Am J Pathol **155**(3): 853-862.

MacBeath, G. and S. L. Schreiber (2000). "Printing proteins as microarrays for high-throughput function determination." Science **289**(5485): 1760-1763.

Magdesian, M. H., M. M. Carvalho, et al. (2008). "Amyloid-beta binds to the extracellular cysteine-rich domain of Frizzled and inhibits Wnt/beta-catenin signaling." J Biol Chem **283**(14): 9359-9368.

Maynard, C. J., A. I. Bush, et al. (2005). "Metals and amyloid-beta in Alzheimer's disease." Int J Exp Pathol **86**(3): 147-159.

McLean, C. A., R. A. Cherny, et al. (1999). "Soluble pool of Abeta amyloid as a determinant of severity of neurodegeneration in Alzheimer's disease." Ann Neurol **46**(6): 860-866.

Mehan, S., H. Meena, et al. (2011). "JNK: a stress-activated protein kinase therapeutic strategies and involvement in Alzheimer's and various neurodegenerative abnormalities." J Mol Neurosci **43**(3): 376-390.

Mendez, M. F. (2006). "The accurate diagnosis of early-onset dementia." Int J Psychiatry Med **36**(4): 401-412.

Meredith, S. C. (2005). "Protein denaturation and aggregation: Cellular responses to denatured and aggregated proteins." Ann N Y Acad Sci **1066**: 181-221.

Metallo, S. J. (2010). "Intrinsically disordered proteins are potential drug targets." Curr Opin Chem Biol **14**(4): 481-488.

Michikawa, M. (2003). "The role of cholesterol in pathogenesis of Alzheimer's disease: dual metabolic interaction between amyloid beta-protein and cholesterol." Mol Neurobiol **27**(1): 1-12.

Miura, T., K. Suzuki, et al. (2000). "Metal binding modes of Alzheimer's amyloid beta-peptide in insoluble aggregates and soluble complexes." Biochemistry **39**(23): 7024-7031.

Necula, M., R. Kayed, et al. (2007). "Small molecule inhibitors of aggregation indicate that amyloid beta oligomerization and fibrillization pathways are independent and distinct." J Biol Chem **282**(14): 10311-10324.

Noy, D., I. Solomonov, et al. (2008). "Zinc-amyloid beta interactions on a millisecond time-scale stabilize non-fibrillar Alzheimer-related species." J Am Chem Soc **130**(4): 1376-1383.

Oh, S., H. S. Hong, et al. (2005). "Amyloid peptide attenuates the proteasome activity in neuronal cells." Mech Ageing Dev **126**(12): 1292-1299.

Ohyagi, Y., H. Asahara, et al. (2005). "Intracellular Abeta42 activates p53 promoter: a pathway to neurodegeneration in Alzheimer's disease." Faseb J **19**(2): 255-257.

Oppermann, U. C., S. Salim, et al. (1999). "Binding of amyloid beta-peptide to mitochondrial hydroxyacyl-CoA dehydrogenase (ERAB): regulation of an SDR enzyme activity with implications for apoptosis in Alzheimer's disease." FEBS Lett **451**(3): 238-242.

Origlia, N., O. Arancio, et al. (2009). "MAPK, beta-amyloid and synaptic dysfunction: the role of RAGE." Expert Rev Neurother **9**(11): 1635-1645.

Pattison, I. H., M. C. Clarke, et al. (1971). "Brain cell cultures from mice affected with scrapie or fed with cuprizone." Res Vet Sci **12**(5): 478-480.

Poorkaj, P., T. D. Bird, et al. (1998). "Tau is a candidate gene for chromosome 17 frontotemporal dementia." Ann Neurol **43**(6): 815-825.

Qiu, C., M. Kivipelto, et al. (2009). "Epidemiology of Alzheimer's disease: occurrence, determinants, and strategies toward intervention." Dialogues Clin Neurosci **11**(2): 111-128.

Roberson, E. D., K. Scearce-Levie, et al. (2007). "Reducing endogenous tau ameliorates amyloid beta-induced deficits in an Alzheimer's disease mouse model." Science **316**(5825): 750-754.

Robinson, D. M. and G. M. Keating (2006). "Memantine: a review of its use in Alzheimer's disease." Drugs **66**(11): 1515-1534.

Robledo, S., R. A. Idol, et al. (2008). "The role of human ribosomal proteins in the maturation of rRNA and ribosome production." Rna **14**(9): 1918-1929.

Rogawski, M. A. and G. L. Wenk (2003). "The neuropharmacological basis for the use of memantine in the treatment of Alzheimer's disease." CNS Drug Rev **9**(3): 275-308.

Roychaudhuri, R., M. Yang, et al. (2009). "Amyloid beta-protein assembly and Alzheimer disease." J Biol Chem **284**(8): 4749-4753.

Sakono, M. and T. Zako (2010). "Amyloid oligomers: formation and toxicity of Abeta oligomers." Febs J **277**(6): 1348-1358.

Sakono, M., T. Zako, et al. (2008). "Formation of highly toxic soluble amyloid beta oligomers by the molecular chaperone prefoldin." Febs J **275**(23): 5982-5993.

Schindowski, K., K. Belarbi, et al. (2008). "Neurotrophic factors in Alzheimer's disease: role of axonal transport." Genes Brain Behav **7 Suppl 1**: 43-56.

Schmitt, E., M. Naveau, et al. (2010). "Eukaryotic and archaeal translation initiation factor 2: a heterotrimeric tRNA carrier." FEBS Lett **584**(2): 405-412.

Shah, Y., E. G. Tangalos, et al. (2000). "Mild cognitive impairment. When is it a precursor to Alzheimer's disease?" Geriatrics **55**(9): 62, 65-68.

Shankar, G. M., B. L. Bloodgood, et al. (2007). "Natural oligomers of the Alzheimer amyloid-beta protein induce reversible synapse loss by modulating an NMDA-type glutamate receptor-dependent signaling pathway." J Neurosci **27**(11): 2866-2875.

Shankar, G. M. and D. M. Walsh (2009). "Alzheimer's disease: synaptic dysfunction and Abeta." Mol Neurodegener **4**: 48.

Sohma, Y., M. Sasaki, et al. (2004). "Design and synthesis of a novel water-soluble A beta 1-42 isopeptide: an efficient strategy for the preparation of Alzheimer's disease-related peptide, A beta 1-42, via O-N intramolecular acyl migration reaction." Tetrahedron Letters **45**(31): 5965-5968.

Spillantini, M. G., J. R. Murrell, et al. (1998). "Mutation in the tau gene in familial multiple system tauopathy with presenile dementia." Proc Natl Acad Sci U S A **95**(13): 7737-7741.

Steitz, T. A. and P. B. Moore (2003). "RNA, the first macromolecular catalyst: the ribosome is a ribozyme." Trends Biochem Sci **28**(8): 411-418.

Stillman, B. A. and J. L. Tonkinson (2000). "FAST slides: a novel surface for microarrays." Biotechniques **29**(3): 630-635.

Sun, W., H. Y. Qureshi, et al. (2002). "Glycogen synthase kinase-3beta is complexed with tau protein in brain microtubules." J Biol Chem **277**(14): 11933-11940.

Takeuchi, N., T. Ueda, et al. (1998). "Expression and characterization of bovine mitochondrial methionyl-tRNA transformylase." J Biochem **124**(6): 1069-1071.

Talaga, P. and L. Quere (2002). "The plasma membrane: a target and hurdle for the development of anti-Abeta drugs?" Curr Drug Targets CNS Neurol Disord **1**(6): 567-574.

Templin, M. F., D. Stoll, et al. (2002). "Protein microarray technology." Drug Discov Today **7**(15): 815-822.

Terry, R. D., N. K. Gonatas, et al. (1964). "ULTRASTRUCTURAL STUDIES IN ALZHEIMER'S PRESENILE DEMENTIA." Am J Pathol **44**: 269-297.

Tompa, P., Ed. (2010). Structure and Function of Intrinsically Disordered Proteins, CRC Press.

Tougu, V., A. Karafin, et al. (2009). "Zn(II)- and Cu(II)-induced non-fibrillar aggregates of amyloid-beta (1-42) peptide are transformed to amyloid fibrils, both spontaneously and under the influence of metal chelators." J Neurochem **110**(6): 1784-1795.

Tseng, B. P., K. N. Green, et al. (2008). "Abeta inhibits the proteasome and enhances amyloid and tau accumulation." Neurobiol Aging **29**(11): 1607-1618.

Uversky, V. N. (2003). "Protein folding revisited. A polypeptide chain at the folding-misfolding-nonfolding cross-roads: which way to go?" Cell Mol Life Sci **60**(9): 1852-1871.

Van Gassen, G., W. Annaert, et al. (2000). "Binding partners of Alzheimer's disease proteins: are they physiologically relevant?" Neurobiol Dis **7**(3): 135-151.

Verdier, Y., M. Zarandi, et al. (2004). "Amyloid beta-peptide interactions with neuronal and glial cell plasma membrane: binding sites and implications for Alzheimer's disease." J Pept Sci **10**(5): 229-248.

Wang, X., B. Su, et al. (2009). "The role of abnormal mitochondrial dynamics in the pathogenesis of Alzheimer's disease." J Neurochem **109 Suppl 1**: 153-159.

Waschuk, S. A., E. A. Elton, et al. (2001). "Cellular membrane composition defines A beta-lipid interactions." J Biol Chem **276**(36): 33561-33568.

Westerman, M. A., D. Cooper-Blacketer, et al. (2002). "The relationship between Abeta and memory in the Tg2576 mouse model of Alzheimer's disease." J Neurosci **22**(5): 1858-1867.

Wisniewski, H. M., H. K. Narang, et al. (1976). "Neurofibrillary tangles of paired helical filaments." J Neurol Sci **27**(2): 173-181.

Xia, W., T. Yang, et al. (2009). "A specific enzyme-linked immunosorbent assay for measuring beta-amyloid protein oligomers in human plasma and brain tissue of patients with Alzheimer disease." Arch Neurol **66**(2): 190-199.

Yamaguchi, H., K. Ishiguro, et al. (1996). "Preferential labeling of Alzheimer neurofibrillary tangles with antisera for tau protein kinase (TPK) I/glycogen synthase kinase-3 beta and cyclin-dependent kinase 5, a component of TPK II." Acta Neuropathol **92**(3): 232-241.

Yan, Y. and C. Wang (2007). "Abeta40 protects non-toxic Abeta42 monomer from aggregation." J Mol Biol **369**(4): 909-916.

Yanagida, M. (2002). "Functional proteomics; current achievements." J Chromatogr B Analyt Technol Biomed Life Sci **771**(1-2): 89-106.

Yang, A. J., D. Chandswangbhuvana, et al. (1998). "Loss of endosomal/lysosomal membrane impermeability is an early event in amyloid Abeta1-42 pathogenesis." J Neurosci Res **52**(6): 691-698.

Yang, D. S., J. McLaurin, et al. (2000). "Examining the zinc binding site of the amyloid-beta peptide." Eur J Biochem **267**(22): 6692-6698.

Yang, L., S. Guo, et al. (2011). "Protein microarrays for systems biology." Acta Biochim Biophys Sin (Shanghai) **43**(3): 161-171.

Yoshiike, Y., K. Tanemura, et al. (2001). "New insights on how metals disrupt amyloid beta-aggregation and their effects on amyloid-beta cytotoxicity." J Biol Chem **276**(34): 32293-32299.

Zhao, W. Q., F. G. De Felice, et al. (2008). "Amyloid beta oligomers induce impairment of neuronal insulin receptors." Faseb J **22**(1): 246-260.

Zhu, H., M. Bilgin, et al. (2001). "Global analysis of protein activities using proteome chips." Science **293**(5537): 2101-2105.

Zhu, H. and M. Snyder (2001). "Protein arrays and microarrays." Curr Opin Chem Biol **5**(1): 40-45.

Zhu, H. and M. Snyder (2003). "Protein chip technology." Curr Opin Chem Biol **7**(1): 55-63.

I.

Two pyridine derivatives as potential Cu(II) and Zn(II) chelators in therapy for Alzheimer's disease†

Andrea Lakatos,*[a] Éva Zsigó,[a] Dominik Hollender,[b] Nóra V. Nagy,[c] Lívia Fülöp,[d] Dóra Simon,[d] Zsolt Bozsó[d] and Tamás Kiss*[a,b]

Received 10th August 2009, Accepted 15th October 2009
First published as an Advance Article on the web 27th November 2009
DOI: 10.1039/b916366b

Two pyridine derivatives, DMAP and ENDIP, have been investigated as possible metal chelators in the therapy of Alzheimer's disease. Their complex formation with Cu(II) and Zn(II) were characterised in detail. In the case of ENDIP a high stability tetradentate ML complex is formed at physiological pH both with Cu(II) and Zn(II). DMAP was found to be a weaker metal binder. At physiological pH, it forms a bidentate ML complex with Zn(II) and MLH_{-1} and ML_2 complexes with Cu(II), depending on the metal ion to ligand ratio. Fluorescence spectroscopy and dynamic light scattering measurements proved that ENDIP effectively competes with aggregated amyloid-β peptides (Aβ) for both Cu(II) and Zn(II) and thus is able to prevent the metal ion-induced amyloid aggregation and to resolubilise amyloid precipitates.

Introduction

Alzheimer's disease (AD) is the most common cause of age-related senile dementia (more than 20 million people in the world today suffer from this disease). It is characterized by cerebral deposits of extracellular amyloid plaques and intracellular tangles.[1] The amyloid plaques comprise mixtures of aggregated amyloid-β peptides (Aβ) with lengths of 39–42 amino acids. From among these Aβ peptides, Aβ(1–40) and Aβ(1–42) are the more common, the latter being the most toxic with the highest tendency to aggregate. Aβ is cleaved off from the amyloid precursor protein (APP) by β- and γ-secretases and is also present in healthy brains in soluble form. According to the amyloid cascade hypothesis, the key of the disease is the aggregation of monomeric Aβ: an increased production and accumulation of Aβ in the synaptic cleft leading to the formation of oligomers, which are proven to be toxic. These oligomers aggregate to protofibrils and finally fibrils which form the amyloid deposits.[2] According to some authors, the problem with this hypothesis is that the self-aggregating properties of Aβ alone are insufficient to explain the accumulation of the peptide in specific brain regions in AD.[3] Thus, the consideration of other factors may also be necessary. Elevated levels of metal ions in these deposits, such as Zn(II), Cu(II) and Fe(III) has been proven.[4] Moreover, several studies have shown dyshomeostasis of these metal ions, especially Cu(II) and Zn(II) in the brain of AD patients.[5,6] Thus, the role of metal ions in the neurodegenerative processes (for example plaque formation) of Alzheimer's disease has become an important research subject.

Both Cu(II) and Zn(II) can be released into the synaptic cleft during neurotransmission.[3,5,7] The nature of this release in the case of Cu(II) is not clearly known. Zn(II) is released from the synaptic vesicles of the hippocampal neurons where they are transported by the zinc transporter protein ZnT3. An overexpression of ZnT3 was found in AD brains, which led to an increased concentration of Zn(II) in the synaptic vesicles and as a consequence, in the synaptic cleft.[6,7] The relationship between the secretion of excess Zn(II) from the synaptic vesicles and the formation of senile plaques was validated by the observation that in ZnT3 knockout mice crossed with transgenic AD mice the cerebral Aβ deposition was diminished due to the reduced release of neuronal Zn(II).[8] Thus, the contribution of Zn(II) to the formation of amyloid plaques has been demonstrated. Cu(II) bound to Aβ can enhance oxidative stress conditions, which play a key role in AD. *In vitro* studies prove that both Zn(II) and Cu(II) can promote aggregation of Aβ, but in a different way. Zn(II) is able to rapidly precipitate Aβ, but forms amorphous aggregates.[9] In contrast, the ability of Cu(II) to promote aggregation is much lower, but the observed aggregates are more fibrillary.[10]

It was also demonstrated that Aβ possesses selective Zn(II) and Cu(II) binding sites that mediate its physicochemical behaviour. The value of dissociation constants for 1 : 1 Cu(II)-Aβ and Zn(II)-Aβ complexes vary with the type of buffer used in the measurements and the methods employed for their determination, and it typically falls in the region of 1 pM to 100 nM for Cu(II) and 1–20 μM for Zn(II).[11] However, in the case of Zn(II), a much higher apparent dissociation constant (2 μM) has been determined when the Zn(II)-Aβ(1–40) sample was pre-incubated before K_D determination allowing aggregation to occur.[12] The most probable binding mode of Cu(II) in its Aβ complex is a 3N1O coordination involving the carboxylate function of Asp1, and either the three His (His6, His13 and His14) imidazole groups, or two His (His6 and His13 or His14) and the terminal amino

[a]*Department of Inorganic and Analytical Chemistry, University of Szeged, Dóm tér 7, H-6720, Szeged, Hungary*
[b]*Bioinorganic Research Group of the Hungarian Academy of Sciences, University of Szeged, POBox 440, H-6701, Szeged, Hungary*
[c]*Institute of Structural Chemistry, Chemical Research Center of the Hungarian Academy of Sciences, Pusztaszeri út 59-67, H-1025, Budapest, Hungary*
[d]*Department of Medical Chemistry, University of Szeged, Dóm tér 8, H-6720, Szeged, Hungary*
† Electronic supplementary information (ESI) available: Experimental details. See DOI: 10.1039/b916366b

group. An equilibrium between these two coordination isomers is very likely. In the case of Zn(II), beside the three His residues, Asp1 can bind through the carboxylate and/or the N-terminal amino function.[11]

In parallel to these findings a so called "metal hypothesis" has arisen, which considers the metal induced Aβ aggregation as a key step, rather than the self-aggregation of Aβ.[3] In line with this hypothesis, the reduction of the aberrant metal-protein interactions by metal-protein attenuating compounds (MPAC), which are molecules able to chelate metal ions, is a possible therapeutic way for AD.[3,7] While Cu(II) and Zn(II) are accumulated in extracellular plaques, the intracellular Cu(II) and Zn(II) levels of the neurons in AD is abnormally low. These low levels can lead, for example, to an enhanced production of the most toxic Aβ peptide, Aβ(1–42). Thus, traditionally used high-affinity metal chelators are unlikely to be good in amelioration of AD symptoms, because they can even worsen the intracellular Cu(II) and Zn(II) deficiency.

The antibiotic Clioquinol (5-cloro-7-iodo-8-hydroxyquinoline, CQ) with moderate affinity towards Cu(II) and Zn(II) was proven to inhibit metal-induced Aβ aggregation and the reactive oxygen generation *in vitro*.[13] A pilot phase IIa clinical study of CQ in AD patients showed its ability to ameliorate cognitive degeneration and lower plasma Aβ(1–42) levels.[14] However, further clinical studies were stopped due to the difficulties in preventing di-iodo-8-hydroxyquinoline contamination upon large scale chemical synthesis.[15] These positive effects of CQ in AD encouraged scientists to propose and design new possible MPACs for therapeutic purposes in AD.[15-18] One of these new compounds PBT2, which is a derivative of CQ, was found to have a favourable safety profile and showed some beneficial effects on AD patients in a recent phase IIa trial. Both CQ and PBT2 are not only metal chelators, but they can act as ionophores being able to transport Cu(II) and Zn(II) across cell membranes.[15] The exact mechanism of action of these compounds is still not clearly known, but it seems reasonable that a ligand-mediated redistribution of metals at a cellular level in the brain may be important. In a very recent paper Orvig *et al*. prepared multifunctional molecules and their glycosylated derivative proved to be very efficient to attenuate metal ion induced amyloid aggregation.[19]

In our present work we have synthesised and characterised the Zn(II) and Cu(II) binding ability of two multifunctional metal chelators: *N*-methyl-1-(pyridine-2-yl)-methaneamine (DMAP) and N^1,N^2-bis(pyridine-2-yl-methyl)ethane-1,2-diamine (ENDIP) (Scheme 1) and characterised their Zn(II) and Cu(II) binding ability in order to assess the possibility to use them as MPACs in AD therapy. The choice of chelator was based on the idea of decreasing the number of donor groups of *N*,*N*,*N*′,*N*′-tetrakis(2-pyridylmethyl)ethylenediamine (TPEN), which is a widely used, membrane permeable, high-affinity Zn(II) chelator in biology. Thus, ENDIP is practically half of TPEN and DMAP represents only one of its four binding units.

Table 1 Overall formation constants and p*K* values of the investigated ligands and complexes formed with Cu(II) and Zn(II) at $I = 0.2$ mol dm^{-3} KCl and $T = 298$ K; and wavelength of the absorption maxima of the molar spectra of the individual Cu(II) complexes of DMAP and ENDIP

	DMAP			ENDIP		
	logβ	pK	$\lambda_{max,\ exp}$	logβ	pK	$\lambda_{max,\ exp}$
HL	8.96 (1)	8.96	—	8.27 (1)	8.27	—
H_2L	10.74 (1)	1.78	—	13.71 (1)	5.44	—
H_3L	—	—	—	15.39[a]	1.68	—
M = Cu(II)						
ML	9.23 (1)	6.78	692	16.62[a]	10.03	615
MLH_{-1}	2.33 (2)	—	614	6.59 (1)	—	655
ML_2	16.09 (1)	10.55	610	—	—	—
ML_2H_{-1}	5.54 (6)	—	n.d.	—	—	—
Fitting parameter	7.54×10^{-3}			7.15×10^{-3}		
M = Zn(II)						
ML	4.86 (1)	9.07		11.35 (2)	9.75	
MLH_{-1}	−4.21 (2)	9.25		1.60 (1)	—	
MLH_{-2}	−13.46 (2)	—		—	—	
ML_2	8.25 (1)	—		—	—	
ML_3	10.19 (8)	—		—	—	
Fitting parameter	5.66×10^{-3}			5.39×10^{-3}		

[a] This value was determined from UV-spectrophotometric titrations.

Results and discussion

Cu(II) and Zn(II) complexes of DMAP

The protonation processes of DMAP were studied by pH-potentiometric titrations in the 2–11 pH range. DMAP has two dissociable protons: one on the pyridine nitrogen and one on the secondary amino group. The pK values determined for these two donor groups are listed in Table 1. The pyridine nitrogen has a very low pK (pK < 2) due to the strong electron attracting effect of the pyridine ring. Thus its determination is rather uncertain. The amino group loses its proton in the basic pH range with a pK of 8.96.

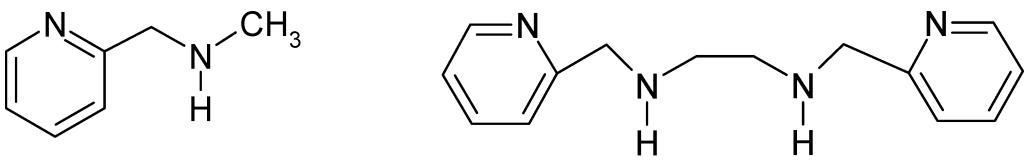

DMAP ENDIP

Scheme 1 Structure of the ligands.

The Cu(II) and Zn(II) binding ability of DMAP was investigated by pH-potentiometry and the former also by Vis-spectrophotometry and EPR spectroscopy, performing the experiments in the 2–10 pH range. Evaluation of the pH-metric titration data led to the speciation model and overall formation constants collected in Table 1. The representative speciation curves are shown in Fig. 1.

In the Cu(II)-DMAP system complex formation starts at pH < 2 by formation of the complex ML. The λ_{max} of this species calculated from the Vis-spectrophotometric data (692 nm, Table 1) agrees relatively well with the predicted value for a $\{N_{amino}, N_{aromatic}, 2\times H_2O\}$ coordination (681 nm) using the semi-empirical equation reported by Sigel and Martin[20] and later by Prenesti *et al*.[21] Thus, a bidentate coordination for this complex can be assumed. At higher pH, deprotonation of the ML complex with a pK of 6.90 leads to the formation of the MLH_{-1} species. Since there is no other deprotonating donor group in DMAP, the MLH_{-1} complex can only be a mixed hydroxo species. However, the λ_{max} of this species

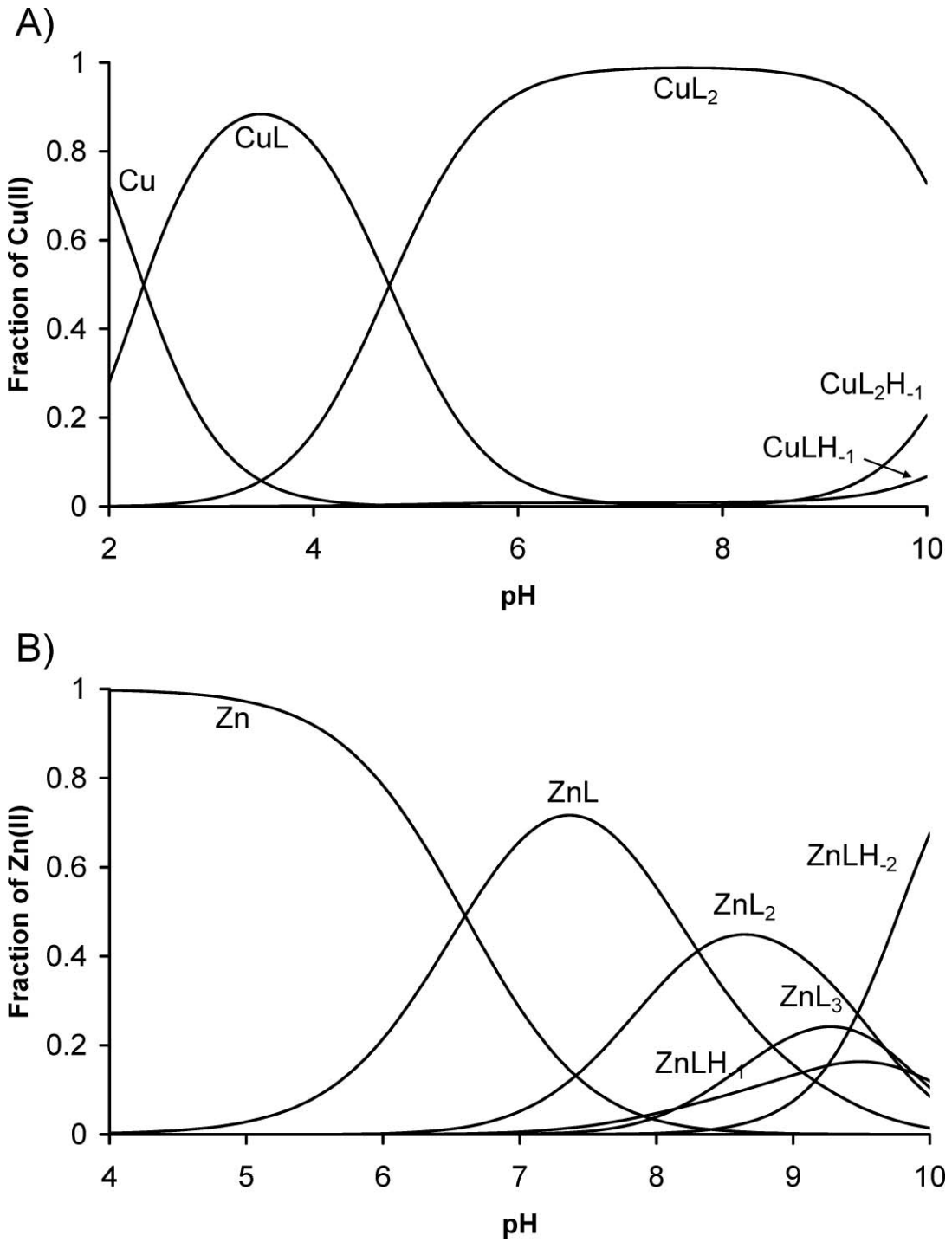

Fig. 1 The speciation diagrams of (A) Cu(II)-DMAP and (B) Zn(II)-DMAP systems at 1 : 4 metal to ligand ratios; $c_{DMAP} = 0.004$ M.

(614 nm) is very different from the estimated value assuming a $\{N_{amino}, N_{aromatic}, OH, H_2O\}$ coordination (640 nm). The reason is a distorted geometry of MLH_{-1} revealed by the anisotropic EPR parameters ($g_{xx} = 2.057$, $g_{yy} = 2.043$ $g_{zz} = 2.251$, $A_{xx} = 26.2$ G, $A_{yy} = 20.7$ G, $A_{zz} = 171.6$ G), since the equation of Prenesti *et al.*[21] gives a good estimation of the λ_{max} value only in the case of a regular arrangement of the equatorial donor groups. We should mention here, that the potentiometric titration data obtained in equimolar solutions were evaluated only until pH 8. Above this pH a poor fitting was obtained between the experimental and the calculated titration curves, although several speciation models have been tried. Isotropic EPR spectra indicated a significant loss in the intensity of the signal in the pH range 8–11, without any sign of precipitation. This could be best described by assuming two EPR silent species: the soluble Cu(II)-hydroxocomplex, $M_2(OH)_2$ and a dinuclear Cu(II)-DMAP species, presumably $M_2L_2H_{-1}$. The $M_2(OH)_2$ complex was considered in our pH-metric calculations too, with a log β of -10.1,[22] but the dinuclear species was barely possible to fit in the speciation model. Thus, no exact description of the probable oligomerization processes could be given occurring at pH > 8 (composition and stability constant of the species). At excess ligand the main species at physiological pH (the pH of our interest) is the complex ML_2, with the two DMAP molecules coordinated in a bidentate manner. The complex has a rhombic symmetry as indicated by the isotropic ($g_o = 2.110$, $A_o = 73.2$ G) and anisotropic: ($g_{xx} = 2.047$, $g_{yy} = 2.050$ $g_{zz} = 2.221$, $A_{xx} = 43.9$ G, $A_{yy} = 29.7$ G, $A_{zz} = 178.4$ G) EPR parameters. This explains again the difference between the calculated and the estimated λ_{max} values (Table 1). Deprotonation of a water molecule in ML_2 occurs in the very basic pH range with the formation of a relatively small amount of species ML_2H_{-1}. (see Fig. 1A).

The complex formation in the case of Zn(II) starts only at pH 5. The stability of the complexes formed with this metal ion are a few orders of magnitude smaller than that of the Cu(II) species (see Table 1) but they may have similar binding modes. The first complex is ML with the same bidentate coordination as was proved for the case of the Cu(II) complex. At higher pH, two deprotonations with pK values of 9.07 and 9.25 occur, resulting in the formation of species MLH_{-1} and MLH_{-2}. These pK values are typical for the deprotonation of water molecules in the coordination sphere of Zn(II). At ligand excess, the fitting between the experimental and the calculated titration curves significantly improved, when besides the ML_2 complex (found also in the Cu(II)-DMAP system) the ML_3 species was also assumed. This complex having an octahedral geometry involves three DMAP molecules bound in a bidentate manner.

The complex formation equilibria in the Zn(II)-DMAP system have also been studied by NMR-spectroscopy. The spectrum recorded at pH 3 in equimolar solution (Fig. S1 in the ESI†) is exactly the same as the spectrum of the free ligand at this pH, indicating that, in accordance with the potentiometric results, there is no complex formation at this pH. Above pH 4 a shift of the signals as compared to the free ligand could be observed, due to fast ligand exchange reactions between the complexes and free DMAP. No information about the structures of the complexes can be drawn from these spectral data.

Cu(II) and Zn(II) complexes of ENDIP

ENDIP has four dissociable protons, on the pyridine nitrogens and on the secondary amino groups. The titration curve of the ligand alone shows three distinct equivalence points (Fig. 2). The first, at two equivalence of base addition, could be assigned to the deprotonations of the pyridine nitrogens, which take place at very acidic pH. Consequently, the other two are related to the deprotonation of the protonated amino groups. The stability

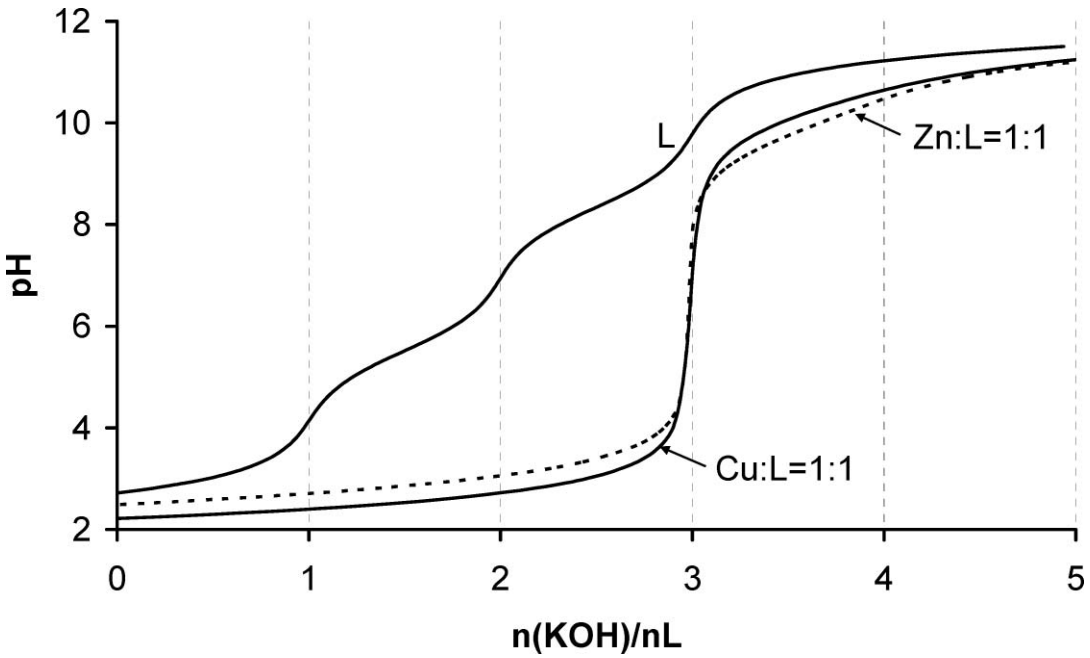

Fig. 2 The comparison of the normalized pH-metric titration curves of ENDIP (L) and its Cu(II) (solid line) and Zn(II) (dashed line) complexes in equimolar solutions. (The KOH consumption by the excess of strong acid has been subtracted from the total amount of KOH.) $c_L = 0.004$ M.

constants and pK values of ENDIP are collected in Table 1. The pK of one of the pyridine nitrogens could not be calculated. This donor group is almost fully deprotonated at the beginning of the titrations. In the presence of metal ions the shape of the titration curves change considerably. Only one, very steep equivalence point can be seen at the addition of four equivalents of base, indicating the simultaneous deprotonation and coordination of the four donor groups.

In the Cu(II)-ENDIP system, the stability constants of the complexes formed in solution could not be determined from the pH-metric titration data, because the complex formation was almost complete at the starting pH (~ 1.8) of the titrations. The stability constants were determined from UV-spectrophotometric measurements. Spectra were recorded in 5×10^{-5} M equimolar solutions of Cu(II) and ENDIP in the 0.9–1.6 pH range. The pH of the solutions (necessary for the calculations) was calculated from the concentration of the strong acid added to the system to reach the desired pH value. This could be done, because at the very low ligand concentrations employed in these measurements the concentration of the protons resulting from the dissociation of the ligand was negligible as compared with that of the strong acid present. From these titration curves the formation constants of the species H_3L and ML were determined. These constants were considered as known values and were fixed during the evaluation of the pH-metric titration data. The speciation model obtained and the stability constants of the detected species are listed in Table 1. The speciation curves calculated for equimolar solution are depicted in Fig. 3.

In equimolar solution and also at ligand excess only mono complexes are formed. The ML species is the only complex in the pH range 2–8. This is supported by spectrophotometric and EPR measurements too, when the same spectra can be seen from the slightly acidic to the neutral pH range. According to the above discussion about the titration curves measured in the presence of metal ions, a tetradentate coordination of ENDIP can be assumed in the ML complex. This type of coordination is supported by both the isotropic ($g_o = 2.093$, $A_o = 71.5$ G) and anisotropic ($g_{xx} = 2.059$, $g_{yy} = 2.029$ $g_{zz} = 2.213$, $A_{xx} = 10$ G, $A_{yy} = 29$ G, $A_{zz} = 172$ G) EPR parameters measured at 298 K and 77 K respectively, for this complex. Unfortunately nitrogen super hyperfine structure is not resolved but the strong ligand field caused by the four equatorially coordinated nitrogen donor atoms resulted in a very low g and high copper coupling values. The rhombic g- and A-tensors indicate a distorted geometry of the complex, where the four donor groups from the equatorial position are not in one plane. This can explain the fact that the λ_{max} calculated for this species assuming a $\{2\times N_{amino}, 2\times N_{aromatic}\}$ type of coordination (570 nm)[21] is rather different from the measured value (615 nm). The proposed structure is depicted in Scheme 2.

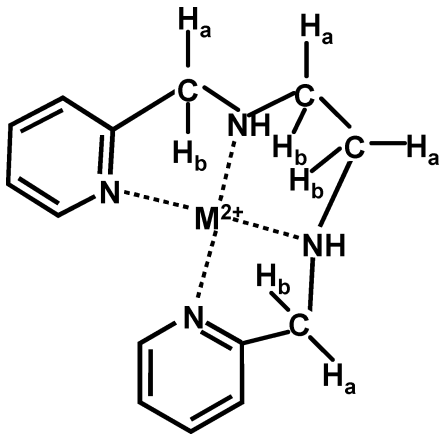

Scheme 2 Proposed binding mode of the ML complexes formed with ENDIP.

Above pH 8 the MLH_{-1} complex is formed, which should be a mixed hydroxo complex. A considerable red shift of the λ_{max} (from 615 to 649 nm) suggests the deprotonation of a coordinated water

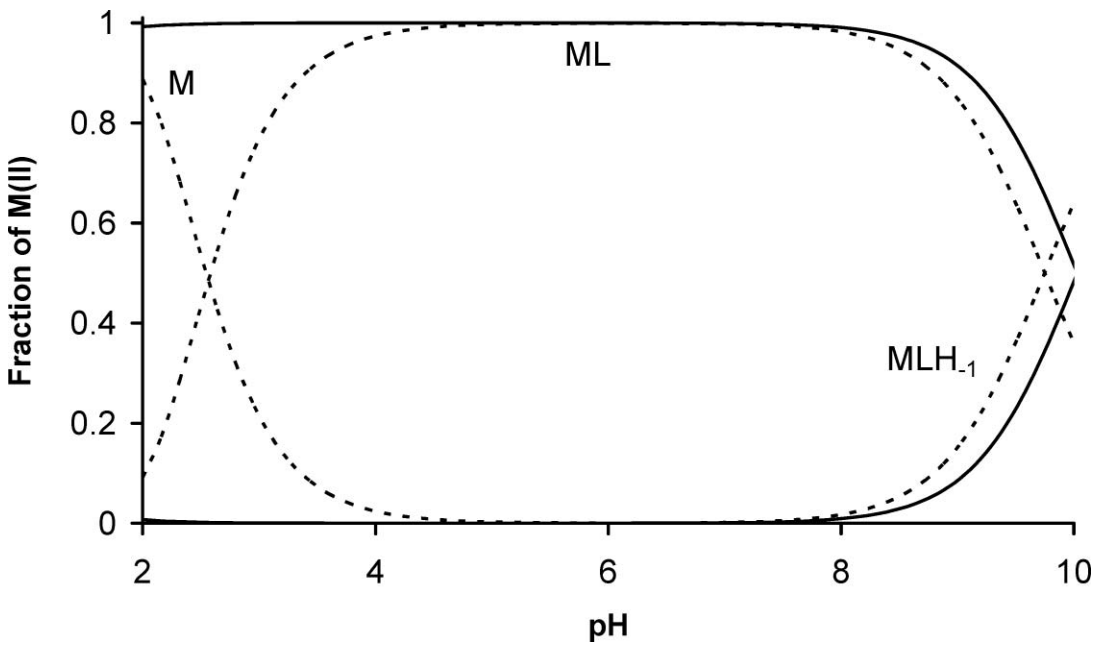

Fig. 3 Speciation curves calculated at 1 : 1 molar ratios in the Cu(II)-ENDIP (solid lines) and Zn(II)-ENDIP (dashed lines) systems; $c_L = 0.004$ M.

molecule from an axial position, in this complex. According to the red shift, decreasing ligand field in the equatorial plane can be observed in the EPR parameters as well. In comparison with ML a small increase in g (isotropic $g_o = 2.105$, and anisotropic $g_{xx} = 2.042$, $g_{yy} = 2.042$ $g_{zz} = 2.235$) and decrease in A values (isotropic $A_o = 63.5$ G, and anisotropic $A_{xx} = 16$ G, $A_{yy} = 16$ G, $A_{zz} = 170$ G) agree with the assumption of an axially coordinated water molecule. This coordination possibly leads to a less distorted equatorial plane as the g- and A-tensor of this mixed hydroxo complex could be described with axial symmetry.

In order to confirm the pH-metric speciation results the EPR spectra of the Cu(II)-ENDIP system were recorded at 298 K in a flow system (see Fig. 4). The EPR titration was carried out under an argon atmosphere. The concentration was identical with that of the pH-potentiometric measurements. The EPR spectra could be perfectly deconvoluted into two species ML and MLH^{-1}. The measured (full line) and calculated (dashed line) spectra show good agreement in the whole pH range 1.7 to –11.4.

Similarly to DMAP, complex formation with Zn(II) starts at a higher pH than with Cu(II) and the stability of the Zn(II)-complexes is a few orders of magnitude lower. The speciation model (Fig. 3) is very similar to that obtained with Cu(II) and the complexes more likely have similar coordination modes. At physiological pH the ML complex is solely formed in the system both in the case of Cu(II) and Zn(II).

In order to confirm our potentiometric results ^{1}H NMR spectroscopic measurements were performed. Fig. 5 shows the spectra recorded in the 4–8 pH range. Spectrum (a) is that of the free ligand at pH 4. Due to the symmetry of the molecule the spectrum is similar to the spectrum of DMAP (Fig S1a†). The signal assignment was made on the basis that TPEN, which has two additional picolyl rings but a symmetrical structure thus gives a very similar ^{1}H spectrum.[24] In the aliphatic region the signal at higher chemical shift values is assigned to the methylene groups bound to the aromatic ring, (Ar-)CH_2, while that at lower ppm to the ethylene protons, CH_2-CH_2. In the aromatic region the typical spectrum pattern of pyridine derivatives can be seen. Due to the electron-attracting effect of the pyridine nitrogen the α protons have the lowest shielding, thus their signal appears at the lowest fields. The asymmetric electron distribution on the pyridine ring (which is enhanced by the presence of the substituent in the *ortho* position) causes a low electron density around the γ protons lower than around those in the β position. This means that the former will give a signal at lower fields than the β protons.

The spectra recorded in equimolar solutions of Zn(II) and ENDIP are very different from that of the free ligand. In the aliphatic region instead of two singlets several doublets appear. Two sets of four signals can be identified: well resolved doublets marked with A, while the broader and lower intensity signals marked with B. The ratio of A and B signals is

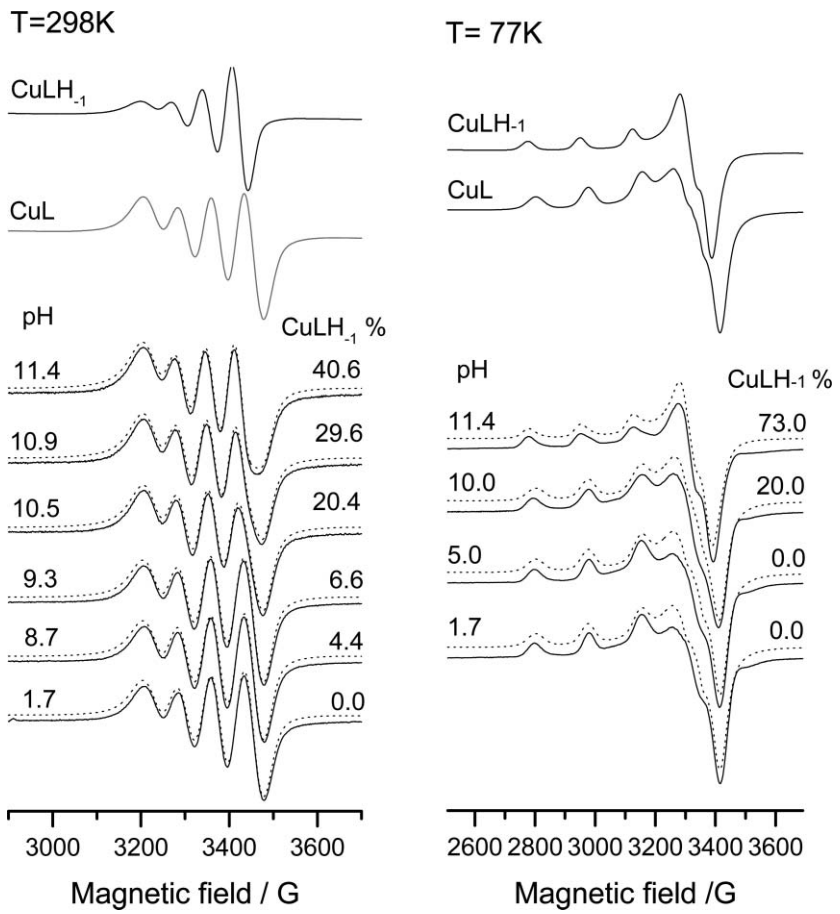

Fig. 4 Experimental (—) and simulated (---) spectra recorded in the Cu(II)-ENDIP equimolar system at different pH values, and the component spectra of CuL and $CuLH_{-1}$ obtained from the deconvolution of the measured spectra.

Table 2 Signal assignment of the two complexes formed in the Zn(II)-ENDIP system at neutral pH

	Chemical shift (ppm)							
	$(NH\text{-})CH_2$		$(Ar\text{-})CH_2$		α	β1	β2	γ
Complex A	2.345	2.913	4.019	4.420	8.602	7.547	7.470	8.043
Complex B	2.500	3.149	3.706	4.472	8.602	7.547	7.470	8.105

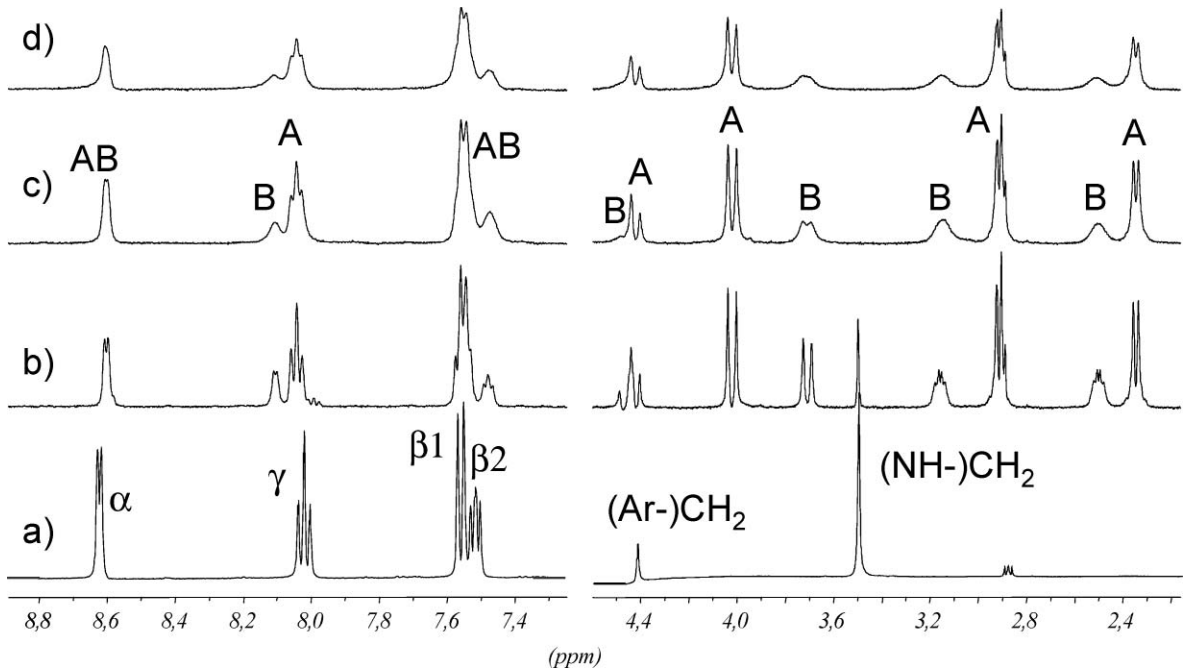

Fig. 5 ^{1}H NMR spectra recorded in (a) solution of ENDIP alone, pH = 4 and solutions of Zn(II)-ENDIP = 1 : 1.1 at different pH values: (b) pH = 4; (c) pH = 6; (d) pH = 7.4; c_L = 0.004 M.

1 : 0.5 and is kept in the entire pH range from 4 to 8. This suggests the presence of two complexes in this pH range. The only difference in the spectra recorded at different pH values is that the signals became broader with increasing pH, due probably to faster ligand exchange processes between the two complexes.

The ^{1}H COSY spectrum recorded at pH 6 shows that pairs of these doublets couple with each other (Fig S2†). The assignment of the peaks based on this 2D measurement is listed in Table 2. This should mean that the geminal protons of the methylene groups, H_a and H_b become magnetically non-equivalent upon coordination, whereas the two methylene groups of each type $(Ar\text{-})CH_2$ and $CH_2\text{-}CH_2$ are in the same chemical and magnetic environment. This presumes a rigid but symmetric structure of these complexes. Similar splitting of the resonances of the geminal protons from the side-arm methylene groups but not from the ethylene group was observed in the case of the Zn(II) complex of TPEN.[23,24] A possible coordination mode which can lead to this spectrum pattern is the tetradentate coordination of ENDIP depicted in Scheme 2. This may be the structure of one of the complexes. The question is what is the other complex?

Although potentiometric data showed only formation of 1 : 1 complexes we tested this phenomenon also by NMR spectroscopy. The spectra taken at pH 6 at different metal to ligand ratios are depicted in Fig. 6. The pattern of these spectra is very similar and integration of the peaks revealed a ratio of 1 : 0.5 between signals A and B at all metal–ligand ratios. This indicates that both complexes are 1 : 1 species.

We also attempted to test whether there is a monomer–dimer (or oligomer) equilibria in solution. Spectra recorded at pH 6 in 1 : 1.1 molar ratio Zn(II)-ENDIP solutions at different concentrations are shown in Fig. 7. Broadening of the signals with increasing concentrations can be observed, but the ratio between the resonances marked with A and those marked with B remains 1 : 0.5 at all concentrations. Thus, these results do not prove the formation of oligomeric species in this system.

According to the NMR results, the two complexes present at slightly acidic and neutral pH are most probably coordination isomers of the ML species. Since our attempts to crystallize these complexes failed, we can only speculate on their structure. However, one of these isomers is more likely to have a tetradentate coordination with all nitrogens in the equatorial position (Scheme 2), which was also proven in the case of the ML complex formed with Cu(II). Another possibility might be coordination with the two amino nitrogens bound equatorially and the two picolyl rings axially. This represents a different structure because the four nitrogens are not in the same plane, but it is still symmetric.

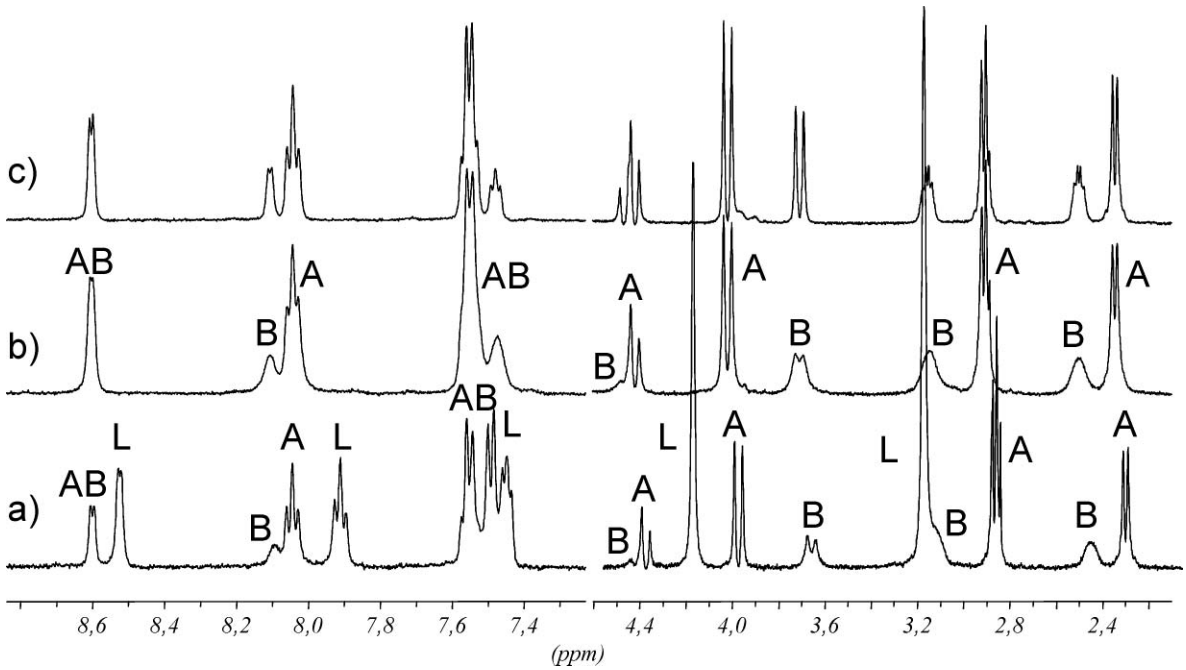

Fig. 6 ^{1}H NMR spectra recorded at pH 6 in Zn(II)-ENDIP solutions at different metal to ligand ratios: (a) Zn(II):ENDIP = 1 : 2; (b) Zn(II):ENDIP = 1 : 1; (c) Zn(II):ENDIP = 2 : 1; = 0.004 M.

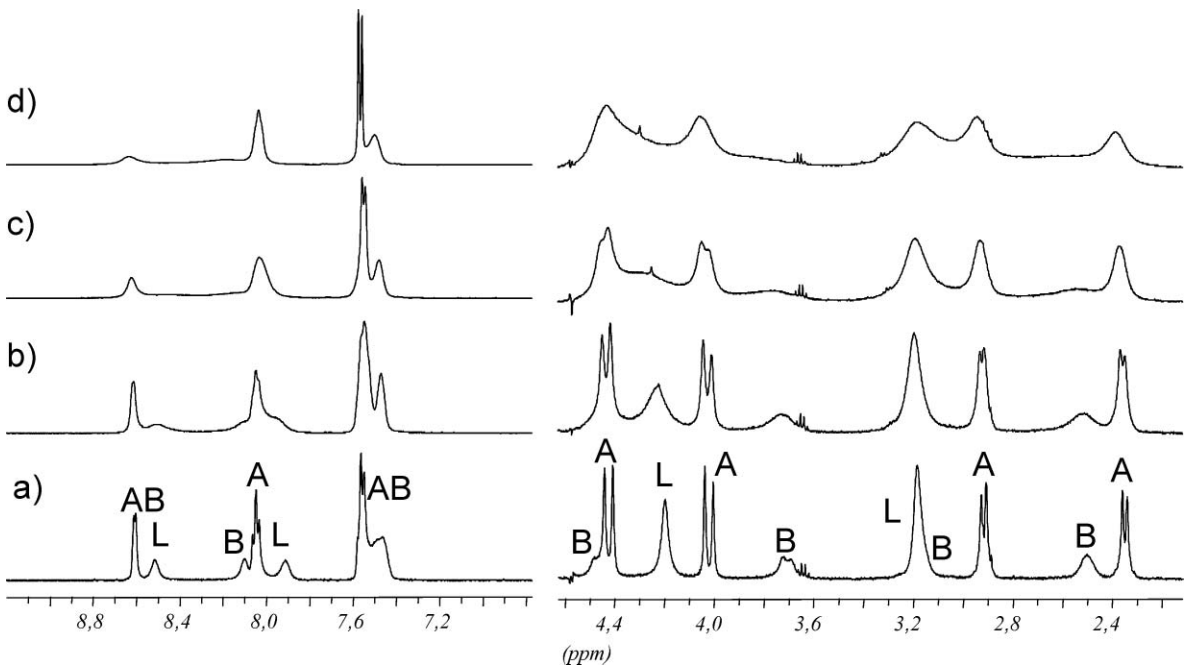

Fig. 7 ^{1}H NMR spectra recorded at pH 6 in equimolar Zn(II)-ENDIP solutions at different concentrations: (a) 0.004 M; (b) 0.01 M; (c) 0.05 M; (d) 0.1 M.

Effect of the chelators on the metal-induced aggregation of Aβ revealed by fluorescence measurements

Fluorescence measurements were based on detection of the intrinsic fluorescence of Aβ, namely, the fluorescence of the single tyrosine residue: Tyr10. The experiments were carried out with the peptide Aβ(1–40).

It is known from the literature,[25] that Cu(II) bound to Aβ quenches the fluorescence of Tyr10, which is very close to the metal binding site of the peptide (His6, His13, His14). Thus, the efficacy of the chelators on binding Cu(II) in the presence of Aβ can be monitored by their effect on the Cu(II)-induced fluorescence quenching.

Solutions containing 44 μM Aβ(1–40), equimolar amount of Cu(II) and Aβ(1–40) and chelator in different concentrations were prepared in HEPES buffer, pH 7.4. Fluorescence of the solutions was measured at an excitation wavelength of 280 nm and emission was recorded in the 290–350 nm range. Taking the value of the

maximum fluorescence intensity at 312 nm, for each sample, Fig. 8 was constructed. In the presence of Cu(II) the intrinsic fluorescence intensity of Aβ(1–40) is reduced by ~55%. Addition of DMAP to the solutions had no effect on the fluorescence quenching caused by Cu(II), indicating that DMAP can not compete with Aβ for the metal ion. When half equivalent (22 μM) of ENDIP was added, a significant increase on the Tyr10 fluorescence was observed. In the presence of one equivalent of ENDIP ~ 90% of the initial Aβ fluorescence was recovered. This means that ENDIP is able to displace Aβ(1–40) from the coordination

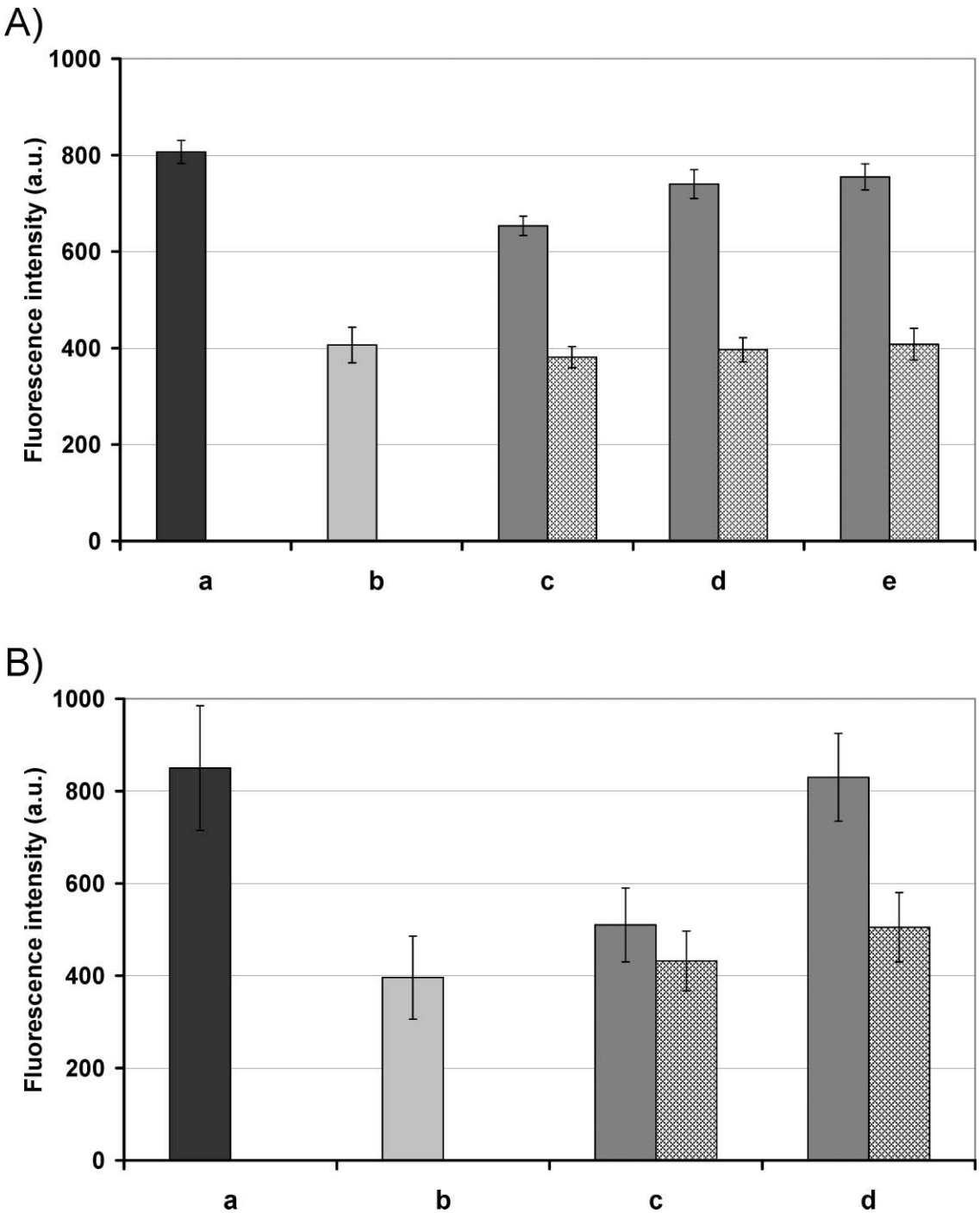

Fig. 8 Changes on Tyr10 fluorescence intensity in the presence of metal ions and chelators. (A) Fluorescence measured in the presence of Cu(II) of the solutions: (a) Aβ(1–40); (b) Aβ(1–42) and equimolar amount of Cu(II); (c) Aβ(1–42), Cu(II) and half equivalent of chelator: ENDIP (middle gray) and DMAP (patterned); (d) Aβ(1–42), Cu(II) and one equivalent of chelator: ENDIP (middle gray) and DMAP (patterned); (e) Aβ(1–42), Cu(II) and two equivalents of chelator: ENDIP (middle gray) and DMAP (patterned); $c_{A\beta} = 44$ μM. (B) Fluorescence measured in the presence of Zn(II) of the solutions: (a) Aβ(1–40); (b) Aβ(1–42) and equimolar amount of Cu(II); (c) Aβ(1–42), Cu(II) and one equivalent of chelator: ENDIP (middle gray) and DMAP (patterned); (d) Aβ(1–42), Cu(II) and five equivalent of chelator: ENDIP (middle gray) and DMAP (patterned); $c_{A\beta} = 44$ μM.

sphere of Cu(II) and thus it is an efficient chelator for this metal ion.

The effect of Zn(II) on the intrinsic fluorescence of Aβ is rather controversial. An increase in Tyr10 intensity upon addition of Zn(II) to Aβ solutions with a poor reproducibility was observed by some authors.[24,25] Using continuous stirring, Tougu *et al*.[12] measured a slight decrease in Aβ fluorescence in the presence of Zn(II) and a better reproducibility of the experimental data was obtained. They also detected a time-dependent decrease in the intrinsic fluorescence of the Zn(II)-Aβ solutions which was not observed in the case of Cu(II). This was explained by the fact, that the initially formed low-affinity Zn(II)-Aβ(1–40) complex (K_D = 60 μM) was transformed/aggregated in time to a higher affinity complex with $K_D = 2$ μM, determined after 30 min incubation.

When we measured directly the effect of Zn(II) and the chelators on the intrinsic fluorescence of Aβ(1–40), the intensity changes were too small and the reproducibility was very poor to draw any conclusion. Thus, to assess the efficacy of our chelators we combined the protocol of Raman *et al*.[24] and Sengupta *et al*.[26] Solutions containing 44 μM Aβ(1–40), equimolar amounts of Zn(II) and Aβ(1–40) and different concentrations of chelator were prepared in HEPES buffer, pH 7.4. The solutions were kept at 37 °C in the dark for 2 h to allow aggregation. After 2 h the solutions were centrifuged at 13000 g to remove highly aggregated species. The fluorescence of the remained soluble Aβ(1–40) was measured on the supernatants. Fig. 8 clearly shows that the amount of the soluble Aβ(1–40) was considerably low in the presence of Zn(II) as compared to the solution of Aβ(1–40) alone. This demonstrates the accelerating effect of Zn(II) on Aβ aggregation. ENDIP present in the solution lowered the Zn(II)-induced aggregation by chelating the metal ion. At a five fold excess of ENDIP to Zn(II) and Aβ(1–40) the same fluorescence intensity was measured as in the case of Aβ(1–40) alone. DMAP has again no significant effect on the Zn(II)-induced aggregation of Aβ(1–40).

Dynamic Light Scattering (DLS) measurements

In order to corroborate our fluorimetric results, DLS measurements were also carried out. DLS is a well established technique for measuring the size of small particles in solution, typically in the submicron region. With DLS the hydrodynamic diameter (d_H) of a given particle can be determined as described in the Experimental section. In these experiments, the so-called iso-Aβ(1–42) peptide[27] was used, which is a structurally modified derivative of the native human amyloid peptide. The structural modification, where Gly[25] is linked to the side chain of Ser[28] through an ester bond, makes the structure of the monomeric form bent, whereby an enhanced solubility of the peptide can be achieved at acidic pH. The peptide rearranges *via* an intramolecular O→N acyl-shift into the native form at physiological pH and aggregates readily into low-n oligomers in a short time-course. The population of the low-n oligomers is proven to be outstandingly stable without the disturbance of extrinsic effects, such as administration of chelating ions, change of ionic strength of the medium, or application of preformed fibrils as seeds.

The change in the Aβ size (d_H) over time was measured in 50 μM iso-Aβ(1–42) solutions with and without addition of metal ions and chelators (Fig. 9). In the sample containing only Aβ(1–42) (+)

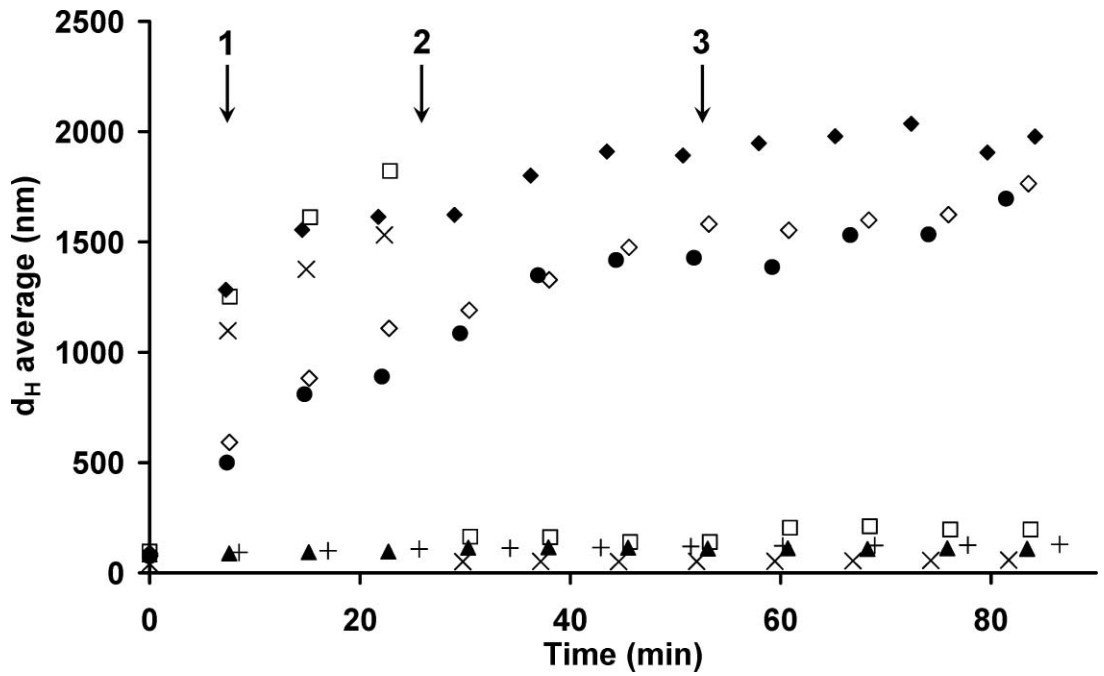

Fig. 9 Time-dependent changes of the hydrodynamic diameter of Aβ(1–42) in different conditions: + Aβ(1–42); ◇ Aβ(1–42) and one equivalent of Zn(II) added after the first measurement point (arrow 1); ◆ Aβ(1–42) and one equivalent of Zn(II) added after the first measurement point (arrow 1) and addition of 2.5 equivalent of ENDIP indicated by arrows 2 and 3; □ Aβ(1–42) and one equivalent of Zn(II) added after the first measurement point (arrow 1) and addition of 5 equivalents of ENDIP indicated by arrow 2; ▲ Aβ(1–42) and 5 equivalents of ENDIP added after the first measurement point (arrow 1) and addition of one equivalent of Zn(II) indicated by arrow 2; ● Aβ(1–42) and one equivalent of Zn(II) added after the first measurement point (arrow 1) and addition of 5 equivalents of DMAP indicated by arrow 2; × Aβ(1–42) and one equivalent of Cu(II) added after the first measurement point (arrow 1) and addition of 5 equivalent of ENDIP indicated by arrow 2; $c_{Aβ} = 50$ μM.

d_H of the peptide did not change during the time of the experiment (~ 2 h), which means that no considerable aggregation occurred. When metal ions were added to the iso-Aβ(1–42) solution (after the first measurement) a significant increase in d_H could be observed (◆, ×), proving that Cu(II) and Zn(II) could promote Aβ precipitation. As expected from the fluorescence measurements, the addition of DMAP (●) had no effect on the particle size. In contrast, ENDIP applied in five fold excess lowered d_H back to its initial value in the case of both metal ions (□, ×). However, application of a five fold excess of ENDIP in two steps gradually (2.5 fold excess each) could not influence the Zn(II)-induced precipitation of Aβ (◆). This may be explained by some kinetic reasons: the ENDIP added in 2.5 fold excess at the beginning is not enough to successfully compete with Aβ for Zn(II). As the aggregation is progressing the Zn(II) will probably become less accessible for the chelator and after 23 min the next 2.5 equivalent of ENDIP (now totally 5 equivalent) is not able any more to displace Zn(II) and redissolve the precipitate. When ENDIP was added to the peptide solution prior to Zn(II) it was able to hinder the Zn(II)-induced precipitation of Aβ, since no increase in d_H was observed (▲).

From these data we can conclude that ENDIP is able to prevent the metal-induced aggregation and to resolubilise Aβ. For this—in our experimental conditions—a five fold excess over the peptide was necessary.

Conclusions

From among the two ligands ENDIP seems to be a good candidate as a metal-protein attenuating compound for the therapy of AD. It forms a very stable ML-type complex at pH 7.4 with both Cu(II) and Zn(II) through tetradentate coordination. With Zn(II) two coordination isomers were detected by NMR spectroscopy. The dissociation constants calculated from the overall stability data are K_D(Cu) = 3.98 pM and K_D(Zn) = 0.6 μM. Faller and Hureau[11] in their critical review estimated the optimal stability of a metal ion chelator to be used in AD therapy. Such a molecule should be strong enough to compete with Aβ, but not too strong to withdraw metal ions from essential metalloproteins. Thus, for Cu(II) they suggested a K_D of ~ 1 pM and for Zn(II) around 1–10 μM. ENDIP more or less fulfils the desired conditions for both Zn(II) and Cu(II). Indeed, our fluorescence and DLS measurements show that ENDIP is able to displace Aβ from its metal complexes and resolubilise the peptide. This means that the optimal K_D values proposed by Faller and Hureau[11] may represent a good estimation. Thus, ENDIP is not expected to perturb the activity of essential metalloproteins. This of course has to be proven by further biological measurements.

Experimental

Compounds

Methylamine, ethylenediamine. 2-pyridinecarboxaldehyde and sodium borohydride used for the synthesis of the ligands were Aldrich products. DCC, *N*,*N*-diicyclohexyl-carbodiimide; DCM, dichloromethane; DIEA, *N*,*N*-diisopropylethylamine; DMF, *N*.*N*-dimethylformamide; HATU, 2-(1*H*-azabenzotriazol-1-yl)-1,1,3,3-tetramethyluronium hexafluorophosphate; HOAt, 1-hydroxy-7-azabenzotriazole; HOBt, 1-hydroxybenzotriazole; Fmoc (fluorenyl-methoxycarbonyl-) and Boc- (*t*-butyloxy-carbonyl) amino acids were purchased from GLBiochem Ltd, Shanghai, PRC. The β-amyloid 1-40 peptide (Aβ(1–40)) was a product of EzBiolab (USA). Iso-Aβ (1–42) was synthesized by our group as given above.

The pH-metric titrations were performed with 0.2 M KOH solution prepared from KOH pellets (Fluka) and 0.2 M HCl solution diluted from 36 (m m^{-1})% HCl (Aldrich). The 0.1 M metal ion solutions were prepared from copper(II) chloride and zinc(II) chloride (Aldrich) and their concentrations was determined gravimetrically *via* the oxinates.

Synthesis of the ligands

A literature search for preparation of the ligands showed that DMAP has been prepared mostly from the reaction of the corresponding 2-methylene chloride derivative of pyridine and methylamine,[29,30] while ENDIP through the Schiff base reaction of the corresponding pyridine-aldehyde and ethylenediamine followed by the reduction of the double bond.[31] Having experience in the latter preparation procedure the Schiff base reaction[32] was used in preparation of both ligands.

***N*-methyl-1-(pyridine-2-yl)-methane amine.** 5 g (0.05 mol) of 2-pyridinecarboxaldehyde was dissolved in 25 cm^3 methanol during continuous stirring in an aqueous bath; 6.5 cm^3 (0.14 mol) methylamine was added drop wise to the solution. The reaction mixture was stirred over 180 min and the completeness of the reaction was checked by GC-MS. The obtained Schiff-base was reduced with sodium borohydride (added slowly, in small portions to the solution of the Schiff-base) to obtain the final product. The solution of the reduced Schiff-base was concentrated in a rotary evaporator and the Schiff-base was extracted with 5 × 20 cm^3 toluene under basic conditions (10% sodium-hydroxide). The toluene phase was dried over magnesium sulfate and the solvent was evaporated to obtain the solid product. The dried material was dissolved in isopropanol, and hydrochloric acid was added in order to transform it in a hydrochloride salt, which was recrystallised from 96% ethanol and dried under vacuum. The product was identified by ESI-MS and NMR spectroscopy. The ESI-MS spectrum shows a base peak at m/z = 123.3 $[M+H]^+$ which agrees well with the calculated monoisotopic mass of DMAP, 122.08. Chemical shifts and assignment of the signals in the ^{1}H NMR spectrum are: 2.79 ppm (CH_3), 4.38 (CH_2), 7.50 (β2), 7.54 (β1), 7.94 (γ) and 8.61 (α).

***N*^{1},*N*^{2}-bis(pyridine-2-yl-methyl)ethane-1,2-diamine.** 10 g (0.093 mol) of 2-pyridinecarboxaldehyde was dissolved in 25 cm^3 methanol during continuous stirring in an aqueous bath (3 days). Then 6.9 cm^3 (0.10 mol) ethylenediamine was added dropwise to the solution. The obtained Schiff-base was reduced with sodium borohydride, which was added in small portions to the mixture in excess. The solution of the reduced Schiff-base was brought to dryness. 10% hydrochloric acid was added to the solution in order to decompose the remaining sodium borohydride. After addition of 10% sodium-hydroxide, the product was extracted with 5 × 20 cm^3 toluene and was dried over magnesium-sulfate for one day. The solvent was evaporated to obtain the solid product. Upon addition of 30 (m m^{-1})% hydrochloric acid in isopropanol to the

crude amine, small, white crystals appeared. The crystals were filtered, dried, recrystallized from isopropanol and finally dried under vacuum. The product was identified by ESI-MS and NMR spectroscopy. The calculated monoisotopic mass: 242.15, which agrees with the ESI-MS data: m/z = 243.3 $[M+H]^+$. Chemical shifts and assignment of the signals in the ^1H NMR spectrum are: 3.54 ppm (CH_2-CH_2), 4.48 (2×(Ar-)CH_2), 7.60 (2×β2), 7.64 (2×β1), 8.07 (2×γ) and 8.63 (2×α).

Synthesis of iso-Aβ(1–42). The synthesis of iso-Aβ(1–42) will be discussed in details elsewhere, briefly: The peptide was synthesized using Boc-chemistry on a Boc-Ala-PAM resin. Acylation of the α-amino groups were done by activating a three fold excess of N^{α}-Boc protected amino acids - or 2-Cl-*Z*-Ser(OtBu)-OH for position 26 - with DCC/HOBt in DCM–DMF (1 : 1) and the peptide resin was reacted with this mixture for 2 h. The coupling was repeated with DCC/HOAt activation, if it was indicated by the qualitative ninhydrin test. Boc and tBu groups were removed by treating the resin with 50% TFA/DCM mixture twice (5+25 min). Neutralization was done with 5% DIEA/DCM (2 × 1 min). Esterification of the hydroxyl group of Ser[28] with Boc-Gly-OH was done by treating the peptide-resin with Fmoc-Gly/DCC/NMI (10-fold excess) in DCM–DMF (3 : 1) for 2 × 4 h.

The peptide was cleaved from the resin with a mixture containing HF (10 ml), anisole (0.2 ml), dimethyl sulfide (DMS; 0.8 ml) and dithiothreitol (DTT; 0.1 g) at 0 °C for 45 min. The crude product was precipitated and washed with diethyl-ether, dissolved in 50% acetic acid/water, lyophilized and purified by HPLC.

Potentiometric measurements

The stability constants of the proton and metal complexes of the ligands were determined by pH-potentiometric titrations of 20 ml samples. The ligand concentrations were 0.004 M and 0.002 M and metal ion to ligand ratios of 1 : 1, 1 : 2 and 1 : 4 were used. The titrations were performed with 0.2 M carbonate-free KOH solution of known concentration under a purified argon atmosphere, using an automatic titration set including a PC controlled Dosimat 665 (Metrohm) autoburette. The ionic strength of all the solutions was adjusted to 0.2 M KCl and the samples were thermostatted at 25.0 ± 0.1 °C. Duplicate titrations were performed. The reproducibility of the titrations was within 0.005 pH unit. The pH was measured with a Orion 710A precision digital pH-meter and a Metrohm Micro pH glass electrode, which was calibrated for hydrogen ion concentration according to Irving *et al*.[33] The complex formation was characterized by the following general equilibrium process:

$$pM + qL + rH = M_pL_qH_r$$

where M denotes the metal ion and L the non-protonated ligand molecule. Charges are omitted for simplicity. The corresponding concentration stability constants $\beta_{pqr} = [M_pL_qH_r]/[M]^p[L]^q[H]^r$ were calculated using the PSEQUAD computer program.[34]

Spectrophotometric measurements

UV-Vis spectra were measured on a Hewlett Packard 8452A diode array spectrophotometer. The metal ion concentration was 5.3 × 10^{-3} M for the visible spectra and 1 : 1 and 1 : 2 metal–ligand ratios were used. In the case of UV-spectrophotometric measurements an ENDIP concentration of 5 × 10^{-5} M were employed. The experiments were performed in a 1 cm cell. The individual spectra of the copper(II) complexes were calculated by the computer program PSEQUAD.[34]

NMR experiments

^1H and ^1H-COSY NMR measurements were performed on a Bruker Avance DRX 500 spectrometer. The chemical shifts δ were measured with respect to DSS as internal reference. The ligand concentrations of 0.004, 0.01, 0.05 M and metal–ligand ratios of 1 : 1, 1 : 2 and 2 : 1 were used. Measurements were made in D_2O and H_2O–D_2O (9 : 1).

EPR measurements

The EPR spectra were recorded at 291 K in a circulating system using a BRUKER EleXsys E500 spectrometer. The EPR titrations were carried out in 8 cm^3 solution under argon atmosphere. The concentrations were identical with the potentiometric measurements. NaOH solution was added to the sample to adjust the chosen pH. A MASTER-FLECX CL peristaltic pump ensured the circulation of the solution through the capillary tube in the cavity. The EPR spectra were recorded after 2 min equilibration at the chosen pH. For several pH's 100 μl of sample were taken out from the stock solution and measured in a Dewar containing liquid nitrogen (77 K). 30 μl of methanol was added to avoid water crystallisation. For all the measurements the microwave frequency 9.51 GHz, microwave power 12 mW, modulation amplitude 5 G and modulation frequency 100 kHz were used.

All recorded EPR spectra were simulated with a spectrum decomposition method by the EPR[30] computer program. Isotropic (g_o and A_o copper coupling and linewidth parameters) or anisotropic ($g_{\parallel}$, $g_{\perp}$, $A_{\parallel}$, $A_{\perp}$ copper couplings, and magnetic field dependent linewidth) parameters were fitted in order to reduce the average square deviation between the experimental and the calculated spectrum. Since the copper(II) used in the solutions was a natural mixture of the isotopes, the spectrum of each species was calculated as the sum of spectra containing ^{63}Cu and ^{65}Cu in their natural abundances. The details of the analysis were published previously.[35]

Fluorescence measurements

Fluorescence measurements were performed on a Hitachi F-4500 fluorescence spectrophotometer equipped with a 150 W xenon light source, with an assay volume of 0.5 ml. Excitation wavelength was set at 280 nm and spectra were recorded in the 290–350 nm range, with excitation and emission slit width of 5 nm. For sample preparation 1 mg Aβ(1–40) peptide was dissolved in 2 ml 0.02 M HEPES buffer and was ultrasonicated for 10 min. Aliquots of this stock solution were mixed with solutions of Zn(II), Cu(II) and chelator to obtain the desired working concentrations and ratios.

DLS measurements

Iso-Aβ was dissolved in MilliQ ultrapure water to a concentration of 500 μM (2.5 mg ml^{-1}) and sonicated for 5 min. The solution was diluted in artificial cerebrospinal fluid buffered with HEPES instead of $NaHCO_3/CO_2$ as the carbogene buffer disturbs the light scattering measurements (constitution of the buffer: 25 mM

HEPES, 125 mM NaCl, 2 mM KCl, 12 mM D-glucose, 2 mM $MgCl_2$, 2 mM $CaCl_2$, pH 7.4) to a final peptide concentration of 50 μM and filtered through a syringe filter equipped with a 0.1 μm pore size PVDF membrane (Millex, Millipore Ireland, Carrigtwohill, Ireland) in order to remove the interfering dust particles.

Prior to the measurements, 0.1 M metal stock solutions of known concentrations were diluted with MilliQ water to get a working solution with a concentration of 500 μM. Working solutions of the examined chelators were similarly prepared: materials were dissolved in MilliQ water to a concentration of 500 μM (in the case of 1 : 1 molar ratio for metal and chelator), or 2.5 mM (in the case of 1 : 5 molar ratio).

All experiments were performed at 25 °C with a Malvern Zetasizer Nano ZS Instrument (Malvern Instruments Ltd. Worcestershire, UK) equipped with a He–Ne laser (633 nm) applying the Non-Invasive Back Scatter (NIBS®) technology, which means detection of the scattered light at an angle of 173°. The translational diffusion coefficients were obtained from the measured autocorrelation functions using the regularization algorithm CONTIN built in the software package Dispersion Technology Software 4.0 (Malvern Instruments Ltd. Worcestershire, UK). Assuming the scattering particles as hard spheres, their apparent hydrodynamic diameter can be calculated from the diffusion parameters by using the Stokes–Einstein equation $d_H = k_B T/(3\pi\eta D_T)$, where k_B is the Boltzmann constant, T is the absolute temperature, η is the viscosity of the medium and D_T is the translational diffusion coefficient. Samples were prepared as given above. Correlation function and distribution of the apparent hydrodynamic diameters (d_H) over the scattered intensity of the samples were monitored according to the following schedule: the DLS instrument was programmed to execute 12 measurements consecutively with 5 min delays in each case. Measurements were conducted either without disturbing the aggregating system (upon the examination of the aggregation of pure Aβ), or aliquots of the working solutions were added between two measurements, routinely after the first and fourth measurements by pipetting a calculated amount of the stock solution carefully into the cell without removing it from the instrument. Control measurements were conducted without the administration of iso-Aβ in each experimental set-up, in order to determine the effect of the working solutions on the scattering intensity. It was found, that the working solutions were able to raise the scattering intensity of the vehicle only to a negligible amount (generally about 1% of the experienced total scattering intensity derived from the measurements with iso-Aβ), therefore their effect on the measurement could be neglected.

Abbreviations

AD	Alzheimer's disease
Aβ	β-amyloid peptide
Boc	*t*-butyloxycarbonyl
DLS	dynamic light scattering
DCC	*N*,*N*-diicyclohexyl-carbodiimide
DCM	dichloromethane
DIEA	*N*,*N*-diisopropylethylamine
DMF	*N*,*N*-dimethylformamide
ESI-MS	electrospray ionization mass spectrometry
Fmoc	9-flourenylmethyloxycarbonyl
HATU	2-(1*H*-azabenzotriazol-1-yl)-1,1,3,3-tetramethyluronium hexaflourophosphate
HOAt	1-hydroxy-7-azabenzotriazole
HOBt	1-hydroxybenzotriazole

Acknowledgements

This work was supported by the National Office for Research and Technology (DNT Subprogram 1) and the Hungarian Scientific Research Found (OTKA NI61786). A.L. and L.F. wish to thank the Hungarian Academy of Sciences for the support of the János Bolyai Research Grant.

References

1 D. J. Selkoe, *Science*, 2002, **298**, 789–791.
2 J. Hardy and D. Selkoe, *Science*, 2002, **297**, 353–356.
3 A. I. Bush, *J. Alzheimers Dis.*, 2008, **15**, 223–240.
4 M. A. Lovell, J. D. Robertson, W. J. Teesdale, J. L. Campbell and W. R. Markesbery, *J. Neurol. Sci.*, 1998, **158**, 47–52.
5 E. Gaggelli, H. Kozlowski, D. Valensin and G. Valensin, *Chem. Rev.*, 2006, **106**, 1995–2044.
6 J. D. Robertson, A. M. Crafford, W. R. Markesbery and M. A. Lovell, *Nucl. Instrum. Methods Phys. Res., Sect. B*, 2002, **189**, 454–458.
7 A. I. Bush, *Neurobiol. Aging*, 2002, **23**, 1031–1038.
8 J. Y. Lee, T. B. Cole, R. D. Palmiter, S. W. Suh and J.-Y. Koh, *Proc. Natl. Acad. Sci. U. S. A.*, 2002, **99**, 7705–10.
9 D. Noy, I. Solomonov, O. Sinkevich, T. Arad, K. Kjaer and I. Sagi, *J. Am. Chem. Soc.*, 2008, **130**, 1376–1383.
10 J. W. Karr and V. A. Szalai, *Biochemistry*, 2008, **47**, 5006–5016.
11 P. Faller and C. Hureau, *Dalton Trans.*, 2009, 1080–94, and references therein.
12 V. Tougu, A. Karafin and P. Palumaa, *J. Neurochem.*, 2007, **104**, 1249–1259.
13 R. A. Cherny, C. S. Atwood, M. E. Xilinas, D. N. Gray, W. D. Jones, C. A. McLean, K. J. Barnham, I. Volitakis, F. W. Fraser and Y.-S. Kim, *Neuron*, 2001, **30**, 665–676.
14 C. W. Ritchie, A. I. Bush, A. Mackinnon, S. Macfarlane, M. Mastwyk, L. MacGregor, L. Kiers, R. A. Cherny, Q. X. Li and A. Tammer, *Arch. Neurol.*, 2003, **60**, 1685–1691.
15 P. A. Adlard, R. A. Cherny, D. I. Finkelstein, E. Gautier, E. Robb, M. Cortes, I. Volitakis, X. Liu, J. P. Smith, K. Perez, K. Laughton, Q.-X. Li, S. A. Charman, J. A. Nicolazzo, S. Wilkins, K. Deleva, T. Lynch, G. Kok, C. W. Ritchie, R. E. Tanzi, R. Cappai, C. L. Masters, K. J. Barnham and A. I. Bush, *Neuron*, 2008, **59**, 43–55.
16 J.-Y. Lee, J. E. Friedman, I. Angel, A. Kozak and J.-Y. Koh, *Neurobiol. Aging*, 2004, **25**, 1315–1321.
17 A. Dedeoglu, K. Cormier, S. Payton, K. A. Tseitlin, J. N. Kremsky, L. Lai, X. Li, R. D. Moir, R. E. Tanzi, A. I. Bush, N. W. Kowall, J. T. Rogers and X. Huang, *Exp. Gerontol.*, 2004, **39**, 1641–1649.
18 G. Liu, M. R. Garrett, P. Men, X. Zhu, G. Perry and M. A. Smith, *Biochim. Biophys. Acta*, 2005, **1741**, 246–252.
19 T. Storr, L. E. Scott, M. L. Bowen, D. E. Green, K. H. Thompson, H. J. Schugar and C. Orvig, *Dalton Trans.*, 2009, 3034.
20 H. Sigel and R. B. Martin, *Chem. Rev.*, 1982, **82**, 385.
21 E. Prenesti, P. G. Daniele, M. Prencipe and G. Ostacoli, *Polyhedron*, 1999, **18**, 3233–3241.
22 R. M. Smith, A. E. Martell, *Critical Stability Constants*, Vol. 4, Plenum Press, New York, 1976.
23 C. A. Blindauer, M. T. Razi, S. Parsons and P. J. Sadler, *Polyhedron*, 2006, **25**, 513–520.
24 B. Raman, T. Ban, K. Yamaguchi, M. Sakai, T. Kawai, H. Naiki and Y. Goto, *J. Biol. Chem.*, 2005, **280**, 16157–16162.
25 W. Garzon-Rodriguez, A. K. Yatsimirsky and C. G. Glabe, *Bioorg. Med. Chem. Lett.*, 1999, **9**, 2243–2248.
26 P. Sengupta, K. Garai, B. Sahoo, Y. Shi, D. J. E. Callaway and S. Maiti, *Biochemistry*, 2003, **42**, 10506–10513.
27 Y. Sohma, Y. Hayashi, M. Kimura, Y. Chiyomori, A. Taniguchi, M. Sasaki, T. Kimura and Y. Kiso, *J. Pept. Sci.*, 2005, **11**, 441–451.
28 F. Ricchelli, D. Drago, B. Filippi, G. Tognon and P. Zatta, *Cell. Mol. Life Sci.*, 2005, **62**, 1724–1733.

29 E. Zara-Kaczian, Gy. Deák and L. György, *Acta Chim. Hung.*, 1989, **126**, 441–451.
30 M. Stollenz, C. Grosse and F. Meyer, *Chem. Commun.*, 2008, 1744–1746.
31 L. Xu, I. A. Setyawati, J. Pierreroy, M. Pink, V. G. Maren, P. O Brien, S. J. Rettig and C. Orvig, *Inorg. Chem.*, 2000, **39**, 5958; M. Martinho, F. Banse, J. Sainton, C. Philouze, R. Guillot, G. Blain, P. Dorlet, S. Lecomte and J.-J. Girerd, *Inorg. Chem.*, 2007, **46**, 1709.
32 J. Costa Pessoa, S. Marcao, I. Correia, G. Goncalves, A. Dörnyei, T. Kiss, T. Jakusch, I. Tomaz, M. Margarida, C. A. Castro, C. F. G. C. Geraldes and F. Avecilla, *Eur. J. Inorg. Chem.*, 2006, 3595.
33 H. M. Irving, M. G. Miles and L. D. Pettit, *Anal. Chim. Acta*, 1967, **38**, 475–481.
34 L. Zékány, I. Nagypál, G. Peintler, *PSEQUAD for Chemical Equilibria*, Technical Software Distribution, Baltimore 1991.
35 T. Szabó-Plánka, A. Rockenbauer and L. Korecz, *Magn. Reson. Chem.*, 1999, **37**, 484–492.

II.

Peptides 31 (2010) 248–256

Contents lists available at ScienceDirect

Peptides

journal homepage: www.elsevier.com/locate/peptides

Controlled in situ preparation of Aβ(1–42) oligomers from the isopeptide "iso-Aβ(1–42)", physicochemical and biological characterization

Zsolt Bozso [a,*], Botond Penke [a,b,c], Dóra Simon [a], Ilona Laczkó [d], Gábor Juhász [b], Viktor Szegedi [b], Ágnes Kasza [a], Katalin Soós [a], Anasztázia Hetényi [a,e], Edit Wéber [e], Hajnalka Tóháti [f], Mária Csete [f], Márta Zarándi [a], Lívia Fülöp [a]

[a] Department of Medical Chemistry, University of Szeged, Szeged, Hungary
[b] BAYGEN, Bay Zoltán Foundation for Applied Research, Szeged, Hungary
[c] Supramolecular and Nanostructured Material Research Group of the Hungarian Academy of Sciences, Szeged, Hungary
[d] Institute of Biophysics, Biological Research Center, Szeged, Hungary
[e] Institute of Pharmaceutical Chemistry, University of Szeged, Szeged, Hungary
[f] Department of Experimental Physics, University of Szeged, Szeged, Hungary

ARTICLE INFO

Article history:
Received 23 July 2009
Received in revised form 1 December 2009
Accepted 1 December 2009
Available online 6 December 2009

Keywords:
β-Amyloid
Oligomers
Aggregation
Alzheimer's disease
Isopeptide

ABSTRACT

β-Amyloid (Aβ) peptides play a crucial role in the pathology of the neurodegeneration in Alzheimer's disease (AD). Biological experiments (both in vitro and animal model studies of AD) require synthetic Aβ peptides of standard quality, aggregation grade, neurotoxicity and water solubility. The synthesis of Aβ peptides has been difficult, owing to their hydrophobic character, poor solubility and high tendency for aggregation. Recently an isopeptide precursor (iso-Aβ(1–42)) was synthesized by Fmoc-chemistry and transformed at neutral pH to Aβ(1–42) by *O*→*N* acyl migration in a short period of time. We prepared the same precursor peptide using Boc-chemistry and studied the transformation to Aβ(1–42) by acyl migration. The peptide conformation and aggregation processes were studied by several methods (circular dichroism, atomic force and transmission electron microscopy, dynamic light scattering). The biological activity of the synthetic Aβ(1–42) was measured by ex vivo (long-term potentiation studies in rat hippocampal slices) and in vivo experiments (spatial learning of rats). It was proven that *O*→*N* acyl migration of the precursor isopeptide results in a water soluble oligomeric mixture of neurotoxic Aβ(1–42). These oligomers are formed in situ just before the biological experiments and their aggregation grade could be standardized.

1. Introduction

Alzheimer disease (AD) is a progressive neurodegenarative disorder. The probability of the disease is exponentially increasing with age. The presence of amyloid deposits and neurofibrillary tangles are the main pathologic features of AD. The main components of the amyloid deposits are β-amyloid (Aβ) peptides. These peptides consist of 39–43 amino acids. The monomeric Aβ peptides are produced from a membrane protein, the amyloid precursor protein (APP) with the cleavage by β and γ secretases [23]. Initially these peptides are water soluble, then explore β-sheet conformation. This conformational transition induces aggregation producing Aβ-oligomers, protofibrils and fibrils, simultaneously the water solubility of these Aβ-species substantially decrease. Aβ-peptides are neurotoxic both in vivo and in vitro [21,35]. The most toxic form of the Aβ peptide is the one that contains 42 residues.

For AD research it is crucial to prepare Aβ(1–42) peptide to study the aggregation process resulting in toxic Aβ-species and the in vitro effects of the peptide in neuronal cells and brain tissues as well as examine the progression of the disease in animal models.

It is well known that the synthesis of Aβ(1–42) is troublesome thus it is considered to be a 'difficult sequence' [4,33,38]. The difficulties arise from the hydrophobic nature of the peptide. The presence of high number of hydrophobic amino acids in the sequence and the high tendency of the peptide to adopt β-sheet conformation – both in solution and on the resin matrix – induces aggregation. The aggregation of the growing peptide chains on the solid support causes steric hindrance during the assembly of the molecule. Several methods were reported to overcome the synthetic problem associated with the aggregation of peptide chains on the resin, such as using different solvents [13,38], adding chaotropic salts [11], performing the synthesis at elevated temperature [34], building up the peptide in resins made from or grafted with

* Corresponding author.
E-mail address: zbozso@yahoo.com (Z. Bozso).

0196-9781/$ – see front matter © 2009 Elsevier Inc. All rights reserved.
doi:10.1016/j.peptides.2009.12.001

polyethylene glycol [15,22], incorporating pseudo-proline residues [36,37] and applying backbone protection [14,24]. Even if the synthesis is successful, it is difficult to dissolve the crude Aβ peptide for loading it into an HPLC column. The broad elution profile – as a result of aggregation – also makes the purification of the peptide troublesome.

Until recently the synthetic commercial Aβ(1–42) samples were not homogeneous as for aggregation grade and water solubility. As a consequence, the biological studies performed by these peptides were not always reproducible. The high sensitivity of peptide conformation to handling (solvents, temperature, pH, peptide concentration) might be the reason for different aggregation grade and solubility. Different procedures were worked out during the years [6,16] to obtain oligomers or fibrils from the altering product of the syntheses. Recent publications outline, that it is important to access oligomers of Aβ, since these are the most toxic form of the peptide [2,7].

Kiso and co-workers [28], Carpino et al. [5] and Mutter and co-workers [10] have independently described a method to ease the synthesis and purification of Aβ(1–42) by preparing a precursor of the peptide with low tendency for aggregation using N^{α}-Fmoc protected amino acids. The serine residue at position 26 was incorporated as Boc-Ser-OH followed by the acylation of its free hydroxyl side chain with the subsequent residue Gly^{25}. After cleavage of the peptide from the resin, the peptide chain contains an ester bond in its backbone ('isopeptide') and a free α-amino group at Ser^{26}. The incorporated ester bond decreases the propensity of the peptide to aggregate, thus the isopeptide (iso-Aβ(1–42)) has an enhanced water solubility. When the pH is raised to the physiological value, a fast *O*→*N* acyl-transfer reaction occurs resulting in Aβ(1–42). The *O*→*N* acyl-shift can occur both in vitro and in vivo, thus iso-Aβ(1–42) can be used as a good precursor for Aβ(1–42).

Some possible drawbacks of the Fmoc-synthesis such as incomplete deprotection of the growing peptide chain by the 20% piperidine in *N*,*N*-dimethylformamide (DMF) [9,18], potential hydrolysis of the ester bond and diketopiperazine formation [8,26] can be minimized if Boc-chemistry is applied for the synthesis of depsipeptides [29].

Our aim was to prepare Aβ(1–42) with a simple and cheap method and characterize the Aβ-peptide assemblies with a series of microscopic, physicochemical and biological methods. Neurobiologists require well characterized, stable and water soluble Aβ(1–42) of standard quality for reproducible biological experiments. First we synthesized iso-Aβ(1–42) in solid phase using Boc-chemistry. The subsequent *O*→*N* acyl-shift at pH 7.4 produced oligomers and other Aβ species with different aggregation state, depending on the time of the assembly formation. Thus iso-Aβ(1–42) can be used as a good precursor for Aβ(1–42), as it was suggested by Sohma and Kiso [27] and recently by us [3]. In vitro and preliminary ex vivo biological experiments were presented by Kiso's [20] group and by us [3], respectively.

In order to follow the aggregation process, conformational and structural studies of the peptide were done by circular dichroism spectroscopy (CD), dynamic light scattering (DLS), transmission electron microscopy (TEM), nuclear magnetic resonance (NMR) and atomic force microscopy (AFM). The biological activity of the Aβ(1–42) formed from the precursor isopeptide was measured in different test systems (ex vivo electrophysiological studies in rat hippocampal slices and spatial learning of rats in Morris water maze).

2. Materials and methods

2.1. Materials

All *N*-terminally protected amino acids were purchased from Orpegen (Heidelberg, Germany) and GL Biochem (Shanghai, China). *N*-(2-chlorobenzyloxycarbonyloxy)succinimide (2-Cl-Z-OSu) and *O*-*tert*-butyl-L-serine (H-Ser(OtBu)-OH), *N*,*N*-dicyclohexylcarbodimide (DCC), 1-hydroxybenzotriazole (HOBt), 1-hydroxy-7-azabenzotriazole (HOAt) were purchased from GL Biochem (Shanghai, China). Solvents and *N*,*N*-diisopropylethylamine (DIEA) were obtained from Sigma–Aldrich. High performance liquid chromatography (HPLC) grade triflouroacetic acid (TFA) was ordered from Pierce.

2.2. Synthesis of 2-Cl-Z-Ser(OtBu)-OH

8.5 g (30 mmol) 2-Cl-Z-OSu in 60 mL DMF were added to 4 g (25 mmol) of H-Ser(OtBu)-OH dissolved in 10% Na_2CO_3 solution (60 mL, pH 9.5). The mixture was stirred on ice for 2 h, then the ice bath was removed and the reaction was continued at room temperature. The pH was maintained between 9 and 9.5 for 3 h, when the change of the pH ceased. Then the mixture was diluted with a three fold amount of water and extracted three times with diethyl-ether. The pH of the aqueous phase was adjusted to 2 with 6 M HCl and was extracted three times with ethyl acetate (EtOAc). EtOAc fractions were pooled, washed with brine solution and dried over $MgSO_4$. The purity of the product was checked by HPLC and thin layer chromatography (TLC; 20% *t*-butanol–acetic acid–water (4:1:1) in EtOAc, $R_f = 0.79$), the molecular weight (MW) was determined with mass spectrometry (MS).

2.3. Solid phase synthesis of iso-Aβ(1–42) with Boc-chemistry

The peptide was synthesized on a Boc-Ala-PAM resin. The loading of the resin was 0.7 mmol/g. The side chains of Asp and Glu were protected with cyclohexyl group. The N^{ε} of Lys was masked with 2-chlorobenzyloxycarbonyl (2-Cl-Z) group. The side chains of Asn and Gln were unprotected. The guanidino group of the Arg was tosylated. The imidazol group of His was protected with benzyloxymethyl group. The aromatic OH of Tyr was masked with 2-bromobenzyloxycarbonyl (2-Br-Z group). The side chain of Ser was benzylated. Free hydroxyl groups of the resin were capped by reacting it with 0.25 M acetic acid anhydride in the presence of 0.25 M *N*-methyl-imidazol (NMI) in dichloromethane (DCM) for an hour. Following removal of the Boc group, 1 g of the resin was treated with a mixture of Boc-Ile-OH/DCC/HOAt (0.35 mmol each) in DCM/DMF (3:1) overnight. The unreacted amino groups of Ala^{42} were acetylated by reacting the peptide-resin with acetic acid/DCC/HOAt (3 mmol each, 1 h). The final loading of the resin was 0.32 mmol/g (determined with picric acid test). Peptide chain elongation were done by activating three fold excess of N^{α}-Boc protected amino acids with DCC/HOBt in DCM/DMF (1:1) and the peptide-resin was reacted with this mixture for 2 h. The couplings were monitored with qualitative ninhydrin test. If the result of the test had indicated, the coupling was repeated either using DCC/HOBt or DCC/HOAt activation. The α-amino protecting groups were removed by treating the resin with 50% TFA/DCM mixture twice (5 + 25 min). Neutralization was done with 5% DIEA/DCM (2 × 1 min). Ser^{26} was introduced into the peptide chain utilizing 2-Cl-Z-Ser(OtBu)-OH and the same conditions as detailed above. The side chain of this serine was deblocked and neutralized with the same method that was used in case of the α-amino groups. Acylation of the hydroxyl group of Ser^{26} with Boc-Gly-OH was done by treating the peptide-resin with Boc-Gly-OH/DCC/NMI (10-fold excess) in DCM/DMF (3:1) for 2 × 4 h. Then the possibly unreacted hydroxyl groups of Ser^{26} were capped as those of the resin mentioned previously.

When the assembly of the isopeptide was completed, 3.0 g peptide-resin was obtained. The peptide was cleaved from the resin with a cleavage mixture containing HF (10 mL), anisol (0.2 mL), dimethyl sulfide (DMS; 0.8 mL) and dithiothreitol (DTT;

0.1 g) for 1 g of peptide-resin at 0 °C for 45 min. The peptide was precipitated and washed with diethyl-ether and dissolved in 50% acetic acid/water and lyophilized. 409 mg peptide was obtained from 1.0 g peptide-resin (85% yield).

2.4. Analytical and preparative HPLC

Analytical analysis was done on a Hewlett-Packard Agilent 1100 Series HPLC apparatus using a Luna C18 column (100 Å, 5 μm, 250 × 4.60 mm, Phenomenex) and the flow rate was 1.2 mL/min. Preparative chromatography was done on a Shimadzu HPLC apparatus equipped with a Jupiter C4 column (300 Å, 10 μm, 250 × 21.2 mm, Phenomenex) with a flow rate of 5 mL/min. 0.1% TFA in d.i. water and 80% acetonitrile (ACN), 0.1% TFA in d.i. water was used as eluent A and eluent B, respectively. 85 mg pure peptide were resulted from the purification of 200 mg crude peptide (42.5% yield).

2.5. Mass spectrometry

Mass spectrometry measurements were done on a FinniganMat TSQ 7000 mass spectrometer in ESI-MS mode.

2.6. Standard Aβ(1–42) sample preparation for microscopic and DLS measurements

To obtain an acidic solution of iso-Aβ(1–42), the peptide was dissolved in 0.1% (v/v) TFA solution, sonicated for 5 min and filtered through a syringe filter equipped with a 0.1 μm pore size PVDF membrane (Millex, Millipore Ireland, Carrigtwohill, Ireland). For a pH 7.4 solution, the peptide was dissolved prior in MilliQ ultrapure water to a concentration of 500 μM (2.5 mg/mL) and sonicated for 5 min. The solution was diluted in HBS (10 mM HEPES, 0.154 M NaCl, pH 7.4) to a final peptide concentration of 50 μM and filtered the same way as written above. The solution was incubated for the required time intervals at ambient temperature. In case of AFM study of the effect of long-term incubation on the aggregation of iso-Aβ(1–42), the peptide solution was seeded with pre-formed fibrils of Aβ(1–42) suspended in MilliQ water; the concentration of the fibrils reached 1 μM in the final volume of the sample.

2.7. Atomic force microscopy measurements

10 μL of peptide solution were pipetted onto freshly cleaved mica (Muscovite mica, V-1 quality, Electron Microscopy Sciences, Washington DC, USA). After 2 min the samples were washed twice 10 μL of distilled water and then dried with nitrogen gas.

The AFM images were obtained using tapping mode on a PSIA XE-100 SPM under ambient conditions. Tapping mode AFM tips (Type NSG01, NT-MDT, Moscow, Russia) were applied with a nominal radius of curvature of 10 nm, the non-contact silicon cantilevers having typical force constant of 5.5 N/m and resonant frequency of 150 kHz. The scan rate was 1 Hz and the resolution of the AFM scans was 512 × 512 pixels.

2.8. Dynamic light scattering measurements

All experiments were performed at 25 °C with a Malvern Zetasizer Nano ZS Instrument (Malvern Instruments Ltd., Worcestershire, UK) equipped with a He–Ne laser (633 nm) applying the non-invasive back scatter (NIBS®) technology. The translational diffusion coefficients were obtained from the measured autocorrelation functions using the regularization algorithm CONTIN built in the software package Dispersion Technology Software 4.0 (Malvern Instruments Ltd., Worcestershire, UK). Assuming the scattering particles as hard spheres, their apparent hydrodynamic radius can be calculated from the diffusion parameters by using the Stokes–Einstein equation $R_h = k_B T/(6\pi\eta D_T)$, where k_B is the Boltzmann constant, T is the absolute temperature, η is the viscosity of the medium and D_T is the translational diffusion coefficient. Samples were prepared as given in the section of sample preparation. Correlation function and distribution of the apparent hydrodynamic radii (R_h) over the scattered intensity of the samples were monitored for the expected time intervals.

2.9. Transmission electron microscopy measurements

10 μL droplets of solutions were placed on 400 mesh carbon-coated copper grids (Electron Microscopy Sciences, Washington, PA), incubated for 2 min, fixed with 0.5% (v/v) glutaraldehyde solution, washed three times with d.i. water, and finally stained with 2% (w/v) uranyl acetate. Specimens were studied with a Philips CM 10 transmission electron microscope (FEI Company, Hillsboro, Oregon, USA) operating at 100 kV. Images were taken by a Megaview II Soft Imaging System at a magnification of ×64,000 and analyzed by an AnalySis® 3.2 software package (Soft Imaging System GmbH, Münster, Germany).

2.10. Circular dichroism spectroscopy

CD measurements were performed at 25 °C on a Jobin–Yvon Mark VI dichrograph using a quartz cell of 0.1 cm pathlength. All the spectra were the averages of four scans and the resolution was 0.2 nm. The iso-Aβ(1–42) was dissolved either in 5 mM phosphate buffer (pH 7.4) or 0.1% TFA (pH 2) at a concentration of 50 μM. The samples were sonicated for 5 min immediately after dissolution and prior to aging at room temperature. CD spectra were expressed as mean residue ellipticity $[\Theta]_{MR}$, in units of deg cm^2 dmol^{-1} using a mean residue weight of 110.

2.11. Nuclear magnetic resonance

All NMR spectra were recorded on a Bruker AV600 spectrometer that was equipped with a 2.5 mm triple-resonance capillary probe at 285 K. The iso-Aβ(1–42) was dissolved in water at a concentration of 0.31 mg/120 μL and pH 2.1, 3.0 or 4.7. The ^{1}H NMR spectroscopy measurements were performed with a WATERGATE solvent suppression scheme. The spectra were recorded with identical conditions (same experimental setup, the same spectrometer and the same probe) after dissolution and a week later. For the relaxation delay, 2 s was used; the delay for binomial water suppression was 150 ms; the number of scans was 256. The NOESY measurements were carried out with a WATERGATE solvent suppression scheme. For the NOESY mixing time 610 ms were used; the number of scans was 64. The TOCSY measurements were carried out with homonuclear Hartman-Hahn transfer with the MLEV17 sequence, with an 80 ms mixing time; the number of scans was 32. For all the 2D spectra, 2024 time domain points and 512 increments were applied. The processing was carried out by using a cosine-bell window function, with single zero filling and automatic baseline correction.

2.12. Pretreatment of rat hippocampal slices with Aβ(1–42) oligomers in artificial cerebrospinal fluid (ACSF)

Using standard procedures, 400 μm thick transverse hippocampal slices were prepared from the brain of 3 months old male Wistar rats using a McIlwain tissue chopper (Campden Instruments, Loughborough, UK). Slices were incubated in a custom-built incubation system in oxygenated standard artificial cerebrospinal fluid (ACSF, composition in mM: NaCl, 130; KCl, 3.5; $CaCl_2$, 2;

$MgCl_2$, 2; NaH_2PO_4, 0.96; $NaHCO_3$, 24; D-glucose, 10 and pH 7.4) at ambient temperature for at least 60 min. Individual slices were transferred to a 3D-MEA (multielectrode array) chip with 60 tip-shaped and 60-μm-high electrodes spaced by 200 μm (Ayanda Biosystems, S.A., Lausanne, Switzerland). The surrounding ACSF solution was removed quickly and the slice was immobilized by a grid. Iso-Aβ(1–42) was dissolved in ACSF at pH 7.4 (1 μM final concentration) and let to transform to Aβ(1–42) and oligomerize in 10 min. The slice was incubated continuously with this solution and perfused with oxygenated ACSF (1.5 mL/min at 34 °C). Incubation was performed for 30 min on the chip before recording commenced. Data were recorded by a standard, commercially available MEA setup (Multi Channel Systems MCS GmbH, Reutlingen, Germany).

2.13. Ex vivo electrophysiological recordings: measurement of long-term potentiation (LTP)

The Schaffer-collateral was stimulated by injecting a biphasic current waveform (−100/+100 μs) through one selected electrode at 0.0166 Hz. Care was taken to choose the stimulating electrode in the same region from one slice to the other one. The peak-to-peak amplitudes of field excitatory postsynaptic potentials (fEPSPs) at the proximal part of stratum radiatum of CA1 were analyzed. After a 30 min incubation period, the threshold and the maximum of stimulation intensity of the evoked responses were determined. To evoke responses, 30% of the maximal stimulation intensity was used. Following a stable 15-min control sequence, LTP was induced using a theta-burst stimulation (TBS) protocol applied at the maximum stimulation intensity. TBS comprised four trains administered at 20 s intervals with 10 bursts given at 5 Hz per train and four pulses given at 100 Hz per burst. LTP was followed for 180 min.

2.14. Learning studies in rats in Morris water maze

A mixture of Aβ(1–42) oligomers was formed in hydrocarbonate buffered saline (HCBS, 20 mM $NaHCO_3$, 130 mM NaCl, purged with CO_2, pH 7.4) containing 50 μM Aβ(1–42) freshly prepared from iso-Aβ(1–42) at 20 °C for 120 h. Aggregation was tested by AFM (average particle diameter was 8.5 nm). This preparation, which contains mostly oligomers and a small amount of protofibrils, will be referred as "oligomeric mixture" later in this paper.

Adult male Wistar rats (age 8–9 weeks, weight 300–350 g) were operated and Morris water maze experiments were performed as published in [25] with some exception, detailed below. In the control (n = 10) and test group (n = 10) 15 μL hydrocarbonate buffered saline (HCBS) and 15 μL of Aβ(1–42) solution in HCBS (c = 50 μM) were administered intracerebroventricularly (icv). Administration was performed bilaterally with Hamilton syringe, 7.5 μL solution was injected in both sides. The coordinates were from Bregma: AP: −1.0; ML: ±1.5; DV 4.3. Rats were treated with antibiotics and analgesics after surgery.

Spatial learning and memory were assessed in Morris water maze on days 8–12 post-surgery. The maze consisted of a circular blue plastic (diameter: 180 cm, height: 60 cm) filled to a depth of 40 cm with water of 23 ± 1 °C. The water was rendered opaque with the addition of milk. The rats had to learn to find a transparent, hidden escape platform (diameter: 10 cm) in the quadrants on the basis of several constant spatial cues around the pool. The position of the platform was stable during the 5 days study. Daily two trials were conducted between 9:00 and 12:00. Rats were given a maximum of 90 s to find the platform and were then allowed to stay on it for 20 s. Animals that did not find the platform were gently guided and placed on it.

The data recorded by video-tracking were used to calculate the time to reach the platform, during learning. Data were evaluated using independent T-test.

3. Results

3.1. Boc-synthesis of iso-Aβ(1–42)

The synthesis of 2-Cl-Z-Ser(OtBu)-OH resulted an oil, which was pure enough to be used in a solid phase synthesis, as it was judged by TLC and HPLC, and it possessed the right molecular weight (MW: 329.7). HPLC chromatogram in Fig. 1A was obtained from the crude product of the synthesis of iso-Aβ(1–42). Peaks a and b have molecular weights of 4530.4 and 4514.2, respectively. (HPLC of the pure iso-Aβ(1–42) is in the Appendix A. Supplementary data).

3.2. Physicochemical characterization of iso-Aβ(1–42)

TEM (Fig. 2) measurements revealed that iso-Aβ(1–42) contains small aggregates even in a pH 2 solution, which are either round-shaped oligomers with an average width of 4–6 nm, or bunches of protofibrils with an average length of 20–30 nm, typical of this type of assembly.

The occurrence of the $O\rightarrow N$ acyl-shift at acidic pH was studied by NMR. The enhanced solubility of iso-Aβ(1–42) caused a satisfying signal dispersion at 285 K, which cannot be observed in case of the native Aβ(1–42) sequence. Based on the 1H, 2D TOCSY and NOESY spectra, signal assignments could be carried out for the residues 1–30 of the iso-Aβ(1–42). Conversion of the peptide was monitored at different pH values (pH 2.1, 3.0 and 4.7) for a week. During the observation period the isopeptide was stable at pH 2.1, but new peaks appeared in the spectra at pH 3.0. The signal assignment of the new peaks confirmed that these resonances can be attributed to the native Aβ(1–42) form. Thus, $O\rightarrow N$ acyl-shift starts even in the pH 3.0 solution: about 16% of the

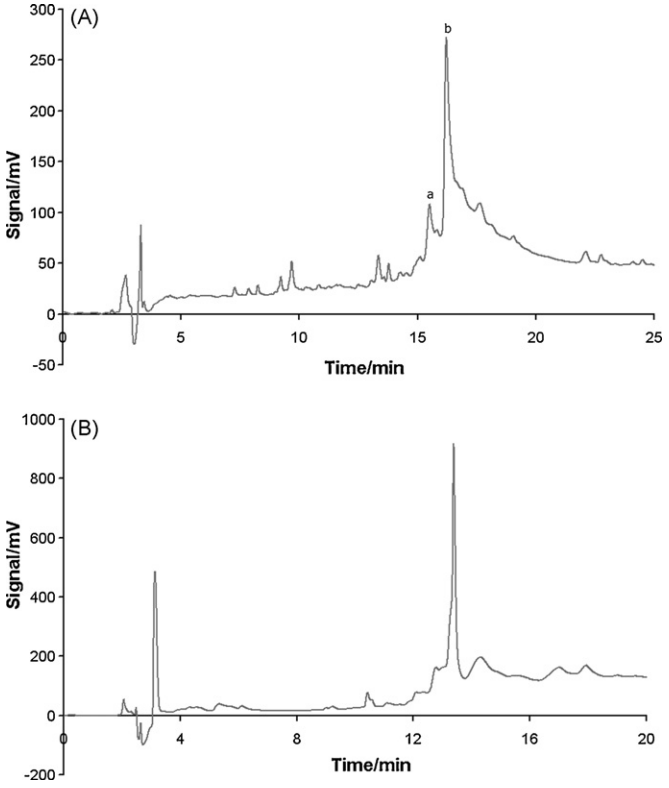

Fig. 1. (A) HPLC of crude iso-Aβ(1–42) synthesized by Boc-chemistry. Gradient: from 5% eluent B in eluent A to 80% eluent B in eluent A over 25 min. (a) $[Met(O)]^{35}$-iso-Aβ(1–42), (b) iso-Aβ(1–42). (B) HPLC of crude iso-Aβ(1–42) dissolved in HFIP. Gradient: from 20% eluent B in eluent A to 60% eluent B in eluent A over 25 min.

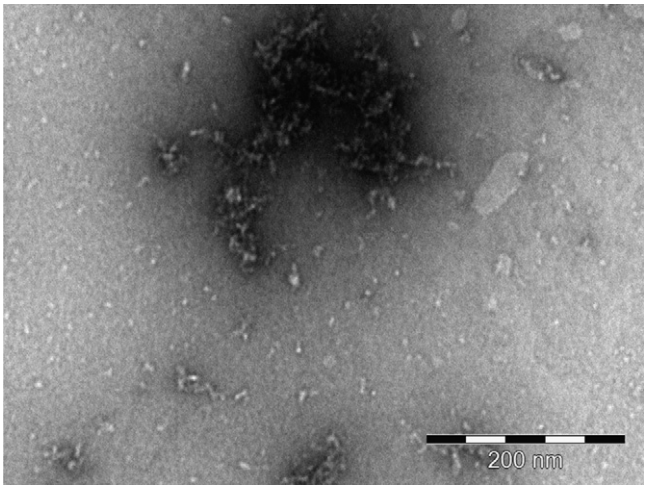

Fig. 2. TEM of iso-Aβ(1–42) dissolved in 0.1% TFA (pH 2.0, c = 50 μM).

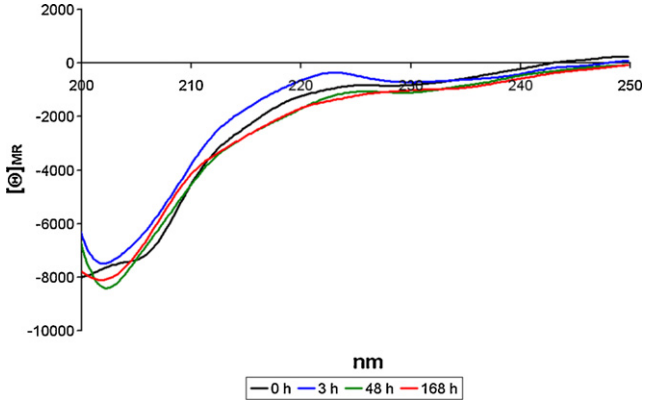

Fig. 3. CD of iso-Aβ(1–42) dissolved in 0.1% TFA (pH 2.0, c = 50 μM).

ester was converted to amide bond in a week. At pH 4.7, the acyl-transfer was instantaneous and some precipitation was observed in the NMR tube.

CD spectroscopy showed that the structure of this peptide is relatively stable in a pH 2.0 solution for a week and it explores mostly random coil conformation (Fig. 3).

3.3. Standard preparation of Aβ(1–42) samples formed by O→N acyl migration of iso-Aβ(1–42)

AFM study showed, that the average width of the particles was 1.8 and 3.4 nm, depending on that the sample was or was not dissolved in d.i. water prior the adjustment of the pH to 7.4, respectively (Fig. 4).

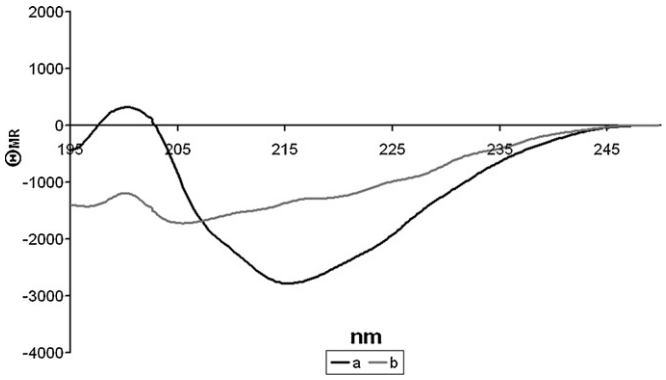

Fig. 5. CD spectra of Aβ(1–42) (a) dissolved in d.i. water, then the pH adjusted to 7.4; (b) first incubated in HFIP overnight, then HFIP is evaporated, followed by the same treatment as that of a (c = 50 μM).

CD spectroscopy (Fig. 5) confirmed that hexaflouro-2-propanol (HFIP) treatment prior the adjustment of the pH to 7.4 of the iso-Aβ(1–42) decreases the negative band intensity at 215 nm (characteristic for β-sheets) of the spectra.

AFM detected the presence of oligomers with regular shape and size (Fig. 4C, average width: 3.9 nm) if the sample was treated with HFIP overnight, and after evaporation of the HFIP the peptide was dissolved in d.i. water followed by the adjustment of pH to 7.4 ('standard sample preparation') and it was incubated in this solution for an hour.

3.4. Characterization of the aggregation process of Aβ(1–42): change of conformation and fibrillization

CD spectroscopy and DLS confirmed that both the β-sheet content of the peptide and the average hydrodynamical diameter of the particles were increasing with time if the iso-Aβ(1–42) was subjected to 'standard sample preparation' (Figs. 6 and 7).

AFM study in Fig. 8, shows the fibrillization of an Aβ(1–42) sample prepared from iso-Aβ(1–42). The isopeptide was dissolved in HBS to a concentration of 50 μM, and seeded with a 100 μM fibrillar suspension of Aβ(1–42) in 1:50 volume ratio. By this method, formation of fibrillar structures (with an average width of 5–7 nm, which is typical for the mature amyloid fibrils) and large globule-like assemblies could be observed in 24 h of incubation time at ambient temperature.

3.5. Biological effect Aβ(1–42) oligomer mixtures: ex vivo and in vivo experiments

In an ex vivo electrophysiology experiment (Fig. 9) control slices exhibited a robust LTP recorded from the proximal part of the str. radiatum (129 ± 8% 180 min after TBS, n = 16 electrodes from

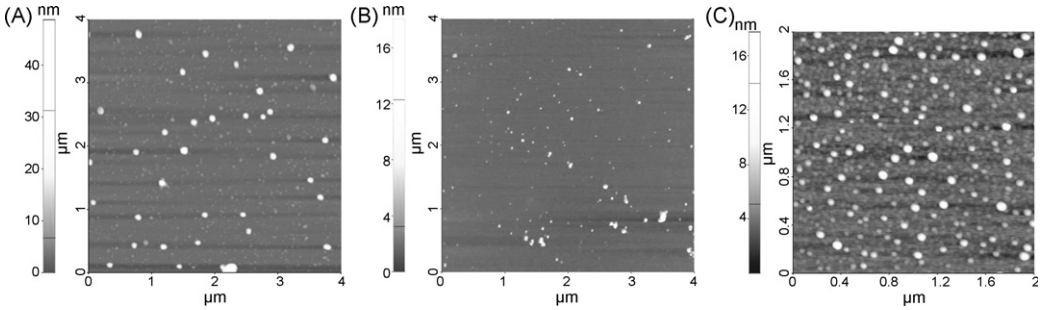

Fig. 4. AFM of Aβ(1–42) after O-N acyl migration of iso-Aβ(1–42) (A) dissolved in pH 7.4 PBS buffer, (B) first taken up into d.i. water followed by adjustment of the pH to 7.4 with PBS buffer and 1 h after 'standard sample preparation' (pH 7.4, c = 50 μM).

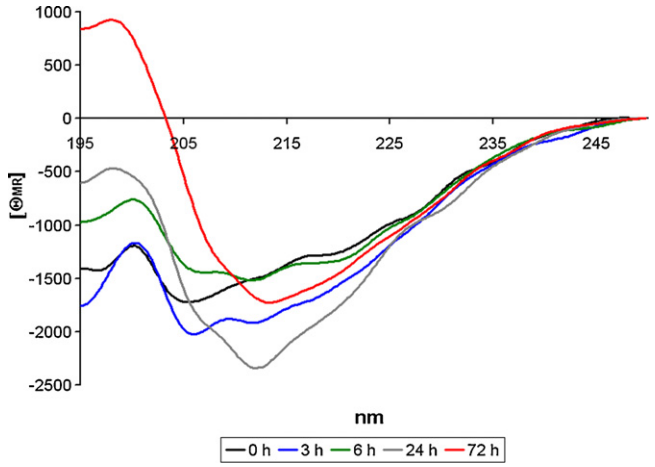

Fig. 6. Aggregation of the Aβ(1–42) peptide after 'standard sample preparation', monitored by CD spectroscopy (pH 7.4, c = 50 μM).

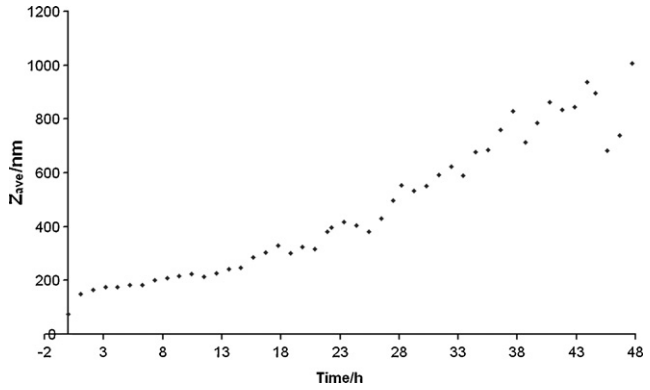

Fig. 7. Aggregation of the Aβ(1–42) peptide after 'standard sample preparation', monitored by DLS measurement (pH 7.4, c = 50 μM).

four slices). On the other hand, Aβ(1–42) treated slices showed a significantly reduced LTP (105 ± 4% 180 min after TBS, n = 15 electrodes from four slices).

The results of the Morris water maze showed, that the performance of the control and Aβ(1–42) treated groups increased across trials. However, statistic analysis of experimental data (time needed to find the platform) revealed that learning was significantly slower in Aβ(1–42) treated rats compared to the control group (Fig. 10) at day 4 ($^{*}P$ = 0.048) and day 5 ($^{**}P$ = 0.017).

4. Discussion

4.1. Boc-synthesis of iso-Aβ(1–42)

The crucial part of devising a Boc strategy for the synthesis of iso-Aβ(1–42) was to determine what kind of protection should be used on the Ser[26]. The side chain of this residue will be masked to avoid unwanted acylation during its activation. The protecting group should be easily removable after the incorporation of the building block. Thus, tBu group was selected for the protection of the side chain of Ser[26], since it is removable with 50% TFA/DCM mixture, routinely used in syntheses utilizing N^{α}-Boc protected

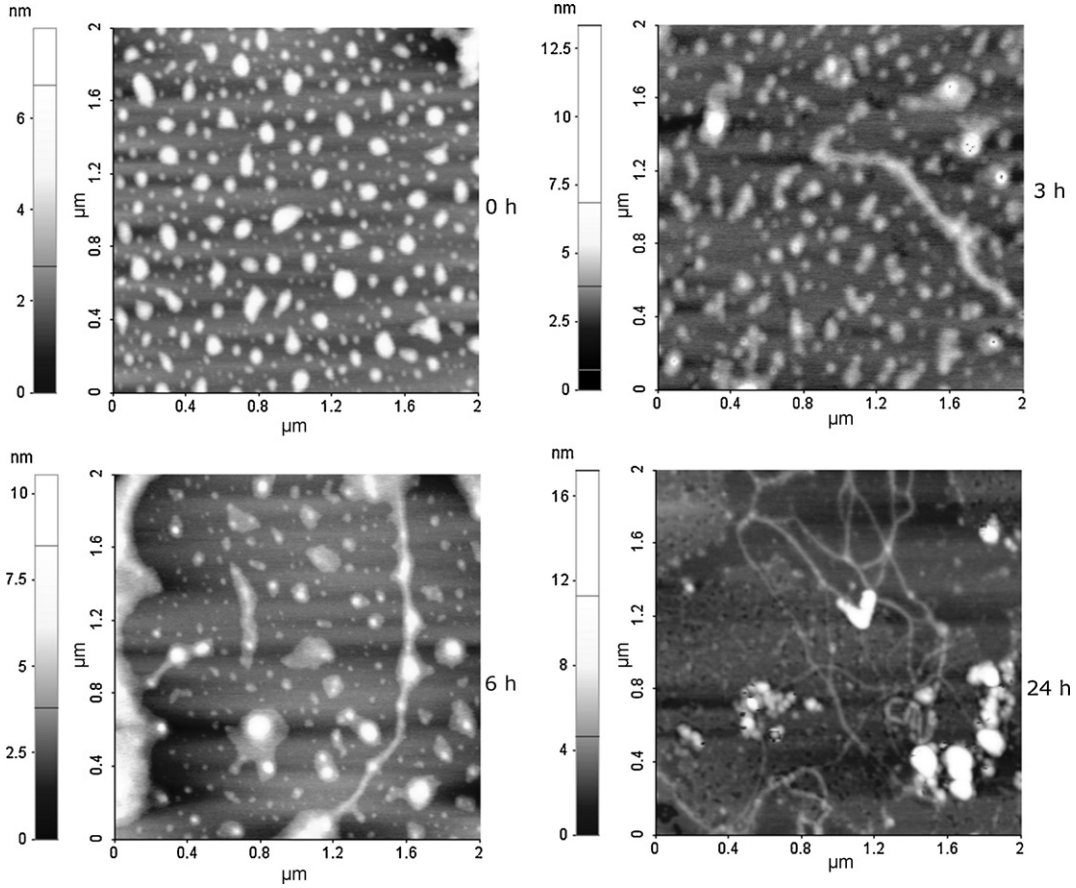

Fig. 8. Aggregation of the Aβ(1–42) peptide (c = 50 μM) after 'standard sample preparation' and seeding with Aβ(1–42) fibrils (c = 1 μM), studied by AFM (pH 7.4).

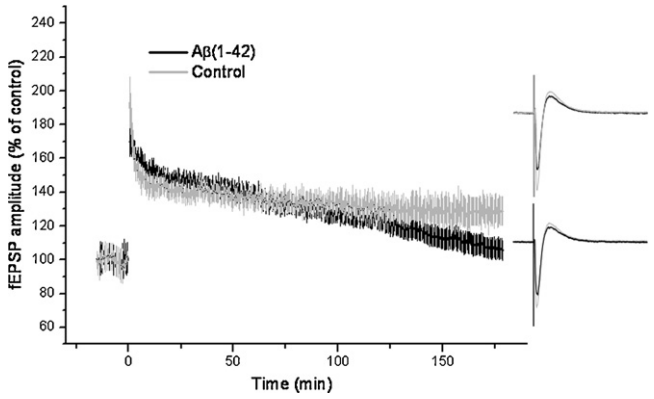

Fig. 9. The effect of Aβ(1–42) oligomer treatment on TBS induced LTP in hippocampal slices. Data are mean ± SEM. Insets show representative superimposed fEPSPs recorded 1 min before (black) and 180 min after (gray) TBS.

amino acids. The protecting group of the α-amino group of the Ser^{26} had to withstand repetitive TFA treatments and be removable during the cleavage of the peptide from the resin to make the precursor ready for the intramolecular *O→N* acyl-shift. Choosing the 2-Cl-Z group was plausible. 2-Cl-Z-Ser(OtBu)-OH was prepared from 2-Cl-Z-OSu and H-Ser(OtBu)-OH as it was detailed in Section 2.2 and later it was used for the incorporation of Ser^{26}.

The presence of Aβ(1–25) as a byproduct was reported by Sohma et al. [26] previously when certain resins were used for the synthesis of iso-Aβ(1–42). It was originated from the simultaneous acylation of the side chain of Ser^{26} and the free hydroxyl groups of the resin during formation of the ester bond between the 25th and 26th residue [8]. To avoid side product formation unreacted free hydroxyl groups of the resin were acetylated. After acylation of the deprotected side chain of Ser^{26} with Boc-Gly-OH using DCC/NMI activation, the free hydroxyl groups were capped.

The major peak of our crude peptide (Fig. 1A, peak b) in the HPLC has a molecular weight of 4514.2 which is in agreement with the molecular weight of iso-Aβ(1–42) (calc. MW: 4514.0). The molecular weight of peak b is by 16 mass unit higher than that of the desired product, thus it is $[Met(O)]^{35}$-iso-Aβ(1–42). This minor byproduct can be completely eliminated, if the 'low-high' cleavage procedure [30] is used, or if the crude peptide is treated with DMS/NH_4I in TFA for 30 min at 0 °C [12]. In our synthesis no hydrolysis product or diketopiperazine formation was detected. It was observed that the main peak had a wide tailing. Fractions belonging to this part of the peak possessed no sign of any byproduct, only iso-Aβ(1–42), when analyzed by MS. If these fractions were sonicated in HFIP for 15 min after lyophilization, a sharp peak was obtained in the HPLC (peaks in Fig. 1B after 14 min are present in the HFIP, see Appendix A. Supplementary data). Thus the tailing can be due to some sort of aggregation of the iso-Aβ(1–42). If we compare Fig. 1B with chromatograms from the literature, where the peptide was synthesized with Fmoc-chemistry and injected into the HPLC in a disaggregating solvent (dimethyl sulfoxide; DMSO) [26,32], it can be concluded that the Boc-synthesis gave comparable results with them.

4.2. Physicochemical characterization of iso-Aβ(1–42)

The findings of other groups have outlined the improved water solubility and stability of the isopeptide that could be explained by its unique structure, lowering its propensity toward aggregation. However, TEM (Fig. 2) measurements showed that iso-Aβ(1–42) forms either round-shaped oligomers, or protofibrils. As no *O→N* acyl migration occurs at pH 2.0 (NMR studies) it seems to be very probable that iso-Aβ(1–42) still has some propensity to form small aggregates. Residues 17–20 and 30–35 play a crucial role in the aggregation of the native Aβ peptides and fragments containing these residues are either enhance aggregation of the full length peptide or themselves are prone to aggregate [19]. These regions are intact in the iso-Aβ(1–42), so the isopeptide can preserve some of their aggregation properties, despite of the structure disrupting effect of the ester bond between residues 25 and 26. Aggregation states of an amyloid peptide are greatly influenced by previous treatments. In our studies no chaotropic agents (e.g. DMSO or HFIP) were applied upon purification to destroy the pre-formed aggregates as it were in [26] and [32]. This can be the cause of the discrepancy between our results and Taniguchi et al.'s [31], who detected isopeptide monomers only with CD and size exclusion chromatography. Our preparation most likely also contains some monomers besides the oligomers, since monomers cannot be detected by AFM. CD spectra of the iso-Aβ(1–42) showed mostly random conformation for a week (Fig. 3). Nevertheless the isopeptide still has superior solubility properties and much lower tendency to aggregate than Aβ(1–42) has.

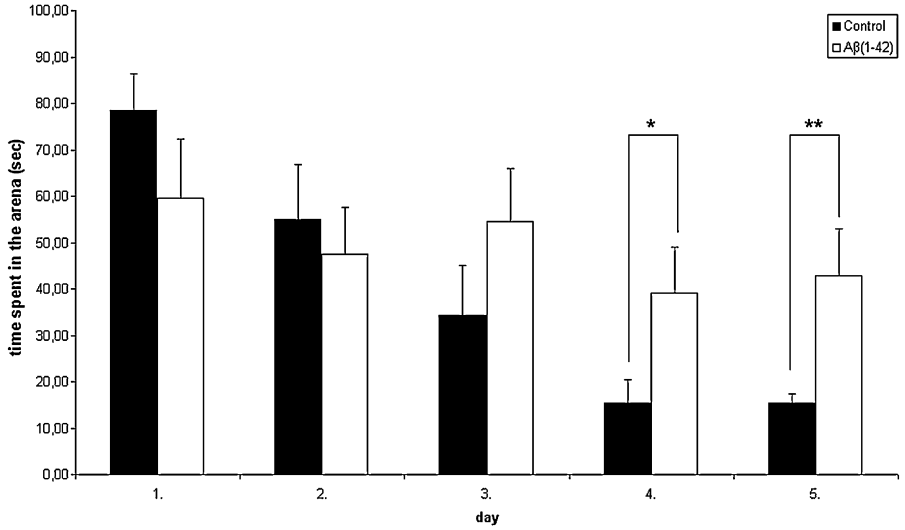

Fig. 10. The effect of Aβ(1–42) treatment (50 μM, icv administration) on the learning of rats during 5 days (Morris water maze, time spent in the arena during the first swims, *T*-test: $^{*}P = 0.048$; $^{**}P = 0.017$).

4.3. Standard preparation of Aβ(1–42) samples formed by O→N acyl migration of iso-Aβ(1–42)

It was confirmed by AFM measurements that particles with smaller size could be obtained if the peptide was dissolved in d.i. water prior to the adjustment of the pH to 7.4 compared to the protocol, which applies only pure pH 7.4 buffer as dissolution media (Fig. 4). CD spectroscopy confirmed that HFIP treatment of the iso-Aβ(1–42) decreased the β-sheet content of the resulting Aβ(1–42) after adjustment of the pH to 7.4 (Fig. 5). Based on these findings, a 'standard sample preparation' protocol was worked out to obtain starting material which possesses reproducible aggregation properties for our future experiments. According to this, the peptide is first treated with HFIP overnight. Followed by the evaporation of the HFIP, the iso-Aβ(1–42) is dissolved in d.i. water, then the pH is changed to 7.4 with an appropriate buffer. In Fig. 4C AFM image taken 1 h after sample preparation followed by the standard preparation protocol shows the overwhelming presence of the small round oligomers of regular shape and size.

4.4. Characterization of the aggregation process of Aβ(1–42): change of conformation and fibrillization

Both CD spectroscopy and DLS (Figs. 6 and 7) showed growing β-sheet content and particle size of the Aβ(1–42) formed from iso-Aβ(1–42) upon incubation. Care must be taken with the interpretation of DLS results, since the increase of the diameters detected by DLS are always distorted by the large particles, as the observed scattering intensity is proportional to the sixth power of the hydrodynamical radius of the scattering particle (the bigger is the scattering particle, the more is its contribution to the scattering intensity). Thus, the increase of the average size in a given time interval is possibly smaller, than that measured by DLS. We observed this phenomenon, when attempted to follow the Aβ(1–42) aggregation by AFM, and found that though the formation of large aggregates could be detected upon incubation of the sample for an elongated time period, their occurrence compared to the small oligomers was reduced. Proper fibrillization could be achieved by seeding the sample with pre-formed fibrils of Aβ(1–42), as it is presented by a series of AFM measurements (Fig. 8).

4.5. Biological effect Aβ(1–42) oligomer mixtures ex vivo and in vivo experiments

The effect of the peptide on synaptic plasticity was studied in an ex vivo electrophysiology experiment. Aβ(1–42) has been repeatedly shown to impair long-term potentiation in hippocampal slices [1,17], thus we investigated LTP. The results in Fig. 9 indicate that Aβ(1–42) formed from the precursor isopeptide hinders the long-term potentiation, thus it decreases synaptic plasticity, a correlate of learning and memory.

Icv administered Aβ(1–42) oligomeric mixture (prepared from iso-Aβ(1–42) and aggregated for 120 h) caused memory deficit in rats (Morris water maze, Fig. 10). The difference of the treated and control group proved to be significant on the 4th and 5th days of the experiments. Icv administration into the 3rd ventricle has an advantage (compared to microinjection into the entorhinal cortex) that soluble Aβ(1–42) oligomers reach large areas of brain beside minimal brain injury.

5. Conclusion

Iso-Aβ(1–42) was successfully synthesized using a Boc strategy. The preparation of the 2-Cl-Z-Ser(OtBu)-OH building block (used to introduce Ser at the position of the ester bond formation) is easy and convenient. The applied protecting groups have been widely used, well known and fulfill the stability requirements toward acidic treatments. Aβ assemblies with different aggregation grade – oligomers and (after prolonged incubation times and seeding) fibrillar structures – can be obtained from iso-Aβ(1–42). It was demonstrated that the isopeptide was a good precursor of Aβ(1–42) for both structural and biological studies. This isopeptide is water soluble, stable and the aggregation of the formed Aβ(1–42) can be well characterized, thus it can be useful to perform reproducible biological experiments. Moreover, by administering this isopeptide chronically into animals, the *O→N* acyl-transfer could happen in situ and in vivo. This chronic administration of the Aβ-isopeptide may serve as a proper model system in order to study Alzheimer's disease from an early onset.

Acknowledgements

This work was supported by the following grants: OTKA NK 73672 from the Hungarian National Sciences Foundation; Memoload FP-7 201159 and Lipididiet FP-7 211696 and the Teller Ede (Napbio) grant of NKTH. L.F. and A.H. acknowledges support from a János Bolyai Postdoctoral Fellowship.

The authors thank to Dr. Zoltán Kele for mass spectrometry and to Dr. Tamás Martinek for providing the NMR facility.

Appendix A. Supplementary data

Supplementary data associated with this article can be found, in the online version, at doi:10.1016/j.peptides.2009.12.001.

References

[1] Barghorn S, Nimmrich V, Striebinger A, Krantz C, Keller P, Janson B, et al. Globular amyloid β-peptide1–42 oligomer–a homogenous and stable neuropathological protein in Alzheimer's disease. J Neurochem 2005;95:834–47.
[2] Bernstein SL, Dupuis NF, Lazo ND, Wyttenbach T, Condron MM, Bitan G, et al. Amyloid-β protein oligomerization and the importance of tetramers and dodecamers in the aetiology of Alzheimer's disease. Nat Chem 2009;1:326–31.
[3] Bozsó Z, Penke B, Juhász G, Szegedi V, Laczkó I, Soós K, et al. The synthesis and structural study of iso-Aβ(1–42). In: Hilkka Lankinen, editor. Peptides 2008, Proceedings of the thirtieth European peptide symposium. Finland: The Finnish Peptide Society; 2008. p. 364–5.
[4] Burdick D, Soreghan B, Know M, Kosmoski J, Knauer M, Henschen A, et al. Assembly and aggregation properties of synthetic Alzheimer's A4/b amyloid peptide analogs. J Biol Chem 1992;267:546–54.
[5] Carpino LA, Krause E, Sferdean CD, Schümann M, Fabian H, Bienert M, et al. Synthesis of "Difficult" peptide sequences: application of a depsipeptide technique to the Jung-Redemann 10- and 26-mers and the amyloid peptide Aβ(1–42). Tetrahedron Lett 2004;45:7519–23.
[6] Chromy BA, Nowak RJ, Lambert MP, Viola KL, Chang L, Velasco PT, et al. Self assembly of Aβ(1–42) into globular neurotoxins. Biochemistry 2003;42:12749–60.
[7] Clemmer DE, Valentine SJ. Protein oligomers frozen in time. Nat Chem 2009;1:257–8.
[8] Coin I, Dölling R, Krause E, Bienert M, Beyermann M, Sferdean CD, et al. Depsipeptide methodology for solid phase peptide synthesis: circumventing side reactions and development of an automated technique via depsipeptide units. J Org Chem 2006;71:6171–7.
[9] Dettin M, Pegoraro S, Rovero P, Bicciato S, Bagno A, Di Bello C. SPPS of difficult sequences. J Peptide Res 1997;49:103–11.
[10] Dos Santos S, Chandravarkar A, Mandal B, Mimna R, Murat K, Saucede L, et al. Switch-peptides: controlling self-assembly of amyloid beta-derived peptides in vitro by consecutive triggering of acyl migrations. J Am Chem Soc 2005;127:11888–9.
[11] Hendrix JC, Halverson KJ, Jarrett JT, Lansbury PT. A novel solvent system for solid-phase synthesis of protected peptides: the disaggregation of resin-bound antiparallel β-sheet. J Org Chem 1990;55:4517–8.
[12] Huang H, Rabenstein DL. A cleavage cocktail for Met containing peptides. J Pept Res 1999;53:548–53.
[13] Hyde C, Owen JD, Quibell M, Sheppard RC. Some 'difficult sequences' made easy. Int J Peptide Protein Res 1994;43:431–40.
[14] Johnson T, Quibell M, Sheppard RC. N,O-bisFmoc derivatives of N-(2-hydroxy-4-methoxybenzyl)-amino acids: usefull intermediates in peptide synthesis. J Pept Sci 1995;1:11–25.

[15] Kates SA, Solé NA, Beyermann M, Barany G, Albericio F. Optimized preparation of deca(L-alanyl)-L-valinamide by 9-flourenylmethyloxycarbonyl (Fmoc) solid-phase synthesis on polyethylene glycol-polystyrene (PEG-PS) graft supports, with 1,8-diazobiciclo[5.4.0]-undec-7-ene (DBU) deprotection. Peptide Res 1996;9:106–13.
[16] Klein WL. Aβ toxicity in Alzheimer's disease: globular oligomers (ADDLs) as new vaccine and drug targets. Neurochem Int 2002;41:345–52.
[17] Klyubin I, Betts V, Welzel AT, Blennow K, Zetterberg H, Wallin A, et al. Amyloid β protein dimer-containing human CSF disrupts synaptic plasticity: prevention by systemic passive immunization. J Neurosci 2008;28:4231–7.
[18] Larsen BD, Holm A. Incomplete Fmoc deprotection in solid-phase synthesis of peptides. Int J Peptide Protein Res 1994;43:1–9.
[19] Liu R, McAllister C, Lyubshenko Y, Sierks MR. Residues 17–20 and 30–35 of beta-amyloid play critical role in aggregation. J Neurosci Res 2004;75:162–71.
[20] Matsuzaki K, Okada T, Tsukuda M, Ikeda K, Sohma Y, Chiyomori Y, et al. Design, synthesis, and biophysical properties of a helical Aβ1–42 analog: inhibition of fibrillogenesis and cytotoxicity. Biochem Biophys Res Commun 2008;371:777–80.
[21] Mattson MP, Cheng B, Davis B, Bryant K, Liederburg I, Rydel RE. β amyloid peptides destabilize calcium homeostasis and render human cortical neurons vulnerable to excitotoxicity. J Neurosci 1992;12:376–89.
[22] Meldal M. PEGA: a flow stable polyethylene glycol dimethyl acrylamide copolymer for solid phase synthesis. Tetrahedron Lett 1992;33:3077–80.
[23] Selkoe DJ. Physiological production of the β-amyloid protein and the mechanism of Alzheimer's disease. Trends Neurosci 1993;16:403–9.
[24] Simmonds RC. Use of Hmb backbone-protecting group in the synthesis of difficult sequences. Int J Peptide Protein Res 1996;47:36–41.
[25] Sipos E, Kurunczi A, Kasza Á, Horváth J, Felszeghy K, Laroche S, et al. β-amyloid pathology in the entorhinal cortex of rats induces memory deficits: implications for Alzheimer's disease. Neuroscience 2007;147:28–36.
[26] Sohma Y, Hayashi Y, Kimura M, Chiyomori Y, Taniguchi A, Sasaki M, et al. The 'O-acyl isopeptide method' for the synthesis of difficult sequence-containing peptides: application to the synthesis of Alzheimer's disease-related amyloid β peptide (Aβ)1–42. J Peptide Sci 2005;11:441–51.
[27] Sohma Y, Kiso Y. "Click peptides"—chemical biology-oriented synthesis of Alzheimer disease-related amyloid β (Aβ) analogues based on the "O-acyl isopeptide method". ChemBioChem 2006;7:1549–57.
[28] Sohma Y, Sasaki M, Hayashi Y, Kimura T, Kiso Y. Design and synthesis of a novel water-soluble Aβ1–42 isopeptide: an efficient strategy for the preparation of Alzheimer's disease-related peptide, Aβ1–42, via O-N intramolecular acyl migration reaction. Tetrahedron Lett 2004;45:5965–8.
[29] Spengler J, Koksch B, Albericio F. Simple machine-assisted protocol for solid-phase synthesis of depsipeptides. Biopolymers 2007;88:823–8.
[30] Tam JP, Heath WF, Merrifield RB. SN2 deprotection of synthetic peptides with a low concentration of HF in dimethyl sulfide: evidence and application in peptide synthesis. J Am Chem Soc 1983;105:6442–55.
[31] Taniguchi A, Sohma Y, Hirayama Y, Mukai H, Kimura T, Hayashi Y, et al. "Click-peptide": pH-triggered in situ production and aggregation of monomer Aβ 1–42. ChemBioChem 2009;10:710–5.
[32] Taniguchi A, Yoshiya T, Abe N, Fukao F, Sohma Y, Kimura T, et al. 'O-Acyl isopeptide method' for peptide synthesis of Aβ 1–42 isopeptide using 'O-acyl isodipeptide unit'. J Peptide Sci 2007;13:868–74.
[33] Tickler AK, Clippingdale B, Wade JD. Amyloid-β as a "Difficult Sequence" in Solid Phase Peptide Synthesis. Protein Pept Lett 2004;11:377–84.
[34] Varanda LM. Miranda MTM Solid-phase peptide synthesis at elevated temperatures: a search for an optimized synthesis condition of unsulfated cholecystokinin-12. J Peptide Res 1997;50:102–8.
[35] Waite J, Cole GM, Frautsky SA, Connor DJ, Thal LJ. Solvent effect on beta protein toxicity in vivo. Neurobiol Aging 1992;13:595–9.
[36] Wöhr T, Mutter M. Pseudo-prolines in peptide synthesis: direct insertion of serine and threonine derived oxazolidines in dipeptides. Tetrahedron Lett 1995;36:3847–8.
[37] Wöhr T, Wahl F, Nefzi A, Rohwedder B, Sato T, Sun X, et al. Pseudo-prolines as a solubilizing, structure-disrupting protection technique in peptide synthesis. J Am Chem Soc 1996;118:9218–27.
[38] Zarándi M, Soós K, Fülöp L, Bozsó Zs, Datki Zs, Tóth GK, et al. Synthesis of Aβ(1–42) and its derivatives with improved efficiency. J Pept Sci 2007;13:94–9.

III.

Journal of proteome research

ARTICLE

pubs.acs.org/jpr

Protein Array Based Interactome Analysis of Amyloid-β Indicates an Inhibition of Protein Translation

Dezso P. Virok,[*,†,#] Dóra Simon,[‡,#] Zsolt Bozsó,[‡] Róbert Rajkó,[§] Zsolt Datki,[†] Éva Bálint,[†] Viktor Szegedi,[†] Tamás Janáky,[‡] Botond Penke,[†,‡] and Lívia Fülöp[‡]

[†]Institute for Plant Genomics, Human Biotechnology, Bioenergy (Bay-Gen) and Szeged, Hungary

[‡]Department of Medical Chemistry, University of Szeged, Szeged, Hungary

[§]Faculty of Engineering, University of Szeged, Szeged, Hungary

Supporting Information

ABSTRACT: Oligomeric amyloid-β is currently of interest in amyloid-β mediated toxicity and the pathogenesis of Alzheimer's disease. Mapping the amyloid-β interaction partners could help to discover novel pathways in disease pathogenesis. To discover the amyloid-β interaction partners, we applied a protein array with more than 8100 unique recombinantly expressed human proteins. We identified 324 proteins as potential interactors of oligomeric amyloid-β. The Gene Ontology functional analysis of these proteins showed that oligomeric amyloid-β bound to multiple proteins with diverse functions both from extra and intracellular localizations. This undiscriminating binding phenotype indicates that multiple protein interactions mediate the toxicity of the oligomeric amyloid-β. The most highly impacted cellular system was the protein translation machinery. Oligomeric amyloid-β could bind to altogether 24 proteins involved in translation initiation and elongation. The binding of amyloid-β to purified rat hippocampal ribosomes validated the protein array results. More importantly, *in vitro* translation assays showed that the oligomeric amyloid-β had a concentration dependent inhibitory activity on translation. Our results indicate that the inhibited protein synthesis is one of the pathways that can be involved in the amyloid-beta induced neurotoxicity.

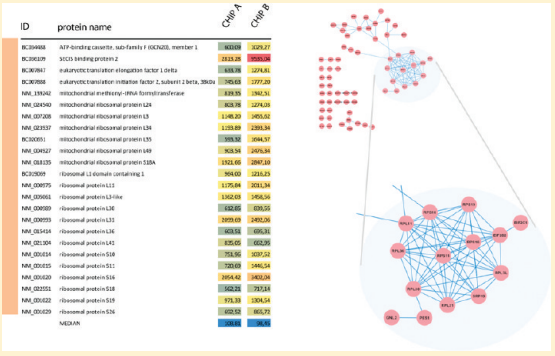

KEYWORDS: Alzheimer's, oligomeric, amyloid-β, protein array, protein chip, proteomics, interactome

INTRODUCTION

Alzheimer's disease (AD) is the most common form of dementia in the developed world and has a severe socioeconomical impact on society. The histological hallmarks of the diseases are the accumulation of amyloid-β (Aβ) fibrils in the extracellular space, the appearance of hyperphosphorylated-tau protein aggregates intracellularly and the progressive loss of neurons. Fibrillar Aβ was suspected of being the primary agent that causes the AD-related histopathology and eventually clinical symptoms. However, the accumulation of the predominantly fibrillar Aβ containing plaques does not correlate well with the clinical symptoms,[1−3] and plaque accumulation appears later than the observed histopathology in animal models.[4,5] Also anti-Aβ immunization leads to the reversal of memory loss without decreasing the plaque concentration.[6,7] Recently, the oligomeric form of Aβ has become the focus of attention, and is regarded as an important specimen that mediates cyto- and synaptotoxicity. The findings supporting the role of oligomeric Aβ in the pathogenesis of AD are numerous and include diverse cellular and supracellular processes. Oligomeric Aβ was shown to perturb potentially AD-related signal transduction cascades including the induction of the ERK/MAPK signaling,[8] increasing calcineurin activity and calcineurin-dependent CREB and BAD dephosphorylation and cell death,[9] inducing tau hyperphosphorylation[10] and inhibiting the phosphatidylinositol-4,5-bisphosphate metabolism.[11] Oligomeric Aβ has an impact on the proteome and phosphoproteome of the cholinergic SN56 cells[12] and transcriptional activity of human neuroblastoma cells.[12] Oligomeric Aβ has also been shown to inhibit axonal transport and the synaptic vesicle rapid endocytosis pathway,[13] and it decreased cellular viability both *in vitro* and *In Vivo*[14,15] in some cases more effectively than fibrillar Aβ.[15,16] Despite its important role in AD pathogenesis, the binding partners by which the oligomeric Aβ mediates its toxicity have not been investigated at a proteome or subproteome level. The protein array technology is a novel postgenomic method to investigate protein−protein interactions in a high-throughput manner. The technology has been successfully used for the identification of protein interaction partners,[17,18] identification of kinase substrates and inhibitors[19,20] and autoantibody profiling.[21−23] To investigate the potential interaction partners of oligomeric Aβ, we used protein arrays with 8163 human proteins covering a significant portion of the

Received: September 6, 2010

   dx.doi.org/10.1021/pr1009096 | *J. Proteome Res.* XXXX, XXX, 000–000

human proteome. We showed that oligomeric Aβ bound to a variety of proteins with diverse functions, indicating that multiple protein interactions mediate the toxicity of the oligomeric amyloid-β. Functional analysis of the interaction partners showed that the most highly impacted cellular system was the protein translation machinery with 24 amyloid binding proteins. The functional effect of amyloid mediated translation inhibition was demonstrated in an *in vitro* translation system.

MATERIALS AND METHODS

Synthesis of the Aβ Peptides

Iso-Aβ 1−42 precursor peptide was synthesized as it was described previously.[24] The sequence of the control scrambled Aβ 1−42 peptide was ^{1}LKAFD^{6}IGVEY^{11}NKVGE^{16}GFAIS^{21}HGVAH^{26}LDVSM^{31}FGEIG^{36}RVDVH^{41}QA. The peptides were synthesized on a Fmoc-Ala-Wang resin using Nα-Fmoc protected amino acids with a CEM Liberty microwave peptide synthesizer (Matthews, NC) on a 0.1 mmol scale. Peptide chain elongation was carried out using 5-fold molar excess of amino acids and HATU/HOAt/DIEA (5:5:10) activation in a DMF at 75 °C for 5 min. Double couplings were performed at residues 1, 2, 4−12, 15, 22−24, 30, 33, 36, and 37. The Fmoc protecting group was removed by treating the peptide-resin twice with 20% piperidine/DMF (75 °C, 3 min). Peptide was cleaved by incubating the resin for 2.5 h in a trifluoroacetic acid/phenol/dithiotreitol/triisopropylsilane/water (36:1:1:1:1) mixture. Crude peptide was precipitated with diethyl ether, dissolved in a mixture of acetic acid and water, lyophilized and purified by HPLC on a Phenomenex Jupiter C4 column (10 μm, 300 Å, 250 × 21 mm) (Torrance, CA).

Preparation of Iso-Aβ Peptide-Derived Amyloid Oligomers

For binding studies, iso-Aβ 1−42 was dissolved in 1,1,1,3,3,3-hexafluoro-2-propanol (HFIP, Sigma, Saint Louis, MO), and incubated for 24 h at room temperature. HFIP was removed in vacuo, followed by dissolution of the oligomeric peptide in Milli-Q ultrapure water (pH 5.0) to 500 μM and sonication for 5 min. The peptide stock solution was diluted to 50 μM in a BSA-free protein array washing buffer (10 mM $NaHCO_3$ buffer, containing 0.45% NaCl, 1% BSA, 5 mM $MgCl_2$, 0.5 mM DTT, 0.05% Triton X-100, 5% glycerol). The iso-Aβ oligomer solution was incubated for 15 min at ambient temperature, and diluted to 10 μM with washing buffer prior to its application on the array. For the Dynamic Light Scattering (DLS) experiments, Transmission Electron Microscopy (TEM) studies, ELISA and *in vitro* translation assay Aβ oligomers were prepared identically, with the only difference that, instead of the washing buffer, the aqueous peptide stock solution was diluted in a solution of 10 mM $NaHCO_3$ and 0.45% NaCl (pH 7.2) to the required peptide concentration.

Transmission Electron Microscopy

Ten microliter droplets of iso-Aβ oligomer or purified ribosome solutions were placed on 400 mesh Formvar-carbon-coated copper grids (Electron Microscopy Sciences, Washington, PA), incubated for 2 min, fixed with a 0.5% (v/v) glutaraldehyde solution, washed three times with Milli-Q water, and finally stained with 2% (w/v) uranyl acetate. Specimens were studied with a Philips CM 10 transmission electron microscope (FEI Company, Hillsboro, OR) operating at 100 kV. Images were taken by a Megaview II Soft Imaging System and analyzed by an AnalySis 3.2 software package (Soft Imaging System, Münster, Germany). Ribosomal images were taken at magnifications of ×64 000 and ×92 000, and ×130 000. The statistical analysis of iso-Aβ oligomers was performed by analyzing the size distribution of the aggregates on 10 images taken from different areas of the grid.

Dynamic Light Scattering

To model the aggregation under the conditions of the on-array binding studies, change of the hydrodynamic radius was monitored for 3 h at 4 °C in a 10 μM iso-Aβ oligomer solution with a Malvern Zetasizer Nano ZS instrument (Malvern Instruments Ltd., Worcestershire, U.K.). The instrument was equipped with a He−Ne laser (633 nm) applying the Non-Invasive Back Scatter (NIBS) technology, detecting the scattered light at an angle of 173°. The translational diffusion coefficients were obtained from the measured autocorrelation functions using the regularization algorithm CONTIN built in the software package Dispersion Technology Software 4.0 (Malvern Instruments Ltd., Worcestershire, U.K.). Assuming the scattering particles to be hard spheres, their apparent hydrodynamic radius can be calculated from the diffusion parameters by using the Stokes−Einstein equation $R_h = k_B T/(6\pi\eta DT)$, where k_B is the Boltzmann constant, T is the absolute temperature, η is the viscosity of the medium, and DT is the translational diffusion coefficient. The correlation function and distribution of the apparent hydrodynamic radii (R_h) over the scattered intensity of the samples were monitored for the expected time interval. The scattering intensity of the background could be neglected compared to the signal intensity of the peptide sample. The results were obtained from three parallel experiments.

Labeling of the Monoclonal Antibody with Alexa Fluor 647 Succinimidyl Ester

Alexa Fluor 647 succinimidyl ester (Invitrogen, Carlsbad, CA) was used for labeling monoclonal anti-Aβ antibody mAb BAM10 (Sigma, Saint Louis, MO). In brief, the antibody was placed in a 3000 MWCO Microcon tube (Millipore, Billerica, MA), repeatedly washed, and finally resuspended in a 50 mM $NaHCO_3$ buffer. A 5-fold excess of the fluorescein dye, dissolved in dimethylformamide, was added to the gently stirred solution of the protein in an ice-bath, and then allowed to warm to an ambient temperature in 2 h protected from light. To neutralize the excess of the succinimidyl ester, 0.1 M of aqueous hydroxylamine solution (pH 8.0) was applied. The labeled antibody was separated from the free dye in the Microcon tube, reconstituted, and stored in the original buffer under the same conditions as that used for the unlabeled antibody.[25]

Probing the ProtoArray Human Protein Microarray

All reagents were purchased from Sigma (Saint Louis, MO). All the steps were performed at 4 °C. The ProtoArray Human Protein microarray 4.0 (Invitrogen, Carlsbad, CA) was blocked in a 10 mM $NaHCO_3$ buffer containing 0.45% NaCl, 1% BSA, and 0.1% Tween-20, pH 7.2, for 1 h with gentle shaking. After the blocking step, excess buffer was drained and iso-Aβ oligomer, prepared as described before, was diluted in washing buffer (10 mM $NaHCO_3$ buffer, containing 0.45% NaCl, 1% BSA, 5 mM $MgCl_2$, 0.5 mM DTT, 0.05% Triton X-100, 5% glycerol) to a final concentration of 10 μM and was added on the top of the array in a total volume of 120 μL. The protein array was covered with a HybriSlip Coverslip (Grace Bio-Laboratories, Brend, OR) and incubated for 1.5 h without shaking at 4 °C. After incubation, the array was washed three times with washing buffer, incubated with Alexa-647 labeled anti-Aβ mAb (BAM10, 1:1000) for 30 min at room temperature protected from light, and finally washed again

dx.doi.org/10.1021/pr1009096 |*J. Proteome Res.* XXXX, XXX, 000–000

three times with washing buffer. The excess solution was decanted, and the protein array was centrifuged for 4 min at 800*g* and dried at an ambient temperature protected from light. Scanning was carried out using a GenePix Personal 4100A microarray scanner (Molecular Devices, Sunnyvale, CA).

ProtoArray Data Processing

The signal intensity of each protein spot was calculated by subtracting the median background value from the median spot value. Protein spots were median normalized so that the median signal intensity of each array became 1. Since every protein had duplicate spots, the average of each duplicate was used as the final signal intensity for a given protein. The corresponding spotted protein concentrations were also averaged. Furthermore, protein signal intensities were concentration normalized so that the median normalized signal intensities were divided by the spot protein concentration values. For further analysis, control spots and spots without accession number were eliminated.

In a two-step procedure, we eliminated the low-concentrations spots and identified the high-concentration normalized signal intensity proteins, the probable Aβ interactors. During the evaluation of the protein array data, robust method[26] was applied, because the low concentrations or high intensities can be considered as outliers from the population. The objective of the least trimmed squares (LTS) estimation as a robust regression procedure is to find the *h*-subset with the smallest least-squares objective function. Its objective is to minimize $\sum_{i=1}^{h}(r)_{i:n}^{2}$, where *r* is the residual. For the functional analysis of the protein array data, a Gene Ontology-based functional grouping was performed using the DAVID Web-based knowledge database.[27] For the network analysis of Aβ interactors, the STRING Web-based interaction database was used.[28]

Preparation and Western-Blot Analysis of Purified Ribosomes

The ribosome purification from human hippocampus was described previously[29] and was applied for rat hippocampus. Protein concentrations of the purified ribosomes were determined by the BCA protein assay kit (Novagen, EMD Chemicals, Gibbstown, NJ). To assess the purity of the purified ribosomes, a Western-blot was performed with the ribosomal protein specific anti-RPL36A antibody (Sigma). Equal amounts (10 μg/lane) of the original homogenized samples and the purified ribosomes were loaded onto a 15% SDS-polyacrylamide gel. The gel was then transferred to a nitrocellulose membrane using an electroblotting apparatus. After blotting, the nitrocellulose membrane was blocked in TBS + 0.5% Tween-20 (TBST) and 5% non-fat dry milk. The membranes were probed with the ribosome specific anti-RPL36A antibody (1:1000) and anti-β-actin antibody (1: 2500) (Sigma, St. Louis, MO), diluted in blocking solution overnight at 4 °C. The following day, the membranes were incubated with an anti-mouse-HRP secondary antibody (1:10000; DakoCytomation, Glostrup, Denmark) and Pierce ECL Western Blotting Substrate (PIERCE, Rockford, IL). Blots were exposed to Kodak film (Sigma).

Enzyme-Linked Immunosorbent Assay (ELISA) Measurement of Oligomeric Aβ-Ribosome Binding

A total of 0.1 μg of purified ribosome was coated in each well of a 96 well plate for 18−20 h at 4 °C, using a coating solution (15 mM Na_2CO_3, 35 mM $NaHCO_3$,, 3 mM NaN_3). After the incubation, the wells were blocked using a blocking solution (10 mM $NaHCO_3$, 0.45% NaCl, 0.1% Tween-20, 1% BSA) at room temperature. Iso-Aβ oligomer (prepared as before) was diluted in a modified washing buffer (10 mM $NaHCO_3$, 0.45% NaCl, 0.05% Tween-20, 1% BSA, 5 mM $MgCl_2$) and was added to the wells in a final concentration of 1, 0.2, 0.1, 0.02, 0.01, 0.002, 0.001, 0.0005, and 0.0001 μM. After 1 h incubation with gentle shaking at room temperature, the plate was washed three times with a washing buffer (10 mM $NaHCO_3$, 0.45% NaCl, 0.1% Tween-20). A monoclonal Aβ oligomer antibody (BAM10, SIGMA) was added to the wells in blocking solution for 1 h at room temperature. After washing twice, the wells were incubated with HRP-conjugated anti-mouse secondary antibody (DakoCytomation, Denmark, Glostrup) in blocking solution. The plate was washed two times, and a TMB reagent (Cell Signaling Technology) was added to the wells. Without using a stopping reagent, the absorbance at 370 nm was constantly monitored using a FLUOstar OPTIMA Multidetection Microplate Reader (BMG LABTECH, Offenburg, Germany). Data values were read at the saturation point of the signal curves.

In Vitro Translation Assay

To permit ribosomal binding, iso-Aβ oligomer was preincubated with the Rabbit Reticulocyte Lysate System, Nuclease Treated *in vitro* translation mix (Promega, WI) in a final concentration of 25, 10, 5, 2.5, 1, 0.5 μM at 37 °C for 60 min. As a control, scrambled Aβ was used in a 10 and 25 μM final concentration. After the preincubation step, 1 μg of the kit's Luciferase control RNA template was added to the reactions, and incubated for 90 min at 30 °C. The luminescence produced by the translated luciferase was measured in a 1:10 dilution of the reaction mixtures according to the Promega Luciferase Assay protocol on a LumiStar Optima luminometer (BMG Labtech, Offenburg, Germany). The expressed luciferase control protein was also investigated by Western-blot. Promega Transcend Biotin-Lysyl-tRNA was added to the *in vitro* translation reaction, in order to detect the *de novo* synthesized biotinylated luciferase, using streptavidin-HRP and chemiluminescent detection. From the translation reaction mixtures, 2 μL aliquots were removed and loaded onto a 10% SDS-polyacrylamide gel. The gel was transferred to a nitrocellulose membrane using an electroblotting apparatus (Bio-Rad Laboratories, CA). The membrane was blocked in TBS + 0.5% Tween-20. For the chemiluminescent detection of the biotinylated proteins, the membrane was incubated in a Streptavidin-HRP solution diluted in TBST for an hour at room temperature and Pierce ECL Western Blotting Substrate (PIERCE, Rockford, IL). Blots were exposed to Kodak film (Sigma, Saint Louis, MO).

RESULTS

Oligomerization of Aβ

We used the iso-Aβ 1−42 peptide, because it possesses advantageous properties compared to the native Aβ 1−42 peptide. The elongation of the iso-Aβ peptide through a side chain between Ser^{26} and Gly^{25} induces a bent structure, which results in a significantly more straightforward synthesis and purification compared to the unaltered sequence. On the other hand, the isopeptide bond readily transforms through an O → N acyl shift into the unaltered, native Aβ 1−42 structure at physiological pH. By using an optimized protocol, an exceptionally stable oligomeric population can be obtained, as was described by our group.[24] The stability of the Aβ 1−42 oligomers was examined by dynamic light scattering. DLS provides quantitative information about the size distribution of an

dx.doi.org/10.1021/pr1009096 |*J. Proteome Res.* XXXX, XXX, 000–000

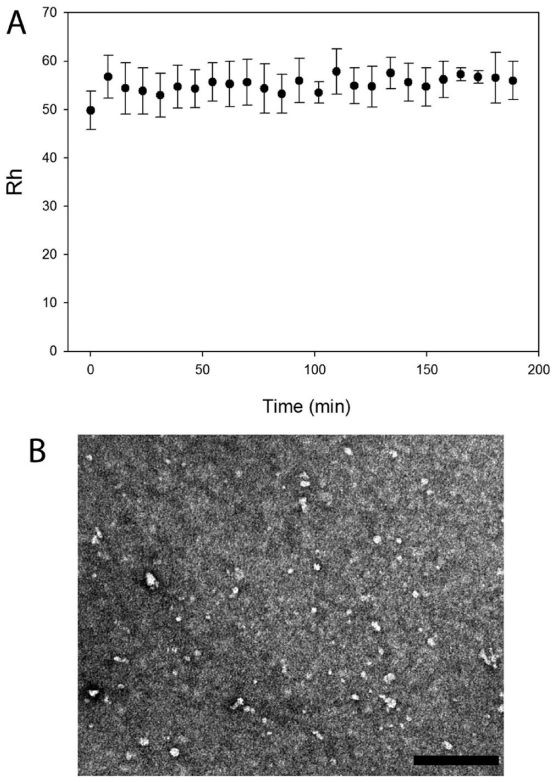

Figure 1. Aggregation of oligomeric Aβ. (A) DLS measurements of Aβ (1−42) oligomers. Measurements were performed in a $NaHCO_3$– solution at pH = 7.2 at 4 °C. Aggregation was monitored for 3 h. (B) TEM image of the Aβ (1−42) oligomers prepared by following the protocol applied in the on-array binding studies. The TEM bar is 100 nm.

oligomer population. In parallel, the actual shape of the oligomers has to be characterized by microscopic techniques working in the submicrometer range. Therefore, we conducted TEM investigations. The results of the DLS measurements are summarized in Figure 1A. The stability of Aβ 1−42 oligomers was monitored at 4 °C for the time interval typically applied in the microarray experiments. Experimental results revealed that the oligomers possessed an average hydrodynamical diameter of 55.1 ± 3.9 nm and were proven to retain their size distribution during the time examined. At the end of the incubation period, oligomers were visualized by TEM (Figure 1B). The shape of the oligomers could be considered to be spherical, as no sign of anisotropic forms could be observed on the TEM images. The statistical analysis of the TEM images revealed an average diameter of 7 ± 3 nm for the aggregates. The discrepancy between the average sizes measured with DLS and TEM can be explained by two phenomena: (i) DLS measures the hydrodynamical sizes; therefore, if the protein chains are fully hydrated, exert an expanded structure and are measured together with their hydrate shell; however, on the TEM grids, the particles are measured in their dehydrated state, and (ii) statistically underrepresented, atypical large aggregates, which are not observed by TEM, can distort the size distribution in DLS, as it is determined from the intensity of the scattered light, which is proportional to the sixth power of the hydrodynamical radius of the scattering particle, resulting in an apparently increased average diameter. Size data derived from DLS measurements were used, therefore, only to demonstrate the stability of the oligomers during the experiment.

Protein Array Based Oligomeric Aβ Interactome Screen

We applied two parallel Protoarray 4.0 protein arrays for the Aβ interactome analysis. These arrays contain duplicate spots for 8163 unique recombinantly expressed human proteins and also control spots. The recombinant expression is performed in an insect cell line; hence, the eukaryotic post-translational modifications are likely present. Since the Aβ binding was visualized with a monoclonal Aβ-antibody, we measured the aspecific binding of the antibody onto the array proteins. When we applied the antibody alone, the hybridization resulted only a dim background fluorescence (data not shown). It was obvious from analyzing the raw images and signal intensities that Aβ could bind to numerous proteins on the array (Figure 2A). To identify the most likely Aβ interactors, a multistep analysis was performed. First, we median normalized the signal intensities on both protein arrays and eliminated all the control spots and proteins without accession numbers from the data set. Since the spotted protein concentration was highly variable within the arrays, we normalized the signal intensities by the spotted protein concentrations. One drawback of this method is that spots with low and extremely low protein concentrations can have a high normalized signal intensity. To circumvent the overrepresentation of small concentration spots and to identify spots with high normalized signal intensities, we applied a two-step LTS-based robust fitting statistical filtering. Instead of the more commonly used least median of squares (LMS), we decided to use LTS. LTS regression has several advantages over LMS. Its objective function is smoother, making LTS less sensitive to local effects than LMS. Its statistical efficiency is better, because the LTS estimator is asymptotically normal whereas the LMS estimator has a lower convergence rate.[26] The breakdown value of LTS equals that for LMS.[26] Intuitively, the breakdown point of an estimator is the proportion of incorrect observations (i.e., arbitrarily large observations) that an estimator can handle before giving an arbitrarily biased result. In our case, the unusable data was fitted and the usable data was treated as outliers; thus, we discriminated the outlying data points from the well-fitted ones. First, LTS analysis calculated a cutoff value of 2021 arbitrary units for the averaged spot concentration for the two arrays (Figure 2B). Only spots with a higher concentration were used further. Second, the signal values were normalized with the spot concentration, and the same LTS method was applied to identify the group of spots with the highest normalized signal intensities (Figure 2C). LTS analysis calculated 560.3 and 647.5 arbitrary units concentration normalized signal intensity cutoff values for the applied two protein arrays. Only proteins that had higher concentration normalized signal intensities than the cutoff values of both arrays were included in the final analysis. Altogether, 324 proteins had higher normalized signal intensities than the cutoff values on both arrays. These proteins were considered as potential interactors of Aβ, and used in the final analysis. The list of the potential Aβ binding proteins can be found in the Supplementary Table.

To gain functional information about the Aβ interactors, we performed a Gene Ontology (GO) analysis, using the DAVID Web-based knowledgebase. DAVID analyzes the GO terms relating to the significantly altered genes/proteins, identifies the terms that contain multiple proteins, and calculates a significance value for the observed enrichment compared to a background protein set—in our case all the proteins on the array. The DAVID analysis revealed that the most highly impacted GO Biological Function category was the protein

dx.doi.org/10.1021/pr1009096 |J. Proteome Res. XXXX, XXX, 000–000

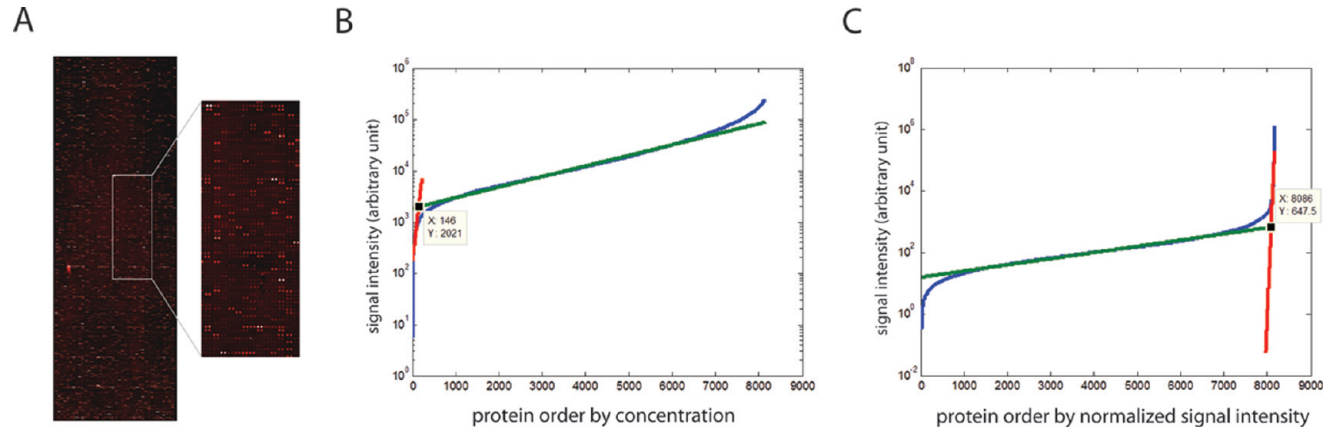

Figure 2. Protein array hybridization and data analysis. (A) Representative image of the protein array after Aβ hybridization. (B) Robust fitting the beginning part (red) and the remaining part (green) of the logarithmic transformed concentrations (blue). The analysis of one array is shown. (C) Robust fitting the beginning part (green) and the remaining part (red) of the logarithmic transformed concentration normalized signal intensities (blue). The analysis of one array is shown.

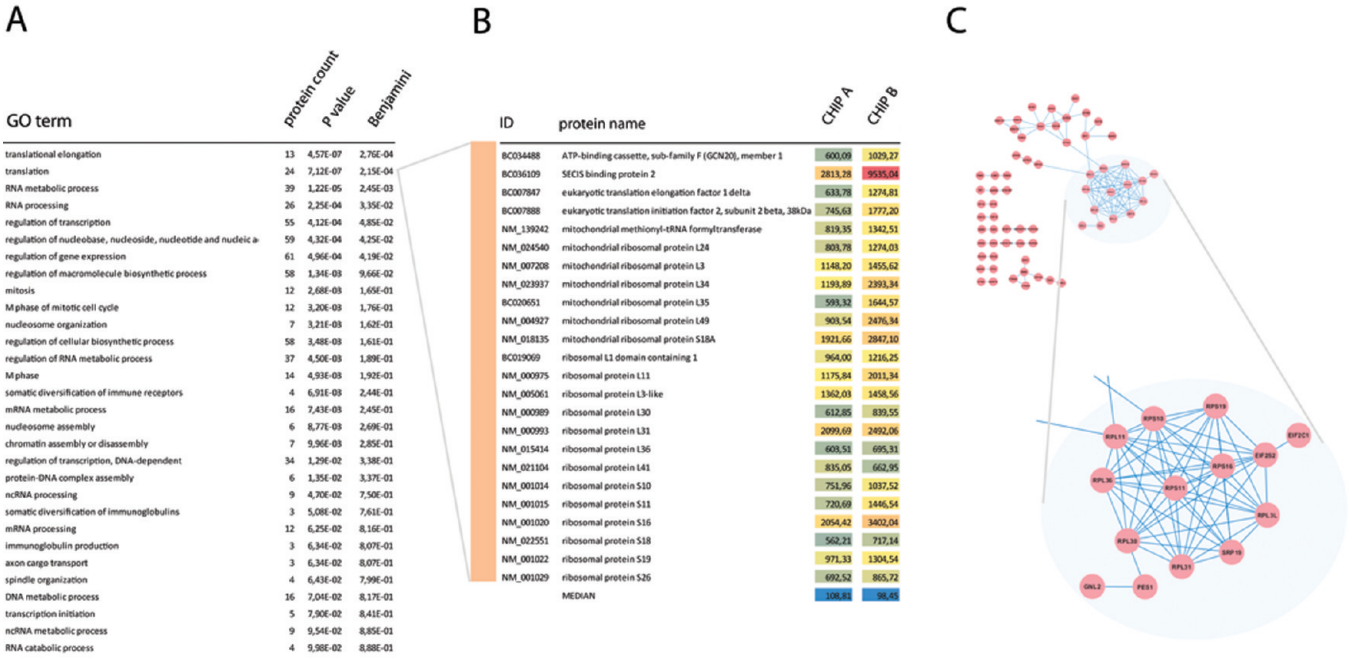

Figure 3. Functional analysis of human proteins interacting with Aβ. (A) GO functional analysis of Aβ binder proteins. The Aβ binder proteins were analyzed for enriched GO functional groups by using the DAVID Web-based knowledge database. The significantly enriched ($P < 0.01$) functional groups are shown with the number of proteins in each group. (B) Members of the GO Biological Function category "translation". The concentration normalized signal intensities from both protein array experiments are shown. On the last row, the median concentration normalized signal intensities on the protein arrays are highlighted. (C) Interaction analysis of the Aβ binding proteins using the STRING interaction database. The connections between ribosomal proteins have been enlarged.

translation with a p-value of 7.12×10^{-7} (Figure 3A,B). The "translation" functional category contained 24 proteins, including several mitochondrial and nonmitochondrial ribosome components along with other proteins required for translation, such as translation initiation factors (Figure 3B). Growing evidence highlights the impact of intracellular Aβ on cellular processes.[30] The GO functional analysis also supported the intracelllular Aβ hypothesis with the highly significant Aβ binding to translation, RNA processing, axon cargo and cell cycle-related proteins (Figure 3A).

In addition to the GO-based functional grouping, a STRING interaction analysis was performed on the individual Aβ binding proteins. STRING screens and visualizes protein/gene interactions based on genomic context, experimental evidence, coexpression and data from other databases such as Pubmed, MINT, KEGG, BIND and BioGRID. The interaction analysis showed that several Aβ binder proteins are connected to each other; moreover, supporting the GO functional analysis a highly interconnected group of ribosomal proteins was prominent in the STRING generated pathway (Figure 3C).

dx.doi.org/10.1021/pr1009096 |J. Proteome Res. XXXX, XXX, 000–000

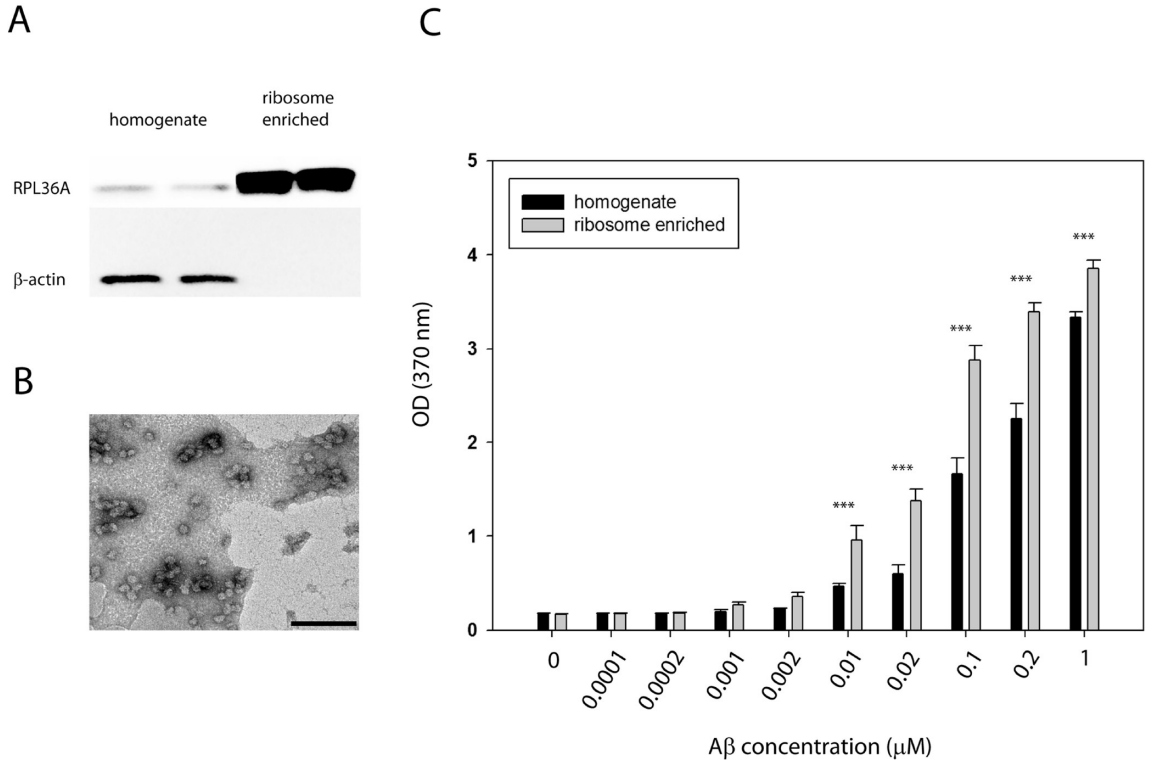

Figure 4. Binding of oligomeric Aβ to purified hippocampal ribosomes. (A) Western blot validation of ribosome purification. Ten micrograms of protein from two rat hippocampus homogenates and two purified ribosomal fractions was loaded. The ribosomal enrichment was verified using the ribosomal protein specific anti-RPL36A antibody. As a control, the β-actin levels were also measured in the samples. (B) TEM visualization of the purified ribosomes. The image shows round-shaped organelles, with an average diameter of 15−20 nm, resembling intact ribosomes. TEM bar is 100 nm. (C) Concentration dependent Aβ binding to purified ribosomal complexes and control homogenates. (n = 6, values are mean ± SEM, P-values were calculated using the Student's t-test). ***$P < 0.01$.

Aβ Binding to Purified Ribosomal Complexes

To support the protein array binding data, we performed an ELISA binding assay on purified rat hippocampal ribosomes. The ribosome purification/enrichment was performed using a sucrose gradient centrifugation, as described earlier.[29] The degree of enrichment was verified using a ribosomal protein (RPL36A) specific and actin specific Western blot (Figure 4A). The Western blots clearly showed that RPL36A was highly enriched in the purified fraction compared to the initial homogenate. On the other hand, the actin signal was only detected in the initial homogenate, but not in the purified fraction, indicating that the purification was specific for ribosomes and ribosomal proteins. The presence of purified intact ribosomes in the purified fraction was also visualized by TEM (Figure 4B). Purified ribosomes and unpurified hippocampus homogenates as controls were adsorbed to an ELISA plate, and Aβ oligomer (1 μM to 0.0001 μM) was added to the immobilized ribosomes and homogenates. As shown in Figure 4C, Aβ bound to immobilized ribosomes in a dose-dependent manner. Moreover, there was a significantly higher binding to the purified ribosomes compared to the hippocampus homogenates when we applied Aβ between 0.01 and 1μM. Aβ binding to the hippocampus homogenates supported the protein array data showing that Aβ probably had multiple targets in the homogenate. On the other hand, the Aβ binding to purified ribosomes was stronger, indicating that the binding strength to ribosomal proteins was significantly higher than the binding to the "background" protein population in the hippocampus homogenate.

Aβ-Mediated Inhibition of *in Vitro* Protein Translation

To test the effect of Aβ on the efficiency of translation, an *in vitro* translation reaction was performed. To increase specificity, we used the nuclease-treated rabbit reticulocyte translation reaction that eliminates the endogenous mRNA background of the translation mix. The same Aβ binding parameters that were used in the protein array study (90 min, 4 °C) were applied, except the temperature was raised to the physiological 37 °C. The 90 min Aβ preincubation step enabled the Aβ−ribosomal binding. After the preincubation step, a luciferase template was added to the reaction and a standard translation reaction was performed. Functionally validating the protein array binding data, the *in vitro* translation results clearly showed a concentration dependent inhibitory effect on the luminescent activity of the luciferase enzyme (Figure 5A). The inhibitory effect was significant, even with a 1 μM Aβ concentration. The inhibitory effect was correlated with the applied Aβ concentration reaching a close to 50% reduction in luminescence at 25 μM Aβ concentration. To exclude the possibility that the reduction of the luminescent signal intensity was due to the Aβ-mediated inhibition of luciferase enzyme function and not to the decreased luciferase translation, a Western-blot experiment was performed. The Western-blot data clearly showed that the observed reduction of luciferase function was the result of the reduction of luciferase protein expression (Figure 5B).

Notably, there was a significant difference between the inhibitory activity of the native and scrambled Aβ. The native form showed a ∼25% inhibitory activity at a 10 μM concentration, while the scrambled form showed a ∼10% inhibition. The

dx.doi.org/10.1021/pr1009096 |*J. Proteome Res.* XXXX, XXX, 000–000

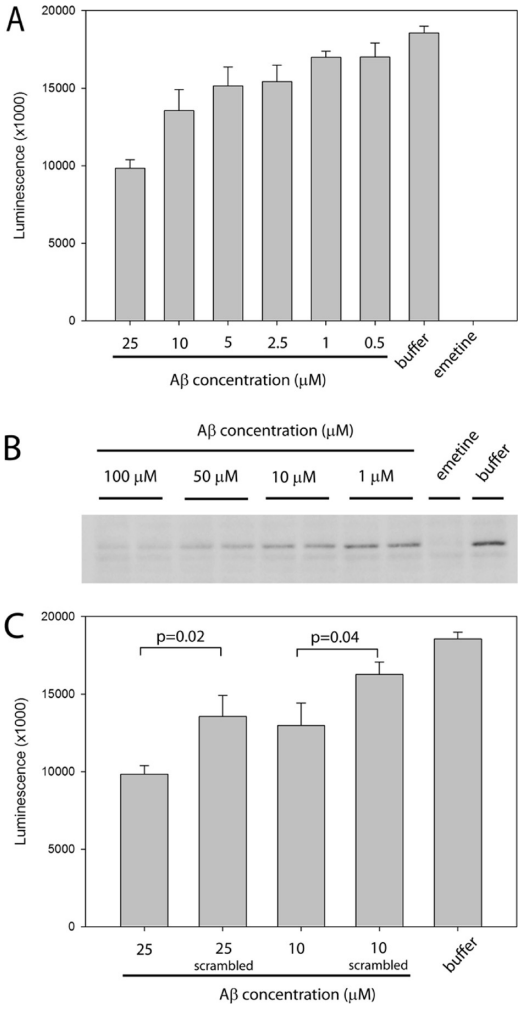

Figure 5. *In vitro* analysis of Aβ mediated translation inhibition. (A) The effect of Aβ on *in vitro* luciferase expression. Aβ was applied in different concentrations in an *in vitro* translation system. The luminescent activity of the translated luciferase was measured with a standard luminometer. The luminescence values were significantly different ($P < 0.05$) from the control "buffer only" values in all applied Aβ concentrations except the 0.5 μM case ($n = 3$, values are mean ± SEM, *P*-values were calculated using the Student's *t*-test). (B) Western blot analysis of luciferase expression. The applied Aβ concentration ranged from 1 to 100 μM. (C) Comparison of the translation inhibition effect of native and scrambled Aβ ($n = 3$, values are mean ± SEM, *P*-values were calculated using the Student's *t*-test). The known translational inhibitor emetine was used as a positive control in both the luminescent measurements and the Western blot experiments. The inhibitory activity of Aβ was compared to the buffer controls containing no amyloid.

difference between the native and scrambled forms was even higher at the 25 μM concentration. Twenty-five micromolar native amyloid caused a ~50% translation inhibition, while the scrambled form showed a ~25% translation inhibition. The translation inhibitory activity was about equal of the 10 μM native Aβ and the 25 μM scambled Aβ (Figure 5C).

DISCUSSION

To explore the Aβ cellular interactome, a protein array method was applied. The applied Protoarray 4.0 array contained 8163 recombinantly expressed human proteins spotted in a defined order onto the array. The protein array method is basically a multiplex hybridization: Aβ is hybridized onto the array and, after washing steps, the bound protein is visualized with a secondary labeled antibody, and the signal intensity is screened with a regular array scanner for each spotted protein. The detected signal intensity in a particular spot is influenced by the K_d of the two interacting proteins and the protein concentrations of the interactors. It should be added that the spotted protein concentration was not the same for each spotted protein on the Protoarray protein array. In fact, there were major differences between the spot concentrations ranging from 0 to ~200 000 arbitrary units. We thought that the large differences in spotted protein concentration should be normalized in such a way that the signal intensity detected on a given spot was divided by the concentration of the spot protein. It is worth mentioning that protein array hybridizations were highly reproducible; the concentration normalized signal intensities had a correlation (R^2) of 0.901 between the arrays. A version of the concentration normalization method was successfully applied earlier in an autoantibody repertoire screening protein array analysis.[31] While the concentration normalization method eliminates false positives from the interactome, it also introduces false negatives. Strong Aβ binder proteins that also had a high spot concentration could be eliminated, while due to the low dissociation constant, a significantly smaller amount of spotted proteins could also produce the same binding signal intensity. As stated previously,[31] the concentration-independent and the concentration-based normalization methods result in interactomes that are not mutually exclusive, but rather complementary with each other.

Our protein array analysis revealed that the Aβ-related protein interaction is not specific; the peptide could interact with at least 324 cellular proteins. The observed nonspecific binding is most likely related to the oligomeric Aβ structure. Aβ oligomers encompass a wide range of species, ranging from low-molecular-weight to high-molecular-weight aggregates. These oligomers belong to the new class of proteins called "intrinsically disordered proteins". All of these proteins have a series of different metastable conformations and interact with a large number of partners, such as other proteins and membrane structures. The flexibility of their structure provides versatile interactions and causes the lack of specificity of binding to partner molecules.[32] The GO-based functional analysis showed that the most highly impacted cellular process was the translation with 24 proteins. Translation consists of three basic processes: initiation, elongation and termination. The protein array data indicates that Aβ might interfere with the initiation and elongation steps. We found that Aβ bound to the important initiation factor eukaryotic initiation factor 2 (EIF2).[33] Aβ also bound to the mitochondrial methionyl-tRNA formyltransferase, a protein involved in mitochondrial translation initiation.[34] Besides translation initiation, Aβ bound to several ribosomal proteins involved in elongation. Despite their importance, the precise roles of ribosomal proteins are not known. These proteins are probably involved in the correct folding and processing of rRNA and in the assembly of the ribosome.[35] Robledo et al. showed that the individual depletion of 9 different small ribosomal subunit and 6 large ribosomal subunit genes lead to a decrease in all ribosomal proteins of both the small and the large subunits and the assembled ribosomes and polysomes. The knockdown of ribosomal proteins also led to an increase of rRNA precursors, suggesting their roles in rRNA processing.[36] From the ribosomal proteins tested by Robledo et al., we showed that Aβ binds to

dx.doi.org/10.1021/pr1009096 |*J. Proteome Res.* XXXX, XXX, 000–000

ribosomal protein S16 (RPS16), RPS19 and RPL11. One of the cellular compartments involved in AD pathogenesis is the mitochondrium. The mechanism(s) of the well described Aβ mediated mitochondrial damage[37,38] is not exactly known, but it probably involves direct binding of Aβ to mitochondrial proteins.[39] Our experiments showed that six mitochondrial ribosomal proteins and the mitochondrial methionyl-tRNA formyltransferase bound to Aβ. If the Aβ binding also has an inhibitory effect on mitochondrial translation, as we showed in the *in vitro* translation system, then the translational blockade might lead to mitochondrial dysfunction. Indeed, the intact protein synthesis is essential to the normal mitochondrial function, as described earlier in the case of genetic diseases such as the Pearson syndrome and the Kearns−Sayre syndrome.[40] Mitochondria are believed to be originally derived from endosymbiotic prokaryotes and share features in common with prokaryotes. Considering the possible inhibition of mitochondrial protein translation, it is worth to note that neuroinflammation, triggered by various bacterial and viral infections, is increasingly considered as an etiological factor of AD.[41−44] It was also shown that one of the most implicated bacteria, the *Chlamydia pneumoniae* could induce amyloid plaque formation in the brains of infected BALB/c mice.[45] The increased Aβ expression could be an innate defense response, as recent data showed that Aβ could function as a natural antibiotic.[46] While one of its major antibacterial mechanisms could be the membrane permeabilization; our results suggest that similarly to other antibiotics, the direct effect of Aβ on bacterial translation might also contribute.

It is important to note that, while we showed the Aβ binding to several translation-related proteins, a simple interaction detection by protein array does not necessarily mean that the proteins bind *In Vivo* or the binding has functional consequence. There could be several reasons, for example, the Aβ and its interactors are not expressed at the same time or cellular compartment or the interactors' Aβ binding site is facing to another molecule in a protein or other complex. Therefore, additional binding and functional studies are needed to validate the protein array results. One of the technical limitations associated with the protein array technology is that the proteins are individually printed onto the array; hence, the Aβ binding to protein complexes such as the ribosomes is not possible. Therefore, we decided to investigate the Aβ binding to native ribosomes purified from rat hippocampus. The binding experiments indicated that Aβ was able to bind to the correctly folded ribosomal complexes. While we clearly showed that Aβ can bind to ribosomal proteins and also to native ribosomal complexes, this binding could occur on ribosomal regions that are not important in translation. Therefore, we functionally tested the Aβ inhibitory effect in an *in vitro* translation system. We discovered that Aβ binding had a concentration dependent inhibitory effect on translation starting at a concentration of 1 μM and became prominent from a 2.5−10 μM Aβ concentration. Importantly, while the scrambled Aβ also had an aspecific inhibitory effect, this inhibitory effect was significantly lower than the native Aβ's, indicating that the effective inhibition requires the native amino acid sequence. While the detection of Aβ mediated translation inhibition is novel here, a problem is that a major inhibitory effect could be observed using the relatively high 2.5−10 μM or higher Aβ concentrations. One explanation could be that the reticulocyte lysate system we used for translation assays had no compartments. Intracellular Aβ via active or passive transports could get into and accumulate in cellular compartments, such as the endoplasmic reticulum, and could reach a relatively high local concentration. Indeed, it was recently described that neuronal cells could take up Aβ oligomers, and the peptides later accumulated in cellular compartments such as late endosomes or lysosomes. The accumulation of Aβ oligomers reached a 2.5 μM local concentration, which was 2 orders of magnitude higher that the extracellular 25 nM.[47]

We also have to underline that while we showed that *in vitro* the Aβ could bind to several proteins involved in translation, and was able to decrease the *de novo* protein expression in an *in vitro* translation system, these findings do not mechanistically mean that this inhibition occurs *In Vivo* and contributes to the pathogenesis of AD. A difficulty with the *In Vivo* validation could be that the detection of the decreased protein content in an AD tissue could just also be a circumstantial evidence, since various AD- and Aβ-related pathways may also lead to decreased local protein content. These altered pathways include the increased apoptosis,[48] impaired neurotrophin function,[49] mitochondrial respiration[37] and microtubular transport.[50,51] A more definitive *In Vivo* validation of our finding could be the isolated investigation of the translation machinery in the brains of AD patients and controls. In fact, these measurements have already been performed by two independent groups.[29,52] In a comparative study by Ding et al.,[52] polyribosomal complexes isolated from different brain areas of 8−8 patients with AD and mild cognitive impairment (MCI) and 10 controls were tested for protein synthesis capability. Ribosomes isolated from AD- related cortical areas such as superior middle temporal gyri and inferior parietal lobule showed a significantly inhibited (30−60%) protein synthesis compared to non-AD controls. Ribosomes from other regions that are not involved in AD pathogenesis such as the cerebellum were unaffected. This difference indicates that the protein synthesis decline is not a general metabolic effect of the disease. Moreover, the fact that patients with MCI, a potentially pre-AD state, also had a significantly decreased protein synthesis indicates that the decreased translation might be one of the causes of AD and not the result of the disease. Since cellular translation is a complex system, the observed inhibition could have various sources. Previous studies focused on the AD-related increased oxidation of the ribosomal RNA and mRNA pools.[52] Our novel data indicates that Aβ could bind to various ribosomal and other translation-related proteins and, importantly, this binding had an functional effect, a significantly decreased protein synthesis. It is possible that *In Vivo* the increased oxidation of rRNA and mRNA and the direct binding of Aβ to various translation-related proteins are parallel mechanisms that might result a decreased protein synthesis in the diseased tissues.

■ ASSOCIATED CONTENT

Supporting Information

The list of the potential Aβ binding proteins. This material is available free of charge via the Internet at http://pubs.acs.org.

■ AUTHOR INFORMATION

Corresponding Author

*Dezso P. Virok, M.D, Ph.D., Institute for Plant Genomics, Human Biotechnology and Bioenergy (BAY-GEN), 2 Derkovits fasor, H-6726 Szeged, Hungary. Phone: +36 30 820 1558. Fax: +36 62 546 974. E-mail: virok@baygen.hu.

Author Contributions

#These authors contributed equally.

■ ACKNOWLEDGMENT

Dezso P. Virok, Zsolt Datki, Viktor Szegedi and Éva Bálint were supported by the Ede Teller Programme of the Hungarian National Office for Research and Technology (NAP_BIO_06). Livia Fulop acknowledges the support of the János Bolyai Fellowship from the Hungarian Academy of Sciences and the Support of the European Union 7th Framework programme (HEALTH-F2-2007-201159, HEALTH-F2-2007-211696). Botond Penke, Tamás Janáky and Zsolt Bozsó were supported by the Hungarian Scientific Research Fund (OTKA NK 73672) and the European Union 7th Framework programme (HEALTH-F2-2007-201159, HEALTH-F2-2007-211696).

■ REFERENCES

(1) Terry, R. D. The pathogenesis of Alzheimer disease: an alternative to the amyloid hypothesis. *J. Neuropathol. Exp. Neurol.* **1996**, *55* (10), 1023–5.

(2) McLean, C. A.; Cherny, R. A.; Fraser, F. W.; Fuller, S. J.; Smith, M. J.; Beyreuther, K.; Bush, A. I.; Masters, C. L. Soluble pool of Abeta amyloid as a determinant of severity of neurodegeneration in Alzheimer's disease. *Ann. Neurol.* **1999**, *46* (6), 860–6.

(3) Lue, L. F.; Kuo, Y. M.; Roher, A. E.; Brachova, L.; Shen, Y.; Sue, L.; Beach, T.; Kurth, J. H.; Rydel, R. E.; Rogers, J. Soluble amyloid beta peptide concentration as a predictor of synaptic change in Alzheimer's disease. *Am. J. Pathol.* **1999**, *155* (3), 853–62.

(4) Westerman, M. A.; Cooper-Blacketer, D.; Mariash, A.; Kotilinek, L.; Kawarabayashi, T.; Younkin, L. H.; Carlson, G. A.; Younkin, S. G.; Ashe, K. H. The relationship between Abeta and memory in the Tg2576 mouse model of Alzheimer's disease. *J. Neurosci.* **2002**, *22* (5), 1858–67.

(5) Billings, L. M.; Oddo, S.; Green, K. N.; McGaugh, J. L.; LaFerla, F. M. Intraneuronal Abeta causes the onset of early Alzheimer's disease-related cognitive deficits in transgenic mice. *Neuron* **2005**, *45* (5), 675–88.

(6) Kotilinek, L. A.; Bacskai, B.; Westerman, M.; Kawarabayashi, T.; Younkin, L.; Hyman, B. T.; Younkin, S.; Ashe, K. H. Reversible memory loss in a mouse transgenic model of Alzheimer's disease. *J. Neurosci.* **2002**, *22* (15), 6331–5.

(7) Dodart, J. C.; Bales, K. R.; Gannon, K. S.; Greene, S. J.; DeMattos, R. B.; Mathis, C.; DeLong, C. A.; Wu, S.; Wu, X.; Holtzman, D. M.; Paul, S. M. Immunization reverses memory deficits without reducing brain Abeta burden in Alzheimer's disease model. *Nat. Neurosci.* **2002**, *5* (5), 452–7.

(8) Young, K. F.; Pasternak, S. H.; Rylett, R. J. Oligomeric aggregates of amyloid beta peptide 1−42 activate ERK/MAPK in SH-SY5Y cells via the alpha7 nicotinic receptor. *Neurochem. Int.* **2009**, *55* (8), 796–801.

(9) Reese, L. C.; Zhang, W.; Dineley, K. T.; Kayed, R.; Taglialatela, G. Selective induction of calcineurin activity and signaling by oligomeric amyloid beta. *Aging Cell* **2008**, *7* (6), 824–35.

(10) De Felice, F. G.; Wu, D.; Lambert, M. P.; Fernandez, S. J.; Velasco, P. T.; Lacor, P. N.; Bigio, E. H.; Jerecic, J.; Acton, P. J.; Shughrue, P. J.; Chen-Dodson, E.; Kinney, G. G.; Klein, W. L. Alzheimer's disease-type neuronal tau hyperphosphorylation induced by A beta oligomers. *Neurobiol. Aging* **2008**, *29* (9), 1334–47.

(11) Berman, D. E.; Dall'Armi, C.; Voronov, S. V.; McIntire, L. B.; Zhang, H.; Moore, A. Z.; Staniszewski, A.; Arancio, O.; Kim, T. W.; Di Paolo, G. Oligomeric amyloid-beta peptide disrupts phosphatidylinositol-4,5-bisphosphate metabolism. *Nat. Neurosci.* **2008**, *11* (5), 547–54.

(12) Joerchel, S.; Raap, M.; Bigl, M.; Eschrich, K.; Schliebs, R. Oligomeric beta-amyloid(1−42) induces the expression of Alzheimer disease-relevant proteins in cholinergic SN56.B5.G4 cells as revealed by proteomic analysis. *Int. J. Dev. Neurosci.* **2008**, *26* (3−4), 301–8.

(13) Moreno, H.; Yu, E.; Pigino, G.; Hernandez, A. I.; Kim, N.; Moreira, J. E.; Sugimori, M.; Llinas, R. R. Synaptic transmission block by presynaptic injection of oligomeric amyloid beta. *Proc. Natl. Acad. Sci. U. S.A.* **2009**, *106* (14), 5901–6.

(14) Kim, H. J.; Chae, S. C.; Lee, D. K.; Chromy, B.; Lee, S. C.; Park, Y. C.; Klein, W. L.; Krafft, G. A.; Hong, S. T. Selective neuronal degeneration induced by soluble oligomeric amyloid beta protein. *FASEB J.* **2003**, *17* (1), 118–20.

(15) El-Agnaf, O. M.; Nagala, S.; Patel, B. P.; Austen, B. M. Non-fibrillar oligomeric species of the amyloid ABri peptide, implicated in familial British dementia, are more potent at inducing apoptotic cell death than protofibrils or mature fibrils. *J. Mol. Biol.* **2001**, *310* (1), 157–68.

(16) Dahlgren, K. N.; Manelli, A. M.; Stine, W. B., Jr; Baker, L. K.; Krafft, G. A.; LaDu, M. J. Oligomeric and fibrillar species of amyloid-beta peptides differentially affect neuronal viability. *J. Biol. Chem.* **2002**, *277* (35), 32046–53.

(17) Schnack, C.; Danzer, K. M.; Hengerer, B.; Gillardon, F. Protein array analysis of oligomerization-induced changes in alpha-synuclein protein-protein interactions points to an interference with Cdc42 effector proteins. *Neuroscience* **2008**, *154* (4), 1450–7.

(18) Satoh, J.; Obayashi, S.; Misawa, T.; Sumiyoshi, K.; Oosumi, K.; Tabunoki, H. Protein microarray analysis identifies human cellular prion protein interactors. *Neuropathol. Appl. Neurobiol.* **2009**, *35* (1), 16–35.

(19) Meng, L.; Michaud, G. A.; Merkel, J. S.; Zhou, F.; Huang, J.; Mattoon, D. R.; Schweitzer, B. Protein kinase substrate identification on functional protein arrays. *BMC Biotechnol.* **2008**, *8*, 22.

(20) Schnack, C.; Hengerer, B.; Gillardon, F. Identification of novel substrates for Cdk5 and new targets for Cdk5 inhibitors using high-density protein microarrays. *Proteomics* **2008**, *8* (10), 1980–6.

(21) Bombaci, M.; Grifantini, R.; Mora, M.; Reguzzi, V.; Petracca, R.; Meoni, E.; Balloni, S.; Zingaretti, C.; Falugi, F.; Manetti, A. G.; Margarit, I.; Musser, J. M.; Cardona, F.; Orefici, G.; Grandi, G.; Bensi, G. Protein array profiling of tic patient sera reveals a broad range and enhanced immune response against Group A Streptococcus antigens. *PLoS One* **2009**, *4* (7), e6332.

(22) Canzler, U.; Bartsch, H.; Ulitzsch, S.; Kurien, B. T.; Dorri, Y.; Scofield, R. H.; Grossmann, K.; Lehmann, W.; Pilarsky, C.; Denz, A.; Grutzmann, R.; Conrad, K.; Schmitz, M.; Rieber, E. P.; Distler, W.; Bachmann, M. P. Detection of autoantibodies to tumour-associated antigens in sera of patients with systemic autoimmunity using a novel protein microblot array. *Scand. J. Immunol.* **2009**, *69* (6), 563–9.

(23) Hudson, M. E.; Pozdnyakova, I.; Haines, K.; Mor, G.; Snyder, M. Identification of differentially expressed proteins in ovarian cancer using high-density protein microarrays. *Proc. Natl. Acad. Sci. U.S.A.* **2007**, *104* (44), 17494–9.

(24) Bozso, Z.; Penke, B.; Simon, D.; Laczko, I.; Juhasz, G.; Szegedi, V.; Kasza, A.; Soos, K.; Hetenyi, A.; Weber, E.; Tohati, H.; Csete, M.; Zarandi, M.; Fulop, L. Controlled in situ preparation of A beta(1−42) oligomers from the isopeptide "iso-A beta(1−42)", physicochemical and biological characterization. *Peptides* **2010**, *31* (2), 248–56.

(25) Brinkley, M. A brief survey of methods for preparing protein conjugates with dyes, haptens, and cross-linking reagents. *Bioconjugate Chem.* **1992**, *3* (1), 2–13.

(26) Rousseeuw, P. J.; Leroy, A. M. *Robust Regression and Outlier Detection*; John Wiley & Sons, Inc.: New York, NY, 1987.

(27) Sherman, B. T.; Huang da, W.; Tan, Q.; Guo, Y.; Bour, S.; Liu, D.; Stephens, R.; Baseler, M. W.; Lane, H. C.; Lempicki, R. A. DAVID Knowledgebase: a gene-centered database integrating heterogeneous gene annotation resources to facilitate high-throughput gene functional analysis. *BMC Bioinf.* **2007**, *8*, 426.

(28) Jensen, L. J.; Kuhn, M.; Stark, M.; Chaffron, S.; Creevey, C.; Muller, J.; Doerks, T.; Julien, P.; Roth, A.; Simonovic, M.; Bork, P.; von Mering, C. STRING 8--a global view on proteins and their functional interactions in 630 organisms. *Nucleic Acids Res.* **2009**, *37* (Database issue), D412–6.

(29) Langstrom, N. S.; Anderson, J. P.; Lindroos, H. G.; Winblad, B.; Wallace, W. C. Alzheimer's disease-associated reduction of polysomal mRNA translation. *Brain Res. Mol. Brain. Res.* **1989**, *5* (4), 259–69.

(30) LaFerla, F. M.; Green, K. N.; Oddo, S. Intracellular amyloid-beta in Alzheimer's disease. *Nat. Rev. Neurosci.* **2007**, *8* (7), 499–509.

(31) Marina, O.; Biernacki, M. A.; Brusic, V.; Wu, C. J. A concentration-dependent analysis method for high density protein microarrays. *J. Proteome Res.* **2008**, *7* (5), 2059–68.

(32) Tompa, P. *Structure and Function of Intrinsically Disordered Proteins*; CRC Press, Taylor & Francis: New York, 2010.
(33) Schmitt, E.; Naveau, M.; Mechulam, Y. Eukaryotic and archaeal translation initiation factor 2: a heterotrimeric tRNA carrier. *FEBS Lett.* **2010**, *584* (2), 405–12.
(34) Takeuchi, N.; Ueda, T.; Watanabe, K. Expression and characterization of bovine mitochondrial methionyl-tRNA transformylase. *J. Biochem.* **1998**, *124* (6), 1069–71.
(35) Steitz, T. A.; Moore, P. B. RNA, the first macromolecular catalyst: the ribosome is a ribozyme. *Trends Biochem. Sci.* **2003**, *28* (8), 411–8.
(36) Robledo, S.; Idol, R. A.; Crimmins, D. L.; Ladenson, J. H.; Mason, P. J.; Bessler, M. The role of human ribosomal proteins in the maturation of rRNA and ribosome production. *RNA* **2008**, *14* (9), 1918–29.
(37) Wang, X.; Su, B.; Zheng, L.; Perry, G.; Smith, M. A.; Zhu, X. The role of abnormal mitochondrial dynamics in the pathogenesis of Alzheimer's disease. *J. Neurochem.* **2009**, *109* (Suppl. 1), 153–9.
(38) Fukui, H.; Moraes, C. T. The mitochondrial impairment, oxidative stress and neurodegeneration connection: reality or just an attractive hypothesis?. *Trends Neurosci.* **2008**, *31* (5), 251–6.
(39) Oppermann, U. C.; Salim, S.; Tjernberg, L. O.; Terenius, L.; Jornvall, H. Binding of amyloid beta-peptide to mitochondrial hydroxyacyl-CoA dehydrogenase (ERAB): regulation of an SDR enzyme activity with implications for apoptosis in Alzheimer's disease. *FEBS Lett.* **1999**, *451* (3), 238–42.
(40) DiMauro, S. Mitochondrial diseases. *Biochim. Biophys. Acta* **2004**, *1658* (1−2), 80–8.
(41) Hammond, C. J.; Hallock, L. R.; Howanski, R. J.; Appelt, D. M.; Little, C. S.; Balin, B. J. Immunohistological detection of Chlamydia pneumoniae in the Alzheimer's disease brain. *BMC Neurosci.* **2010**, *11*, 121.
(42) Miklossy, J.; Kis, A.; Radenovic, A.; Miller, L.; Forro, L.; Martins, R.; Reiss, K.; Darbinian, N.; Darekar, P.; Mihaly, L.; Khalili, K. Beta-amyloid deposition and Alzheimer's type changes induced by Borrelia spirochetes. *Neurobiol. Aging* **2006**, *27* (2), 228–36.
(43) Kountouras, J.; Tsolaki, M.; Gavalas, E.; Boziki, M.; Zavos, C.; Karatzoglou, P.; Chatzopoulos, D.; Venizelos, I. Relationship between Helicobacter pylori infection and Alzheimer disease. *Neurology* **2006**, *66* (6), 938–40.
(44) Itzhaki, R. F.; Lin, W. R.; Shang, D.; Wilcock, G. K.; Faragher, B.; Jamieson, G. A. Herpes simplex virus type 1 in brain and risk of Alzheimer's disease. *Lancet* **1997**, *349* (9047), 241–4.
(45) Little, C. S.; Hammond, C. J.; MacIntyre, A.; Balin, B. J.; Appelt, D. M. Chlamydia pneumoniae induces Alzheimer-like amyloid plaques in brains of BALB/c mice. *Neurobiol. Aging* **2004**, *25* (4), 419–29.
(46) Soscia, S. J.; Kirby, J. E.; Washicosky, K. J.; Tucker, S. M.; Ingelsson, M.; Hyman, B.; Burton, M. A.; Goldstein, L. E.; Duong, S.; Tanzi, R. E.; Moir, R. D. The Alzheimer's disease-associated amyloid beta-protein is an antimicrobial peptide. *PLoS One* **2010**, *5* (3), No. e9505.
(47) Hu, X.; Crick, S. L.; Bu, G.; Frieden, C.; Pappu, R. V.; Lee, J. M. Amyloid seeds formed by cellular uptake, concentration, and aggregation of the amyloid-beta peptide. *Proc. Natl. Acad. Sci. U.S.A.* **2009**, *106* (48), 20324–9.
(48) Ohyagi, Y.; Asahara, H.; Chui, D. H.; Tsuruta, Y.; Sakae, N.; Miyoshi, K.; Yamada, T.; Kikuchi, H.; Taniwaki, T.; Murai, H.; Ikezoe, K.; Furuya, H.; Kawarabayashi, T.; Shoji, M.; Checler, F.; Iwaki, T.; Makifuchi, T.; Takeda, K.; Kira, J.; Tabira, T. Intracellular Abeta42 activates p53 promoter: a pathway to neurodegeneration in Alzheimer's disease. *FASEB J.* **2005**, *19* (2), 255–7.
(49) Schindowski, K.; Belarbi, K.; Buee, L. Neurotrophic factors in Alzheimer's disease: role of axonal transport. *Genes Brain Behav.* **2008**, *7* (Suppl. 1), 43–56.
(50) King, M. E.; Kan, H. M.; Baas, P. W.; Erisir, A.; Glabe, C. G.; Bloom, G. S. Tau-dependent microtubule disassembly initiated by prefibrillar beta-amyloid. *J. Cell Biol.* **2006**, *175* (4), 541–6.
(51) Islam, K.; Levy, E. Carboxyl-terminal fragments of beta-amyloid precursor protein bind to microtubules and the associated protein tau. *Am. J. Pathol.* **1997**, *151* (1), 265–71.
(52) Ding, Q.; Markesbery, W. R.; Chen, Q.; Li, F.; Keller, J. N. Ribosome dysfunction is an early event in Alzheimer's disease. *J. Neurosci.* **2005**, *25* (40), 9171–5.

IV.

THE JOURNAL OF BIOLOGICAL CHEMISTRY VOL. 286, NO. 39, pp. 34088–34100, September 30, 2011

Interactions of Pathological Hallmark Proteins

TUBULIN POLYMERIZATION PROMOTING PROTEIN/p25, β-AMYLOID, AND α-SYNUCLEIN[*] [S]

Received for publication, March 25, 2011, and in revised form, July 29, 2011 Published, JBC Papers in Press, August 8, 2011, DOI 10.1074/jbc.M111.243907

Judit Oláh[‡], Orsolya Vincze[‡], Dezső Virók[§], Dóra Simon[¶], Zsolt Bozsó[¶], Natália Tőkési[‡], István Horváth[‡], Emma Hlavanda[‡], János Kovács[‖], Anna Magyar[**], Mária Szűcs[¶‡‡], Ferenc Orosz[‡], Botond Penke[¶§§], and Judit Ovádi[‡1]

From the [‡]Institute of Enzymology, Biological Research Center, Hungarian Academy of Sciences, H-1113 Budapest, Hungary, the [§]Institute of Clinical Microbiology, University of Szeged, H-6725 Szeged, Hungary, the [¶]Department of Medical Chemistry, University of Szeged and the [§§]Supramolecular and Nanostructured Material Research Group of the Hungarian Academy of Sciences, H-6720 Szeged, Hungary, the [‖]Department of Anatomy, Cell, and Developmental Biology and the [**]Research Group of Peptide Chemistry, Hungarian Academy of Sciences, Eötvös Loránd University, H-1117 Budapest, Hungary, and the [‡‡]Institute of Biochemistry, Biological Research Center, Hungarian Academy of Sciences, H-6726 Szeged, Hungary

Background: The disordered TPPP/p25 is a hallmark of synucleinopathies.
Results: Tight binding of TPPP/p25 with β-amyloid results in the formation of massive aggregates both *in vitro* and *in vivo*.
Conclusion: The presence of intracellular pathological-like TPPP/p25-β-amyloid aggregates elucidates the partial co-localization of β-amyloid and TPPP/p25 in Lewy body dementia with Alzheimer disease.
Significance: This new type of aggregation may form bridge to conjoin synucleopathies with other neuropathologies.

The disordered tubulin polymerization promoting protein (TPPP/p25) was found to be co-enriched in neuronal and glial inclusions with α-synuclein in Parkinson disease and multiple system atrophy, respectively; however, co-occurrence of α-synuclein with β-amyloid (Aβ) in human brain inclusions has been recently reported, suggesting the existence of mixed type pathologies that could result in obstacles in the correct diagnosis and treatment. Here we identified TPPP/p25 as an interacting partner of the soluble Aβ oligomers as major risk factors for Alzheimer disease using ProtoArray human protein microarray. The interactions of oligomeric Aβ with proteins involved in the etiology of neurological disorders were characterized by ELISA, surface plasmon resonance, pelleting experiments, and tubulin polymerization assay. We showed that the $A\beta_{42}$ tightly bound to TPPP/p25 (K_d = 85 nM) and caused aberrant protein aggregation by inhibiting the physiologically relevant TPPP/p25-derived microtubule assembly. The pair-wise interactions of $A\beta_{42}$, α-synuclein, and tubulin were found to be relatively weak; however, these three components formed soluble ternary complex exclusively in the absence of TPPP/p25. The aggregation-facilitating activity of TPPP/p25 and its interaction with Aβ was monitored by electron microscopy with purified proteins by pelleting experiments with cell-free extracts as well as by confocal microscopy with CHO cells expressing TPPP/p25 or amyloid. The finding that the interaction of TPPP/p25 with Aβ can produce pathological-like aggregates is tightly coupled with unusual pathology of the Alzheimer disease revealed previously; that is, partial co-localization of Aβ and TPPP/p25 in the case of diffuse Lewy body disease with Alzheimer disease.

Alzheimer disease (AD)[2] (1) and Parkinson disease (PD) (2), the hallmark proteins of which are Tau/β-amyloid (Aβ) and α-synuclein, respectively, are the most common age-related conformational diseases causing serious socioeconomic problems (3). AD is characterized by two major neuropathological hallmarks, extracellular plaques of Aβ and neurofibrillary tangles consisting of abnormally phosphorylated Tau (4). Aβ is a product of proteolytic processing of amyloid precursor protein (APP) of undetermined function (5). Aβ is a 39–43-amino acid peptide that is the main constituent of amyloid plaque in the brains of AD patients that is a consequence rather than necessarily a cause of cell pathology (6). One of the most common isoforms is $A\beta_{42}$, which is typically produced by proteolytic cleavage occurring in the trans-Golgi network (7). Accumulation of $A\beta_{42}$ also occurs intracellularly with cytotoxicity resulting from initial oligomer formation. In the past attention was focused on mature β-sheet-rich amyloid fibrils and recently on the critical role of intraneuronal Aβ aggregates and smaller, soluble Aβ oligomers (8) as risk factors for AD (9, 10).

The β-amyloid hypothesis provided the basis for the therapeutic strategies of AD (11). However, this concept has been in the center of ongoing discussions because the plaque load in AD brains, in contrast to the load of Tau neurofibrillary tangles

* This work was supported by Hungarian National Scientific Research Fund Grants OTKA T-067963 (to J. Ovádi) and PD 76793 (to J. Oláh), the European Commission (DCI-ALA/19.09.01/10/21526/245–297/ALFA111(2010)29; to J. Ovádi), a János Bolyai Research Scholarship of the Hungarian Academy of Sciences (to J. Oláh), and EC-7 Health Grant 201159 ("Memoload").
[S] The on-line version of this article (available at http://www.jbc.org) contains supplemental Table 1.
[1] To whom correspondence should be addressed: Institute of Enzymology, Biological Research Center, Hungarian Academy of Sciences, Budapest, Karolina út 29, H-1113, Hungary. Tel.: 36-1-279-3129; Fax: 36-1-466-5465; E-mail: ovadi@enzim.hu.

[2] The abbreviations used are: AD, Alzheimer disease; APP, amyloid precursor protein; Aβ, β-amyloid; GO, Gene Ontology; PD, Parkinson disease; SPM, synaptic plasma membrane; TPPP/p25, tubulin polymerization promoting protein; Fmoc, *N*-(9-fluorenyl)methoxycarbonyl.

(12), does not correlate with the disease state. A series of cytosolic and mitochondrial proteins has been identified that bind Aβ aggregates (protofibrils and fibrils) (13).

Recent data have shown that a significant part (even up to 50%) of AD exhibits a third prevalent neuropathology, aggregation of α-synuclein into Lewy bodies (14), whereas Tau pathology was found in PD as well (15). Evidence has been reported for the critical role of the interaction between Aβ and α-synuclein in AD pathology by enhancing mitochondrial failure (16) as well as promoting α-synuclein aggregation with serious toxicity (17).

Tubulin polymerization promoting protein (TPPP/p25) was identified as a disordered protein; its primary target is the microtubular system (18, 19). TPPP/p25 is expressed predominantly in oligodendrocytes of the human brain, where it plays crucial role in their differentiation likely via its role in the rearrangement of the microtubular network during the projection elongation before the onset of myelination (20). However, it was found to be enriched and colocalized with α-synuclein, another disordered protein, in pathological inclusions characteristic for synucleinopathies such as PD and multiple system atrophy (21–23); therefore, it was proposed to be considered as a marker of synucleinopathies. TPPP/p25 promotes the formation of α-synuclein filament, which is probably a crucial pathological process in the cases of certain neurological diseases (23). TPPP/p25 immunolabeled α-synuclein-immunoreactive dystrophic globular neurites at the periphery of β-amyloid plaques in diffuse Lewy body disease with AD (21). Immunopositivity of TPPP/p25 was also documented by immunoelectron microscopy in post mortem brain tissue of AD patients at the pre-tangles but not at the Tau-laden neurofibrillary tangles, and dot-like TPPP/p25 immunoreactivity was also seen in neuronal cytoplasm in areas with abundant Tau pathology in AD (21).

In this paper we identified TPPP/p25 as a potential interacting partner of $A\beta_{42}$ oligomer mutually influencing their structural and functional properties. Apart from opening new avenues in the research of conformational diseases with mixed type pathology, identification of new protein complexes, ultrastructures, and interfaces could provide a potentially valuable target for pharmacological intervention.

EXPERIMENTAL PROCEDURES

Chemicals—Fmoc amino acids were purchased from IRIS Biotech GmbH (Germany). Other chemicals for peptide synthesis were product of Merck. Peptide synthesis reagent (1,3-diisopropylcarbodiimide, piperidin, 1-hydroxybenzotriazole, diisopropylethylamine, trifluoroacetic acid) and solvents were of reagent grade.

Synthesis of Peptides—Peptide synthesis was carried out on "MULTIPIN NCP" non-cleavable pins (Chiron Technologies) using solid-phase peptide synthesis (Fmoc/*t*-butyl strategy) according to Geysen et al. (24) with some modifications at the 66-nmol scale. Decapeptides overlapping by 5 amino acid residues were synthesized. The following side chain-protecting groups were used: *t*-butyl for Asp, Glu, Ser, Thr, and Tyr, *t*-butoxycarbonyl for Lys and Trp, trityl for Asn, Gln, and His, 2,2,4,6,7-pentamethyldihydrobenzofuran-5-sulfonyl for Arg, and acetamidomethyl for Cys. Coupling was performed with 1,3-diisopropylcarbodiimide/1-hydroxybenzotriazole in *N*,*N*-dimethylformamide and monitored with bromphenol blue added to the reaction mixture (25). After the final coupling cycle the Fmoc-protecting groups were removed, and the N terminus of the peptides were acetylated using Ac_2O-diisopropylethylamine-*N*,*N*-dimethylformamide (5:1:50 (v/v/v)). All side chain protecting groups were cleaved from the peptides with trifluoroacetic acid containing 2.5% ethanedithiol and 2.5% anisole except the acetamidomethyl group of Cys. Peptides were prepared in duplicate, except additional peptides produced only for amino acid analysis as a control for the synthesis.

$A\beta_{42}$ Preparation—$A\beta_{42}$ was prepared as described earlier (26). Then 0.2 mg of dry peptide was dissolved in 40 μl of Milli-Q ultrapure water and sonicated for 5 min, and 360 μl of PBS was added to the peptide, which was further sonicated for 5 min. The solution was filtered through a 0.2-μm filter (Millipore) and then was kept at 37 °C for 24 h before use.

TPPP/p25 Purification—Human recombinant TPPP/p25-possessing His tag tail at the N or C terminus was expressed in *E. coli* BL21 (DE3) cells and isolated on HIS-Select™ Cartridge (Sigma H8286) as described previously (21). Comparative studies performed with the preparations showed virtually no difference either in the structural or in the interacting features of TPPP/p25 depending on the position of the His tag.

Tubulin Preparation—Tubulin was prepared from bovine brain according to the method of Na and Timasheff (27).

α-Synuclein Purification—Human recombinant α-synuclein was prepared as described previously (28). Protein concentration was determined from the absorbance at 280 nm using an extinction coefficient of 5960 M^{-1} cm^{-1}.

Purification of Synaptic Plasma Membrane (SPM) Fraction—Highly purified SPM fraction was prepared from the forebrains of rats (Wistar, 200–300 g) as described earlier (29).

Preparation of Extract from Amyloid-expressing CHO7PA2 Cells—Cells were collected at 2000 × *g* at 4 °C for 15 min and then were diluted into 20 mM Tris buffer, pH 7.0, containing 1 mM EDTA, 1% Triton X-100, and protease inhibitors. The cells were then lysed by sonication with 5 short bursts of 5 s followed by intervals of 30 s for cooling in ice and centrifuged at 16,000 × *g* at 4 °C for 25 min, and this supernatant was used for a co-precipitation binding assay and affinity chromatography.

Protein Determination—The protein concentration was measured by the Bradford method (30) using the Bio-Rad protein assay kit.

Probing and Data Processing of the ProtoArray Human Protein Microarray—Processing of the ProtoArray Human Protein microarray 4.0 (Invitrogen) was performed according the manufacturer's protocol with small modifications as described in Virok *et al.* (31). Briefly, 10 μM Aβ oligomer was added on the top of the array and incubated for 1.5 h without shaking at 4 °C. The Aβ binding to the protein array was visualized by a fluorescently labeled monoclonal Aβ antibody (Sigma A3981). Array scanning was carried out using a GenePix Personal 4100A microarray scanner (Molecular Devices, Sunnyvale, CA). The localization of spots on the raw array images was performed by GenePix Pro 7.0 software (Molecular Devices).

The generated "gpr" files were further analyzed by the protein-protein interaction module of the Protoarray Prospector Analyzer software (Invitrogen). The significantly Aβ binder protein spots were identified by the Z-factor-based analysis of the Prospector Analyzer software. The Z-factor for a pair of protein spots indicates how far the mean of that spot pair deviates from the mean of the array negative controls comparing the variation associated with that spot pair and negative controls. The negative controls of the same sub-array were chosen as the spot pair for comparison. Two parallel protein array experiments were performed. Proteins were considered significant Aβ binders if each of the four protein spots (1-1 duplicate spots from each array) was found to be significant by the Z factor analysis using the cutoff value of 0.4. The signal intensity of a protein spot was calculated by subtracting the median background value from the median spot value. Protein spot signal intensities were median-normalized so that the median signal intensity of each array became 1. Because every protein had duplicate spots, the average of each duplicate was used as the final signal intensity for a given protein.

The potential cellular compartments that could be influenced by the Aβ binding were investigated by a Gene Ontology (GO) Cellular Content analysis using the DAVID Web-based knowledgebase (32). DAVID analyzes the GO terms relating to the Aβ binding proteins, identifies the GO terms that contain multiple proteins, and calculates a significance value for the observed enrichment compared with all the proteins on the array.

Surface Plasmon Resonance—The direct binding of Aβ to TPPP/p25 was monitored in real time with a BIAcore X instrument (GE Healthcare). The TPPP/p25 was immobilized onto the nickel nitrilotriacetic acid chip through its His tags in 0.01 M Hepes buffer, pH 7.4, containing 0.15 M NaCl and 0.005% P20 detergent. Aβ in PBS buffer was injected onto the immobilized protein surface in various concentrations for 2 min at a flow rate of 10 μl/min at 25 °C. After a 3-min dissociation, the surface was washed with 0.01 M Hepes, pH 7.4, containing 0.15 M NaCl, 50 μM EDTA, and 0.005% P20 detergent. Bound Aβ was removed from the chip with a pulse of 6 M guanidine-HCl solution. All experiments were repeated at least three times.

ELISA—The synthesis of solid-phase peptides on polyethylene pins and immunoscreening with an ELISA type of analysis were carried out similarly to established Pepscan procedures (24). TPPP/p25 peptides coupled to polyethylene pins were tested for Aβ binding by ELISA in 96-well microtiter plates (Greiner Bio-one). Each peptide-carrying pin was immersed in 200 μl of PBS buffer containing 20 mg/ml BSA (blocking buffer) overnight at 4 °C to block nonspecific binding. 4 μM Aβ or 1.5 μM α-synuclein diluted in blocking buffer was added to the wells and incubated for 1 h at room temperature. Each pin was incubated with anti-Aβ (1:7500, Sigma A3981) or anti-α-synuclein (1:5000, Sigma S5566) diluted in blocking buffer for 1 h at room temperature, then with anti-mouse IgG conjugated to horseradish peroxidase (1:5000, dilution in blocking buffer, Sigma) for 1 h at room temperature. Between each incubation step, the wells were washed three times with PBS containing 0.05% Tween 20 for 10 min. The presence of antibodies was detected using *o*-phenylenediamine in the concentration of 3.7 mM with 0.03% peroxide as substrate solution. The peroxidase-catalyzed reaction was stopped after 10 min with 1 M H_2SO_4; absorbance was read at 490 nm with a Wallace Victor 2 multiplate reader (PerkinElmer Life Sciences). After completion of the assay, pins were sonicated for 20 min in a water bath with PBS buffer containing 1% SDS and 0.1% 2-mercaptoethanol at 65 °C. The pins were subsequently washed 3 times in hot water (65 °C) and immersed in methanol for 1 min. Pins were allowed to air-dry for a minimum of 20 min and were ready to be used for another assay. Peptides retained their antibody binding capacity for several assays (more than 50). The reaction of a pin-coupled peptide was scored positive (significance level) when the ELISA absorption was significantly higher than the 2-fold average absorption of the peptides.

In the other sets of experiments the microtiter plate was coated with 5 μg/ml (100 μl/well) protein solution (TPPP/p25, tubulin or α-synuclein) in PBS overnight at 4 °C. The wells were blocked with 1 mg/ml BSA in PBS for 1 h at room temperature. Next, the plate was incubated with serial dilutions of an interacting partner (Aβ or other protein) for 1 h at 37 °C in PBS. Where indicated, after the addition of the interacting partner, a further protein was added to the plate in constant concentration (without washing), and the plate was incubated with both partners for 1 h at 37 °C in PBS. Then the plate was sequentially incubated with the corresponding antibody produced against Aβ (1:5000, Sigma A3981) or the appropriate protein (1:5000, tubulin antibody Sigma T6199; α-synuclein antibody Sigma S5566; TPPP/p25 antibody (33) or (21)) and with the secondary IgG-peroxidase conjugate (1:5000, Sigma). Both antibodies were in PBS buffer containing 1 mg/ml BSA and incubated for 1 h at room temperature. Between each incubation steps the wells were washed three times, and *o*-phenylenediamine was used as the substrate solution as described above.

Turbidity Measurements—The assembly of tubulin (15 μM for paclitaxel-induced, 7 μM for TPPP/p25-induced polymerization) was assessed in polymerization buffer (50 mM MES buffer, pH 6.6, containing 100 mM KCl, 1 mM dithioerythritol, 1 mM $MgCl_2$, and 1 mM ethylene glycol tetraacetic acid) at 37 °C in the absence and presence of $A\beta_{42}$ (10–15 μM) and/or α-synuclein (5–10 μM). The tubulin polymerization into microtubules was induced by the addition of either 3 μM TPPP/p25 or 20 μM paclitaxel. The optical density was monitored at 350 nm by a Cary 100 spectrophotometer (Varian, Walnut Creek, Australia). At the final state of polymerization, some of the samples were prepared for electron microscopic analysis and analysis by SDS-PAGE.

Pelleting—Aβ peptide was incubated with the proteins for 15 min at 37 °C, or the samples at the quasi end-point of the polymerization were used. After centrifugation at 15,000 × *g* for 15 min at 37 °C, the pellet and the supernatant fractions were separated. The pellet fraction was washed with PBS buffer and resuspended in PBS buffer. Then the pellet and the supernatant fractions were analyzed by SDS-PAGE, separated on a Tris-Tricine three-layer gel and stained with Coomassie Brilliant Blue R-250 containing 2-mercaptoethanol and dithioerythritol. The S.E. of the determinations was ± 10% ($n = 3–5$).

Co-precipitation Binding Assay—The extract of amyloid expressing CHO7PA2 cells was incubated overnight at 4 °C

with 20 μM human recombinant TPPP/p25. The samples were then centrifuged at 16,000 × *g* at 4 °C for 15 min. Amyloid expressing CHO7PA2 cells were also transiently transfected with human recombinant TPPP/p25, collected at 2000 × *g* at 4 °C for 15 min, and then diluted into 20 mM Tris buffer, pH 7.0, containing 1 mM EDTA, 1% Triton X-100, and protease inhibitors. The cells were then lysed by sonication with 5 short bursts of 5 s followed by intervals of 30 s for cooling in ice and were centrifuged at 16,000 × *g* at 4 °C for 25 min. In both sets of experiments the resulting supernatant and pellet fractions were separated; the pellet fractions were washed with 20 mM Tris buffer, pH 7.0, containing 1 mM EDTA, 1% Triton X-100, and protease inhibitors and resuspended in the same buffer. The samples were analyzed by SDS-PAGE and electrotransferred onto Immobilon-P^{SQ} transfer membranes. The filters were subjected to immunoblotting with an antiserum directed against TPPP/p25 in rat (1:5000 (21)) or with an antibody directed against Aβ_{42} in mouse (1: 5000, Sigma A8978). Antibody binding was revealed by using anti-rat or anti-mouse IgG coupled with peroxidase, ECL® (enhanced chemiluminescence) Western blotting Detection reagents (Amersham Biosciences), and Kodak X-Omat AR film or 3-amino-9-ethylcarbazole as substrate.

Affinity Chromatography—TPPP/p25 or Aβ_{42} was immobilized to CNBr-activated Sepharose 4B (Amersham Biosciences) according to the manufacturer's instructions. The TPPP/p25 or Aβ_{42} bound to Sepharose was packed into column. After each experiment columns were regenerated using 3 cycles of 0.1 M sodium acetate, pH 4.0, buffer containing 0.5 M NaCl and 0.1 M Tris, pH 8.0, buffer containing 0.5 M NaCl. The columns were stored in 20% ethanol, 0.01% NaN_3 solution at 4 °C. The affinity columns were equilibrated with 10 mM phosphate buffer, pH 7.2, containing 10 mM NaCl. SPM fraction was loaded to the Aβ_{42} column, whereas extract of CHO7PA2 cells expressing amyloid was loaded to the TPPP/p25 column. The columns were washed with at least 10 volumes of 10 mM phosphate buffer, pH 7.2, containing 10 mM NaCl. The bound proteins were eluted with 100 mM glycine buffer, pH 3.0, and concentrated using an Amicon ultrafiltration stirred-cell apparatus fitted with a YM-10 or PLAC membrane for the Aβ_{42} or TPPP/p25 column, respectively. The bound proteins were analyzed by SDS/PAGE, separated on a Tris-Tricine two-layer gel, and stained with Coomassie Brilliant Blue R-250 containing 2-mercaptoethanol and dithioerythritol. A Western blot was carried out as described above for the co-precipitation binding assay.

Electron Microscopy—Microtubule-containing samples were fixed in a mixture of 2% glutaraldehyde, 0.2% tannic acid, and 0.1 M sodium cacodylate, pH 7.4, for 1 h, post-fixed in 0.5% OsO_4, and embedded in Durcupan (Fluka, Buchs, Switzerland). Thin sections were contrasted with uranyl acetate and lead citrate and examined in a JEOL CX 100 electron microscope. For negative staining, a drop from the unpelleted samples was applied to Formvar/carbon-coated glow-discharged copper grids for 30 s. The solution was then removed, and the grid was stained with one drop of freshly filtered 1% aqueous uranyl acetate for 30 s. The excess stain was removed by blotting with filter paper.

Cell Cultures—CHO7PA2 cells expressing human APP and processing it to Aβ (kind gift of Dr. Michael Rowan, Dublin) were cultured in DMEM supplemented with 10% FCS, 100 units/ml streptomycin, 100 μg/ml penicillin, 200 μg/ml G418, and 200 μg/ml L-proline (all reagents from Sigma) in a humidified incubator at 37 °C with 5% CO_2. The expression of APP/Aβ was induced by withdrawal of the L-proline. The TPPP/p25 stable-expressing clone (CHO10) was selected after subcloning from the CHO-K1 Tet-On cell line transfected with pTRE2hyg-TPPP/p25 (34). Expression of TPPP/p25 in CHO10 cells was induced by doxycycline as described previously (34). Transfection of induced CHO7PA2 cells with human recombinant TPPP/p25 and that of induced CHO10 cells with Aβ_{42} was carried out with ProteoJuice (Novagen) or Pro-DeliverIn (OZ Bioscience) transfection reagent, respectively, according to the manufacturer's instructions. The cells were grown on 12-mm diameter coverslips for microscopic analysis and on 60-mm dishes for all other experiments.

Immunocytochemistry—For immunofluorescence microscopy analysis, cells were fixed with 2.5% formaldehyde at 37 °C for 10 min. Next, samples were blocked for 30 min in PBS containing 0.1% Triton X-100 and 5% FCS. Samples were stained with a mouse monoclonal Aβ antibody (1:1000, Sigma A8978), a rat polyclonal TPPP/p25 serum (1:300 (21)), and a rabbit LC3 antibody (1:1000, a kind gift of Ron R. Kopito) followed by Alexa-488-, Texas-Red-, and Alexa 633-conjugated anti-mouse, anti-rat, or anti-rabbit antibody, respectively (1:1000, Invitrogen). Samples were washed for 7 min, 3 times with PBS containing 0.1% Triton X-100 between incubations. Nuclei were counterstained with DAPI. For staining cellular membranes, the CHO10 cells were preincubated with 50 μM BODIPY 500/510 dodecanoic acid (BODIPY 3823, Invitrogen) for 1 min before fixation, and LC3 staining was omitted. After processing of samples, the coverslips were mounted with GelMount and sealed with Clarion (reagents from Biomeda).

Microscopy—The pictures of fixed samples were acquired on a Zeiss LSM710 inverted microscope with 63× objective. To minimize the cross-talk between imaged channels, sequential image collection was used. Cells are shown as single confocal section. All images were processed using ZEN software (Zeiss).

RESULTS

Protein Array-based Oligomeric Aβ Interactome Screen—The introduction of protein arrays provided a suitable method for the analysis of Aβ protein interactions on a large scale. We applied two parallel Protoarray 4.0 protein arrays with more than 8100 unique recombinant human proteins immobilized on a matrix for the Aβ interactome analysis. The Aβ binding to the protein array was visualized by a fluorescently labeled monoclonal Aβ antibody, and the fluorescent signal intensities were detected by a regular array scanner. The proteins that bound to the oligomeric Aβ were identified by Z-factor statistical analysis extended with a new type quantitative analysis of the protein array data reported very recently (31) that is based upon the normalization of the signal intensities of the spots by the concentrations. This analysis of the arrays revealed that altogether 2242 proteins displayed significant binding to the oligomeric Aβ (supplemental Table 1). Among the Aβ binding

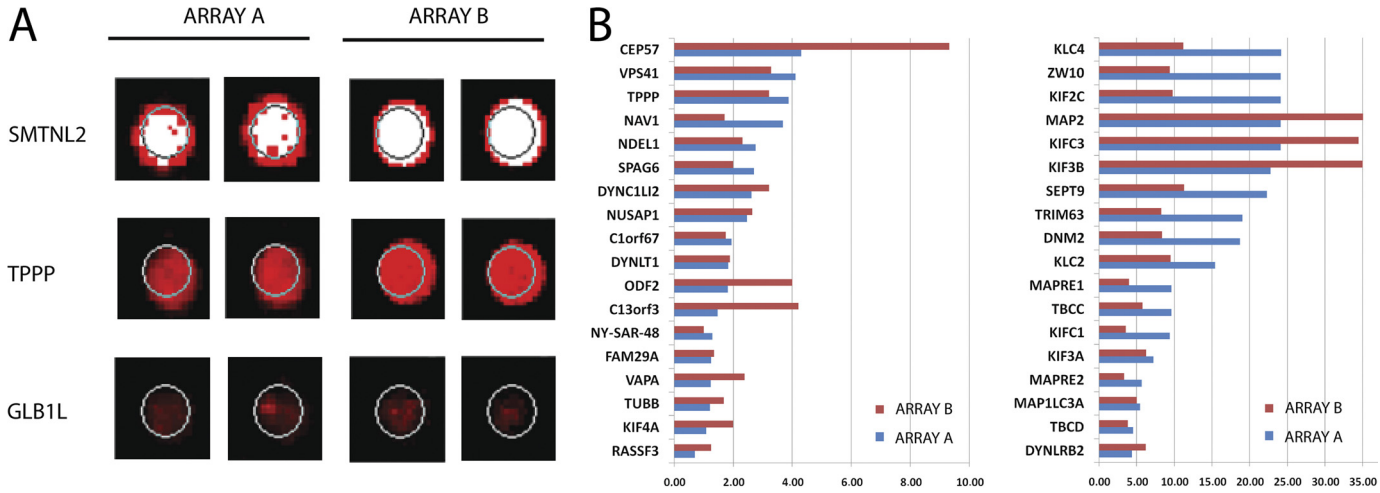

FIGURE 1. **Protein array-based interactome analysis of oligomeric Aβ_{42}.** *A*, to explore the interacting protein partners of β-amyloid, 10 μM Aβ_{42} peptide was hybridized onto the Protoarray 4.0 protein array. Duplicate spot images show a strong Aβ_{42} binder smoothelin-like protein 2 (*SMTNL2*), the TPPP/p25, and a weak Aβ_{42} binder β-galactosidase-1-like protein (*GLB1L*) on both applied protein arrays. *B*, the cellular localization of the Aβ_{42} interacting proteins were characterized using the GO data base. Members of the microtubule GO cellular content category are shown, with their normalized signal intensities on both applied arrays.

partners, several members of the cellular microtubular network, including tubulin and TPPP/p25, were identified. Our protein chip data were validated by the fact that several previously described Aβ binding proteins such as tubulin β (TUBB) (35), glyceraldehyde-3-phosphate dehydrogenase (GAPDH) (36), synuclein (37), CD36 (38), apolipoprotein A-I (APOA1) (39), various ribosomal proteins (31), heat shock proteins (HSP27, HSP60, HSP70) (40), and various histone proteins (41) were identified as Aβ interacting partners. However, it should be added that not all reported interacting partners of Aβ were detected; some of them were not immobilized on the array (ApoE receptors, p75 neurotrophin receptor, nicotinerg receptors) or they did not fulfill all the statistical requirements (integrin β1).

The proteins with related intracellular functions and significant Aβ binding were identified by GO Cellular Content analysis using the DAVID Web-based knowledgebase (32), which quantifies the enrichment of anti-Aβ signal for a given protein compared with that of all proteins on the array. This GO analysis showed that one of the impacted cellular systems displaying distinct affinity to Aβ was the microtubule-related proteins, which includes cytoskeleton, microtubule-associated proteins, microtubule organizing center, and microtubule itself (The GO Cellular Content category "microtubule cytoskeleton" had a p value of 0.000056, "microtubule-associated complex" had a p value of 0.0015, "microtubule organizing center" had a p value of 0.017, and "microtubule" had a p value of 0.03). A key member of this family in which we were specifically interested is the TPPP/p25. The relative Aβ binding intensities of TPPP/p25 were more than 3-fold higher in two different array experiments as compared with the median binding intensity of 1. The spot images of the TPPP/p25 are shown in Fig. 1*A* together with that of a strong and a weak Aβ-binding protein. The signal intensities of the 37 members of the "microtubule-related proteins" according to the GO Cellular Content category are shown in Fig. 1*B*. Instead, to extend the *ProtoArray* experiments by varying the Aβ-oligomer concentration, we carried

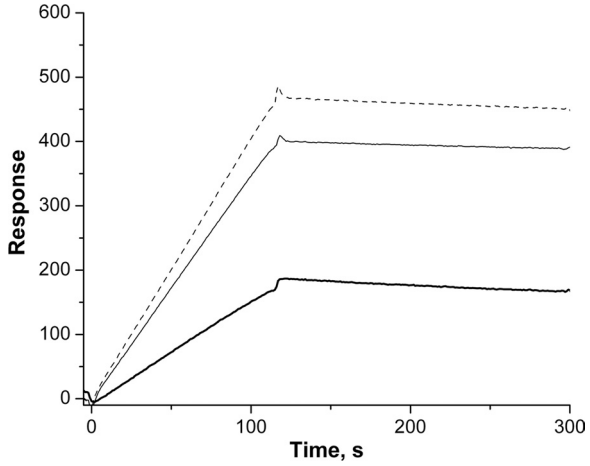

FIGURE 2. **TPPP/p25-Aβ_{42} interaction monitored by surface plasmon resonance.** Representative surface plasmon resonance curves are shown. 2.5 μM (*bold line*), 5 μM (*solid line*), 7.5 μM (*dashed line*) Aβ_{42} was injected onto TPPP/p25 immobilized on the nickel nitrilotriacetic acid chip through its His tag. Three independent experiments were performed. S.E. = ±10%.

out extensive studies with isolated proteins relevant to the neurological diseases with mixed type pathology.

Detection and Characterization of the Direct Interactions of Aβ_{42}—Biophysical and biochemical techniques were used to characterize the direct interaction of Aβ_{42} oligomer with human recombinant TPPP/p25, human recombinant α-synuclein, and tubulin isolated from bovine brain that had been successfully used in our previous studies (26, 42).

First, the interaction of Aβ_{42} with TPPP/p25 was tested by surface plasmon resonance, a sensitive method to detect direct complex formation. TPPP/p25 was immobilized onto the surface of a sensorchip, and Aβ_{42} oligomer solution at different concentrations were injected (binding phase) followed by the injection of buffer alone (dissociation phase). The registered sensorgrams are shown in Fig. 2, which clearly demonstrates the ability of the Aβ_{42} to associate with the immobilized TPPP/p25. However, as illustrated, the dissociation parts of sensorgrams appeared to be almost horizontal; apparently there is no

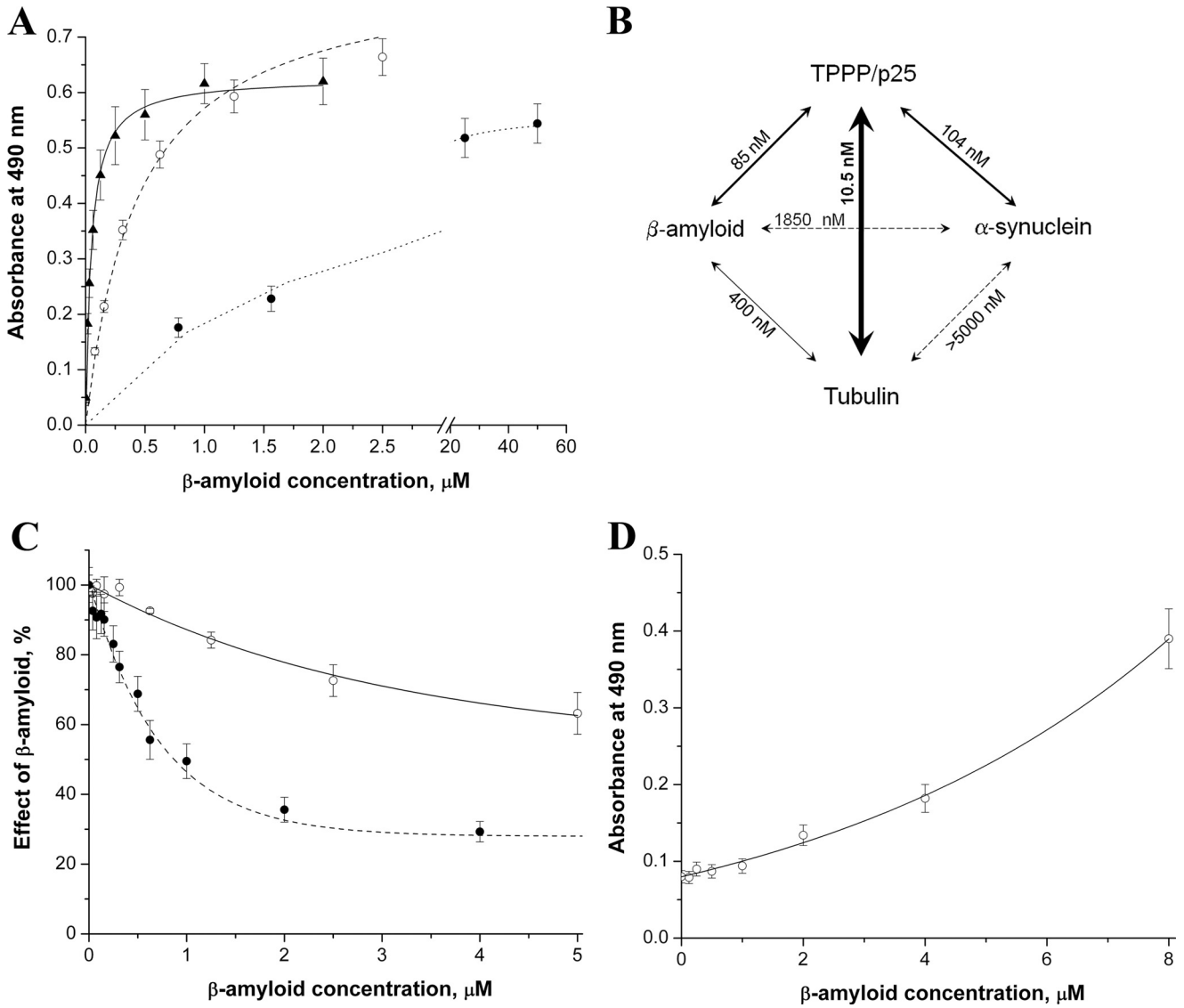

FIGURE 3. **The interaction of oligomeric Aβ_{42} with different proteins followed by ELISA.** *A*, the plate was coated with 0.5 μg/well TPPP/p25 (▲), tubulin (○), or α-synuclein (●), then it was incubated with Aβ_{42} at different concentrations. *B*, the apparent dissociation constants (K_d) characteristic for the interactions were evaluated by non-linear fitting of the hyperbolic saturation curves using the Microcal Origin 6.0 software. *C*, ○, the plate was coated with TPPP/p25 then incubated with Aβ_{42}. After incubation, tubulin was added in constant concentration (100 nM). After further incubation, anti-tubulin was added. ●, the plate was coated with TPPP/p25 and incubated with Aβ_{42}, 100 nM α-synuclein was added, and then anti-α-synuclein was added. The effect of the Aβ_{42} was calculated as the absorbance at a given Aβ_{42} concentration divided by the absorbance without Aβ_{42}. *D*, ○, the plate was coated with α-synuclein, then incubated with Aβ_{42}. After incubation, tubulin was added in constant concentration (100 nM). After further incubation, anti-tubulin was added. The average of three-five independent experiments and the S.E. is shown.

effective dissociation of amyloid oligomers from the coated TPPP/p25. Thus, the evaluation of the k_{on} and k_{off} values of the interaction were not possible, which is similar to the cases published for other protein systems (19, 43).

Next, in the ELISA assay, TPPP/p25, α-synuclein, or tubulin were immobilized on the wells of ELISA plates then incubated with Aβ_{42} oligomer at various concentrations. The binding of the Aβ_{42} to the immobilized proteins was detected by specific antibody for Aβ_{42} as described under "Experimental Procedures." The titration curves are shown in Fig. 3*A*. The binding constants were evaluated from the computed curves fitted to the experimental points by nonlinear fitting of the hyperbolic saturation curves; accordingly, the apparent dissociation constants ($K_d \pm$ S.E.) for interaction of Aβ_{42} with TPPP/p25, tubulin, or α-synuclein were 0.085 ± 0.016, 0.40 ± 0.03, or 1.85 ± 0.15 μM, respectively (Fig. 3*B*). These data indicate order of magnitude differences in the binding affinities, and the tightest interaction was found between Aβ_{42} and TPPP/p25.

Similar sets of experiments were carried out with TPPP/p25, α-synuclein, and tubulin (no Aβ_{42}) to obtain comparative data for the pair-wise interactions of these proteins; the dissociation constants evaluated from the ELISA experiments are summarized in Fig. 3*B*. These data show that the affinity of TPPP/p25 to Aβ_{42} oligomer is weaker than that to tubulin (K_d = 0.0105 ± 0.0012 μM), its physiological interacting partner, but it is in the same order of magnitude as that to α-synuclein (K_d = 0.104 ± 0.011 μM), its pathological interacting partner (23). However, the interactions of α-synuclein with either Aβ_{42} oligomer or tubulin are weak and can be characterized with a K_d in the micromolar concentration range.

Then the effect of a third partner on bis-protein interactions was investigated by ELISA. In one set of experiments (Fig. 3*C*) TPPP/p25 was immobilized on the plate, and Aβ_{42} oligomer was added at various concentrations at constant tubulin or α-synuclein concentration. In the other set, α-synuclein was immobilized, tubulin was constant, and the titration was performed with Aβ_{42} oligomer as in the other set. In both cases the concentrations of the third partners (the constant ones) were visualized by specific antibodies. If Aβ_{42} oligomer does not influence the protein-protein interaction, the signal should be constant as a function of Aβ_{42} oligomer concentration. However, as seen in Fig. 3*C*, this was not the case; the presence of Aβ_{42} impeded the association of tubulin as well as that of α-synuclein to the immobilized TPPP/p25. As expected on the basis of the dissociation constants of bis-protein complexes, a higher Aβ_{42} concentration was required for the displacement of the tubulin than that of α-synuclein from the immobilized TPPP/p25, an indicating alternative binding mechanism (Fig. 3*C*). Similarly, tubulin impeded the TPPP/p25 interaction with α-synuclein, corresponding to an alternative binding mechanism (data not shown). Rather surprisingly, when TPPP/p25 was omitted from the system, more and more tubulin was associated to the immobilized α-synuclein by increasing the concentration of Aβ_{42} oligomers (Fig. 3*D*), which is suggestive for the formation of ternary complex of tubulin-Aβ_{42}-α-synuclein.

Identification of the Binding Domain on TPPP/p25—The ELISA-Pepscan method developed by Geysen *et al.* (24) is suitable to identify the binding motifs involved in heteroassociation, particularly in the case of unstructured proteins. The amino acid sequence of human recombinant TPPP/p25 was used to synthesize a complete set of overlapping decapeptides covalently attached to the surface of pins in a format compatible with standard ELISA. As described under "Experimental Procedures," pins were incubated with Aβ_{42} or α-synuclein, and then the reaction was visualized by the addition of Aβ or α-synuclein antibodies, respectively. The reaction of a pin-coupled peptide was scored positive (significance level) when the ELISA absorption was higher than the 2-fold of the average absorption of the peptides. Fig. 4, *A* and *B*, show signal intensities along the sequence of TPPP/p25 incubated with Aβ_{42} or α-synuclein. The 142–166 and 147–166 amino acid sequences are indicated to be the specific binding motifs of TPPP/p25, which are targeted by Aβ_{42} or α-synuclein.

Functional Effect of Aβ_{42} on TPPP/p25-promoted Tubulin Polymerization-Microtubule Assembly—Our large scale protein array experiment (*cf.* supplemental Table 1) as well as experiments with purified proteins (*cf.* Fig. 3) provided evidence for the association of Aβ_{42} with both TPPP/p25 and tubulin. Previously we showed that TPPP/p25 induced assembly and bundling of microtubules as well as tubulin aggregations (18–20, 34, 44). In addition, the association of these proteins with α-synuclein has been reported as well (23). To establish the effect of Aβ_{42} and its interacting partners on tubulin polymerization, turbidity measurements were performed induced by paclitaxel or TPPP/p25, and the samples at the quasi endpoints were pelleted followed by analysis of the supernatant and pellet fractions.

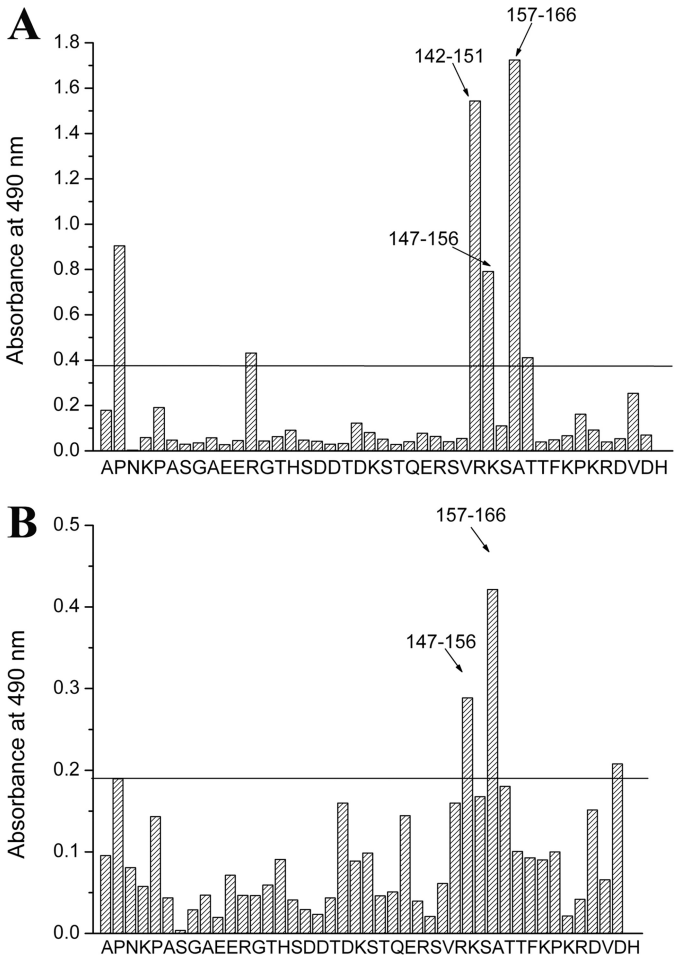

FIGURE 4. **Mapping of possible binding sites between Aβ_{42} or α-synuclein and TPPP/p25 by MULTIPIN peptide technology (Pepscan analysis).** The amino acid sequence of the TPPP/p25 was used to synthesize a complete set of overlapping decapeptides covalently attached to the surfaces of derivative polyethylene pins in a format compatible with standard ELISA. These overlapping peptides covered the entire sequence of the protein. Pins were coated with 4 μM Aβ_{42} (*A*) or 1.5 μM α-synuclein (*B*), then anti-Aβ or anti-α-synuclein was added, respectively. The absorbances of the peptides (indicated by *letters of the first amino acid of the decapeptides*) are shown. The reaction of a pin-coupled peptide was scored positive (significance level, indicated by a *line*) when the ELISA absorption was significantly higher than the 2-fold average absorption of the peptides.

Typical time courses are shown in Fig. 5, *A* and *C*. The initial time course of the TPPP/p25-induced tubulin polymerization does not show lag phase as observed with paclitaxel, indicating that TPPP/p25 induced tubulin aggregation beside microtubule assembly as demonstrated by electron microscopy (19). The addition of Aβ_{42} oligomer to tubulin at equimolar concentrations resulted in partial inhibition in the polymerization induced by paclitaxel or TPPP/p25 (Fig. 5, *A* and *C*), indicating the inhibitory effect of Aβ oligomers on the formation of tubulin assemblies. The pelleting experiments showed that although Aβ_{42} was partitioned between the supernatant and pellet fractions in the case of paclitaxel-induced tubulin polymerization (Fig. 5*B*), it was detected exclusively in the pellet (Fig. 5*D*) when the polymerization was promoted by TPPP/p25. This finding suggests that the self-association of Aβ_{42} oligomers is promoted by the presence of TPPP/p25; indeed, the interaction of TPPP/p25 with Aβ_{42} oligomers resulted in aggregation (Fig.

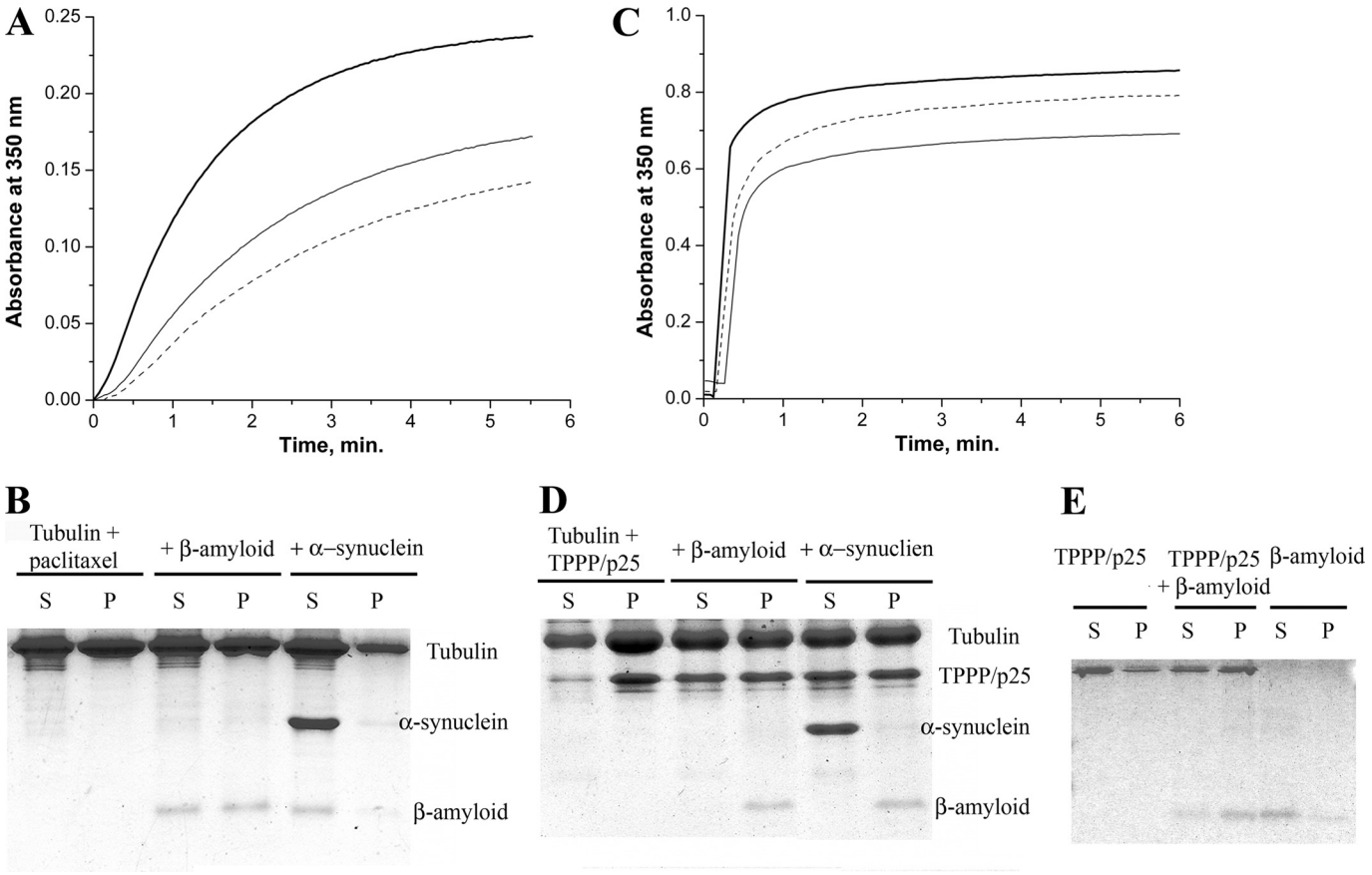

FIGURE 5. **The effect of the interacting partners on tubulin assembly as determined via a turbidimetric assay followed by pelleting experiments.** Tubulin polymerization was induced by paclitaxel (*A* and *B*) or by TPPP/p25 (*C* and *D*). For the turbidimetric assay (*A* and *C*), control (*bold line*), in the presence of Aβ_{42} (*solid line*) or Aβ_{42} and α-synuclein (*dashed line*) are shown. For the pelleting experiments (*B* and *D*), at the quasi endpoints of the polymerization curves the assay mixtures were centrifuged at 15,000 × *g* for 15 min at 37 °C, and the pellet (*P*) and the supernatant (*S*) fractions were separated followed by SDS-PAGE analysis on Tris-Tricine three-layer gels. Tubulin alone, incubated with Aβ_{42} or with both Aβ_{42} and α-synuclein as indicated. The concentration of tubulin was 15 μM (*A* and *B*) or 7 μM (*C*) or 10 μM (*D*) and the concentration of Aβ_{42} was 15 μM (*A* and *B*) or 10 mM (*C*) or 25 μM (*D*), whereas that of the TPPP/p25 was 3 μM (*C*) or 10 μM (*D*) and that of the α-synuclein was 10 μM (*A*, *B*, and *D*) or 5 μM (*C*). *E*, for the pelleting experiment, 2 μM TPPP/p25 alone, TPPP/p25 incubated with 25 μM Aβ_{42}, and Aβ_{42} alone as indicated were used. Three-five independent experiments were performed; S.E. for turbidimetry and pelleting were ± 5 and ± 10%, respectively.

5*E*). Although the α-synuclein slightly reduced the paclitaxel-induced tubulin polymerization, no protein aggregation could be detected (data not shown).

To elucidate the ELISA data showing the binding of α-synuclein to tubulin in the presence of Aβ_{42} oligomer, we measured tubulin polymerization induced by paclitaxel or TPPP/p25 combined with pelleting studies. In the case of paclitaxel-induced polymerization, the mixture of α-synuclein and Aβ_{42} oligomer further inhibited the polymerization as compared with that without α-synuclein (Fig. 5*A*), and both proteins appeared in the supernatant (Fig. 5*B*). In contrast to that, in the presence of TPPP/p25 the tubulin polymerization was slightly inhibited by the mixture of α-synuclein and Aβ_{42} oligomer (Fig. 5*C*), and the pellet fraction did not contain α-synuclein, but Aβ_{42} oligomer was found exclusively in this fraction (Fig. 5*D*). This finding, therefore, further supports that Aβ_{42} oligomer and α-synuclein can form a ternary complex with tubulin, a specific soluble ultrastructure that does not occur in the presence of TPPP/p25, displaying an alternative binding mechanism which concerns the ELISA Pepscan data, namely, the α-synuclein and Aβ_{42} could compete each with other for the common binding motifs on the TPPP/p25, which is maintained in the case of tubulin-bound TPPP/p25.

Ultrastructural Studies; Electron Microscopy—Aberrant (non-physiological) associations of unfolded/misfolded proteins are considered as initiators of pathological protein aggregations leading to formation of inclusions. Our tubulin polymerization and pelleting experiments showed that Aβ_{42} oligomers affected the microtubule assembly depending on whether the polymerization was induced by paclitaxel or TPPP/p25 (*cf.* Fig. 5). To visualize the morphologies of the protein assemblies, electron microscopic studies were carried out on sections from resin-embedded pellets. Transmission electron microscopy pictures from samples prepared by the addition of paclitaxel to tubulin solution revealed the presence of large amounts of intact-like microtubules, about 25 nm in diameter, between which small patches of thread-like oligomers were occasionally seen (Fig. 6*A*). The amount of these threads greatly increased in samples formed in the presence of Aβ_{42} oligomers without causing visible tubulin aggregation, indicating the effect of Aβ_{42} on the paclitaxel-induced microtubule assembly (Fig. 6*B*).

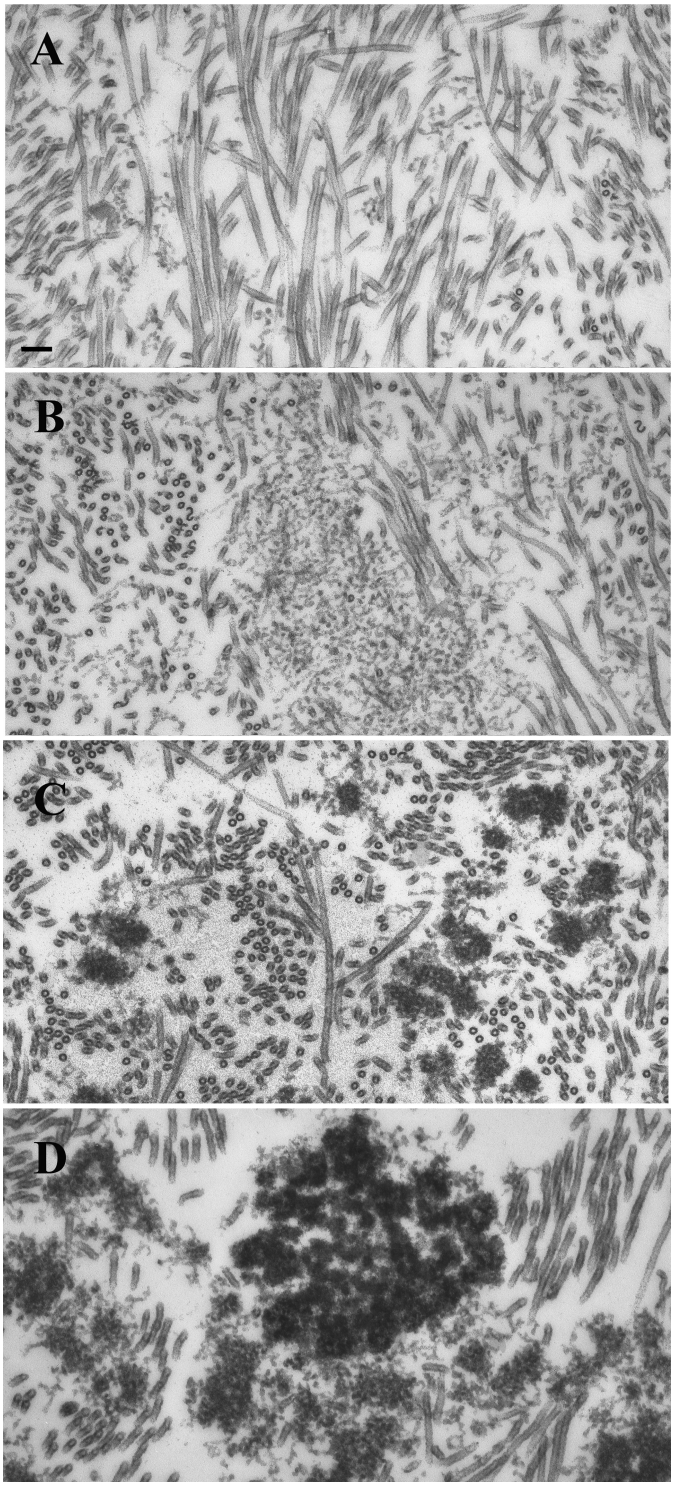

FIGURE 6. **Electron microscopic analysis of the effect of Aβ_{42} oligomers on paclitaxel- or TPPP/p25-induced tubulin polymerization.** Samples were prepared with 20 μM paclitaxel (*A* and *B*) or with 1.5 μM TPPP/p25 (*C* and *D*) in the presence of 10 μM Aβ_{42} (*B* and *D*) or in its absence (*A* and *C*). The tubulin concentration was 10 μM (*A* and *B*) or 7 μM (*C* and *D*). *Scale bar*, 100 nm.

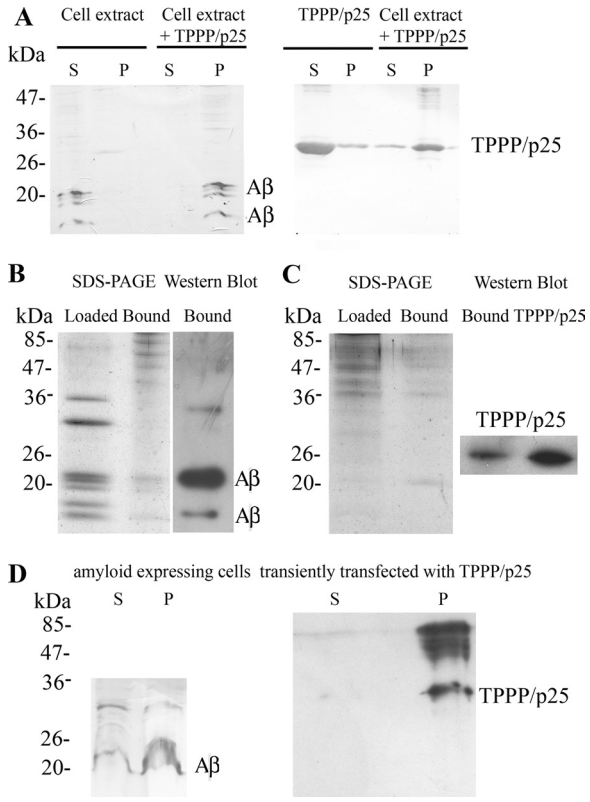

FIGURE 7. **Interaction of TPPP/p25 and Aβ at cell level.** *A*, shown is a co-precipitation assay. Extract of amyloid expressing CHO7PA2 cells was incubated without or with 20 μM TPPP/p25 overnight at 4 °C, or 20 μM TPPP/p25 alone was incubated under the same conditions, and after centrifugation, the supernatant (*S*) and the pellet (*P*) fractions were subjected to Western blot to test the partition of Aβ and TPPP/p25 as indicated. *B*, extract of amyloid expressing CHO7PA2 cells loaded to TPPP/p25 affinity column is shown. SDS-PAGE analysis of the cell extract loaded to the column and the bound proteins. After elution, the bound proteins were subjected to Western blot using Aβ antibody. *C*, extract of the SPM fraction loaded to Aβ affinity column. SDS-PAGE analysis of the SPM extract loaded to the column and the bound proteins. After elution, the bound proteins and 0.9 ng of human recombinant TPPP/p25 were subjected to Western blot using TPPP/p25 antiserum. *D*, shown is a co-precipitation assay. Amyloid-expressing CHO7PA2 cells were transiently transfected with human recombinant TPPP/p25 and were lysed by sonication. After centrifugation, the supernatant and the pellet fractions were subjected to Western blot to test the partition of Aβ and TPPP/p25 as indicated.

Previously we showed (42) that the TPPP/p25-induced tubulin polymerization can produce intact-like microtubules as well as ones effectively bundled by TPPP/p25; however, small tubulin aggregates were also formed as illustrated in Fig. 6*C*. The addition of Aβ_{42} oligomers resulted in few but larger aggregates without a significant amount of intact-like microtubules as shown in Fig. 6*D*. These data suggest that the potency of TPPP/p25 to produce microtubule assembly and bundling coupled with extensive stabilization of the microtubules (42) was impeded due to its interaction with Aβ_{42}.

The Interaction between TPPP/p25 and Aβ at Cell Levels—To further investigate the TPPP/p25 and Aβ interaction, three different sets of experiments were carried out. Two kinds of extracts were used for these studies, extracts of amyloid-expressing CHO7PA2 cells and SPM fraction prepared from rat brain, where TPPP/p25 is endogenously expressed. In the first set of experiments, the aggregation of TPPP/p25 and Aβ was studied by a co-precipitation binding assay in amyloid expressing CHO7PA2 cell extract incubated without or with human recombinant TPPP/p25. The partition of the proteins in the supernatant and the pellet fractions was analyzed by Western blot. As shown in Fig. 7*A*, TPPP/p25 or Aβ alone was found in the supernatant fractions, whereas in the presence of both part-

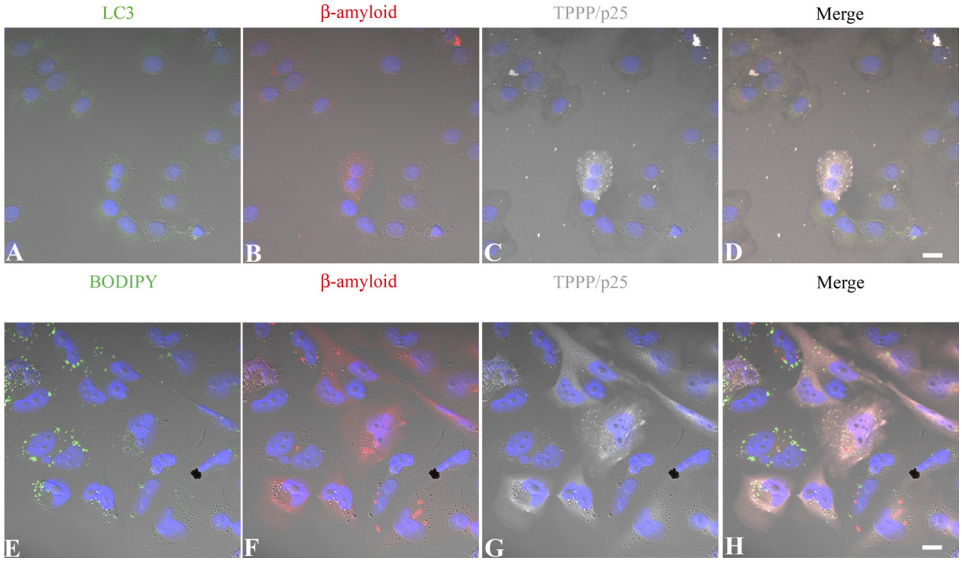

FIGURE 8. **Representative pictures of intracellular Aβ and TPPP/p25 aggregation in CHO7PA2 and CHO10 cells.** Amyloid expressing CHO7PA2 cells (*A–D*) and TPPP/p25 expressing CHO10 cells (*E–H*) were transiently transfected with human recombinant TPPP/p25 and Aβ_{42}, respectively, and immunostained for TPPP/p25 (*C* and *G*, *gray*), Aβ (*B* and *F*, *red*), and the autophagic marker LC3 (*A*, *green*), whereas the general intracellular membrane marker (BODIPY 500/510) was detected by its own signal (*E*, *green*). Note the appearance of cytoplasmic aggregates in the case of TPPP/p25 and β-amyloid co-expression on the merged pictures (*D* and *H*) that show no co-localization with either *vacuole* markers. *Blue*, DAPI. *Scale bar*, 10 μm.

ners the protein and the different Aβ oligomers/peptides were found in the pellet fraction, indicating their interaction.

In the second set of experiments the binding of Aβ to TPPP/p25 affinity column was investigated from the same extract used above (Fig. 7*B*). In the third set the binding of endogenous TPPP/p25 from SPM extract to Aβ was studied by affinity chromatography, where monomeric Aβ_{42} was immobilized to the column (Fig. 7*C*). In both cases the bound proteins were analyzed by SDS-PAGE and then subjected to Western blot using Aβ antibody and TPPP/p25 antiserum, respectively. The affinity chromatography experiments corroborated the interaction between TPPP/p25 and Aβ.

In Vivo Non-physiological Aggregation Induced by the Interaction of TPPP/p25 and Amyloid—The colocalization of TPPP/p25 and Aβ was visualized by confocal microscopy in amyloid-expressing CHO7PA2 cells transfected with human recombinant TPPP/p25 (Fig. 8, *A–D*) as well as in CHO10 cells expressing TPPP/p25 and transfected with Aβ_{42} (Fig. 8, *E–H*) as described under "Experimental Procedures." TPPP/p25 and the amyloid were immunostained for TPPP/p25 (*gray*) and Aβ (*red*). As shown in Fig. 8, the co-enrichment of TPPP/p25 and amyloid in the aggregates with distinct sizes is visible within the cytoplasm, whereas no protein aggregation can be visualized in the absence of TPPP/p25.

To study whether the aggregation process was related to vacuolization, the cells were stained with anti-LC3 (Fig. 8, *A* and *D*), a specific autophagic marker (kindly provided by Prof. Kopito), or BODIPY (Fig. 8, *E* and *H*), a dye-conjugated lipid accumulating in the membranes. None of these markers showed co-labeling with the immunodetected intracellular protein aggregates; therefore, the colocalization of the aggregates did not result from vacuolization but from the mutual interaction of TPPP/p25 and amyloid.

To confirm the intracellular association of the two hallmark proteins, the aggregates formed in amyloid-expressing CHO7PA2 cells transiently transfected with TPPP/p25 were isolated by a pelleting experiment after cell lysis and immunostained for the presence of TPPP/p25 and amyloid (Fig. 7*D*). The TPPP/p25 was exclusively found in the pellet fraction, whereas the amyloid was found both in the supernatant and the pellet fractions (due to the presence of untransfected cells in the sample). Control data showed that in CHO7PA2 cells not transfected with TPPP/p25, the amyloid was not pelleted at all (Fig. 7*A*). These data show that their mutual pelleting was detected due to their hetero-association.

DISCUSSION

Cognitive impairment and synaptic dysfunction, which are early changes preceding the accumulation of the hallmark pathological lesions, were found to correlate with the accumulation of intracellular Aβ (45, 46). Recent evidence has also suggested that APP and Aβ accumulate in mitochondrial membrane in AD, and the oligomeric Aβ can induce mitochondrial damage, proteasome dysfunction, calcium dyshomeostasis via structural, and functional alterations (47). In our studies we used a specific amyloid preparation in which the 42-amino acid amyloid peptide occurred in a well established soluble oligomeric form (26), which is considered to be the most toxic form of the Aβ peptides (3). Accumulation of intraneuronal oligomeric Aβ is an early event in the pathogenesis of AD (48).

In this study using protein array we identified 2242 proteins including TPPP/p25 as the interacting partner of the oligomeric Aβ of the 8100 recombinantly expressed human proteins, representing a significant portion of the human proteome (*cf.* Fig. 1). Several previously described Aβ-binding proteins (35–41) were found among the interacting partners. The recombinant protein expression was performed in an insect cell line; therefore, the eukaryotic posttranslational modifications could be present. Analysis of the Aβ hybridization pattern revealed that more than 2200 human proteins bound to the

oligomeric peptide. Although we detected a high number of interactions, it is likely that many of these interactions are not relevant *in vivo*. The reason could be numerous, *e.g.* the Aβ and these interacting proteins are not expressed at the same compartment or the binding domains of these proteins are not available for Aβ. The high number of interacting partners *in vitro* is not surprising because of the structural flexibility of the Aβ peptide, which displays a series of different metastable conformations and interacts with a large number of partner molecules (49).

Ontological analysis of the Aβ binding partners revealed that various members of the microtubular network were its potential interacting partners, which suggests that cumulative impact of Aβ on microtubule function could be significant. TPPP/p25, a modulator of the dynamics and stability of the microtubular network (50), seems to be an interacting partner of Aβ. Although the protein array data suggested that Aβ could bind to TPPP/p25 and other members of the microtubular network, these results should be considered as an output of an initial high-throughput interactome screen, which we validated in this work.

Synergistic interactions among Aβ, Tau, and α-synuclein have been proposed that could mutually promote their accumulations within the inclusions leading to accelerated cognitive dysfunction (51). In fact, deposition of multiple proteins in the brain of demented people is more the rule than exception, which alters the prognosis and therapeutic response. Therefore, TPPP/p25 as a new protein player could be involved in multiple pathological interactions leading to protein aggregations characteristic for a subtype of neurological disorders.

In this work multiple interactions of Aβ_{42} oligomer as well as that of TPPP/p25 were characterized at molecular and cellular levels. As illustrated in the Fig. 3 scheme, the binding of Aβ_{42} to TPPP/p25 appears to be the tightest (K_d = 85 nM), whereas its interaction with tubulin and α-synuclein are one and two orders of magnitude weaker, respectively. The binding affinities of other interacting partners to the APP or Aβ peptide, characterized with K_d values also in the nanomolar range, suggest the pathological relevance of these interactions (52–54). Recently, proteomic analysis of hippocampal and cortical tissue from an animal model of AD has been performed where the most important groups of significantly altered proteins included those involved in synaptic plasticity, neurite outgrowth, and microtubule dynamics (55). Moreover, the levels of both tubulin and TPPP/p25 were found to increase both in the cortex and the hippocampus as compared with that of control samples (55), and the increase of TPPP/p25 level was similar to the increase of the α-synuclein level as well as that of the Tau level (55). However, our data offer the first evidence to the direct binding of TPPP/p25 to Aβ_{42} oligomer, which is stronger than that of the Aβ_{42} to α-synuclein.

The peptide/proteins used in the present studies are considered as hallmark proteins of neurological diseases; they are disordered or have an extended unfolded region. The studied proteins do not form a ternary complex with TPPP/p25, but they exhibited alternative binding; the formation of binary complexes was detected (*cf.* Figs. 3*C* and 5). This is in agreement with the results obtained by ELISA-Pepscan analysis, suggesting (partial) overlap of the binding sequences of TPPP/p25 for α-synuclein and Aβ_{42} in addition to tubulin as demonstrated previously (42).

A surprising result was obtained when the tubulin, α-synuclein, and Aβ_{42} system was investigated (*cf.* Figs. 3*D* and 5). The association of α-synuclein to tubulin is weak; however, Aβ_{42} oligomer was able to promote its binding in a concentration-dependent manner indicated by ELISA (*cf.* Fig. 3*D*). This soluble ternary complex is likely of functional importance because it causes a more extensive decrease of the tubulin assembly as compared with the decrease without α-synuclein (*cf.* Fig. 5). The synergistic interaction of these three proteins/peptide, similar to that recently demonstrated in the case of Tau, Aβ_{42}, and α-synuclein leading to more pronounced aggregation coupled with accelerated cognitive dysfunction (51), might be of pathological relevance.

Aβ_{42} effectively stimulates the oligomerization of α-synuclein (56), and vice versa, the α-synuclein promotes the oligomerization of Aβ_{42} leading to its *in vitro* precipitation (57) and formation of hybrid ring-like structures (17). TPPP/p25 can also induce α-synuclein aggregation (23).

Proteomics methods identified TPPP/p25 in various synaptic preparations (58). AD is associated with synapse loss, and emerging evidence links intraneuronal Aβ accumulation to the development of synaptic pathology, which is an early marker for this disease (for review, see Refs. 59–61). Aβ generated from axon-transported APP is released from presynaptic sites and subsequently accumulates close to the nerve terminal. Moreover, it has recently been suggested that monomeric Aβ_{40} and Aβ_{42} are the predominant forms required for synaptic plasticity and neuronal survival at physiological circumstances, and Aβ may act as a positive regulator presynaptically and as a negative regulator postsynaptically (61). Previously several synaptosomal proteins were identified to interact with the Aβ peptide including vacuolar proton-pump ATP synthase, glyceraldehyde-3-phosphate dehydrogenase, synapsin I and II, β-tubulin, and 2′,3′-cyclic nucleotide 3′-phosphodiesterase, but for these experiments the fibrillar form of the peptide was used (13). Our affinity chromatographic experiments provided the first evidence that Aβ_{42} peptide can bind TPPP/25 from the SPM fraction. The identification of synaptosomal molecular partners of Aβ is of great importance both physiologically and pathologically, as there is a bell-shaped relationship between Aβ and synaptic transmission; higher or lower than optimal concentration of Aβ impairs synaptic transmission.

Here we presented *in vitro* and *in vivo* evidence for the TPPP/p25-promoted aggregation of Aβ_{42}. Single cell experiments showed the colocalization of TPPP/p25 with amyloid in massive aggregate forms (*cf.* Fig. 8). We noticed that relatively large particles are formed exclusively in the cells where both TPPP/p25 and Aβ are present, as indicated by their colocalization in CHO cells (*cf.* Fig. 8), which is the consequence of their mutual interaction within the cytoplasm shown by the isolation of the protein aggregates by pelleting experiment (*cf.* Fig. 7*D*).

The formation of protein aggregates with specific ultrastructures might be an early event in AD. In fact, TPPP/p25 was found at the pretangles as well as in neuronal cytoplasm (21), supporting the possibility of its interaction with the intracellu-

lar Aβ, which might modify/determine the aggregate formation. In addition, in a previous work we noticed TPPP/p25 immunopositivity with antibody raised against TPPP/p25 peptide for the neurites at the intracellular amyloid plaques in the case of diffuse Lewy body disease with Alzheimer disease (21). Similar immunopositivity for α-synuclein was observed in the case of the same disease. Consequently, the detection of aggregates including amyloid and α-synuclein/TPPP/p25 could be indicative for the development of a new subtype of neurological disorders that forms a functional bridge to conjoin the co-pathologies of synucleopathies and amyloid plaque formation. Further immunohistochemical studies on human brain samples are in progress to identify specific subtypes of dementias.

Acknowledgments—We are grateful to Gergely Róna (Institute of Enzymology, Biological Research Center, Hungarian Academy of Sciences, Budapest, Hungary) for providing the Pro-DeliverIn, BODIPY 500/510 reagents, and the Alexa 633-conjugated secondary antibody.

REFERENCES

1. Hardy, J., and Selkoe, D. J. (2002) *Science* **297,** 353–356
2. Spillantini, M. G., Crowther, R. A., Jakes, R., Hasegawa, M., and Goedert, M. (1998) *Proc. Natl. Acad. Sci. U.S.A.* **95,** 6469–6473
3. Irvine, G. B., El-Agnaf, O. M., Shankar, G. M., and Walsh, D. M. (2008) *Mol. Med.* **14,** 451–464
4. Avila, J. (2006) *FEBS Lett.* **580,** 2922–2927
5. Hiltunen, M., van Groen, T., and Jolkkonen, J. (2009) *J. Alzheimers Dis.* **18,** 401–412
6. Carrell, R. W. (2005) *Trends Cell Biol.* **15,** 574–580
7. Hartmann, T., Bieger, S. C., Brühl, B., Tienari, P. J., Ida, N., Allsop, D., Roberts, G. W., Masters, C. L., Dotti, C. G., Unsicker, K., and Beyreuther, K. (1997) *Nat. Med.* **3,** 1016–1020
8. Roychaudhuri, R., Yang, M., Hoshi, M. M., and Teplow, D. B. (2009) *J. Biol. Chem.* **284,** 4749–4753
9. Wirths, O., Breyhan, H., Cynis, H., Schilling, S., Demuth, H. U., and Bayer, T. A. (2009) *Acta Neuropathol.* **118,** 487–496
10. Shah, S. B., Nolan, R., Davis, E., Stokin, G. B., Niesman, I., Canto, I., Glabe, C., and Goldstein, L. S. (2009) *Neurobiol. Dis.* **36,** 11–25
11. Hardy, J., and Allsop, D. (1991) *Trends Pharmacol. Sci.* **12,** 383–388
12. Braak, H., and Braak, E. (1991) *Acta Neuropathol.* **82,** 239–259
13. Verdier, Y., Huszár, E., Penke, B., Penke, Z., Woffendin, G., Scigelova, M., Fülöp, L., Szucs, M., Medzihradszky, K., and Janáky, T. (2005) *J. Neurochem.* **94,** 617–628
14. Crews, L., Tsigelny, I., Hashimoto, M., and Masliah, E. (2009) *Neurotox. Res.* **16,** 306–317
15. Lei, P., Ayton, S., Finkelstein, D. I., Adlard, P. A., Masters, C. L., and Bush, A. I. (2010) *Int. J. Biochem. Cell Biol.* **42,** 1775–1778
16. Kazmierczak, A., Strosznajder, J. B., and Adamczyk, A. (2008) *Neurochem. Int.* **53,** 263–269
17. Tsigelny, I. F., Crews, L., Desplats, P., Shaked, G. M., Sharikov, Y., Mizuno, H., Spencer, B., Rockenstein, E., Trejo, M., Platoshyn, O., Yuan, J. X., and Masliah, E. (2008) *PLoS One* **3,** e3135
18. Hlavanda, E., Kovács, J., Oláh, J., Orosz, F., Medzihradszky, K. F., and Ovádi, J. (2002) *Biochemistry* **41,** 8657–8664
19. Tirián, L., Hlavanda, E., Oláh, J., Horváth, I., Orosz, F., Szabó, B., Kovács, J., Szabad, J., and Ovádi, J. (2003) *Proc. Natl. Acad. Sci. U.S.A.* **100,** 13976–13981
20. Lehotzky, A., Lau, P., Tokési, N., Muja, N., Hudson, L. D., and Ovádi, J. (2010) *Glia* **58,** 157–168
21. Kovács, G. G., László, L., Kovács, J., Jensen, P.H., Lindersson, E., Botond, G., Molnár, T., Perczel, A., Hudecz, F., Mezo, G., Erdei, A., Tirián, L., Lehotzky, A., Gelpi, E., Budka, H., and Ovádi, J. (2004) *Neurobiol. Dis.* **17,** 155–162
22. Orosz, F., Kovács, G.G, Lehotzky, A., Oláh, J, Vincze, O., and Ovádi, J. (2004) *Biol. Cell* **96,** 701–711
23. Lindersson, E., Lundvig, D., Petersen, C., Madsen, P., Nyengaard, J. R., Højrup, P., Moos, T., Otzen, D., Gai, W. P., Blumbergs, P. C., and Jensen, P. H. (2005) *J. Biol. Chem.* **280,** 5703–5715
24. Geysen, H. M., Meloen, R. H., and Barteling, S. J. (1984) *Proc. Natl. Acad. Sci. U.S.A.* **81,** 3998–4002
25. Krchnák, V., Vágner, J., and Lebl, M. (1988) *Int. J. Pept. Protein Res.* **32,** 415–416
26. Bozso, Z., Penke, B., Simon, D., Laczkó, I., Juhász, G., Szegedi, V., Kasza, A., Soós, K., Hetényi, A., Wéber, E., Tóháti, H., Csete, M., Zarándi, M., and Fülöp, L. (2010) *Peptides* **31,** 248–256
27. Na, G. C., and Timasheff, S. N. (1986) *Biochemistry* **25,** 6214–6222
28. Paik, S. R., Lee, J. H., Kim, D. H., Chang, C. S., and Kim, J. (1997) *Arch. Biochem. Biophys.* **344,** 325–334
29. Fábián, G., Bozó, B., Szikszay, M., Horváth, G., Coscia, C. J., and Szücs, M. (2002) *J. Pharmacol. Exp. Ther.* **302,** 774–780
30. Bradford, M. M. (1976) *Anal. Biochem.* **72,** 248–254
31. Virok, D. P., Simon, D., Bozsó, Z., Rajkó, R., Datki, Z., Bálint, É., Szegedi, V., Janáky, T., Penke, B., and Fülöp, L. (2011) *J. Proteome. Res.* **10,** 1538–1547
32. Sherman, B. T., Huang da, W., Tan, Q., Guo, Y., Bour, S., Liu, D., Stephens, R., Baseler, M. W., Lane, H. C., and Lempicki, R. A. (2007) *BMC Bioinformatics* **8,** 426
33. Höftberger, R., Fink, S., Aboul-Enein, F., Botond, G., Olah, J., Berki, T., Ovadi, J., Lassmann, H., Budka, H., and Kovacs, G. G. (2010) *Glia* **58,** 1847–1857
34. Tokési, N., Lehotzky, A., Horváth, I., Szabó, B., Oláh, J., Lau, P., and Ovádi, J. (2010) *J. Biol. Chem.* **285,** 17896–17906
35. Oyama, R., Yamamoto, H., and Titani, K. (2000) *Biochim. Biophys. Acta* **1479,** 91–102
36. Verdier, Y., Földi, I., Sergeant, N., Fülöp, L., Penke, Z., Janáky, T., Szücs, M., and Penke, B. (2008) *J. Pept. Sci.* **14,** 755–762
37. Henning Jensen, P. (2001) *Methods Mol. Med.* **62,** 61–65
38. Coraci, I. S., Husemann, J., Berman, J. W., Hulette, C., Dufour, J. H., Campanella, G. K., Luster, A. D., Silverstein, S. C., and El-Khoury, J. B. (2002) *Am. J. Pathol.* **160,** 101–112
39. Koudinov, A. R., Berezov, T. T., Kumar, A., and Koudinova, N. V. (1998) *Clin. Chim. Acta* **270,** 75–84
40. Wilhelmus, M. M., de Waal, R. M., and Verbeek, M. M. (2007) *Mol. Neurobiol.* **35,** 203–216
41. Duce, J. A., Smith, D. P., Blake, R. E., Crouch, P. J., Li, Q. X., Masters, C. L., and Trounce, I. A. (2006) *J. Mol. Biol.* **361,** 493–505
42. Hlavanda, E., Klement, E., Kókai, E., Kovács, J., Vincze, O., Tökési, N., Orosz, F., Medzihradszky, K. F., Dombrádi, V., and Ovádi, J. (2007) *J. Biol. Chem.* **282,** 29531–29539
43. Vincze, O., Tökési, N., Oláh, J., Hlavanda, E., Zotter, A., Horváth, I., Lehotzky, A., Tirián, L., Medzihradszky, K. F., Kovács, J., Orosz, F., and Ovádi, J. (2006) *Biochemistry* **45,** 13818–13826
44. Lehotzky, A., Tirián, L., Tökési, N., Lénárt, P., Szabó, B., Kovács, J., and Ovádi, J. (2004) *J. Cell Sci.* **117,** 6249–6259
45. Oddo, S., Caccamo, A., Shepherd, J. D., Murphy, M. P., Golde, T. E., Kayed, R., Metherate, R., Mattson, M. P., Akbari, Y., and LaFerla, F. M. (2003) *Neuron* **39,** 409–421
46. Billings, L. M., Oddo, S., Green, K. N., McGaugh, J. L., and LaFerla, F. M. (2005) *Neuron* **45,** 675–688
47. Reddy, P. H. (2009) *Exp. Neurol.* **218,** 286–292
48. LaFerla, F. M., Green, K. N., and Oddo, S. (2007) *Nat. Rev. Neurosci.* **8,** 499–509
49. Tompa, P. (2009) *Structure and Function of Intrinsically Disordered Proteins*, CRC Press, New York
50. Ovádi, J. (2008) *IUBMB Life* **60,** 637–642
51. Clinton, L. K., Blurton-Jones, M., Myczek, K., Trojanowski, J. Q., and LaFerla, F. M. (2010) *J. Neurosci.* **30,** 7281–7289
52. Hughes, S. R., Khorkova, O., Goyal, S., Knaeblein, J., Heroux, J., Riedel, N. G., and Sahasrabudhe, S. (1998) *Proc. Natl. Acad. Sci. U.S.A.* **95,** 3275–3280
53. Golabek, A. A., Soto, C., Vogel, T., and Wisniewski, T. (1996) *J. Biol. Chem.*

271, 10602–10606
54. Ahn, H. J., Zamolodchikov, D., Cortes-Canteli, M., Norris, E. H., Glickman, J. F., and Strickland, S. (2010) *Proc. Natl. Acad. Sci. U.S.A.* **107,** 21812–21817
55. Martin, B., Brenneman, R., Becker, K. G., Gucek, M., Cole, R. N., and Maudsley, S. (2008) *PLoS One* **3,** e2750
56. Masliah, E., Rockenstein, E., Veinbergs, I., Sagara, Y., Mallory, M., Hashimoto, M., and Mucke, L. (2001) *Proc. Natl. Acad. Sci. U.S.A.* **98,** 12245–12250
57. Mandal, P. K., Pettegrew, J. W., Masliah, E., Hamilton, R. L., and Mandal, R. (2006) *Neurochem. Res.* **31,** 1153–1162
58. Orosz, F., Lehotzky, A., Oláh, J., and Ovádi, J. (2009) in *Protein Folding and Misfolding: Neurodegenerative Diseases* (Ovádi, J., and Orosz, F., eds) pp. 225–250, Springer-Verlag, New York
59. Parihar, M. S., and Brewer, G. J. (2010) *J. Alzheimers Dis.* **22,** 741–763
60. Gouras, G. K., Tampellini, D., Takahashi, R. H., and Capetillo-Zarate, E. (2010) *Acta Neuropathol.* **119,** 523–541
61. Palop, J. J., and Mucke, L. (2010) *Nat. Neurosci.* **13,** 812–818